

This item was submitted to Loughborough University as a PhD thesis by the author and is made available in the Institutional Repository (<https://dspace.lboro.ac.uk/>) under the following Creative Commons Licence conditions.



For the full text of this licence, please go to:
<http://creativecommons.org/licenses/by-nc-nd/2.5/>

Pilkington Library

Author/Filing Title Cook, M.

Accession/Copy No. 040129797

Vol. No.	Class Mark
---------------	------------------

LOAN COPY

~~THIS VOLUME IS NOT TO BE LOANED~~

25 JUN 1999

14 JAN 2000

14 APR 2000

0401297977



The Influence of Magnesium Hydroxide Morphology on the Mechanical Properties of Polypropylene

by

Mark Cook

Doctoral Thesis

Submitted in partial fulfilment of the requirements for the award of


DOCTOR OF PHILOSOPHY of Loughborough University

November 1996

Supervisor: Mr J. F. Harper

Institute of Polymer Technology and Materials Engineering

© Mark Cook 1996

 Loughborough University LE11 3TU	
Date	Apr 97
Class	
Acc No	060129797

9 9102506

CONTENTS

	<i>PAGE</i>
<i>DEDICATION</i>	i
<i>ACKNOWLEDGEMENTS</i>	ii
<i>ABSTRACT</i>	iv
<i>TABLES</i>	vi
<i>FIGURES</i>	viii
 <i>CHAPTER 1- INTRODUCTION</i>	 1
1.1 Polypropylene	1
1.2 Flame Retarding Polymers	3
1.3 Flame Retardants	4
1.4 Hydrated Mineral Fillers	6
1.5 Premier Periclase Limited	7
1.6 Aims	8
 <i>CHAPTER 2 - LITERATURE SURVEY</i>	 9
2.1 Magnesium Hydroxide	9
2.1.1 Flame retardant effects of $Mg(OH)_2$	9
2.1.2 Morphology of magnesium hydroxide	11
2.1.3 Production of magnesium hydroxide	11
2.1.3.1 Sea water method	12
2.1.3.2 Brines method	12
2.1.3.3 Raw mineral method	14
2.1.3.4 Kyowa method	14
2.2 Effect of Mineral Fillers on Polymer Properties	15
2.2.1 Filler particle size and morphology	17
2.2.2 Composite modulus	20
2.2.3 Composite tensile strength	25
2.2.4 Composite toughness	29
2.2.5 Filler dispersion	32
2.2.6 Processing	35
2.3 Effect of Filler Modification	37
2.3.1 Reasons for surface modification	38
2.3.2 Fatty acid surface modifiers	39
2.3.3 Silane surface modifiers	41
2.3.4 Surface tension and wettability	43
2.3.5 $Mg(OH)_2$ /PP interactions	45
2.4 Polypropylene Crystallinity and Morphology	46
2.4.1 Unfilled polypropylene	47
2.4.2 Influence of fillers on crystallisation	47
 <i>CHAPTER 3 - EXPERIMENTAL METHODS</i>	 51
3.1 Materials	51
3.1.1 Polypropylene	51
3.1.2 Magnesium hydroxide	52
3.1.3 Coating agents	53
3.1.4 Coating methods	53
3.1.5 Filler coding	55

	<i>PAGE</i>
3.2 Characterisation of fillers	55
3.2.1 X-ray diffraction	57
3.2.2 Particle sizing	58
3.2.3 Surface area	59
3.2.4 Scanning transmission electron microscopy (STEM)	59
3.2.5 Bulk density	60
3.2.6 Oil absorption	60
3.2.7 FTIR DRIFT analysis	61
3.3 Sample Preparation	62
3.3.1 Formulation	62
3.3.2 Compounding	65
3.3.2.1 Continuous mixing	65
3.3.2.2 Batch mixing	66
3.3.3 Injection moulding	67
3.4 Characterisation of Compounds	67
3.4.1 Final filler content	68
3.4.2 Melt flow index	68
3.4.3 Capillary rheometry	69
3.5 Characterisation of Moulded Composites	69
3.5.1. Flexural testing	69
3.5.2 Impact testing	70
3.5.3. Thermal analysis	71
3.5.3.1 Differential scanning calorimetry (DSC)	71
3.5.3.2 Dynamic mechanical thermal analysis (DMTA)	72
3.5.3.3 Vicat softening point	72
3.5.4 Flame retardancy	72
3.5.4.1 UL94 vertical burning test	72
3.5.4.2 Limiting oxygen index (LOI)	73
3.5.4.3 Cone calorimetry	74
3.5.5 Fracture surface analysis	75
3.5.6 Filler dispersion analysis	75
CHAPTER 4 - RESULTS	78
4.1 Filler Characterisation	78
4.1.1 X-ray diffraction	78
4.1.2 Particle structure and size distribution	80
4.1.3 Surface area	88
4.1.4 Packing properties	89
4.1.5 FTIR DRIFT analysis	90
4.2 Compounding Characteristics	91
4.3 Characterisation of Pelletised Compounds	94
4.3.1 Final filler content	94
4.3.2 Melt flow index	95
4.3.3 Capillary rheometry	96
4.4. Mechanical Properties	100
4.4.1 Flexural testing	100
4.4.2 Impact testing	104

	<i>PAGE</i>
4.5 Thermal Analysis	106
4.5.1 Differential scanning calorimetry (DSC)	106
4.5.2 Differential mechanical thermal analysis (DMTA)	114
4.5.3 Vicat softening point	114
4.6 Flame Retardancy	115
4.6.1 UL94 vertical burning test and LOI	115
4.6.2 Cone calorimetry	118
4.7 Fracture Surface Analysis	119
4.8 Filler Dispersion Analysis	123
<i>CHAPTER 5 - DISCUSSION</i>	128
5.1 Filler Morphology	128
5.1.1 Filler structure	128
5.1.2 Replication of morphology	130
5.1.3 Dry packing properties	131
5.1.4 Wet packing properties	131
5.1.5 Compounding	132
5.1.6 Rheology	133
5.1.7 Crystallinity	134
5.1.8 Flexural properties	137
5.1.9 Impact properties	139
5.1.10 Flame retardancy	140
5.1.11 Fracture surface analysis	142
5.1.12 Filler dispersion	143
5.2 Coating Agent	144
5.2.1 Filler structure	144
5.2.2 Particle size distribution	145
5.2.3 Surface area	145
5.2.4 Packing properties	146
5.2.5 Compounding	147
5.2.6 Rheology	147
5.2.7 Crystallinity	148
5.2.8 Flexural properties	149
5.2.9 Impact properties	150
5.2.10 Flame retardancy	151
5.2.11 Fracture surface analysis	151
5.2.12 Filler dispersion	152
5.3 Coating Type	152
5.3.1 Filler structure	152
5.3.2 Particle size distribution	153
5.3.3 Surface area	154
5.3.4 Packing properties	155
5.3.5 Coating consistency	156
5.3.6 Compounding	157
5.3.7 Rheology	158
5.3.8 Crystallinity	161
5.3.9 Ageing of vinyl silane composites	162
5.3.10 Flexural properties	165
5.3.11 Impact properties	167
5.3.12 Flame retardancy	168

	<i>PAGE</i>
5.3.13 Fracture surface analysis	170
5.3.14 Filler dispersion	172
5.4 Coating Level	173
5.4.1 Filler structure	173
5.4.2 Particle size distribution	174
5.4.3 Surface area	174
5.4.4 Packing properties	175
5.4.5 Coating consistency	176
5.4.6 Compounding	177
5.4.7 Rheology	177
5.4.8 Crystallinity	178
5.4.9 Flexural properties	179
5.4.10 Impact properties	181
5.4.11 Flame retardancy	182
5.4.12 Fracture surface analysis	183
5.4.13 Filler dispersion	184
CHAPTER 6 - CONCLUSIONS	185
6.1 Filler Morphology	185
6.2 Coating Agent	186
6.3 Coating Type	186
6.4 Coating Level	187
REFERENCES	188
APPENDIX A X-ray diffraction peaks $Mg(OH)_2$ fillers	194
APPENDIX B Particle sizing parameters and data	195
APPENDIX C BET surface area calculations and data	198
APPENDIX D Filler packing data	201
APPENDIX E FTIR analysis and data	203
APPENDIX F Filler content data	205
APPENDIX G Melt flow calculations and data	210
APPENDIX H Capillary rheometry calculations and data	214
APPENDIX I Flexural calculations and data	224
APPENDIX J Impact parameters and data	236
APPENDIX K DSC analysis and parameters	248
APPENDIX L DMTA theory and data	249

Dedicated to
Janet and John Cook

In memory of Alf Heaton
(1913 to 1995)

ACKNOWLEDGEMENTS

During the three and a half years that it has taken me to prepare this thesis, I have experienced many difficulties. To overcome these problems I have required practical, academic and financial assistance along with a lot of friendship, love and laughs provided by many people. I would therefore like to take this opportunity to thank the following people:

Mr John Harper, my supervisor, who has been exceptionally kind to me. He has not only provided valuable academic input and financial backing, but has been available and understanding when times have been difficult. Thank you John.

Roger Rotheron, my industrial supervisor who instrumented the project and provided me with the understanding required to complete the project.

Premier Periclase Ltd (Ireland) for funding the project, particularly Adrian Ryder and Tony Bourke.

The Engineering and Physical Sciences Research Council (EPSRC) for providing sponsorship for 3 years.

John Long (Montell Polyolefins, Milton Keynes), for selecting and providing the polypropylene.

My friends, particularly my best friends Martin Reeves, David Mandley (Shandy), Mark Foster (Sharky) and Roland Kotzian, who have made my time at Loughborough such a laugh. Cheers!

Jim and Penny White at William Morris Hall, where I was a Sub-Warden for 3 years.

Ceri, my girlfriend, who I love dearly. Thanks for all the love and support.

I would also like to thank the following people within IPTME at Loughborough University:

Dr Gilbert (Director of Research), for allowing me to commence the project, Andy Trotter (processing), Ray Owens (characterisation), Trevor Atkinson (photographic), Frank Page (SEM), John Bates (STEM), Dave Hitt (XRD), Carole Birchenough (assistance) and to Colin Lines, Mick Hallum and Ken Ellison (workshop).

Thanks also go to Martin Evans (Zeneca Resins) for particle size analysis, Martin Kerry (Chem. Eng.) for surface area analysis, Derek Hemsley (Polymer Microscopy Services) for providing valuable consultancy work and to Dr Lee Martin for being such a good mate throughout his time in IPTME.

Finally, a special thanks go to Barry Haworth, for getting me there in the end.

ABSTRACT

Magnesium hydroxide is of growing interest as a halogen-free flame retardant, and has a high thermal stability, so it can be melt processed into most thermoplastics without premature decomposition. The hydrated mineral filler commences endothermic decomposition at approximately 340°C, withdrawing heat from the polymer substrate, releasing water of crystallisation to dilute the fuel supply. However, to be an effective flame retardant filler, high loadings up to 66% are required. This may cause detrimental effects on both rheological and mechanical properties of composites produced.

Two synthetic seawater magnesium hydroxide fillers (DP393 and DP390s), of different morphologies but similar surface area, were selected as flame retardant fillers for polypropylene. These were coated with stearate, oleate, rosin and vinyl silane and compounded at 60% by weight into an injection moulding grade of polypropylene. The effect of filler morphology, coating agent, coating type and coating level on the crystallisation, rheological and mechanical properties of polypropylene were studied.

DP393 is a one-micron platey structure which was found (by XRD) to be orientated parallel to the flow direction, whereas DP390s is a five-micron porous sphere residing isotropically within the matrix. Incorporation of uncoated magnesium hydroxide increased the overall crystallisation rate of polypropylene, causing orientation of the polymer b axis parallel to the flow direction, this being induced by the 001 crystal face of magnesium hydroxide.

Particle sizes and surface areas were difficult to replicate using the current production methods. Filler coating changed the particle size distribution of the primary particles. Filler coating also reduced the surface area and wet packing properties of the fillers.

PP compounds containing uncoated magnesium hydroxide filler have very high shear viscosities, but filler coatings reduced melt viscosities, with fatty acids having the most pronounced effect. Filler coatings had a greater influence than particle size on such

rheological changes. Vinyl silane and fatty acid coatings facilitated good dispersion during twin screw compounding whereas the rosin coating did not promote dispersion to the same extent. Crystallisation rates were reduced with filler coatings, this being most significant at higher coating levels.

Stearate and oleate coatings yielded composites with similar rheological and mechanical property trends. Flexural modulus and strength decreased with increased coating levels, which was attributed to a reduction in interfacial adhesion at the filler/matrix interface. However, an increase in flexural modulus as a function of ageing time is experienced for silane coated fillers. Vinyl silane coating produced composites with the highest impact properties. Fatty acid treatment reduced these below the uncoated. However, increased coating levels improved material toughness by increasing failure deflections. Filler loading level was the main factor governing flame retardancy, as determined by LOI and UL94 techniques. Flame retardant formulations significantly reduced the heat evolved during polypropylene pyrolysis in cone calorimetry experiments.

TABLES

<i>Table</i>	<i>Description</i>	<i>Page</i>
2.1	Some models for predicting composite modulus	21
3.1	Codes for DP393 coated fillers	56
3.2	Codes for DP390s coated fillers	57
3.3	DP393 LOT 1 uncoated and fatty acid formulations	62
3.4	DP393 LOTS 1 and 2 vinyl silane formulations	63
3.5	DP393 LOT 2 fatty acid formulations	63
3.6	DP393 LOT 3 uncoated and fatty acid formulations	64
3.7	DP390s LOT 1 uncoated fatty acid formulations	64
3.8	DP390s LOT 2 fatty acid formulations	64
3.9	Screw configurations for both compounds	65
3.10	Barrel temperature profile of each APV compounder	66
3.11	Conditions employed for injection moulding of test specimens	68
4.1	DP393 LOT 1 uncoated and fatty acid compounding characteristics	92
4.2	DP393 LOT 2 fatty acid compounding characteristics	92
4.3	DP393 LOT 3 uncoated and fatty acid compounding characteristics	92
4.4	DP393 LOT 1 and 2 vinyl silane compounding characteristics	93
4.5	DP390s LOT 1 uncoated and fatty acid compounding characteristics	93
4.6	DP390s LOT 2 fatty acid compounding characteristics	94
4.7	Effect of stearate coating agent on flexural properties of DP393 composites	101
4.8	Comparison of flexural properties of DP393 LOT 1 uncoated & coated fillers	102
4.9	Comparison of flexural properties of DP390s LOT 1 uncoated & coated fillers	102
4.10	Comparison of fatty acid coating level on flexural properties of DP393 LOT 1 fillers	102
4.11	Comparison of fatty acid coating level on flexural properties of DP390s LOT 1 fillers	103
4.12	Effect of 55% magnesium hydroxide level on impact properties of PP	104
4.13	Effect of coating agent on impact properties of DP393 fillers	104
4.14	Comparison of impact properties of DP393 LOT 1 uncoated & coated fillers	105
4.15	Comparison of impact properties of DP390s LOT 1 uncoated & coated fillers	105
4.16	Comparison of stearate coating level on impact properties of DP393 LOT 1 fillers	105
4.17	Comparison of oleate coating level on impact properties of DP390s LOT 1 fillers	106
4.18	Thermal properties of polypropylene	106
4.19	Thermal properties of DP393 LOT 1 uncoated and fatty acid composites	107
4.20	Thermal properties of DP393 LOT 2 fatty acid composites	107
4.21	Thermal properties of DP393 LOT 3 uncoated and fatty acid composites	107
4.22	Thermal properties of DP390s LOT 1 uncoated and fatty acid composites	108
4.23	Thermal properties of DP390s LOT 2 fatty acid composites	108
4.24	Maiti parameters for some DP393 LOT 1 composites	109
4.25	Maiti parameters for some DP390s LOT 1 composites	109
4.26	Maiti parameters for polypropylene	109
4.27	Onset temperature of vinyl silane coated DP393 LOT 1A composites	110
4.28	Crystallinity (XL) of vinyl silane coated DP393 LOT 1A composites	110
4.29	Crystallinity (RC) of vinyl silane coated DP393 LOT 1A composites	110
4.30	Onset temperature of vinyl silane coated DP393 LOT 1B composites	110
4.31	Crystallinity (XL) of vinyl silane coated DP393 LOT 1B composites	111
4.32	Crystallinity (RC) of vinyl silane coated DP393 LOT 1B composites	111
4.33	Thermal analysis of batch mixed polypropylene & uncoated DP393 compound	111
4.34	Thermal analysis of batch mixed vinyl silane coated DP393 LOT 2 compounds	112
4.35	Overall crystallisation rate of vinyl silane coated DP393 LOT 1B composites	112

<i>Table</i>	<i>Description</i>	<i>Page</i>
4.36	Nucleation rate of vinyl silane coated DP393 LOT 1B composites	112
4.37	Crystallite size distribution of vinyl silane coated DP393 LOT 1B composites	113
4.38	Maiti analysis of polypropylene and uncoated DP393 batch mixed compounds	113
4.39	Maiti analysis of vinyl silane coated DP393 batch mixed compounds	113
4.40	Vicat softening point for polypropylene and some vinyl silane composites	114
4.41	UL94 and LOI results for DP393 LOT 1 uncoated and fatty acid composites	115
4.42	UL94 and LOI results for DP393 LOT 2 fatty acid composites	116
4.43	UL94 and LOI results for DP393 LOT 3 fatty acid composites	116
4.44	UL94 and LOI results for DP393 LOT 1 vinyl silane composites	116
4.45	UL94 and LOI results for DP390s LOT 1 uncoated and fatty acid composites	116
4.46	UL94 and LOI results for DP390s LOT 2 fatty acid composites	117
4.47	UL94 and LOI results for polypropylene	117
4.48	Cone calorimetry data for some magnesium hydroxide filled composites	119

FIGURES

<i>Figure</i>	<i>Description</i>	<i>Page</i>
1.1	Simple model of burning process	4
3.1	Flow chart indicating the production routes to obtain DP390s and DP393	52
4.1	XRD pattern for DP393 and DP390s fillers	78
4.2	XRD pattern for unfilled polypropylene	79
4.3	XRD pattern for polypropylene filled with 55% DP393	79
4.4	XRD pattern for polypropylene filled with 55% DP390s	80
4.5	STEM micrograph of DP393 (x50k)	81
4.6	STEM micrograph of DP390s (x50k)	81
4.7	PSD for DP393 and DP390s fillers	82
4.8	PSD for standard and high density DP393	83
4.9	SEM micrograph of HD-DP393	83
4.10	PSD for different LOTS of DP393 fillers	84
4.11	Effect of coating agent on PSD of DP393 LOT 1 fillers	84
4.12	Effect of coating agent on PSD of DP393 LOT 1 fillers	85
4.13	Effect of coating agent on PSD of DP390s LOT 2 fillers	85
4.14	PSD of stearate, oleate and rosin coated DP393	86
4.15	PSD of vinyl silane coated DP393	86
4.16	PSD of stearate and oleate coated DP390s	87
4.17	PSD for stearate and oleate coated DP393 LOT 1 fillers at high and low levels	87
4.18	PSD for stearate and oleate coated DP390s LOT 1 fillers at high and low levels	88
4.19	Effect of stearate coating level on surface area of magnesium hydroxide fillers	89
4.20	Effect of increased coating level on the wet packing properties of magnesium hydroxide fillers	90
4.21	Effect of increase in applied fatty acid coating level on the CH/OH ratio of DP393 LOT 1 fillers	91
4.22	Bar chart showing discrepancies between MFI and volumetric output	95
4.23	Shear flow curves for DP393 and DP390s filled polypropylene	96
4.24	Shear flow curves for DP393 with stearate coating agents	96
4.25	Shear flow curves for DP393 with oleate coating agents	97
4.26	Shear flow curves for DP390s with oleate coating agents	97
4.27	Shear flow curves of vinyl silane coated DP393 filled compounds	98
4.28	Shear flow curves of stearate, oleate, rosin & silane coated DP393 filled compounds	98
4.29	Shear flow curves of stearate and oleate coated DP390s filled compounds	99
4.30	Effect of increased oleate coating level on the rheological properties of DP393 filled polypropylene	99
4.31	Effect of increased stearate coating level on the rheological properties of DP390s filled polypropylene	100
4.32	Change in PP modulus with 55% addition of magnesium hydroxide	101
4.33	Change in flexural modulus with time for vinyl silane coated DP393 composites	103
4.34	Effect of DP393 filler loading on the LOI of polypropylene composites	117
4.35	Heat release curves for selected Mg(OH) ₂ /PP composites	118
4.36	Impact fracture surface of composite DP393 LOT 3 (x5k)	120
4.37	Impact fracture surface of composite DP390s LOT 1 (x5k)	120
4.38	Flexural fracture surface of composite 4.5AMST LOT 1 (x5k)	121
4.39	Flexural fracture surface of composite DP393 LOT 1 (x5k)	121
4.40	Flexural fracture surface of composite 2.0VS65A (x5k)	122
4.41	Flexural fracture surface of composite 4.5AMROS LOT 1 (x5k)	122

<i>Figure</i>	<i>Description</i>	<i>Page</i>
4.42	Flexural fracture surface of composite DP390s LOT 2 (x5k)	123
4.43	Etched surface of composite DP393 LOT 1 showing filler dispersion (x5.5k)	124
4.44	Etched surface of composite DP390s LOT 1 showing filler dispersion (x5.5k)	124
4.45	Etched surface of composite 2.0VS70A showing filler dispersion (x5.5k)	125
4.46	Etched surface of composite 4.5NAOL LOT 1 showing filler dispersion (x5.5k)	125
4.47	Etched surface composite 4.5AMROS LOT 1 showing filler dispersion (x5.5k)	126
4.48	Etched surface of composite AMST4.0 showing filler dispersion (x5.5k)	126
4.49	Etched surface of composite AMOL4.0 showing filler dispersion (x5.5k)	127

CHAPTER 1

INTRODUCTION

Polypropylene is one of the most widely used engineering thermoplastics in the world today. Since the number and severity of disasters involving flammable polymeric materials has increased, fire retardancy is of great importance. Hence, the need for flame retarding polypropylene is required.

Several methods have been devised to reduce the flammability of polymers, many of which have been well documented. This project is associated with the flame retardancy of polypropylene using what has been termed 'an environmentally friendly' fire retardant. The reasons for the selection of this fire retardant and its effect on the physical and mechanical properties of polypropylene have been concisely presented within this thesis.

1.1 Polypropylene

Crystalline, high molecular weight polymers of polypropylene (PP) were first prepared by Professor Giulio Natta using catalysts of the type used by Zeigler for the low pressure polymerisation of ethylene. In the early slurry processes, polymerisation took place in a liquid hydrocarbon carrier. Catalyst residues and non-crystalline polymer were removed in an additional separation stage after polymerisation, prior to drying [1]. More recently, catalysts having progressively higher activities and stereospecifications have been developed. These catalysts eliminate the need for residue removal stages. Propylene (monomer) can be produced commercially by 3 principal processes leading to naphtha, refinery and natural gas propylene [2]. The naphtha process is the most common in Western Europe and it is expected that by the year 2000 the world wide capacity for PP will be 10M tonnes per annum [3].

Propylene copolymerises readily with alpha-olefins, the most widely used of which is ethylene. Random or 'block' copolymers of propylene and ethylene are used to extend the performance range of polymers to include high toughness, good low temperature

performance, flexibility and improved clarity. Co-ordination polymerisation is far from simple in terms of mechanism, kinetics and application. The Zeigler-Natta catalyst is a co-ordination complex, with a transition metal being the active centre, and the uniformity of its surface giving a direct bearing on the isotacticity of the polymer being produced [2,4]. The delta TiCl_3 and $\text{TiCl}_4/\text{MgCl}_2$ supported catalysts are the main industrial systems used at present [2,5]. Typical catalysts are 10-30 microns in diameter, consisting of loosely bound agglomerated fine crystallites. The morphology of the polypropylene particles are determined by the catalyst morphology (shape, size and porosity) since nascent particles produced by such catalysts replicate the original morphology [3,6,7].

Polypropylene is available in three forms of tacticity; atactic, syndiotactic and isotactic. Atactic chains are completely disorganised in structure and consequently do not crystallise. Syndiotactic and isotactic polypropylene, because of their regular structure can crystallise. Due to the poor properties of syndiotactic polypropylene, commercial polypropylene is isotactic. Isotactic polypropylene (iPP) cannot crystallise in the planar zig zag form like PE because of the steric hindrance of the methyl side group [8]. Instead, the isotactic chain assumes a helical configuration and ternary system. This means that the structure is repeated after 3 monomeric units at an identity period of 0.65nm giving rise to four helical arrangements [2].

Polypropylene is a semi-crystalline polymer and has a series of ordered crystalline regions (crystallites) and a non ordered amorphous region. It crystallises from the melt via spherulites and the maximum achievable crystallinity is 70% [1] due to restriction by molecular hindrance. Also the great length of the polymer molecules leads to chain entanglement. Rapid freezing of the polymer melt is another factor that restricts crystallinity as structural transitions take time to complete. Indeed fully crystallised PP's tend to be brittle since it is the amorphous regions that convey toughness. Crystalline regions are therefore more densely packed than amorphous regions, a typical density for polypropylene is 905kg/m^3 .

1.2 Flame Retarding Polymers

Since the 1950's, polymeric materials have replaced conventional materials in the construction and furnishing of homes, commercial and public buildings. These synthetic polymers are mostly organic compounds which are often more flammable than the conventional materials and thus involve a much increased fire hazard. The number of people killed by fire is only a small problem. When synthetic polymers are involved, additional hazards such as reduced visibility and suffocation by smoke and poisoning by volatile fumes are major contributory factors.

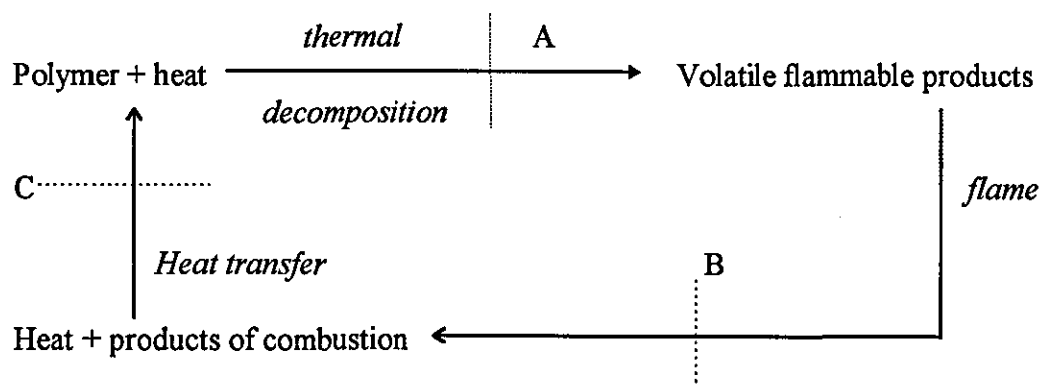
Polymeric materials, mainly organic compounds, are essentially comprised of carbon and hydrogen. Like most organic compounds, polymers are unstable at quite low temperatures upward from 200°C, producing a range of small, volatile, organic compounds which are highly flammable. It is these products of thermal degradation which burn, evolving large amounts of heat, which causes further degradation, rapidly accelerating combustion.

With polypropylene, little monomer is observed in the volatile gaseous products, indicating that little chain depolymerisation by unzipping from chain ends takes place [9]. The principal mechanism for the formation of volatiles appears to be a homolytic chain scission followed by inter and intramolecular chain transfer. Radical transfer occurs more readily at hydrogens attached to tertiary carbon atoms. The initial bond scission may involve regular C-C bonds, bonds beta to oxygen containing chain carbons or branch points, or other weak bonds that may have been incorporated into the polymer during resin manufacture. The principal volatile products are a homologous series of low molecular weight saturated and unsaturated hydrocarbons, all of which are flammable.

A simple model of the burning process can be seen in Fig.1.1 [10]. For continuous burning, sufficient heat must be applied to decompose the material and ignite the products of degradation, and sufficient heat from the combustion must be transferred

back to the polymer to maintain the cycle when heat is withdrawn. Therefore to make a material fire retardant, the cycle must be broken at one of three points A, B or C.

Fig 1.1 Simple model of a burning process



- A) modifying the thermal degradation process,
- B) quenching the flame
- C) reducing the flow of heat from the flame back to the degrading polymer.

1.3 Flame Retardants

An additive that can interfere with any of the above stages by physical or chemical means is termed a flame retardant. As flame retardancy is an essential property of many polymeric products, it was originally normal practice to use halogenated polymers which were inherently flame retardant (often in combination with halogenated organic additives). The main advantage of halogenated flame retardant additives is the low concentration level required for them to work effectively, hence retaining mechanical properties. Halogens are effective because they interfere with the chemical chain reaction that propagates fire [11]. The use of such halogenated organics, such as halogenated diphenyl esters bears significant health risks by forming toxic products such as dibenzofuranes and polyhalogenated dibenzodioxines [12]. The halogenated polymers themselves liberate toxic hydrochloric acid.

Antimony trioxide is itself a popular fire retardant but its flame retarding effect also depends on the presence of organic halides (unless it is used with a chlorinated

polymer). On heating, in the presence of the organic halide, the antimony trioxide is converted to antimony trichloride. This boils at 219°C and on evaporation participates in flame retardation by acting in the gaseous phase [13]. This synergistic effect, occurring in the gas phase, leads to increased soot formation and smoke density [12]. The above undesirable effects are the main reasons for the requirement of halogen free flame retardants.

Increased resistance to flammability can also be achieved using melamine salts to promote dripping and red phosphorus through enhanced condensed phase char formation [14]. Dripping will remove heat from the substrate but may lead to the ignition of fresh unburned material. Red phosphorus is a well documented health hazard, especially as air-borne particles, which will be experienced during compounding.

Sometimes, inert fillers are added to polymers, acting like a diluent by reducing the amount of combustible material. This inhibits smoke formation in proportion to the loading. This diluent effect does not work with all fillers, especially for those that react with the pyrolysis products active in the combustion mechanism. For example, calcium carbonate will react with HCl liberated during PVC pyrolysis. This elimination of hydrogen chloride (capable of reducing flammability) will cause an effective decrease in the materials resistance to ignition [13]. Alternatively, the filler may react with products of material degradation, producing active flame suppressants, char and cross linking reactions all contributing to increased flammability.

Due to the disadvantages of these flame retardants, alternatives, such as hydrated minerals have been utilised as flame retardant fillers for polypropylene.

1.4 Hydrated Mineral Fillers

Hydrated inorganic compounds such as metal hydroxides are of growing interest as flame retardants for polymers. They release water of crystallisation by decomposing endothermically on heating. Before they can be used as flame retarding fillers, they must meet certain criteria; the material must be inexpensive, freely available in quantity, non toxic, non coloured, of low solubility and with a morphology suitable for filler use. Furthermore, the decomposition temperature must be high enough to survive polymer processing but low enough to exhibit a fire retarding effect.

Until recently, the market has been dominated by one material, aluminium hydroxide (alumina trihydrate, ATH) [15]. Its endothermic decomposition commences at about 180°C and withdraws heat from its polymer substrate. The accompanying release of inert gases (water vapour) on thermal breakdown dilutes the fuel supply present in the gas phase [16]. Although ATH is reasonably cheap it is the relatively low thermal stability that drives the inherent interest in alternatives.

Other hydrated fillers with a potential use in polymers are [16,17,18] calcium hydroxide, nesquehonite ($\text{MgCO}_3 \cdot 3\text{H}_2\text{O}$), basic magnesium carbonate ($3\text{MgCO}_3 \cdot \text{Mg}(\text{OH})_2 \cdot 3\text{H}_2\text{O}$), magnesium hydroxide ($\text{Mg}(\text{OH})_2$) and a naturally occurring deposit comprised of huntite ($\text{Mg}_3\text{Ca}(\text{CO}_3)_4$) and hydromagnesite ($\text{Mg}_4(\text{CO}_3)(\text{OH})_2 \cdot 3\text{H}_2\text{O}$, known as 'Ultracarb. Zinc borate compounds are also used, of which the most commercial variant is $2\text{ZnO} \cdot 3\text{B}_2\text{O}_3 \cdot 5\text{H}_2\text{O}$. Calcium hydroxide decomposes endothermically to the oxide at 450° having a high thermal stability. However, calcium hydroxide has given disappointing results, since during combustion carbonate rather than oxide forms, which is an exothermic reaction [16]. Basic magnesium carbonate is more stable than nesquehonite but its platy, high surface area particles are not suited to filler applications. Nesquehonite is an effective flame retardant but suffers from a low decomposition temperature. Ultracarb occurs naturally and is cheaper to produce than ATH but its morphology is not perfect for use in polymers. Zinc borate decomposes endothermically to release water, producing boric acid which is a highly effective char promoter in oxygen containing substances [18].

Apart from ATH (zinc borate which will not be considered further), only Ultracarb and to some extent, magnesium hydroxide have achieved any commercial significance. Enthalpies of decomposition of these 3 hydrated minerals are broadly similar (around 1300kJ/g), their respective percentage water loss by weight is 34.5, 31.4 and 20% on complete breakdown [18]. Ultracarb has been used within a polypropylene matrix and has been shown to be effective as a flame retardant but has limitations due to its incomplete decomposition at high filler loadings [19]. Further differences between aluminium hydroxide and magnesium hydroxide can be found between their decomposition temperatures, 180 and 330°C respectively, breaking down to the oxide and water vapour. This higher thermal stability of magnesium hydroxide permits its use in polymers processed at higher melt temperatures, without premature filler degradation, giving rise to an attractive range of compound properties which has stimulated interest in this specific project.

1.5 Premier Periclase Limited

Premier Periclase Limited has been a leading producer of high quality sintermagnesia (magnesium oxide) since the company began production in 1980. The plant has a rated capacity of 100,000 tonnes per annum and is located in Drogheda, Ireland.

In 1991, Premier Periclase commenced the production of large crystal sintermagnesia with a high bulk density, large crystal size, low boron content and balanced chemistry setting standards in terms of quality and performance within the refractory industry [20]. The production of sintermagnesia is based on the reaction of lime with magnesium salts dissolved in seawater producing an intermediate magnesium hydroxide slurry. Based on a joint research project with ICI Chemicals and Polymers Limited, Premier Periclase developed a synthetic magnesium hydroxide, from this slurry intermediate, with a carefully controlled particle morphology. When incorporated into copolymers of polyethylene, high mechanical properties and fire retardancy have been produced [21]. Investigations of the incorporation of this new grade of magnesium hydroxide into other engineering thermoplastics are now being undertaken in order to determine possible commercial markets.

1.6 Aims

The major aim of this project is to investigate the effect of magnesium hydroxide filler morphology and surface coating treatment on the physical, rheological and mechanical properties of flame retardant polypropylene formulations. This will involve utilising two synthetic (and experimental) grades of magnesium hydroxide, DP393 and DP390s, which are different to those currently available. These fillers have essentially the same surface area but have distinctly different morphologies. Both fillers will be treated with stearate and oleate fatty acid coatings at addition levels up to saturation coverage, whereas DP393 will also be coated with vinyl silane and a rosin gum at this upper limit. Work will be focused on studying four discrete areas: filler morphology, coating agent, coating type and coating level. Characteristics and properties to be measured will include PSD, filler packing, rheology, crystallinity, flexural and impact properties, filler dispersion and flame retardancy.

The main objectives of this work are to improve the knowledge which has been previously generated in this area. This will involve a range of objectives:

- To undertake a comprehensive filler characterisation programme.
- To identify the necessary morphological features of magnesium hydroxide which influence the nucleation and morphology of polypropylene.
- To examine any differences between stearate and oleate treated magnesium hydroxide and to investigate their influence on particle size distribution, crystallisation characteristics, rheology and mechanical properties.
- To develop an optimised filler dispersion technique for magnesium hydroxide filled PP, in order to investigate the effectiveness of twin screw extrusion.
- To assess the burning characteristics of $\text{Mg}(\text{OH})_2/\text{PP}$ composites using a range of tests including LOI, UL94 and cone calorimetry.

CHAPTER 2

LITERATURE REVIEW

2.1 Magnesium Hydroxide

Magnesium hydroxide has the chemical formula $\text{Mg}(\text{OH})_2$ and occurs naturally as the mineral brucite. Magnesium hydroxide is a crystalline, inorganic salt of alkaline nature (in slurry form it has a pH of 9). It has a hexagonal (trigonal) crystallographic structure with lattice parameters $a = 0.3174\text{nm}$ and $c = 0.4769\text{nm}$, with its basal plane lying in the 001 direction. This crystallographic structure consists of close packed hydroxyl anions with magnesium cations occupying half of the octahedral holes. The normal crystal shape consists of hexagonal plates formed from layers of HO-Mg-OH . However, magnesium hydroxide's final structure is dependent on its production method [22]. The bulk density will therefore differ for different types of $\text{Mg}(\text{OH})_2$.

Magnesium hydroxide is chemically stable and has a specific gravity of approximately 2.3, this depending on its water content. In the pure form it exists as a white, odourless powder with low toxicity. It has a refractive index of 1.57 and a Mohr's hardness of 2.5 [13]. Magnesium hydroxide is practically insoluble in water but is soluble in acids and ammonium salts [23].

$\text{Mg}(\text{OH})_2$ belongs to a group of materials termed magnesia products. In the past, magnesia products have been essentially used for refractory applications and more recently in effluent treatment [24]. Over the last five years there has been a growing interest in magnesium hydroxide as a flame retardant for plastics [25].

2.1.1 Flame retardant effects of $\text{Mg}(\text{OH})_2$

Until recently the market for hydrated mineral as flame retardant fillers has been dominated by one material, aluminium hydroxide (alumina trihydrate, ATH) [16]. Like ATH, magnesium hydroxide decomposes endothermically to release water of hydration which contributes to its flame retarding action [22,25,26]. On decomposition, the

thermogravimetric weight loss of water between 350 and 500°C, for a series of $\text{Mg}(\text{OH})_2$ variants, was shown to be between 26 and 28% [27]. The theoretical weight loss of magnesium hydroxide to yield magnesium oxide and water is 30.9% [22]. Magnesium hydroxide can therefore be incorporated into most thermoplastics without premature decomposition during melt processing [28,29].

Magnesium hydroxide is thought to exert its flame retardant properties through a combination of factors [15,28]. Initially the endothermic decomposition commencing at 350°C withdraws heat from the substrate and retards the rate of thermal degradation. The accompanying release of inert gases (water vapour) on thermal breakdown dilutes the fuel supply present in the gas phase. The heat capacities and their decomposition products further reduce the thermal energy available to degrade the substrate. The decomposition products may better insulate the substrate from the heat source, through the promotion of char formation. Also, the high filler content necessary to attain an adequate level of fire retardancy in polypropylene, acts as a solid phase diluent. The decomposition process is thought to occur in two stages [16]. The first stage comprises conversion to a high surface area, disordered magnesium oxide lattice. The surface area of this material is still heavily hydrated. Only at temperatures well above 500°C does this lattice rearrange to a more stable phase by the loss of surface area and by water sintering. This second step comprises about 15% of the overall endotherm and water loss but may not contribute to the fire retarding effect.

Although magnesium hydroxide has advantages over halogenated flame retardant additives, due to its non-toxicity, filler levels of 50 to 60% are required to produce flame retardant properties when incorporated into polymer matrices [26,30]. However this new particulate filler advantageously affects some mechanical properties and flammability because of the wide range of morphologies available [31]. Due to the low surface energy of polyolefins into which it is commonly compounded, magnesium hydroxide is often surface treated to aid dispersion and compatibility.

2.1.2 Morphology of magnesium hydroxide

According to Rothon [16], there are 3 principal forms of magnesium hydroxide that can be produced, which are either synthetic or natural in origin. Synthetic crystals can be small or large in size. Small synthetic crystals are less than 1 micron in size. These can aggregate tightly into polycrystalline particles, of typical size 1 to 10 microns. This form, the easiest to produce, is obtained by reacting a base with a magnesium salt solution. The large synthetic crystals range in size from 0.5 to 5 microns. Although more difficult and expensive to produce, the crystals are considered to be more perfect. Aggregation of crystals is reduced and the final particle size is not too indifferent from the crystal size. Finally there are natural forms of $\text{Mg}(\text{OH})_2$, existing within the mineral 'brucite'. For use in plastics these come as a white powder made of hexagonal shapes [32], the purity depending on the nature of the deposit.

Hornsby [22] claims that the production method of magnesium hydroxide will define its structure. This in turn will influence the crystallite size, particle surface area and chemical composition of the final product. The morphology of particles may also vary. Small hexagonal crystals may agglomerate to form near spherical configurations or alternatively high aspect ratio platelets may be formed. Under special conditions, fibrous magnesium hydroxide can be produced. Current particle sizes and surface areas of magnesium hydroxide employed in polymers reach a maximum of 8 microns and 20 m^2/g respectively.

2.1.3 Production of magnesium hydroxide

Magnesium hydroxide is probably the second most widely used flame retardant filler but is currently more expensive to produce than ATH. Unlike aluminium hydroxide (Bayer process), there is no dominant large scale production process. There are 4 different techniques employed commercially for the large scale production of magnesium hydroxide, two of which are a variation of the same theme. Three of these methods produce the synthetic types while the other produces the natural form. The principle of each is detailed below.

2.1.3.1 Sea water method

This method was first used in 1937 [24] and is now operated world-wide. The magnesium hydroxide obtained by the sea water method is actually a precursor encountered during the manufacture of magnesia (magnesium oxide).

In the process [15,28,33], magnesium salts in sea water react with calcium hydroxide obtained from 'limes'. The sea water is decarbonated and desulphonated with sulphuric acid and clarified to remove any solids prior to reaction. Limes used in magnesium hydroxide production are slurried lime (dolomite) and dolime (calcined dolomite). These are calcined and subsequently hydrated before being introduced to the treated sea water. The magnesium hydroxide precipitate settles and is allowed to thicken, which can be aided by seeding.

This magnesium hydroxide intermediate is of unsuitable morphology for general use as a flame retardant filler. $\text{Mg}(\text{OH})_2$ precipitates as high surface area crystals which are difficult to wash, unless induced to agglomerate. The morphology can be improved however by hydrothermal recrystallisation of the primary precipitates and controlled hydration of magnesium oxide [34].

2.1.3.2 Brines method

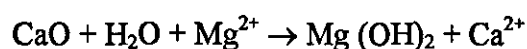
Because of the low content of magnesium in seawater, it is necessary to produce large quantities of it which causes the fixed costs and operating costs to be high. In addition, it is necessary to have available high purity dolomite and limestone. Sources richer in magnesium are the residual brines from seawater desalination and sodium chloride plants [35]. Brines can also be pumped from the surface of the earth from deposits ranging from 1000 to several thousand feet below the surface.

Production of magnesium hydroxide involves precipitation of magnesium ions from solution of magnesium salts by the use of strong bases such as sodium hydroxide (NaOH) and calcium hydroxide ($\text{Ca}(\text{OH})_2$). Although calcium hydroxide is more

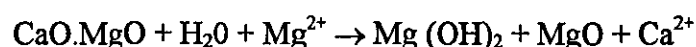
common, sodium hydroxide is used if a product low in calcium oxide is desired. It is produced using calcined limestone (lime) or calcined dolomite (dolime). Lime is produced through the calcination of limestone in rotary kilns. It is then reacted with water to yield calcium hydroxide.

When using dolime only 50% of the quantity of brine water is required as compared to the same process when using lime.

When using lime



When using dolime



The resulting precipitation stage is in the form of a slurry of magnesium hydroxide with calcium chloride present. This slurry is thickened and filtered to remove the calcium chloride [36]. However, the high sulphate ion concentration (in the presence of calcium hydroxide) causes the precipitation of calcium sulphate and magnesium hydroxide. The separation of both products is difficult and expensive. High quality $\text{Mg}(\text{OH})_2$ can be produced if the ammoniation of brines is utilised. Here, the brine from sodium chloride plants is concentrated to a 1.31 specific gravity and then mixed with ammonia. The magnesium hydroxide formed is separated from the liquor by filtration, washed with water and dried [35].

2.1.3.3 Raw mineral method

This method was devised by Veitscher Magnesitwerke AG Company [37]. This process leads to a high purity magnesium hydroxide providing a regular crystal lattice with low surface energy, minimising agglomeration. This special magnesium hydroxide was introduced into the market in 1989 under the brand name Magnifin™. For the first time $\text{Mg}(\text{OH})_2$ was used in flame retardancy rather than pharmaceutical applications as was usually the case for seawater based grades.

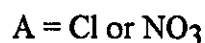
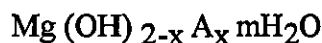
The mineral raw material, containing magnesium silicate, is leached by circulating HCl using a specially controlled two step precipitation process to separate any impurities. This leaves a pure magnesium chloride liquor which undergoes thermal decomposition to magnesium oxide. At this stage the circulating HCl is removed. The magnesium oxide is then rehydrated and the magnesium hydroxide produced undergoes controlled recrystallization.

The very regular hexagonal platelet particles produced have a median particle size of about 1 micron. This magnesium hydroxide has a purity of 99.8%, the highest impurity level being oxides [38]. Magnifin is currently available in 12 different grades, half of which are suitable for polypropylene formulations.

2.1.3.4 Kyowa method

In 1979, the Kyowa Chemical Industry Company Ltd. filed a patent [39] which defined the production route of a new type of magnesium hydroxide. It stated that the traditional materials crystals had a high polarity inducing strains and the crystallites were relatively small and produced a high specific surface area. This caused secondary aggregation with water particles 10 to 100 microns in size.

This new magnesium hydroxide was prepared by hydrothermal treatment (in an aqueous medium at an elevated temperature) of a novel magnesium chloride or nitrate, according to the following formula:



$$x > 0 \text{ but } x < 0.2$$

$$m = 0 \text{ to } 6$$

This basic magnesium chloride (or nitrate) can be formed by reacting magnesium chloride (or nitrate) with an alkaline substance in an aqueous media. The amount of alkaline substance is controlled with respect to the magnesium salt used. Also, the hydroxyl ion ratio of the alkaline substance to the magnesium ion ratio remains at a predetermined value. The reaction is best carried out between 10 and 20°C. The novel magnesium chloride (or nitrate) is hydrothermally treated, at a preferred pressure of at least 5kg/cm² and a temperature of 200°C.

As compared with conventional magnesium hydroxides, this new structure will have a small strain in the 101 direction, a large crystallite size in the same direction and a very low specific surface area. Because of these structural characteristics, the surface polarity of the crystallites is extremely small, and the secondary aggregation of the crystallites does not occur. The novel magnesium hydroxide crystals produced have a crystallite size of at least 80nm in the 101 direction and a specific surface area of less than 20m²/g.

2.2 Effects of Mineral Fillers on Polymer Properties

Mineral filled polymers are one type of composite polymeric materials. The properties of the base polymer can be modified by the incorporation of discontinuous filler particles into the continuous polymer matrix. There are over 2000 minerals recognised as valid fillers but only a fraction are utilised.

Fillers were traditionally used to reduce the price of the final polymeric product [40] whereas properties are now tailored by use of the correct filler selection. Effective filler

incorporation is a complex process and cannot be limited to alterations in one property at a time. Property modification however is dependent on filler dispersion within the matrix, as this will influence the system's rheology [41]. However, often certain properties can be grouped together because of their similarity of influence. Filled polymer systems are practically isotropic, if the geometry of the filler particles is isotropic too, or if no orientation of anisotropic fillers occurs during processing [42].

Conventionally fillers are divided into reinforcing, active and inert, depending on their particle size [43,44]. Fillers have also been classified in terms of their chemical composition [13]. However, it has been reported that fillers must be classified in terms of their primary properties [45]. These can be seen below:

- a) Particle shape,
- b) Particle size distribution,
- c) Surface area,
- d) Particle packing,
- e) Chemical composition.

The main effect of adding rigid filler particles to a polymer matrix is to cause an increase in the elastic modulus in proportion to the filler loading. Other properties that may be favourable are increased hardness and reduced mould shrinkage. However, certain other useful properties such as toughness, extension at break and tensile strength may show a decline.

Fillers can strongly affect the crystallisation of polymers in both primary nucleation and growth steps [46]. This nucleation effect will influence the size and distribution of the crystalline phase and modify the matrix morphology, which will effect the final mechanical properties of the composite.

Surface tension, hence wettability has been shown to significantly influence the properties of filled composites [47]. This can influence the agglomeration of filler particles within a polymer matrix. Agglomeration or variable dispersion of filler

particles will affect mechanical strength of a composite and may lead to void formation.

Finally, the coefficients of thermal expansion of mineral fillers and polymers differ considerably. This can lead to the formation of stress concentrations around the filler particles as the composite cools from the melt [48]. This will result in residual stresses being formed in the moulding and may cause premature failure.

2.2.1 Filler particle size and morphology

Filler particles can be defined by their particle size [43]:

Active (reinforcing), 0.01 to 0.1 microns

Semi-active, 0.1 to 1 microns,

Inactive, 1 to 50 microns,

Impairing, 50 to 100 microns.

Active fillers are used to improve the properties (primarily mechanical), whereas inactive fillers are used to reduce the cost of the product while retaining the basic characteristics of the material. In reality, this relationship is more complex.

Filler particles are rarely symmetrical in shape. To overcome this problem, particles can be characterised in terms of three diameters:

- a) Equivalent sphere diameter (most common),
- b) Equivalent circle diameter,
- c) Statistical diameter.

The description of particle size distribution (PSD) can be represented by cumulative or frequency distribution. Cumulative distribution is useful for numerical information whereas frequency distribution is most useful for mass or volumetric information.

Measurement of particle size distribution can be performed by several methods [49]. The principles can be outlined below.

<i>Method</i>	<i>Principle</i>	<i>Size Range</i>	<i>Distribution</i>
Sieve Analysis	Amount retained by each sieve shows PSD.	5-4000 μm	By mass.
Sedimentation	Concentration change shows PSD	0.01-100 μm	By mass or area.
Coulter Principle	Output from non-conducting particles.	0.3-1000 μm	By number.
Light Scattering	Laser diffraction of dilute solution.	0.1-2000 μm	By volume.
Microscopy	Inspection using optical or electron microscope.	0.001-150 μm	By number.

When filler particles are added to a polymer matrix, the volume occupied by an individual particle (V_i) has been based upon a simple model [50]:

$$V_i = \sum V_e V_f \quad (2.1)$$

where,

V_e is the volume of material in which these particles are contained,

V_f is the volume fraction of filler.

When the point is reached where each filler particle is in contact with its neighbour, critical packing concentration (V_{fc}) is reached where:

$$V_{fc} = V_e / V_o \quad (2.2)$$

where,

V_e is the total volume occupied by filler particles,

V_0 is the total volume of the filled polymer.

An additional component of V_0 may occur if the particles do not fill all of the interstitial free spaces.

Hard uniform spheres can be ideally packed into four regular geometric arrangements, these being cubic, orthorhombic, tetragonal and rhombohedral. Depending on filler geometry and free volume changes, fillers could pack in these arrangements. In reality, a single geometry does not exist but a few packing geometries coexist [13]. A good example of the maximum packing fraction attainable by a range of morphologically different fillers is provided by Bigg [51].

At the maximum packing fraction, the voidless composite attains its maximum modulus and viscosity. When a composite is formulated below its maximum packing fraction, flow is obtained. Almost all compounds are formulated well below the maximum packing fraction of their discontinuous filler content [52].

In a polymeric matrix, the filler particles are always more or less agglomerated. Microscopic studies have shown that two types of primary structures can exist. These are filler aggregates, filler particles bound firmly together, and agglomerates, systems of weakly bound aggregates [44]. Neilson [53] however, believed that an agglomerate is like a body of contacting primary particles. Assuming that the agglomerates behave like hard particles below a low stress threshold, high stresses should cause the particles constituting an agglomerate to move relative to each other.

It is known that platy fillers have a tendency to align in the direction of flow when in the melt state [54,55], therefore the composite has a certain degree of anisotropy. Jancar proposed the agglomerate theory for unidirectional aligned microfibrillar magnesium hydroxide/PP composites [56]. An assumption is made so that each microfibrillar particle can be represented by a circle of area fraction equal to the volume fraction V_f . The surface is immobilised by an interlayer of PP, thus creating space packing, the cross section being divided into hexagons. A two particle

agglomerate is formed when two hexagons adjoin each other. From this it can be deduced that the concentration of non agglomerated particles, V_{f1} , is:

$$V_{f1} = (V_f - V_{fA}) \div (1 - Q_{A2}) \quad (2.3)$$

where,

V_{fA} is the concentration of agglomerates in the cross section,

Q_{A2} is the area fraction occupied by all agglomerates.

The immobilised layer of PP on the fibrous surface was considered to act as a 'bonding agent' for the agglomerates. Each agglomerate is characterised by its elastic modulus and aspect ratio. The agglomerates will possess different physical and geometrical properties to magnesium hydroxide single, non-fibrous particles.

2.2.2 Composite modulus

There is a large body of literature discussing the mechanical property behaviour of filled polymers. Composite modulus is the easiest to model, because it is a bulk property and depends primarily on the geometry, modulus, particle size distribution and concentration of filler. Models used frequently for predicting the modulus of filled polymers can be seen below in Table 2.1 [51]. E_R is the relative modulus, V_f is the volume fraction of filler, G_f is the shear modulus of filler, G_p is the shear modulus of polymer, ν is Poisson's ratio of polymer and V_{fm} is the maximum packing fraction of filler.

Einstein's equation describes experimental data for low filler concentrations, but can be modified to include aspect ratio [13]. Guth's equation is a further modification to account for interparticle interaction at higher filler concentrations. Thomas's equation is an empirical one, based on monodispersive particles. Quemada used a variable coefficient to account for particle geometry and interparticle interactions [51].

Table 2.1 Some models predicting composite modulus [51]

MODEL	EQUATION
Einstein (2.4)	$E_R = 1 + 2.5 V_f$
Guth (2.5)	$E_R = 1 + 2.5 V_f + B V_f^2$ B usually equals 14.1
Mooney (2.6)	$E_R = \exp \left[\frac{K}{1 - \left(\frac{V_f}{V_{fm}} \right)} \right]$ K usually equals 14.1
Kerner (2.7)	$E_R = \frac{G_f V_f \div [(7-5\nu)G_p + (8-10\nu)G_f] + V_f \div [15(1-\nu)]}{G_p V_f \div [(7-5\nu)G_p + (8-10\nu)G_f] + V_f \div [15(1-\nu)]}$
Thomas (2.8)	$E_R = 1 + 2.5 V_f + 10.05 V_f^2 + 0.00273 \exp [16.6 V_f]$
Frankle-Acrivos (2.9)	$E_R = 1 + \frac{9}{8} \frac{\left(\frac{V_f}{V_{fm}} \right)^{\frac{1}{3}}}{1 - \left(\frac{V_f}{V_{fm}} \right)^{\frac{1}{3}}}$
Quemada (2.10)	$E_R = \frac{1}{(1 - 0.5KV_f)^2}$ K usually equals 2.5
Neilson (2.11)	$E_R = \frac{1 + AV_f}{1 - \psi V_f}$ $\psi = 1 + \left(\frac{1 - V_{fm}}{(V_{fm})^2} \right) V_f$ A = f(geometry), 1 for spheres

Mooney, Frankle and Acrivos developed this concept by introducing the concept of maximum packing fraction [51]. Kerner's equation is one of the most frequently used

models to predict experimental data [13]. However, Neilson modified the Kerner equation to take into account the maximum packing fraction, interparticle interactions and the relative modulus of the two constituents [51]. Other equations based upon Kerner's are the Chow, Counto and Cox models [13]. Only the Sato-Furwaka model exists for the analysis of the dependence of elastic moduli on the strength of interfacial adhesion [56]. Unfortunately, this model was derived for the case of reinforced rubbers, and cannot be applied to filled thermoplastics.

The modulus of fillers is typically ten to one hundred times larger than that of the base polymer. If mathematical models are to be utilised, knowledge of the bulk modulus must be known. As these values cannot be directly measured, they can be estimated considering the relation between elastic modulus and hardness of the material. Typical bulk modulus values for differing filler morphologies are shown below [57].

Filler	Young's Modulus (GPa)	Shear Modulus (GPa)	Morphology	Aspect Ratio
Mg(OH) ₂	64	25	Hexagonal	5
Mg(OH) ₂	64	25	Needle	25
CaCO ₃	72	28	Irregular	1

Jancar [58] found that the application of the Tsai equation was adequate for modelling PP/Mg(OH)₂ composites filled with randomly orientated hexagonal plate and microneedle particles. The Tsai equation can be seen below.

$$M = \frac{3}{8} M_L + \frac{5}{8} M_T \quad (2.12)$$

where, M is overall composite modulus and M_L and M_T are parallel and perpendicular values of elastic moduli.

A good relationship between experimental and theoretical results was observed. Discrepancies occurred due to two reasons. Firstly, void formation was detected, and

was attributed to the great extent of matrix immobilisation at the interlayer. Secondly, creation of clusters of filler particles accounted for the matrix volume insufficiency in the bulk (determined by density measurements). The average aspect ratio of particles decreased with filler volume, particularly needles, and was caused by mechanical destruction. Reinforcement was most predominant for needles, but was less apparent for volume fractions above 0.3.

Jancar also utilised the Halpin-Tsai equation for similar composites which purposely had their filler particles unidirectionally aligned upon moulding, to compare their longitudinal and transverse modulus values. The Halpin-Tsai equation can be seen below:

$$\frac{M_c^{LT}}{M_m} = \frac{1 + A_{LT}B_{LT}V_f}{1 - B_{LT}V_f} \quad (2.13)$$

where A and B are constants dependent on the particle's shape and elastic modulus nature and V_f is filler volume fraction. M_m and M_c are the matrix and composite moduli respectively. L and T refer whether the model is applied in the parallel or perpendicular direction to flow.

In these findings, platey particles were shown to have a lower orientability due to their superposition of flow field and particle shape. Therefore, little difference between modulus in the longitudinal and transverse directions was observed. For microneedle particles, this was not the case. In the transverse direction, the modulus increased with filler volume fraction. However in the longitudinal direction, modulus yielded a sharp increase around $V_f = 0.12$. This again was attributed to a reduction in the aspect ratio of filler particles caused by mechanical destruction.

The simple Tsai equation proved adequate for modelling the elastic modulus of randomly orientated compounds, whereas the Halpin modification was required when orientation was involved.

Jancar [56] also utilised the above equations for PP/Mg(OH)₂ composites of similar nature, but with enhanced adhesion between the polymer/filler interface. This was achieved by grafting polypropylene with maleic anhydride. Maleated polypropylene influenced both the filler/matrix interface and bulk matrix due to the interactions of carboxyl groups with base centres on the surface or on impurities in the matrix bulk. The greater extent of immobilised PP on the filler surface caused the creation of a particles hyperstructure and hence higher modulus at a lower magnesium hydroxide content than in systems with no interfacial adhesion.

Jancar [57], further modified the Halpin-Tsai equation for agglomerated particles, by making assumptions, derived from previous work [56,58]. These were that a magnesium hydroxide agglomerate has a constant value of elastic modulus, independent of the number of agglomerated particles. The value of 7MPa was obtained by extrapolation of the experimental composite modulus from the maximum volume fraction down through a low filler volume fraction. To find the concentration dependence of the elastic modulus of a composite with unidirectional aligned microfibrillar filler, constants A^{eff} and B^{eff} have been substituted into the Halpin-Tsai equation:

$$\frac{E_c}{E_m} = \frac{(1 + A^{\text{eff}} B^{\text{eff}} V_f)}{(1 - B^{\text{eff}} V_f)} \quad (2.14)$$

where A^{eff} is an estimate of the mechanically reduced aspect ratio and B^{eff} is dependent on the effective 'agglomerate' filler modulus, E^{eff} .

Qualitative agreement was found between theory and data describing the concentration dependence of the elastic modulus accounting for unidirectionally aligned fibres. A steep increase in modulus occurred at a critical volume fraction of 0.2. Here it was assumed that the origins of filler agglomeration begin.

2.2.3 Composite Tensile Strength

The tensile strength of a filled polymer is more difficult to predict. The tensile strength depends in a complex way on the microstructure (including interfacial microstructure), since the load transfer between phases and also the stress concentration is determined by structural factors. These being shape, size distribution and spatial distribution of the filler along with the thickness of the interface [59].

Two general tensile strength-filler concentration responses are possible [51], these being the lower and upper bound responses. The lower bound response assumes weak or no adhesion and the total load is carried by the matrix [59]. The lower bound response, derived by Nicolais, can be seen below [51]:

$$\sigma_c = \sigma_p (1 - aV_f^b) \quad (2.15)$$

where,

σ_c is the tensile strength of the filled composite,

σ_p is the tensile strength of the polymer,

a is a constant related to stress concentrations,

V_f is volume fraction,

b is a constant related to filler geometry.

The upper bound response assumes strong polymer/filler adhesion. This is more difficult to predict as some degree of reinforcement is implied, and flakey fillers with low aspect ratio provide limited reinforcement. Two forms of the upper bound response exist [51].

The first, derived by Leidner and Woodhams indicated a linear strength response to filler concentration and did not imply an upper bound response with a maximum.

The alternative representation accounts for the filler reinforcement by improved polymer/filler adhesion, and the competing loss in strength due to stress concentrators. This empirical formula is an extension of the lower bound formula, and is given below.

$$\sigma_c = \sigma_p (1 - aV_f^b + cV_f^d) \quad (2.16)$$

With four constants (V_f is filler volume fraction), it is flexible enough to match a wide range of data. However, because it does not have a theoretical basis, it cannot be used to predict the performance of untested composites. Determination of the constants will give evidence of the degree of adhesion. The values c and d should be strong indicators of polymer/filler adhesion, whereas a and b should not be too dissimilar to the lower bound case [51].

Turcsanyi [59,60] furthered this approach to determine a one parameter equation for tensile yield strength. He stated that the composite strength will be dependent on the minimum value of matrix area in the cross section perpendicular to the load direction. This will be influenced by filler packing, hence filler particle shape and distribution. The equation can be seen below.

$$\sigma_{yc} = \frac{1 - V_f}{1 + 2.5V_f} \sigma_{ym} \exp(BV_f) \quad (2.17)$$

where,

σ_{ym} is the matrix yield stress

V_f is filler volume fraction

B is a semi-empirical integral.

Parameter B accounts for interfacial interactions, filler specific area and properties of both the immobilised layer and unfilled matrix.

Other similar models, involving power laws, have been built to predict the strength of particulate composites derived by Neilson, Nicolais-Narkson, Landon and Leidner-Woodhams [13].

Jancar [61] utilised the equation derived by Turcsanyi, but found for $\text{Mg}(\text{OH})_2/\text{PP}$ composites, that an acceptable agreement between calculated and experimental data was only valid at low filler concentrations. Introduction of the relative yield stress, Q ,

$$Q = \frac{\sigma_{yc}}{\sigma_{ym}} \left[\frac{(1 - 2.5V_f)}{(1 - V_f)} \right] \quad (2.18)$$

where,

σ_{yc} is the composite yield stress,

σ_{ym} is the matrix yield stress.

made it possible to calculate the integral interaction parameter, B . It was found that B was higher for needle type as opposed to platey particles, indicating that filler shape is influential on composite yield strength.

The anisometric shape and size of magnesium hydroxide particles caused a steep drop in the yield strength above a filler volume fraction of 0.25 and a ductile to quasi-brittle transition occurred. Above this critical volume fraction, stress concentration near the filler particles is greater than in the matrix and microelastic deformation occurs. In PP, it was pseudocrazing which accounted for the location of matrix strain and quick spread of the main crack.

Jancar also found that filler surface treatment facilitated better dispersion but the tensile yield strength is reduced due to the lower thermodynamic work of adhesion. This reduced the immobilised layer of PP on the filler surface.

For greater load transfer across an interface, it has been suggested that chemical bonding between the filler and matrix is necessary. Although a full understanding of

this mechanism still unknown, Jancar [62] has proposed a mechanism for maleated PP (MPP) filled with different morphologies of magnesium hydroxide. Maleated polypropylene molecules chemically bond onto the fillers surface due to the acid-base interaction between the hydroxyl (OH) group from the filler surface and the carboxyl group (COOH) grafted onto PP by maleation.

At a constant filler volume fraction of 0.18, yield stress increased steeply to a concentration of 0.162% COOH and composites failed in a ductile manner. Above 0.162%, a slow increase in yield stress was observed and composites failed in a quasi-brittle manner. At this critical carboxyl coating level, either 100% of the filler sites were covered with MPP or the interfacial strength of adhesion was greater than the matrix yield stress before failure occurred.

A non monotonic dependence of yield stress on maleic anhydride concentration was observed for PP/Mg(OH)₂ needle type compositions at room temperature. This could be explained in terms of particle shape and orientation. For platelet type Mg(OH)₂/PP compositions, a clear transition filler volume fraction was observed. The integral interaction parameter, B, was found to increase as a function of carboxyl content, hence interfacial adhesion.

The Leidner-Woodhams model was applied to composites to calculate the interfacial strength of adhesion as a function of concentration of maleic anhydride content. A good qualitative agreement with SEM micrographs was observed.

The TBT equation [59,60] was also applied to CaCO₃/PP composites where the effective interlayer thickness and yield stress of immobilised PP were calculated.

The effects of filler volume fraction and strength of adhesion on the mode of tensile failure of particulate reinforced polypropylene have been studied by Jancar [63] using finite element simulation (FES). The model was applied to CaCO₃/PP composites. A particle size of 10 microns was assumed (experimentally, 97% of particles were smaller than this value). The properties of calcium carbonate filled homopolymer were

measured over a wide range of filler volume fractions. For the model to work, two cases were assumed. The first was zero adhesion, and this was represented experimentally by treating the filler surface with 0.8% stearic acid. Secondly, perfect adhesion was represented by grafting maleic anhydride with PP [62].

A good agreement was found between experimental data and those calculated using the proposed model. The model described the upper bound of tensile strength satisfactorily. When there is no adhesion between constituents, a modified version of the Nicholais-Narkis equation adequately described the lower bound of the tensile strength of the material.

For the case of stearic acid treated filler, the failure mechanism was primarily by microcavitation and crazing. Slightly higher values of tensile yield strength compared to the experimental prediction were probably caused by the polydispersive size distribution and irregular shape of the filler particles.

In the case of the maleated PP, at volume fractions above 0.35, a brittle failure mechanism dominated. For filler volume below 0.2, yielding of the composite by combined microcavitation and shear deformation was the principal deformation. At intermediate filler volumes, both failure modes were seen.

2.2.4 Composite toughness

Current impact tests used on thermoplastic profiles are well documented [64]. Impact properties of mineral filled polypropylene are thought to be primarily governed by particle size, distribution, shape, surface structure and content of its particulate filler [65]. Inclusions within a matrix, such as voids, particles, fibres, notches, cracks and even crystallites can all act as stress concentrators [45]. However, according to Bigg [51], there are no viable theoretical relationships between filler characteristics and concentration that can be used to predict the impact strength of filled polymers.

Currently, there are two proposed mechanisms for toughening of polymer matrices. The first mechanism [66] occurs in a system where rubber particles, a few microns or less, are dispersed in a rigid matrix. With this mechanism of rubber toughening, impact energy is absorbed by crazing and shear yielding in the glassy phase, both of which are induced by the rubber inclusions. Unfortunately, the modulus is reduced as a consequence. The second mechanism occurs within particulate composites comprised of a ductile matrix and dispersed brittle particles. Here the fracture energy in a particulate composite may be expected to rise over an unfilled polymer due to the dispersed particles making the crack propagation path longer. The fillers themselves will absorb a portion of the energy and enhance plastic deformation of the polymer. This mechanism is termed the 'cold drawing concept'.

According to Hornsby [67], the degree of interfacial adhesion at the polymer/filler interface has a direct bearing on the composite to resist crack propagation, hence its impact behaviour. If the filler/matrix interface is extremely strong, the failure pathway is confined to the matrix. When the strength of the interface is equal to the matrix, the crack will propagate along the interface. If filler cohesion is weak, such as in an agglomerate, the crack will pass through the particle.

Suetsuga [68] correlated the state of dispersion in filled polypropylene with the failure mechanisms from falling weight impact tests. Notched Izod impact strength was found to be constant, regardless of the state of dispersion. Failure was initiated near the notch, which was the greatest stress concentrator. The existence of agglomerates, did not affect initiation and propagation of the crack within the range of agglomeration studied. However, the state of dispersion had a pronounced effect in falling weight impact tests. Unfilled polypropylene and poorly dispersed composites always exhibited brittle fracture. Highly dispersed compounds tended to fail in a ductile fashion and enhanced impact properties without lowering the modulus. Failure in the falling weight impact test initiated at agglomerates which were roughly greater than 10 microns. Large sample deviation, often observed in the falling weight impact tests, were caused by the change in distance between the dart head collision point and the failure initiation point where the agglomerate existed.

Factors affecting the impact properties of mineral filled polypropylene were determined by Riley [69]. Of these factors, the particle size was of greatest importance. Large particles (or aggregates of small ones) acted as flaws from which cracks could initiate. Stress analysis indicated that high aspect ratio fillers had the largest stress concentration in the region of their sharp edges. He suggested that the situation would be worsened if the sharp edges had the inclination to nucleate crystal growth in the polymer. Low aspect fillers will act as crack blockers, and the coalescence of a crack with such a particle will result in the lowering of stress. Again, the dispersion of the filler in the matrix will be important in determining this mechanism.

Hutley [70,71], found that the falling weight impact strength (FWIS) for a series of highly filled polypropylene compounds produced discrepancies. Limited differential scanning calorimetry (DSC) analysis revealed a correlation between onset temperature of the polypropylene recrystallisation and the FWIS. Generally, it was found that a polypropylene matrix with a low impact strength crystallised at high temperature (and vice versa).

Varying the particle size and distribution of the limestone filler produced a change in FWIS and affected the failure mechanism. Generally, the coarser particles produced the greater reduction in impact strength. It appeared that a change in filler variables affected the FWIS of the composite by enhancing the rate of PP crystallisation, changing the matrix morphology. Hence, materials with a brittle mode of failure (low impact strength) would be expected to have a higher nucleation density.

Work on $\text{Mg}(\text{OH})_2/\text{PP}$ composites revealed that the notch impact strength was at its maximum when the filler loading level was 30% by weight [29]. This was 2.4 times that of the base polymer. At 60% loading (required for flame retardancy), the impact strength dropped below that of the base polymer. Although no explanation of the fracture mechanics was given, it was found that superior impact strength was obtained for magnesium hydroxide fillers with a low surface area. This was attributed to the fillers having a larger crystallite size (up to 2 microns) and a lower degree of agglomeration.

2.2.5 Filler dispersion

Many authors have stated that good filler dispersion yields optimal mechanical properties of particulate filled thermoplastics [61,72,73,74]. Filler dispersion is not to be confused with distribution. Good distribution involves the progressive reduction in size of particle domains to attain a random distribution throughout the polymer. Good dispersion involves the rupture of agglomerates of solid particles, within a domain, into smaller fragments. Practically, it is possible with melt mixing to achieve both of these.

Wypych [13] defined the most important criterion for fillers to agglomerate in terms of a simple equation:

$$T_a = \frac{\sum_i B_i}{\sum_j E_j} \quad (2.19)$$

where,

T_a is the tendency towards adhesion,

B_i are binding forces (Van der Waal's, hydrogen bonding, magnetic etc.)

E_j are environmental forces (gravitational, drag, inertia etc.)

For agglomeration, $T_a > 1$. Agglomeration forces could be measured by determining the tensile strength of compacted fillers. In turn the tensile strength could be determined by the packing density and filler morphology.

Wypych also stated, that incorporation of fillers into polymer matrices by melt mixing can be subdivided into four stages, these being:

Subdivision (breaking up large lumps)

Incorporation (wetting of filler by forcing polymer into the interstitial gaps)

Deagglomeration (breaking down agglomerates)

Distribution (uniform scatter of agglomerates/primary particles in matrix)

Suetsuga [68], determined the state of dispersion in terms of a dispersion index (DI),

$$DI = 1 - V_{fa} \quad (2.20)$$

where,

V_{fa} is the area fraction of agglomerates defined by,

$$V_{fa} = \frac{\pi}{4AV_f} \sum d_i^2 n_i \quad (2.21)$$

where,

A is the area of observation,

V_f is the volume fraction of filler,

d_i is agglomerate diameter,

n_i is number of agglomerates.

The dispersion index varies between 0 (indicating worst dispersion where all filler particles exist in the form of agglomerates) and 1 (where no agglomeration exists).

This model was applied to a series of CaCO_3/PP composites with varying levels of filler agglomeration. Correlation between the state of dispersion and various mechanical properties was obtained. Tensile modulus, yield strength and notched Izod impact strength were found to be independent of the state of dispersion. However, tensile strength and more dramatically falling weight impact strength increased with the improvement of dispersion state.

Suetsuga [75] also used a practical approach to study the effect of filler agglomeration. As the extent to which filler particles can be dispersed is directly related to the rate at which they agglomerate, various grades of calcium carbonate were immersed in organic solvents (the procedure is referred to as the sedimentation volume method).

Agglomeration was found to increase with decreasing particle size. However, surface treatment with stearic acid sharply reduced the tendency of agglomeration.

Dispersion analysis of a particulate filled polymeric system involves direct inspection of the dispersed filler in specially prepared samples. A crude assessment often used industrially is the blown film method. This involves blowing a tubular film of the particulate filled compound and hauling it off at increasing speed. The speed at which the film ruptures is indicative of the tensile strength of the compound, when compared to that of the unfilled polymer. Visual or optical microscopy of the film can be used to assess filler dispersion. However, this method is not a true assessment of filler dispersion since it does not represent the compound in its true bulk state.

The British Standards Institute (BSI) has two methods for the inspection of pigments [76] and carbon blacks [77] respectively, in polyolefin matrices. Samples are prepared by microtoming thin sections of the particulate filled composites and examining by viewing them in transmitted common light. Examples of sections comprised of good, indifferent and bad dispersions are provided, to which the prepared sample can be compared. However, these methods are not quantitative and the qualitative analysis will be operator dependent.

Burke [78] examined the dispersion of titanium dioxide in HDPE and PP using a series of different methods. Sample preparation was identical for each method, whereby a 10 micron section was taken from the centre of injection moulded bars, perpendicular to the flow direction.

One dispersion technique involved the extraction of pigment particles from etched samples, assuming that the pigment extraction was not selective. Samples were viewed using TEM and their dispersion quantified using one of two equations:

$$\text{Number average} = \frac{\sum N_i C_i}{\sum N_i} \quad (2.22)$$

$$\text{Weight average} = \frac{\sum N_i C_i^2}{\sum N_i C_i} \quad (2.23)$$

where,

N_i is the number of agglomerates,

C_i is the number of particles in each agglomerate.

Secondly, samples with filler particles intact were viewed using TEM with an electron dispersive X-ray mapping (EDX) facility. EDX mapping studies replicated the corresponding TEM image of a pigmented sample. This method required less sample preparation than the etching technique and the degree of particle agglomeration could be readily investigated.

Burke found that the etching technique could reveal the detailed morphology of particulate filled polyolefins. From the dispersion analysis methods, it was found that higher number of agglomerates were present in composites loaded with higher filler levels, the deagglomeration being caused by compounding.

Finally, Liauw [79] reviewed filler dispersion techniques and also found that both electrical and dynamic melt properties can be utilised to measure the state of filler dispersion.

2.2.6 Processing

Particulate filled thermoplastics are processed in the melt state by either batch or continuous methods. Batch mixing is advantageous because machinery is versatile and good dispersive mixing is usually achieved. Unfortunately due to the changeover time between adjacent batches, the system is not very efficient. However, continuous mixers are more efficient and can be directly linked to the next stage of processing. Continuous mixers are generally used for large throughputs of material. Examples of batch and continuous mixers can be seen below.

<i>BATCH MIXER</i>	<i>CONTINUOUS MIXER</i>
Internal mixers	Single & twin screw extruders
Two roll mills	Motionless mixers

The most versatile continuous mixer on the market at the moment is the twin screw extruder with its segmented design and self wiping action [80]. The basic design and operation process are well documented [80,81,82]. The trend in the plastics industry towards the incorporation of higher filler levels, especially for flame retardant applications has resulted in manufacturers of compounding machines developing twin screw extruders which have enabled more effective and efficient compounding at higher outputs [81].

According to Dillon [82], there are several factors that influence filler dispersion when melt mixing in a twin screw extruder. These can be seen below:

- Surface chemistry of filler (determines the tendency to form agglomerates),
- Premixing (this reduces segregation if more than one filler is used),
- Viscosity of matrix (influenced by the shear rate),
- Method of addition (influences viscosity, shear rate and temperature),
- Shear rate and residence time (influences filler deagglomeration).

Twin screw extruders are normally starve fed, therefore they only have two primary control variables, these being feed rate and screw speed. Secondary variables are feed, barrel and screw temperature. Step changes that can be selected are length, diameter and design of the screw along with feed and die design. These will influence the process parameters such as torque, material throughput, melt temperature, residence time and most importantly the state of mixing [80]. When the above variables have been correctly selected and the mixing process is running efficiently, the operating window is said to be established.

Hornsby [83] documented the flow characteristics of polypropylene in a co-rotating intermeshing twin screw. He stated that the geometry of the intermeshing zone is of

fundamental importance to the mixing characteristics of a co-rotating twin screw extruder. Here, a positive pump displacement is achieved where the melt is transferred by interchannel flow (the major route for material transfer). If the screw is tapered and the barrel clearance decreases, enhanced shear 'micromixing' can be attained. Cross channel flow also occurs and is caused by variation in melt viscosities, generating material turbulence and complex flow patterns across the screw. A screw design has been developed for use with highly filled particulate compounds for use in a co-rotating intermeshing twin screw extruder [81].

Rheological studies by Hornsby [84] were performed on highly filled $\text{Mg}(\text{OH})_2/\text{PP}$ compounds (containing magnesium hydroxide of different grades) in order to predict their ease of processing. It was found that the presence of magnesium hydroxide caused a significant increase in the shear viscosity of polypropylene relative to unfilled material. This effect was less pronounced at low shear rates. Lower viscosities were also achieved for smaller particle sizes of magnesium hydroxide and it was assumed that crystallite size and morphology controlled the rheological changes.

2.3 Effect of Filler Modification

The addition of inorganic materials in the form of minerals offers both benefits and disadvantages to polymer systems. It is known [41] that difficulties in dispersion, wetting and stability occur when using minerals with a high polar nature and high surface area. Poor dispersion leads to the production of non homogeneous products. Poor wet-out and bonding encourages attack by moisture and reduces physical properties. The addition of fillers often results in a loss of strength. This is because under deformation, the resin is more elastic than the filler which causes debonding and void formation [85]. Highly filled compounds also suffer high viscosity and flow problems. The correct selection of a filler surface treatment can often eliminate some of these problems.

Fillers may be coated by a range of different methods, but the four most common methods [86] are detailed below.

<i>Method</i>	<i>Technique</i>	<i>Comment</i>
Dry blend.	Coating agent is sprayed into a well agitated filler.	No solvent or diluents required.
Slurry.	Filler is dispersed in water and the coating agent is added to the agitated slurry.	Ideal for fillers produced in slurry form. Requires water removal.
Integral blend.	Undiluted coating agent added directly to polymer just prior to filler.	Cheap but may limit mixing with the polymer.
Spray.	Solution of coating agent is added to the hot filler, discharged from a furnace.	Filler is dry after surface treatment. Temperature of oven is about 100°C.

Other small scale methods employed for filler surface treatment methods are variations on solvent extraction, such as solvent refluxing.

Sometimes fillers undergo a further stage called after treatment or heat set. Reasons for after treatment are to bind the coating (often silane) more completely to the filler surface, while driving off solvents and liberated side products.

2.3.1 Reasons for surface modification

Surface modification is mainly used to optimise the reinforcement of the filler and to improve the dispersion and flow properties. Surface modification is defined as the result of the chemical reaction of an organic compound with a filler, pigment or reinforcement surface, to permanently alter the organophilic nature of the surface [45]. Surface modification occurs either by chemisorption or ionic and covalent bonding or by interfacial molecular entanglement.

The most common reagents used in the plastics industry are coupling and wetting agents. According to Griffiths [73], coupling agents act by modifying the interfacial region between the inorganic mineral filler and the organic polymer to provide bonding between the two. Wetting agents serve to wet out the mineral filler. Low molecular weight coupling agents cannot form a strong bond between PP and fillers. High molecular weight couplants are therefore preferred which create strong bonds with the filler surface and form physical entanglements with the matrix [58]. The most common surface modifiers used are silanes, fatty acids and titanates, whereas zircoaluminates and phosphates (to name a few) are also used.

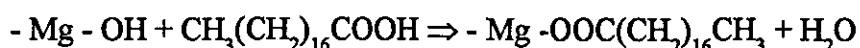
2.3.2 Fatty acid surface modifiers

Fatty acids have the functional group structure RCOOH , where R is a saturated or unsaturated straight chain. Fatty acids and their salts are applied to filler surfaces by dry and wet coating techniques. Surface treatment with these reagents has been found to increase melt flow and improve physical properties of highly filled polyolefins [73].

Stearic acid is the most commonly used fatty acid, it is comprised of 16 straight chain CH_2 segments and is fully saturated. Oleic acid, also used, is of the same chain length but contains a double bond in the centre. Workers [87] investigated the effect of the aliphatic coating's chain length on the mechanical properties of magnesium hydroxide/polyethylene composites. Fatty acids studied were stearic, behenic (C-20) and decanoic acid (C-8). The chemical structure of these four fatty acids above can be seen below.

<i>Fatty Acid</i>	<i>Structure</i>	<i>Total Number of Carbons</i>	<i>Melting Point (°C)</i>
Decanoic	$\text{CH}_3(\text{CH}_2)_8\text{COOH}$	10	31
Stearic	$\text{CH}_3(\text{CH}_2)_{16}\text{COOH}$	18	70
Oleic	$\text{CH}_3(\text{CH}_2)_7\text{CH}=\text{CH}(\text{CH}_2)_7\text{COOH}$	18	4
Behenic	$\text{CH}_3(\text{CH}_2)_{20}\text{COOH}$	22	81

Surface analysis of fatty acid treated magnesium hydroxide is not well published. FTIR DRIFT (diffuse reflectance infra-red) with a sampling depth of several microns has been utilised to characterise fatty acid coated magnesium hydroxide surfaces [88]. Although not surface specific, a very high signal to noise ratio is achievable allowing the effects at about the monolayer thickness to be studied. The reaction with stearic acid was described as:



The reaction was quantified by ratioing the peak area produced by the aliphatic chain to that of the substrate hydroxyl (OH) peak. Any unreacted fatty acid could be detected by observing the carboxyl region (C=O). When the peak CH/OH ratio was reached, it was assumed that this was the amount of stearic acid to cause saturation coverage. The porous grade of magnesium hydroxide required substantially more stearic acid to fully coat its surface when compared to the non porous grade. This was attributed to the larger surface area of the porous filler.

The same workers [88] utilised X-ray photoelectron spectroscopy (XPS) to measure the thickness of the applied surface coating. This method could only sample the surface to a depth of 2-3nm and gave an indication of the level at which monolayer coverage took place.

ESCA (electron spectroscopic chemical analysis) has been used [89] to calculate the monolayer coverage of stearic acid on calcium carbonate. This technique probes on an atomic scale, 2 or 3 atoms below the surface. From this, it was proposed that only one stearic acid molecule was attached to each calcium cation. At monolayer coverage, the stearic acid molecules were said to align themselves vertically to the filler surface.

Some work on stearic acid coated magnesium hydroxide using more standard test methods has been performed [90]. This involved measuring the amount of coating retained after the coating process using CHN analysis and measuring the heat of immersion using calorimetry. With CHN analysis, the amount of stearic acid retained

on the filler surface was compared to that added at the coating stage. The coating is burned off and the amount of carbon released (as carbon dioxide) is compared to the amount of carbon in the acid group (COOH) prior to burning. The amount of stearic acid retained on the filler surface increased with increasing surface coating. With calorimetry, magnesium hydroxide was immersed in heptane, a non polar substance (like polypropylene) and the heat of immersion was measured. Measurements showed that for uncoated and high coating levels, fast temperature changes were experienced. This was due to the totally exposed filler surface and the fact that densely populated filler surfaces with alkyl chains in fixed positions, reached equilibrium quickly. However, at low levels, the temperature change was slow. This may have been due to the alkyl chains reorienting themselves to cover the filler surface to some degree.

2.3.3 Silane surface modifiers

Unlike fatty acids, the variety of silane coating agents (traditionally called coupling agents) are much more diverse. The type of silane is tailored to suit the particular functionality of the filler and/or matrix. A variety of silane coating agents can be seen below [43,74,86].

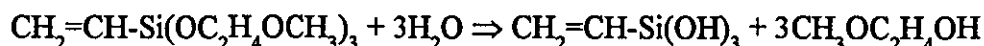
<i>Name</i>	<i>Structure</i>	<i>Comment</i>
Vinyltriethoxy silane	$\text{CH}_2=\text{CHSi}(\text{OC}_2\text{H}_5)_3$	General. Improves dispersion/compatibility.
Amyltriethoxy silane	$\text{CH}_3(\text{CH}_2)_4\text{Si}(\text{OC}_2\text{H}_5)_3$	General. Improves water repellency.
Vinyl-tris (2methoxyethoxy) silane	$\text{CH}_2=\text{CHSi}(\text{OCH}_2\text{CH}_2\text{OCH}_3)_3$	Polyolefins. Improves dispersion/compatibility.
γ -Aminopropyltriethoxy silane	$\text{NH}_2(\text{CH}_2)_3\text{Si}(\text{OC}_2\text{H}_5)_3$	PP, PVC and PC. Thermosets.

When used with thermoplastics, the silane coating agent may react with the filler surface by becoming permanently attached through a primary bond. The reaction of

vinyl-tris (2 methoxy ethoxy) silane (the silane used in this study) with magnesium hydroxide can be represented by a two step mechanism [86].

Step 1.

Initially the silane reacts with water to form a silanol:-



Step 2.

Reaction of the silanol with the filler surface:-



According to Venables [91], silanes have been characterised on traditional filler surfaces by FTIR, radioisotope labelling, inverse gas chromatography (IGC), gel permeation chromatography (GPC) and desorption studies to name a few. However, with vinyl silanes (used in this study), all of the published literature involved the use of FTIR DRIFT analysis.

Porro [92] studied the effect of increasing silane concentration level on a clay substrate. The degree of silanation by the coupling agent was obtained quantitatively by measuring the carbon-hydrogen stretching absorption bands between 2600 and 3200 cm^{-1} . The amount of silane present on the substrate surface could be analysed quantitatively to concentration differences less than 0.1%. The analysis was difficult due to low IR reflections from the coated materials being only slightly higher than for the uncoated substrate.

Further work [93] involved aluminium hydroxide as a substrate for vinyl silanation. The Kubelka-Monk correction was required to compensate for the ordinate reflectance non-linearity induced by the diffuse reflectance process occurring in the range 2600 to

3200cm⁻¹. CH absorption's located at 3060cm⁻¹, were used for quantifying the coatings in terms of a least square fit of overlapping IR peaks at progressive coating levels up to 1.5%. From this a model could be deduced and it was assumed that a model could be applied to any silane treated mineral substrate, such as magnesium hydroxide.

The detectable IR groups from the vinyl silane group -CH=CH₂ are:-

-CH between 2925 and 3100cm⁻¹

=CH between 2850 and 2925cm⁻¹

2.3.4 Surface Tension and Wettability

Mechanical properties of filled polymers depend on the uniformity of filler dispersion in the matrix and the adherence of the filler surfaces to the matrix, which depends upon the fillers wettability. Wypch provides an excellent description of wettability theory [13]. Surface tension and contact angle measurements can be used to quantify filler wettability. The equation defining these parameters can be seen below:

$$\gamma_{SV} = \gamma_{SL} + \gamma_{LV} \cos\theta \quad (2.24)$$

where,

γ_{SV} is the free surface energy of solid or solid/vapour surface tension,

γ_{SL} is the liquid/solid surface tension,

γ_{LV} is the liquid/vapour surface tension,

θ is the contact angle.

When spontaneous wetting occurs, air is displaced and the contact angle is zero. Here, spontaneous spreading occurs which is characterised by the following equation:

$$S_I = \gamma_S - \gamma_{SL} - \gamma_{SV} \quad (2.25)$$

where,

S_i is the initial spreading coefficient,

γ_s is the surface tension before any liquid molecules are adsorbed.

After the monomolecular layer of liquid was adsorbed on the surface of the solid, a further process of surface wetting occurs between the modified surface of solid and liquid, described by:

$$S = \gamma_{SV} - \gamma_{SL} - \gamma_{LV} \quad (2.26)$$

where,

S is the equilibrium spreading coefficient.

The first equation is dependent on the free energy of the solid surface and surface tension of the liquid. The second equation is dependent on the physical and chemical interaction of liquid and solid.

Determination of the critical surface tension for a given liquid is possible by plotting the cosine of the contact angle versus surface tension and extrapolating back to zero. If the critical surface tension of the liquid (or polymer) is lower than that of the solid (filler), wetting will occur. Hence, surface treatment will modify wettability.

Work on stearic acid coated calcium carbonate [47], involved relating surface tension measurements to composite mechanical properties. Here, surface tension was split into a polar (γ_s^P) and dispersive component (γ_s^D), as can be seen below:

$$\gamma_s = \gamma_s^P + \gamma_s^D \quad (2.27)$$

It was found that increased stearic acid treatment not only caused a decrease in surface tension but also caused a decrease in interfacial tension, work of adhesion and wettability. At high coating levels, there was a dramatic drop in the polar component of surface tension, which caused wettability values to become negative. From this finding, it was deduced that wettability values could not be directly related to

composite mechanical properties by an existing model. However, to prove the generality of the established relationships, experiments had also to be carried out on cases of increased interfacial interactions.

Further work [89] on similar composites also showed the surface area decreased with filler coating level, as well as surface tension which could be explained by stearic acid's amphiphilic nature. The addition of 0.25% by weight of stearic acid reduced the surface tension to one quarter of the original value. The minimum value was reached at 0.75 to 1.00% weight level. These values were confirmed by ESCA to be approximately monomolecular coverage. Up to this coating level, the drop in the polar component of surface tension was more prominent than the dispersion component. Above this level, surface tension increased. It was deduced that above the monomolecular level, multimolecular absorption of the stearic acid chains occurs in a tail to tail configuration. The dispersion component increased due to the hydrophilic acid groups (and not the hydrophobic groups) being exposed to the polymer matrix.

2.3.5 $\text{Mg}(\text{OH})_2/\text{PP}$ Interactions

According to Galeski [46], the application of a surface treatment to a filler in PP can produce an increase in toughness of the composite by reducing the brittle to ductile transition temperature. This effect can be explained by various synergistic effects; change in the morphology of polymer interfacial layers, change in the localisation of plastic deformation zones, physical contacts between the surface treated filler and polymer during deformation, improved heat withdrawal during polymer deformation, production of pores instead of cracks and reorientation of anisotropic fillers.

Jancar [62] proposed a mechanism for reactions at the interface of $\text{Mg}(\text{OH})_2/\text{PP}$ composites with different levels of adhesion, perfect adhesion (using maleated PP) and zero adhesion (using stearic acid). With perfect adhesion, the maleated PP molecules were chemically bonded onto the filler surface due to the acid/base reaction between carboxyl groups grafted on maleated PP and hydroxyl groups from the filler surface. The maleated PP molecules are significantly long to create physical entanglements with

PP from the matrix bulk. Maleated PP activates nucleation centres on the filler surface, producing transcrystalline regions. Consequently, the load can be transferred from the matrix to the filler particles, enhancing the composite yield strength. For zero adhesion, stearic acid reduced the interfacial thermodynamic work of adhesion below that of the uncoated filler. This reduction was caused by the occupation of part of the interaction centres on the filler surface by stearic acid molecules. The carboxyl group of the stearic acid deactivates the reactive centres on the filler surface. The stearic acid chains were too short to form physical entanglements with the bulk PP and a reduction in the composite yield strength is produced.

Jancar [94] also proposed the idea of a physical network of bonded filler particles. PP immobilised on the filler surface, he suggested, created a new continuous phase due to the interpenetration of interlayers absorbed on the neighbouring particles. The majority of PP however existed in the dispersed (non continuous) domains and it was this primary dispersed polypropylene phase that permitted higher loadings at elevated temperatures. The hindered continuous phase with reduced chain mobility had a poorer temperature/load dependence when compared to the primary PP.

Finally, Jancar [95] further utilised DMTA measurements to characterise $\text{Mg}(\text{OH})_2/\text{PP}$ composites. Neither platey nor needle type fillers changed the molecular mobility pattern in the glass transition region, only the extent of segmental mobility was reduced. Enhanced interfacial adhesion did not change this PP mobility pattern in the glass transition region. Needle type filler particles did however liberate a higher immobilised matrix content than platey particles. This was attributed to them having higher specific surface areas.

2.4 Polypropylene Crystallinity and Morphology

Polypropylene undergoes a large amount of supercooling upon crystallisation which may be altered by cooling rate and heterogeneous nucleation. A controlled cooling rate from the melt will influence the spherulitic structure of polypropylene. This in turn will influence the physical and mechanical properties of the material. At low cooling rates,

just below T_m , the spherulitic growth rate predominates over the nucleation rate and few but large spherulites are formed producing an overall high crystallinity. Alternatively at high cooling rates, nucleation rate (homogeneous) dominates over spherulite growth rate resulting in many smaller spherulites with a lower amount of crystallinity. Therefore the polymers morphology and crystallinity are functions of cooling rate, overall rate of nucleation and spherulitic growth rate [96].

2.4.1 Unfilled polypropylene

Isotactic polypropylene is a polymorphic material and can exhibit numerous crystal forms [97]. The main form is the α form (monoclinic) but β (hexagonal), χ (triclinic) and smectic (liquid crystal) forms also occur. The β form is occasionally found in commercial PP, usually at low levels but is less stable than the α form, since under tensile stress it will spontaneously convert into the α form [98]. The β form can however be obtained by the addition of nucleating agents [97]. X-ray diffraction patterns have been produced for the isolated α , β and χ forms of iPP [98], therefore the presence of any form can be detected in a PP sample. It has also been reported [99] that some workers believe that the β form has unique properties such as a higher impact strength and undergoes stress whitening during tensile deformation.

2.4.2 Influence of fillers on crystallisation

By the addition of foreign materials to polypropylene it is possible to increase the rate of nucleation [96]. These 'nucleants' act as heterogeneous sites for polymer crystallisation. This increased nucleation rate with respect to spherulitic growth allows smaller spherulites to be formed at higher temperatures than with homogeneous nucleation. Higher densities are observed even with small spherulites compared with homogeneous nucleation. Therefore heterogeneous nucleation increases the overall rate of crystallisation and increases the total amount of crystallinity.

Little is known about the nature of heterogeneous nuclei and their mechanism of nucleation. Polypropylene is complicated because nucleation has been exhibited by

solid, liquid and gaseous materials and the effect varied in different grades of commercial PP [100]. Binsbergen [101] stated that most inorganic substances show little nucleation activity and Beck [96] found that alkali metal or aluminium salts of aromatic or alicyclic carboxylic acids were the most efficient nucleants.

The intense number of catalyst residues within a polypropylene make them excellent candidates as heterogeneous nuclei. Their quantity is several orders of magnitude larger than the number of spherulites, but not every particle possesses the surface structure for heterogeneous nucleation. Rybníkar [102] found a second type of stable heterogeneous nuclei formed in a talc/PP nucleated system. This was attributed to the residues of polymerisation catalysts and the interaction was similar to that of the talc. The catalyst formed a nucleation substrate from which a lamellae structure could form. This was of different dimensions to that formed heterogeneously by the talc particles.

It was shown [96] that by progressively increasing the concentration of heterogeneous nuclei PP supercooling was reduced (anomalies were seen at very low concentrations). This supercooling effect was observed by measuring the peak temperature, T_p , of the crystallisation exotherm. Subtraction of T_p from the onset point (T_c) of nucleation was found to be a good measure of nucleation rate, the smaller the value the higher the rate. It was found that heterogeneous nucleation caused more rapid crystallisation compared with non nucleated systems. Also other factors that increased as a function of T_p were tensile yield stress, clarity and density. It was deduced that heterogeneous nucleation formed small, less coarse spherulites which filled in the interstices between larger spherulites before spherulite growth rate became too slow.

Maiti et al [103] investigated the behaviour of calcium carbonate in iPP using differential scanning calorimetry (DSC) and wide angle X-ray diffraction. By the utilisation of various parameters from DSC crystallisation exotherm peaks, they found it was possible to obtain information relating to cooling rate, nucleation rate, crystallisation rate and crystallite size distribution. The degree of crystallinity could also be estimated from X-ray diffractograms by the knowledge of certain intensity values.

Taylor [104] studied the effect of reported β phase nucleants on the properties of filled polypropylene. The β phase nucleants were quinacridone dye and azelaic acid coated calcium carbonate. The β phase content was measured by XRD and expressed as an index [98]:

$$\beta \text{ phase index} = \frac{I_{\beta 300}}{(I_{\alpha 110} + I_{\alpha 040} + I_{\alpha 130} + I_{\beta 300})} \quad (2.28)$$

The treated calcium carbonate filler gave no increase in the β phase index. The level of β phase was dependent on processing conditions. Compression moulding was the only compounding process that significantly increased the β phase content of polypropylene and retention of the grain boundary was observed. However, the influence of the β phase content was found to have negligible effect on impact strength and the toughening effect produced by the calcium carbonate filler could not be attributed to the β phase crystallisation.

Burke [78] reported that in injection moulded polypropylene samples (which naturally undergo non-isothermal cooling in the atmosphere) there are three main zones. These were the skin zone (high elongational flow, fast cooling), shear zone (thermal gradients, fine morphology) and the core zone (slow cooling, less molecular orientation). Additions of up to 40% TiO_2 were incorporated into the matrix, prior to injection moulding to investigate its effect on matrix morphology. All three of the morphological zones in the PP mouldings were approximately 45% crystalline. The presence of the pigment did not significantly affect the nature of the skin and shear zones. Burke deduced that processing parameters were the main factors governing the morphology in these regions and not the filler. The core zone crystallised at a lower temperature and a higher nucleation density was produced. The lower crystallisation temperature appeared to overwhelm the filler's nucleating effect. However, in identical composites, isothermal cooling yielded larger spherulites and the spherulitic nucleation density was enhanced by the incorporation of TiO_2 .

Alonso [111] utilised differential scanning calorimetry (DSC) and wide angle X-ray diffraction (WAXD) to characterise talc filled polypropylene. Filler loadings up to 10% strongly affected crystallisation characteristics, loadings above this had a minor influence. Samples with 10% loading had the highest level of crystal orientation and degree of crystallinity. This small filler loading influenced the orientation of practically all of the PP crystallites. At higher talc content, the influence of the filler diminished. This was reported to be due to the increase in nucleation centres, producing smaller PP crystallites, some of which did not even take part in the process of crystallisation.

Talc is a platey filler and was shown [54,55,111] to align parallel to the mould cavity wall, produced by flow. The crystallisation proceeded with the (004) plane of polypropylene crystals piling up on the plate (001) planes of the talc particles and the b direction being aligned parallel to the thickness and cooling direction of injection moulding. The c and a axes of the polypropylene were bimodally orientated to the flow direction.

Although the morphology of magnesium hydroxide filled polypropylene composites has not been well documented, the diversity of it's filler morphology has been shown to influence the crystallinity of injection moulded samples [67].

CHAPTER 3

EXPERIMENTAL METHODS

3.1 Materials

The two main materials used in this study were a commercial grade of polypropylene and magnesium hydroxide (in various development grades). Comprehensive details of these two materials can be seen in sections 3.1.1 and 3.1.2 respectively.

3.1.1 Polypropylene

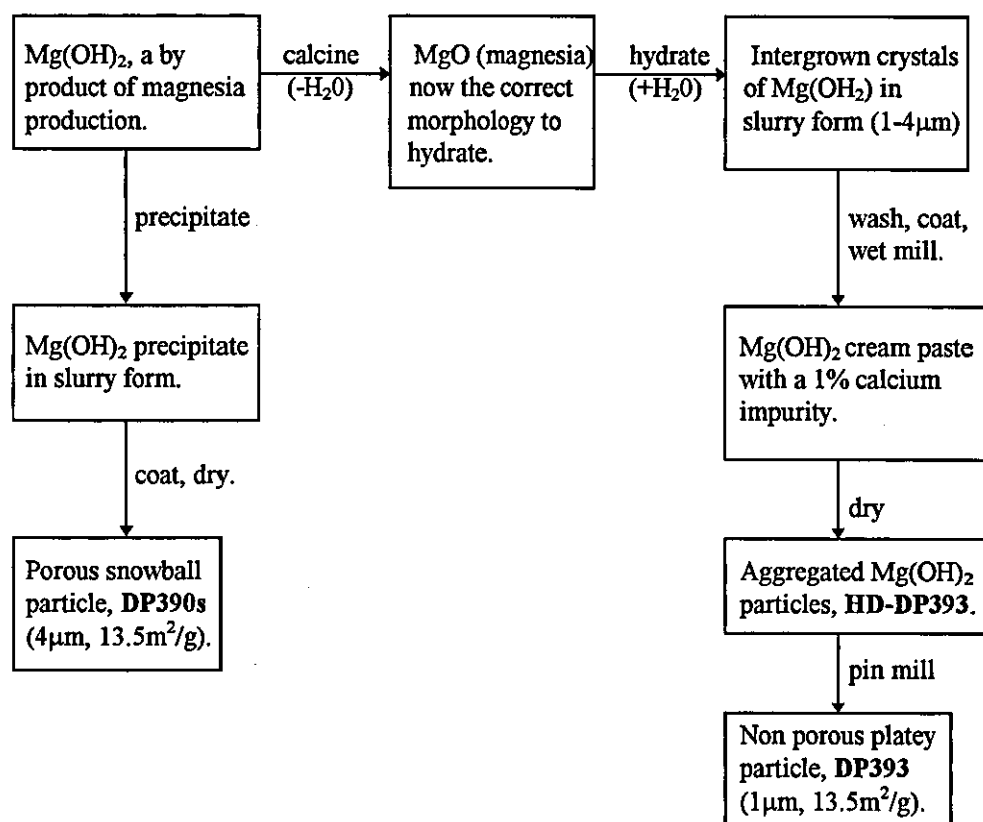
The sole polymer used throughout this project was Valtec CG108, an injection moulding grade of a heterophasic ethylene/propylene (EP) copolymer (Montell Polyolefins, Milton Keynes Limited). It was chosen to maximise the flow properties of the highly filled $Mg(OH)_2$ /PP designated to be produced from it. This copolymer differs from traditional EP copolymers. It has a higher ethylene content (about 8%) which will enhance toughness. This ethylene content exists as a discrete phase of discontinuous ethylene/propylene rubber particles, introduced during polymerisation. This new polypropylene, with controlled morphology, was manufactured using the spheripol™ process. The polymer is in the form of spherical white translucent particles with diameters in the range 0.5 to 4.0mm. This heterophasic copolymer was chosen, since it has been shown that the ethylene/propylene phase has an affinity for hydrated mineral fillers [79]. Some physical properties of Valtec CG108 can be seen below.

<i>PROPERTY</i>	<i>VALUE</i>	<i>METHOD</i>
Density (kg/m^3)	900	ASTM D 1505
M.F.I (230°C, 2.16kg)	13	ASTM D 1238L
Rockwell Hardness	89	ASTM D 785 (R scale)
Vicat Softening Point	151°C	ASTM D 1525 (10N)
Accelerated oven ageing	360 hours	ASTM D 3012 (150°C)

3.1.2 Magnesium hydroxide

During this project two distinctly different morphological forms of magnesium hydroxide than those commercially available were selected as fire retardant fillers for polypropylene. These had almost identical surface areas, but one was platey in nature whereas the other was pseudo-spherical, enabling a better understanding of the effect of magnesium hydroxide morphology on polypropylene properties to be evaluated. These fillers were produced by Premier Periclase Limited, Drogheda, Ireland using a pilot plant. The uncoated magnesium hydroxides were coded DP390s and DP393 (where DP refers to 'development product'). An attempt to utilise a high density form of DP393 was also made, this simply being an aggregated unmilled form of DP393 sub-coded HD-DP393. The production method of the two different filler morphologies along with the points at which filler coatings were introduced onto both magnesium hydroxide morphologies can be seen below in Fig 3.1.

Fig 3.1 Flow chart indicating the production routes to obtain DP390s and DP393.



3.1.3 Coating agents

In an attempt to improve the processing characteristics and the final $\text{Mg}(\text{OH})_2/\text{PP}$ composite properties, both magnesium hydroxide morphologies (DP390s and DP393) were coated with various organic coating agents. The silane coating agent was added direct but the rosin gum and fatty acid coating agents were applied in salt form. The rosin gum and fatty acid salts (either sodium or ammonium) were prepared at Premier Periclase Limited by reacting the fatty acid with sodium or ammonium hydroxide. Some characteristics of the original coating agent can be seen below.

<i>Coating Agent</i>	<i>Supplier</i>	<i>Structure</i>	<i>Mol. Wt.</i>	<i>M.Pt (°C)</i>
Stearic acid (Pristerine 4931)	Unichema Ltd.	$\text{CH}_3(\text{CH}_2)_{16} \text{COOH}$	272	55
Oleic acid (Prioline 6900)	Unichema Ltd.	$\text{CH}_3(\text{CH}_2)_7\text{CH}=\text{CH}(\text{CH}_2)_7 \text{COOH}$	270	13
Rosin Gum (Portuguese type)	Langley Smith and Company.	Mainly abietic acid $\text{C}_{20}\text{H}_{30}\text{O}_2$	~302	70
Vinyl-tris (2 methoxy-ethoxy) silane.	OSi Specialities.	$\text{CH}_2=\text{CHSi}(\text{OCH}_2\text{CH}_2\text{OCH}_3)_3$	280	-70

3.1.4 Coating methods

A summary of the coatings added to both the filler morphologies (DP390s and DP393) can be seen below.

<i>COATING</i>	<i>DP390s</i>	<i>DP393</i>
Stearate	Yes	Yes
Oleate	Yes	Yes
Rosin	No	Yes
Vinyl silane	No	Yes

Due to DP393 requiring more precipitation stages than DP390s slurry coatings were required to be applied at different stages in the milling process using different coating methods. Once dried, different coating methods could be employed.

DP390s was precipitated by a special seeding process in the slurry form and the fatty acid salts were added hot, directly to the well agitated slurry. This is done because slurry coating is cheap and further washing stages are possible. The dried filler was hydrocycloned to remove particles above 10 microns in diameter and washed further.

DP393 precipitated in a form that was unsuitable for washing, therefore filler coating had to be employed earlier in the production route prior to wet (bead) milling. This was done using the rosin gum and the fatty acid salts. At this stage the magnesium hydroxide was again in slurry form but was composed of larger particles of smaller surface area than the final DP393 particles. No further washing was undertaken. The filler was dried and existed as the high density HD-DP393 form. Pin milling this material reduced the crystallite aggregation into a finer form, DP393.

The coating agents were simply poured into the slurry as a hot solution as it was being agitated. In all cases the desired final coating weight percentage corresponds to that of the stearate, oleate or rosin chain and not that of the carrier salt. All coated fillers were oven dried at 80°C to facilitate full reaction at the filler surface.

Silane coatings were applied to the DP393 filler using a large scale spray process and at a laboratory size using a small scale dry coating technique. The large scale spray coating was performed by ECC International Limited and the exact coating conditions were not revealed. The small scale mixing was performed in a plastic bag. One hundred grams of DP393 were weighed out into the bag before the vinyl silane was added dropwise using a dropping pipette. The bag was shaken and squeezed to maximise coating efficiency. The coating process lasted in total for 5 minutes. In both cases, the total weight percentage of vinyl silane was at 2 wt/wt percentage which was expected to produce monolayer coverage.

As an optimum coating agent and coating level were sought, several different batches (referred to by LOT numbers) of fillers DP390s and DP393 were used in order to determine this. The characteristics of the different batches were expected to be the same as the production method of both filler morphologies should be reproducible.

The comprehensive list of both filler morphologies with and without coatings can be seen in section 3.1.5.

3.1.5 Filler coding

Filler coding for all DP393 and DP390s coated fillers along with their coating agent, coating type, coating level and LOT number can be seen in tables 3.1 and 3.2. For the case of DP393 fillers, the numerical prefix corresponds to the weight percentage of coating applied to the filler. For the case of the DP390s fillers, the numerical suffix corresponds to the weight percentage of coating applied to the filler. The maximum coating levels, calculated prior to coating, were expected to produce total surface coverage.

3.2 Characterisation of Fillers

Before any of the magnesium hydroxide fillers were compounded into polypropylene, they were comprehensively characterised in terms of their morphology, packing ability and surface coverage.

Table 3.1 Codes for DP393 coated fillers

<i>CODE</i>	<i>COATING AGENT</i>	<i>COATING TYPE</i>	<i>PERCENTAGE COATING (wt/wt)</i>	<i>LOT NUMBERS</i>
2.0VS	Vinyl silane	Vinyl silane	2.0	1 & 2
1.5AMST	Ammonium stearate	Stearate	1.5	1
3.0AMST	Ammonium stearate	Stearate	3.0	1
4.5AMST	Ammonium stearate	Stearate	4.5	1 & 3
1.5AMOL	Ammonium oleate	Oleate	1.5	1
3.0AMOL	Ammonium oleate	Oleate	3.0	1
4.5AMOL	Ammonium oleate	Oleate	4.5	1, 2 & 3
4.5NAST	Sodium stearate	Stearate	4.5	1
4.5NAOL	Sodium oleate	Oleate	4.5	1, 2 & 3
4.5AMROS	Ammonium rosinate	Rosin	4.5	1
1.5NAOL	Sodium oleate	Oleate	1.5	3
3.0NAOL	Sodium oleate	Oleate	1.5	3

Table 3.2 Codes for DP390s coated fillers

<i>CODE</i>	<i>COATING AGENT</i>	<i>COATING TYPE</i>	<i>PERCENTAGE COATING (wt/wt)</i>	<i>LOT NUMBERS</i>
AMST2.0	Ammonium stearate	Stearate	2.0	1
AMST4.0	Ammonium stearate	Stearate	4.0	1
AMST6.0	Ammonium stearate	Stearate	6.0	1
AMOL2.0	Ammonium oleate	Oleate	2.0	1
AMOL4.0	Ammonium oleate	Oleate	4.0	1 & 2
NAOL1.5	Sodium oleate	Oleate	1.5	2
NAOL3.0	Sodium oleate	Oleate	3.0	2
NAOL4.5	Sodium oleate	Oleate	4.5	2
NAOL6.0	Sodium oleate	Oleate	6.0	2
AMOL6.0	Ammonium oleate	Oleate	6.0	2

3.2.1 X-ray diffraction

The resolution of scanning transmission electron microscopy has only been adequate to resolve the shape of the primary particle structure of the DP393 and DP390s fillers. In order to assess whether the crystallographic systems differ, X-ray diffraction was employed. Uncoated DP393 and DP390s samples were mounted in windows based in aluminium housings. These were packed tightly and uniformly to promote all possible

diffraction patterns. The samples were mounted individually into a Hiltonbrooks X-ray diffraction machine fitted with a goniometer detection device. Nickel filtered $\text{CuK}\alpha$ radiation of wavelength 0.1542nm was aimed at the samples in turn. The anode was set at 40KV and the filament current was 30mA. The goniometer was set to scan X-rays diffracted from the samples in the 2θ range 10° to 90° at a speed of $0.1^\circ/\text{s}$. The relative intensities of the diffraction peaks can be obtained and the d spacing can be calculated using Bragg's equation ($2d\sin\theta = n\lambda$).

Polypropylene can exist in various forms, the most common being the α form. XRD can also be used as a tool to detect the presence of different forms (β or χ). Hence, XRD can be used to investigate whether the loading content of magnesium hydroxide fillers affected the morphology of the base polypropylene. Uncoated DP393 and DP390s filled composites were therefore selected along with an unfilled sample. Samples were cut from tensile bars and had their outer skins removed. These were then mounted in windows of aluminium housings so that the X-rays could be aimed at the through (normal) direction of the compounds i.e. perpendicular to the injection induced flow. Diffracted X-rays were collected between 2θ values of 5° and 40° (polypropylene diffracts between these limits). By observation of the traces produced by the unfilled polypropylene and the DP393 filled composites and comparing them to standard PP traces, it can be deduced what forms of polypropylene exist within the mouldings and how it is orientated.

3.2.2 Particle sizing

In order to measure the particle size and volumetric distribution of the two uncoated filler morphologies and the twenty eight coated fillers (17 of DP393 and 11 of DP390s), a Malvern Mastersizer X version 1.0 particle size analyser was used. These tests were performed at Zeneca Resins Limited, Runcorn. Prior to sizing, uncoated fillers were dispersed in Dispex A40 while the coated fillers were dispersed in surfactant AQ3. Samples were then sonicated for periods of 2, 5 and 15 minutes before being inserted into the particle sizer. From the data, it was possible to obtain the mean particle size (d_{50}) of each filler. Also, the extent to which the mean particle size was

affected by prolonged ultrasound indicated the cohesive strength of the filler particles. A typical particle size distribution and definitions of the parameters measured can be found in Appendix B.

3.2.3 Surface area

Surface area measurements for the uncoated and coated fillers for both morphologies were measured using the Haynes single point Brunauer-Emmett-Teller (BET) method and more rigorously through construction of nitrogen gas adsorption and desorption isotherms using the accelerated surface area and porosimetry machine (ASAP 2000) within the Department of Chemical Engineering at Loughborough University. An individual sample of each filler was dried and placed into a sample cell. This was then fixed onto the ASAP 2000 rig. The rig comprised of 3 ports: helium, nitrogen and one for evacuating the sample cell. The sample cell was evacuated to obtain a pressure of less than 50 μ m of mercury. The sample cell was immersed in liquid nitrogen and filled with a known volume of helium (carrier) gas. The system was then dosed with a known volume of nitrogen (adsorbate) gas. The relative pressure of adsorbate (at room temperature) was known. Nitrogen adsorbed onto the surface of the filler sample, and when adsorption was complete, the pressure transducer reached an equilibrium value which was recorded by the pressure. The system was then dosed with known volumes of nitrogen over a preselected range of relative pressure values. From the data obtained (measured equilibrium pressure, relative pressure at room temperature) the volume of nitrogen adsorbed at each relative pressure may be calculated. A plot of adsorbed volume against relative pressure of adsorbate gave the adsorption isotherm. This isotherm was utilised for calculating the BET surface area, the method for calculating specific surface area can be found in Appendix C.

3.2.4 Scanning transmission electron microscopy (STEM)

To fully characterise each magnesium hydroxide filler (whether coated or uncoated), information about the primary and secondary structure must be obtained. Primary structure refers to the primary crystals characterised by X-ray diffraction. Secondary

structure refers to the aggregation of these primaries into particles. Initially scanning electron microscopy (SEM) was used, but the resolution was not good enough to characterise the particles. Therefore STEM was utilised as a more powerful method, where secondary electrons from the TEM provide the source of information. A higher acceleration voltage was available (100kV), providing a smaller electron wavelength, hence providing better resolution. Also the working distance between the sample and lens was also very small.

Sample preparation was simple. Both filler morphologies were dispersed in methanol and a drop was placed onto a clean glass slide. After the solvent had evaporated, the glass slide was gold sputter coated using an Edwards E12 evaporation unit. The samples were then mounted onto the copper specimen holder within a Joel JEM 100CX combined scanning/transmission electron microscope. Examination of the fillers was undertaken in a scanning mode at magnifications of 10, 20 and 50K.

3.2.5 Bulk density

The dry packing properties of the fillers were assessed by measuring their compacted bulk (tap) density. This was done in accordance with BS2782: Part6: Method 621D: 1978 [104], except that 60-70g of filler powder was used to avoid overfilling the measuring cylinder. The accurately weighed samples were placed in a tap pack volumeter and repeatedly tapped at a rate of 85 taps per minute until a constant volume was attained. The compacted apparent bulk density was expressed as mass per unit volume of powder (g/ml). An average of 3 determinations was obtained.

3.2.6 Oil absorption

The oil absorption determination of all of the fillers was performed in accordance with BS3483: Part B7: 1982 [106]. The only difference in the method was that the palette knife dimensions were 20mm wide by 100mm long. The curved end of the knife permitted more controlled mixing. Traditionally, linseed oil (which is slightly acidic) is used for determining the oil absorption coefficient of pigments and extenders.

However, for simulating the behaviour of magnesium hydroxide fillers in polypropylene, an oil of similar solubility and polarity was used. The oil selected was a mineral oil (white, heavy paraffin oil) from Aldrich Chemicals Limited.

3.2.7 FTIR DRIFT analysis

Infra-red (IR) analysis of an organic compound involves the exposure of a sample to IR radiation. Each compound specifically absorbs certain wavelengths to produce a characteristic absorption spectrum for that sample. The Fourier Transform Infra-Red method, DRIFT (diffuse reflectance) was utilised so that a quantitative assessment of filler coatings could be made. The DRIFT facility was installed on a Unicam Matteson 3000 spectrometer. The attachment removes the spectral component from the main IR beam and allows only the diffuse component onto the sample surface, making the technique very surface specific.

For FTIR DRIFT analysis, the absorbance must be less than one for the response to be linear. Above this value, samples cannot be directly compared. To ensure this occurs, the filler samples were diluted in KBr (Aldrich, spectroscopic grade). This was ground in a Braun coffee grinder for 20 one minute intervals to obtain sub ten micron diameter particles. For DRIFT analysis, the KBr must be of a similar particle size to that of the filler under analysis. From a practically constructed calibration curve, it was found that 3.0 wt/wt% of magnesium hydroxide in KBr yielded an absorption spectrum just below one. All fillers were diluted to 3.0%, dried at 105°C to remove water and stored in a desiccator prior to analysis.

When the FTIR machine was initialised, samples were compacted in aluminium cups and the surface smoothed with a clean spatula. KBr was analysed to obtain a background reading by introducing it into the diffuse beam at 150 scans over a range of 400 to 4000 cm^{-1} at a resolution of 4.0. Samples were then placed within the IR beam until all of the fillers were scanned under the same conditions. The peak areas of the substrate OH peak and the alkyl CH peak were measured between 2970-2800 and 3735-3625 cm^{-1} respectively. The CH/OH ratio was then calculated for each coated

filler [88]. A typical trace of a fatty acid coated magnesium hydroxide filler indicating the relevant peaks can be found in Appendix E.

3.3 Sample Preparation

Sample preparation techniques used are given below.

3.3.1 Formulation

A total of 45 polypropylene formulations were compounded using the 28 different magnesium hydroxide fillers. These comprised different morphologies (DP393 and DP390s), different coatings (stearate, oleate, rosin or vinyl silane), different coating levels (uncoated up to total coverage) along with different filler loading levels (unfilled up to nominally 70% by weight). The formulation of the polypropylene compounds along with their specific coding can be seen below in Tables 3.3 to 3.8..

Table 3.3 DP393 LOT 1 uncoated and fatty acid formulations

<i>CODE</i>	<i>COATING</i>	<i>LOT</i>	<i>NOMINAL FILLER LOADING (%)</i>	<i>COMPOUNDING METHOD</i>
DP393	Uncoated	1	60	Continuous
DP393	Uncoated	1	60	Batch
HD-DP393	Uncoated	1	60	Continuous
1.5AMST	Stearate	1	60	Continuous
3.0AMST	Stearate	1	60	Continuous
4.5AMST	Stearate	1	60	Continuous
1.5AMOL	Oleate	1	60	Continuous
3.0AMOL	Oleate	1	60	Continuous
4.5AMOL	Oleate	1	60	Continuous
4.5NAST	Stearate	1	60	Continuous
4.5NAOL	Oleate	1	60	Continuous
4.5AMROS	Rosin	1	60	Continuous

Table 3.4 DP393 LOTS 1 and 2 vinyl silane formulations

<i>CODE*</i>	<i>COATING</i>	<i>LOT</i>	<i>NOMINAL FILLER LOADING (%)</i>	<i>COMPOUNDING METHOD</i>
2.0VS50A	Vinyl silane	1	50	Continuous
2.0VS55A	Vinyl silane	1	55	Continuous
2.0VS60A	Vinyl silane	1	60	Continuous
2.0VS65A	Vinyl silane	1	65	Continuous
2.0VS70A	Vinyl silane	1	70	Continuous
2.0VS20B	Vinyl silane	1	20	Continuous
2.0VS30B	Vinyl silane	1	30	Continuous
2.0VS40B	Vinyl silane	1	40	Continuous
2.0VS50B	Vinyl silane	1	50	Continuous
2.0VS60B	Vinyl silane	1	60	Continuous
2.0VS70B	Vinyl silane	1	70	Continuous
2.0VS20	Vinyl silane	2	20	Batch
2.0VS60	Vinyl silane	2	60	Batch

* Where A & B refer to LOT 1 compounds containing the same filler but produced at different periods in time on slightly different extruders.

Table 3.5 DP393 LOT 2 fatty acid formulations

<i>CODE</i>	<i>COATING</i>	<i>LOT</i>	<i>NOMINAL FILLER LOADING (%)</i>	<i>COMPOUNDING METHOD</i>
1.5NAOL	Oleate	2	60	Continuous
3.0NAOL	Oleate	2	60	Continuous
4.5NAOL	Oleate	2	60	Continuous
4.5AMOL	Oleate	2	60	Continuous

Table 3.6 DP393 LOT 3 uncoated and fatty acid formulations

<i>CODE</i>	<i>COATING</i>	<i>LOT</i>	<i>NOMINAL FILLER LOADING (%)</i>	<i>COMPOUNDING METHOD</i>
DP393	Uncoated	3	60	Continuous
4.5AMOL	Oleate	3	60	Continuous
4.5AMST	Stearate	3	60	Continuous
4.5NAOL	Oleate	3	60	Continuous

Table 3.7 DP390s LOT 1 uncoated and fatty acid formulations

<i>CODE</i>	<i>COATING</i>	<i>LOT</i>	<i>NOMINAL FILLER LOADING (%)</i>	<i>COMPOUNDING METHOD</i>
DP390s	Uncoated	1	60	Continuous
AMST2.0	Stearate	1	60	Continuous
AMST4.0	Stearate	1	60	Continuous
AMST6.0	Stearate	1	60	Continuous
AMOL2.0	Oleate	1	60	Continuous
AMOL4.0	Oleate	1	60	Continuous

Table 3.8 DP390s LOT 2 fatty acid formulations

<i>CODE</i>	<i>COATING</i>	<i>LOT</i>	<i>NOMINAL FILLER LOADING (%)</i>	<i>COMPOUNDING METHOD</i>
NAOL1.5	Oleate	2	60	Continuous
NAOL3.0	Oleate	2	60	Continuous
NAOL4.5	Oleate	2	60	Continuous
NAOL6.0	Oleate	2	60	Continuous
AMOL4.0	Oleate	2	60	Continuous
AMOL6.0	Oleate	2	60	Continuous

3.3.2 Compounding

Compounding methods used, including mixing conditions and temperatures are given below.

3.3.2.1 Continuous mixing

The compounding of the majority of the filled compounds was performed using a continuous mixer. The DP393 LOT 1 uncoated, DP393 LOT 1 fatty acid coated and DP393 LOT 1 vinyl silane coated compounds were produced on an APV (MP2015) high intensity intermeshing co-rotating compounding extruder with an L/D ratio of 15/1. The remaining DP393 compounds and all of the DP390s compounds were produced on an APV (MP30TC) high intensity intermeshing co-rotating compounding extruder with an L/D ratio of 30/1. An unfilled formulation was also passed through the MP30TC compounding extruder to act as a control compound. The screw configurations for each extruder can be seen below.

Table 3.9 Screw configurations for both extruders

<i>MP2015</i>	<i>MP30TC</i>
Feed screws: 5D	Feed screws: 5.5D
Mixing paddles: 10 at 60°	Mixing paddles (block): 4 at 30°
Mixing paddles : 4 at 90°	Mixing paddles (block): 4 at 30°
Orifice plug: 0.5D	Full bore orifice plug: 0.5D
Feed screws: 5.5D	Feed screws : 6D
Camel back discharge: 1.5D	Mixing paddles: 12 at 60°
Die	Feed screws: 4D
	Mixing paddles: 6 at 60°
	Full bore orifice plug: 0.5D
	Feed screws: 4.5D
	Single lead discharge screw: 1.5D
	Die

The polypropylene and fillers were fed independently into each extruder using two K-Tron T20 volumetric twin screw feeders. The hoppers were calibrated manually to produce extrudates containing the desired filler loading level. With the MP2015 machine, the total calibrated output was set at 6 kg/hr. With the MP30TC machine, the total calibrated output was set at 12 kg/hr. In every case, low output rates were used to starve feed the extruder to overcome compounding difficulties. A continuous strand of extrudate was formed via a single strand die from the MP2015 at a constant screw speed of 200rpm. For the case of the MP30TC machine, the extrudate was formed via a four strand die at a constant screw speed of 250rpm. In each case the extrudate was cooled in a water bath and granulated. The barrel temperature profiles were kept constant for each extruder, but temperatures were higher with the MP2015 extruder (due to mixing limitations with its short barrel), and can be seen below.

Table 3.10 Barrel temperature profile of each APV compounding extruder (°C)

<i>MP2015</i>	230	235	235	240	240	245	Die
<i>MP30TC</i>	200	210	210	220	220	220	Die

While each filled compound was being produced, the compounding torque was measured and could be related to the ease of processing. Due to the poor mixing quality and porous extrudate made on the MP2015 compounder, all of the pellets for each compound were dried and re-compounded. This was achieved by feeding the pellets of the compounds into the APV using just one of the hoppers (with the pellet feed screws attached). The output speed of the hopper was set arbitrarily in order to attain a compounding torque between 60 and 70%. The screw configuration and barrel temperature profile were left as for the first extrusion (except the first zone temperature was decreased to 125°C).

3.3.2.2 Batch mixing

Three filled compounds along with an unfilled formulation were produced by small scale batch mixing on a Haake Reocord 90 co-rotating internal mixer with roller rotors. These compounds were the DP393 LOT 2 vinyl silane compounds and

uncoated DP393 (LOT 1). The Haake Rheocord consists of a heated chamber (230°C) with a maximum charge volume of 45cm³. A fill factor of 0.9 was used for all of the formulations. The rotors were activated (50rpm) and the polypropylene was introduced into the mixing chamber over a one minute period via a feed chute. Filler was then added (at the appropriate quantity) again via the feed chute over a one minute period. The chamber was then closed and the two components were allowed to homogenise for a further eight minutes. After this time, the chamber was opened immediately, and the batch was dropped while it was still hot. No further processing was performed on these small scale mixes.

3.3.3 Injection moulding

All pelletised compounds that had been produced by continuous mixing, were moulded into suitable shaped test specimens. This was performed using a Negri Bossi NB55 injection moulding machine with Dimigraph 80 control. Two types of moulds were used. The first was a four piece tensile mould producing tensile bars of dimensions in accordance with BS 2782: Part 3: Method 320B: 1976 [107]. The second was a 9 piece Izod impact bar mould producing specimen samples of dimensions 630 x 12 x 6mm. Three of the samples were unnotched, three contained a sharp notch and three contained a blunt notch. All of the extruded pellets were predried in an oven at 70°C for at least 6 hours just prior to injection moulding. The conditions employed for injection moulding of both sets of test specimens can be seen in Table 3.11.

3.4 Characterisation of Compounds

The dried pelletised compounds were characterised in terms of their final filler content and rheological properties prior to injection moulding.

Table 3.11 Conditions employed for injection moulding of test specimens

<i>PARAMETER</i>	<i>4 PIECE TENSILE</i>	<i>9 PIECE IZOD</i>
Shot size (mm)	50	58
Temperature profile (°C)	Barrel: 190	Barrel: 190
	Barrel: 200	Barrel: 200
	Barrel: 210	Barrel: 210
	Nozzle: 220	Nozzle: 220
	Sprue: 240	Sprue: 240
	Mould: 60	Mould: 60
Injection settings	1st: 50%	1st: 50%
	2nd: 50% @ 0mm	2nd: 50% @ 0mm
Back pressure (bar)	10	10
Screw position trip (mm)	6	10

3.4.1 Final filler content

Ash analysis was performed in accordance with BS 2782: Part 4: Method 470A: 1991 [108] using an oven temperature of 1000°C. The compounds were placed in silicon crucibles which were thermally stable up to 1500°C. The crucibles were handled with hot tongs. In order to calculate the final filler content of a compound, a calibration graph was constructed and was used to reveal the true filler content. From this value, the volume fraction of filler could be calculated for each composite. Procedures to determine filler content and filler volume fraction can be found in Appendix F.

3.4.2 Melt flow index

The MFI of the compounds was determined in accordance with BS 2782: Part 7: Method 720A: 1979 [109] using the standard 2.16 Kg load at 230°C. Three determinations for each compound were made and an average taken. From the melt flow index and final filler content, it was also possible to calculate the volumetric

output rate of polypropylene in each compound. The method for determining melt flow rate and volumetric output can be found in Appendix G.

3.4.3 Capillary rheometry

To assess the rheological properties of all of magnesium hydroxide filled polypropylene compounds (along with the unfilled) over a wide range of shear rates, a Davenport capillary rheometer was used. The internal diameter of the barrel was 20mm and the diameter of the piston 19mm. Two dies were used at a standard test temperature of 230°C. These were a 20/2 and a 0/2 (zero length) die, where the first figure is the die length and the second figure is the internal diameter (in mm). Pellets of the magnesium hydroxide filled compounds were charged into the barrel of the rheometer and allowed to soften for 5 minutes. These were subsequently extruded, separately, through both dies at piston speeds of 5, 10, 25, 50, 100, 150 and 250mm/min. A pressure transducer was situated at the die and the extrusion pressure was recorded for each piston speed. This was carried out for all of the compounds. To account for die end errors, the pressure caused by the zero length die was subtracted from that of the extrusion die giving a true pressure (two die technique). Equations used for determining rheological parameters can be found in Appendix H.

3.5 Characterisation of Moulded Composites

The moulded composites were characterised using a vast array of testing procedures, all of which are given below.

3.5.1 Flexural testing

Initially, tensile testing of the filled composites was attempted using an external clip on extensometer. However due to the large errors over the low extensions to yield, the method was very inaccurate, so was discontinued. Flexural testing was performed on a T5002 JJ Lloyd universal testing machine fitted with a 3 point bend testing jig. The mounting points used on the 3 point jig were knife edge in nature with radius of 5mm,

to ensure point contact with the test specimens. The test speed was 5mm/min and a 500N load cell was incorporated. Tests were carried out in accordance with ASTM D70-86 [110]. The span length was 60mm. In all cases 8 samples were tested (at room temperature). The testing equipment was interfaced to DAP2 computer software for data acquisition and analysis. The method of determining flexural parameters along with a typical trace can be found in Appendix I.

3.5.2 Impact testing

A Rosand instrumented falling weight impact tester was used to assess the impact properties of the filled compounds along with the virgin material. The test specimens used were sharp notched Izod bars of notch radius 0.25mm. The samples were mounted on a two point support jig of span length 40mm. A Kistler transducer was positioned between the impactor dart and the impact weight. On drop release, the impactor dart accelerated towards the sample on the jig. The dart assembly flagged an optic trigger which activated a transient recorder to begin data collection of the force signal with time. The fracture event could be only a few thousands of a second, but the 12 bit transient recorder could obtain 2000 data points during this time. Correct filtering reduced adventitious vibrations. The sweep time sets the length of time that recording will be taken after the data capture has been triggered. Data analysis was performed on a BBC microcomputer. A sample size of 8 specimens was used in order to obtain a good statistical presentation. The peak force and peak energy were found to be the most suitable parameters of impact resistance to differentiate between the different compounds. The peak force is related to the flexural strength of a compound and is the force required to cause crack initiation. The peak energy is a measure of material toughness and is the energy to initiate failure. Deflection of the specimens at peak force was also recorded. Total energy absorbed during failure was also measured, but the determination of the end point of the test was more difficult. These values were therefore omitted from this thesis. The test conditions and parameters obtained from a typical impact trace can be seen in Appendix J.

3.5.3 Thermal analysis

3.5.3.1 Differential scanning calorimetry (DSC)

The melting temperature (T_m), onset of recrystallization (T_c), heat of crystallisation on melting (ΔH_c) and heat of recrystallisation on cooling (ΔH_{rc}) were determined for every filled compound along with the unfilled reference compound. This was achieved using a Du Pont 2000 thermal analyser fitted with a differential scanning calorimeter (DSC) cell. Samples were encapsulated in a sealed aluminium pan and along with an empty pan, were placed on the sample and reference areas of the DSC cell. The samples were heated at $10^\circ\text{C}/\text{min}$ from room temperature to 220°C . To remove any thermal history, the samples were fluxed for 5 minutes at this temperature before they were cooled to 70°C at a rate of $10^\circ\text{C}/\text{min}$ (with liquid nitrogen assist). In all cases, the sample size was 10 to 17 mg. Where possible, two runs were performed on each composite.

The melting point, T_m , of the composites was obtained from the peak of the heating endotherm. The onset temperature, T_c , was defined by the intercept of the line of greatest gradient with the extrapolated baseline and could be used to determine whether the filler is causing a nucleating effect. The heats of crystallisation, ΔH_c , and recrystallization, ΔH_{rc} , were obtained from the area of the heating endotherm and cooling exotherm respectively. The values produced were for the whole sample weight, and as the filler has no effect on ΔH_c or ΔH_{rc} , the values had to be corrected for pure polymer. The corrected H_c and ΔH_{rc} were converted to percentage crystallinity values by dividing them by the ΔH_c for 100% pure polypropylene. This value is accepted as 209J/g [111]. Parameters [103] such as overall crystallisation rate ($T_c - T_p$), nucleation rate (S_i) and crystallite size distribution (ΔW) were measured for selected composites and were obtained from the cooling endotherm. The method of determining such crystallisation parameters from a DSC cooling endotherm can be found in Appendix K.

3.5.3.2 Dynamic mechanical thermal analysis (DMTA)

A DuPont 983 dynamic mechanical analyser was used in order to study how incorporating high loadings of magnesium hydroxide fillers into polypropylene affects its glass transition temperature. Samples used were unnotched impact bars of DP393 vinyl silane coated filled composites that had been milled to a thickness of 3.2mm by removing the outer edges (skins) of the mouldings. The samples were subsequently mounted in the DMA head and firmly secured using a torque wrench. The samples were subjected to a sinusoidally varying stress of frequency 1Hz over a temperature range -50°C to 80°C. This was attained by use of a liquid nitrogen cooling unit and heater coils. The theory of DMTA along with a typical trace can be found in Appendix L.

3.5.3.3 Vicat softening point

The Vicat softening point of a selection of DP393 LOT 1B vinyl silane coated filled compounds of widely ranging filler loading levels were determined in accordance with BS2782: Part 1: Method 120A: (10N load) [112]. The samples were taken from the centre 2cm strip of tensile bars, and placed in the Vicat softening unit with the indenter being perpendicular to the flow direction. Transformer oil was used as the heating medium, at a heating rate of 50°C/hour. The temperature at which the 10N load is forced 1mm into the samples is defined as the Vicat Softening Point. Three readings were taken for each compound and an average was taken.

3.5.4 Flame retardancy

Flame retardance was assessed using UL94, LOI and cone calorimetry methods.

3.5.4.1 UL94 vertical burning tests

To assess the flame resistance of the injection moulded composites, tensile bars were milled and tested in accordance with the UL94 standard [113] for testing plastics

flammability. The test set-up was simple. The milled tensile bars (3.2mm thick) were clamped vertically above a Tirrel burner which was used to ignite the bottom end of each test specimen. The apparatus was housed in a fume cupboard and surrounded by a draught exclusion hood. The standard states that test specimens must be ignited then reignited (after self extinction), the burning time in each case is recorded to produce a combined burning time. Five different specimens for each compound must be tested. Each composite can be given a flammability rating according to the total burning time of all 5 of the test specimens and their dripping characteristic,. If the combined burning time for each composite is less than 50s and do not drip and ignite cotton wool situated below, the composite will obtain the maximum desired V0 classification. Two other ratings, V1 (where the total burning times are longer) and V2 (these materials will have longer total burning times and will drip and ignite the cotton wool).

3.5.4.2 Limiting oxygen index (LOI)

Limiting oxygen index values were measured on Stanton Redcroft fire testing apparatus. Test samples were 125 x 10 x 3mm. The LOI apparatus was initially calibrated. The oxygen valve was closed and the nitrogen valve opened. The flow rate was adjusted to 18 l/min and the potentiometer adjusted to zero. The nitrogen valve was then closed and the oxygen valve opened. The oxygen flow rate was adjusted to 18 l/min. Samples were mounted vertically in the steel holder. The oxygen/nitrogen mix (oxygen index) could be pre-set by altering the flow rate using the valves. In all cases, the flow rate was maintained at 18 l/min. Samples are alighted using an ignitor. If the sample burns for more than 3 minutes or for more than 5cm, the oxygen content is too rich. The oxygen/nitrogen content is adjusted as to reduce the oxygen index. If the samples don't burn for 3 minutes or 5cm, the oxygen content is too low. When the oxygen index just permits burning for 3 minutes or 5 cm, this is defined as the limiting oxygen index.

3.5.4.3 Cone calorimetry

Five compounds, 60% filled with DP393 or DP390s were selected for use in the cone calorimeter. Two of the compounds contained DP393 LOT 2 and two contained DP390s LOT 2 filler, both with 1.5 or 4.5% oleate coating. A DP393 LOT 1 vinyl silane coated filled polypropylene was also selected. The pelletised compounds were injection moulded using the standard barrel and mould temperatures. A one piece mould was used to produce test plaques, of dimensions 4 inches by 4 inches square and 3mm thick, so that their burning characteristics could be assessed using a Fire Test Technology cone calorimeter. Testing followed BS 476: Part 15: 1993 [114], except that only one determination was performed on each compound.

The cone calorimeter itself is an oxygen depletion calorimeter as it works on the basis that 13.1×10^3 J/g of heat released by a burning material is proportional to 1kg of oxygen consumed in the burning process. The name 'cone' is derived from the shape of the truncated conical heater element capable of irradiating samples with fluxes up to 100kW/m^2 . The heat resistant sample holder $100 \times 100 \times 50\text{mm}$ thick was orientated in the horizontal position. Test plaques were placed on an electronic load cell accurate to 0.1g, the sample mass being automatically recorded by the computer. A 10kV spark generator was situated directly above the test plaque and activated in order to ignite any volatile gases during burning. At the start of the test, the heat shield was removed from the sample and it was irradiated with a constant heat flux of 50kW/m^2 at a distance of 1 inch. Via a remote handset the computer was informed that the test has commenced. When the sample started to burn the computer was informed again manually via a remote handset. Any pyrolised materials were drawn up a stainless steel exhaust system at a constant rate of 24 litres per second. Gas sampling was then performed using a ring sampler, cold trap and drying columns. Oxygen could be detected using a paramagnetic oxygen analyser whereas carbon monoxide and carbon dioxide were monitored using a NDIR gas analyser. Smoke obscuration was measured with a 0.5mW helium-neon laser and twin photodiodes for main and reference beam detection. Finally, when burning has totally ceased the test is stopped. The information

is stored and analysed by the computer. Data collection was collected via a 16 channel A-D interface and software linked to an IBM compatible PC. A wide range of results were obtained relating to ignition and extinction time, heat of combustion, mass loss rate, specific extinction area, smoke release rate and CO₂/CO yields were provided both statistically and graphically.

Calibration of the instrument was most important and was performed on the day of analysis. The oxygen detector was set to zero by flushing it through with nitrogen. The CO₂/CO detectors were automatically calibrated using a fixed ratio of CO₂/CO from a pre-prepared cylinder. The calibration burner was connected to a metered supply of methane of at least 99.5% purity (heat of combustion being 50×10^3 kJ/kg) in order to calibrate the conical heater. A temperature controller which compared the temperature of the calibration burner to the conical heater could be adjusted to provide the desired heat flux of the cone.

3.5.5 Fracture surface analysis

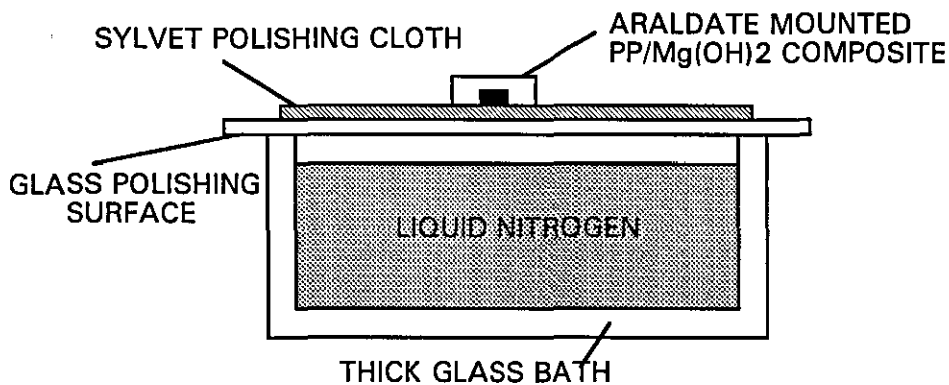
Fracture surfaces of composites that had broken during either flexural or impact testing were observed at magnifications x500, x1.5K, x5K and x10K using a Cambridge Stereoscan scanning electron microscope (SEM). The fracture surfaces of samples were untouched after fracture but the samples were cut across their section to a 1cm specimen sizes. These could be easily mounted on aluminium stubs before they were gold sputter coated using an Edwards E12 evaporation unit. Samples were then placed into the evacuated sample chamber of the SEM. Accelerating voltages between 10 and 20kV were used at a working distance of about 8mm. Areas were photographed which showed the general representation of the type of failure mechanism and microstructure of each composite viewed.

3.5.6 Filler dispersion analysis

Optical and X-ray mapping techniques have proved inconclusive in providing firm evidence about filler dispersion in highly filled compounds. X-ray mapping is prone to

detecting subsurface particles and microtoming can often produce excellent results but often it is difficult to obtain sections that are not buckled. Polishing the face of a bulk sample is more time consuming but can regularly produce a superior finish. A new filler dispersion analysis technique has therefore been utilised.

Centre portions of impact bars of DP393 and DP390s filled composites were obtained by slicing them with a sharp blade. The samples were placed in turn on a microtome stage transverse face upwards and the face was sectioned in 10 micron portions using a steel knife until a flat surface was obtained. When this had been done individual samples were placed smooth side down into circular plastic holders with 'pop out' bottoms. An epoxy resin (araldite MY750 and hardener HY951 in ratio 10:1) was mixed. 4 parts by weight of a toughener (desmocap 11) was added to 100 parts by weight of the resin. The toughened resin system was poured over the sample until it was fully submerged, and the resin was allowed to cure for 24 hours at room temperature. Initially the samples were polished with increasing grades of silicon carbide paper, these being 220, 400, 800 and 1200. The use of finer polishing agents (grades of alumina powder) were then used to obtain a well polished surface finish. However, the polypropylene matrix had to be cooled well into its glassy state to prevent any of the hard filler being dislodged by the polishing motion or smearing of the polished surface. This was achieved by liquid nitrogen cooling on the apparatus shown below.



A thick circular glass bath (approximate diameter 12cm) was almost completely filled with liquid nitrogen and insulated with foamed polystyrene (not shown). A flat glass polishing surface was placed on top of the arrangement and the total glass area was allowed to cool. While this was happening a sylvet polishing cloth was affixed to the glass plate using masking tape. Alumina of gradually decreasing particle size (5.00, 1.00 and 0.05 micron) was then used as the polishing media with methanol as the lubricant. The araldite mounted composites were then slowly polished, ensuring minimal heat build up during the polishing motion. The glass bath was constantly maintained at its almost full level.

When the smallest grade alumina had been used the samples were washed several times with distilled water to remove any surface residue. Samples were then immersed in 1M HCl for at least 12 hours to etch out the filler particles from the PP matrix. The samples were then left in air to dry before being gold sputter coated and subsequently viewed using a scanning electron microscope, where the dark holes represent the etched filler particles.

CHAPTER 4

RESULTS

4.1 Filler Characterisation

The 33 fillers were fully characterised in terms of their morphological structure and coating content. The results of this characterisation can be seen below.

4.1.1 X-ray diffraction

The X-ray diffraction patterns for the two uncoated fillers, DP393 and DP390s can be seen below in Fig 4.1. X-ray diffraction patterns for unfilled polypropylene, and polypropylene filled with 55% DP393 and DP390s can be found in Figs. 4.2, 4.3 and 4.4 respectively. Raw data for 2θ , d spacings and relative intensities can be found in Appendix A.

Fig 4.1 XRD patterns for DP393 and DP390s fillers

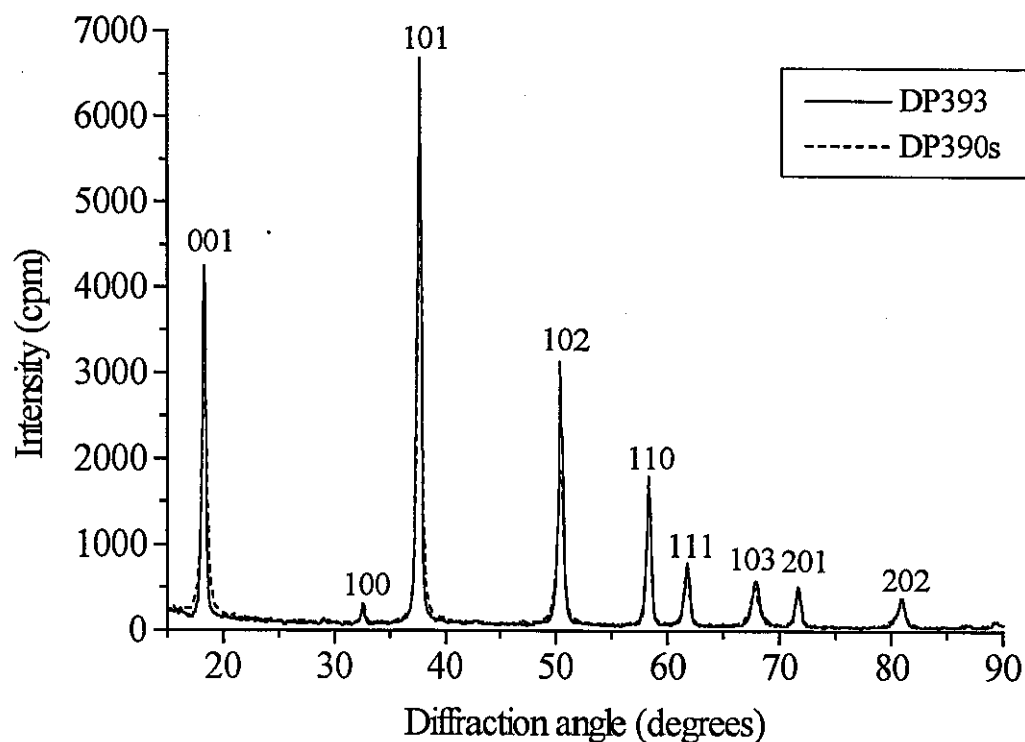


Fig 4.2 XRD pattern for unfilled polypropylene

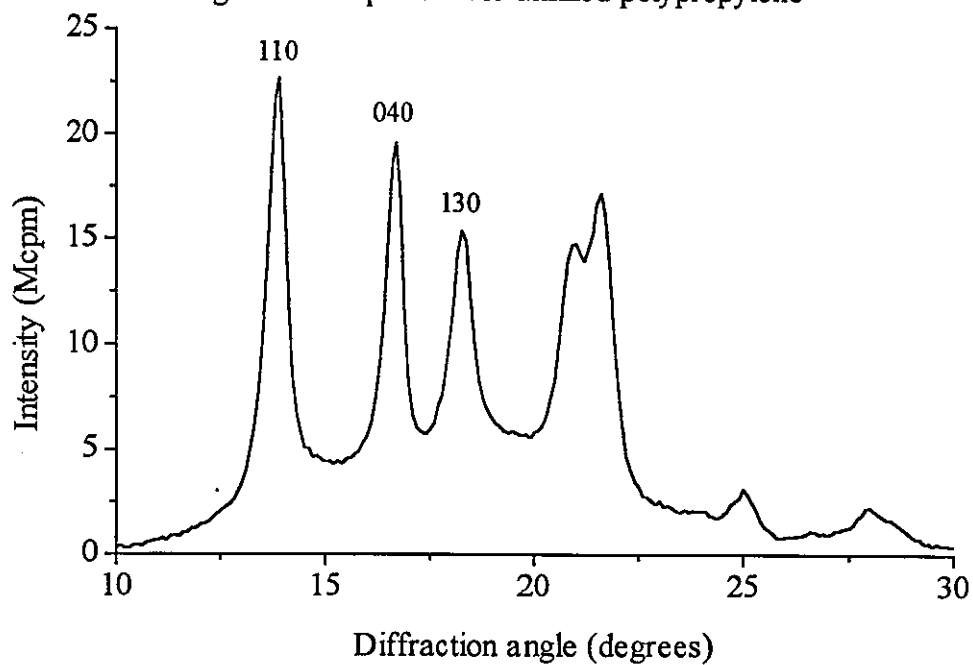


Fig 4.3 XRD pattern for polypropylene filled with 55% DP393

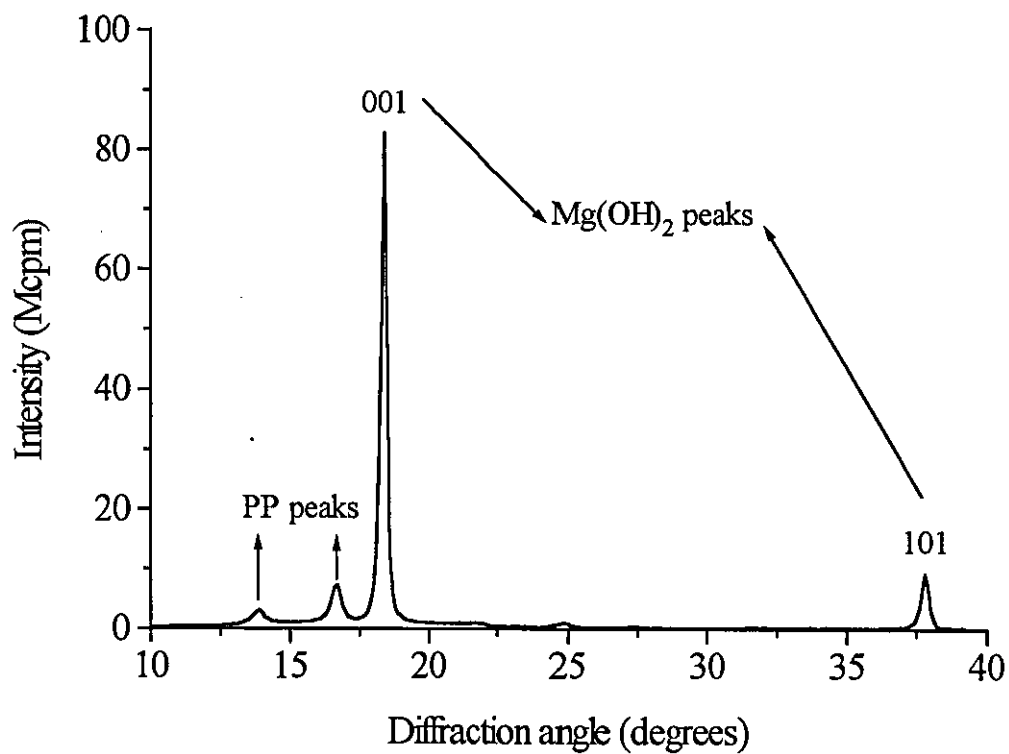
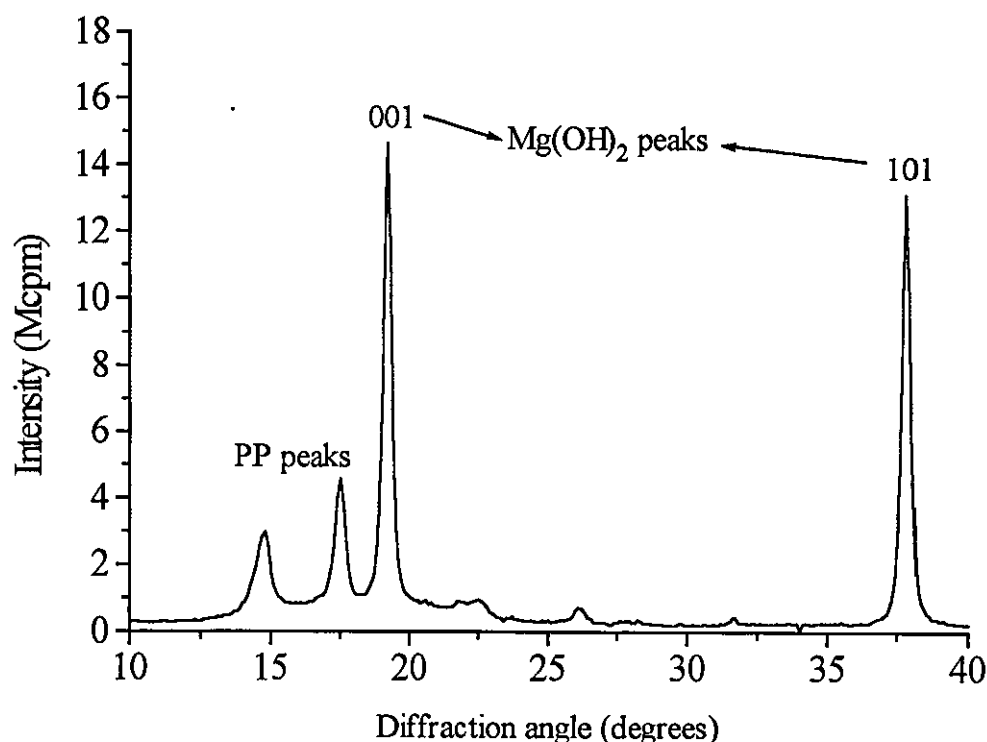


Fig. 4.4 XRD pattern for polypropylene filled with 55% DP390s



From the overlap of the XRD diffraction patterns of fillers DP393 and DP390s (Fig. 4.1) it can be seen that they have identical crystallographic structure (trigonal). The characteristic 110, 040 and 130 peaks for unfilled polypropylene can be seen in Fig. 4.2. The relative intensities of magnesium hydroxide diffraction peaks compared to those produced by polypropylene can be seen in Figs. 4.3 and 4.4. The presence of the strong $\text{Mg}(\text{OH})_2$ 001 peak for both DP393 and DP390s filled polypropylene can also be depicted from these figures.

4.1.2 Particle structure and size distribution

Fillers were analysed in terms of both their primary and secondary structure. Primary structure was revealed using scanning transmission electron microscopy (STEM) whereas particle size distribution (PSD) and secondary particle size (d_{50}) were revealed using particle sizing. An example PSD curve, explanation of the parameters used and data for all fillers can be found in Appendix B.

Fig. 4.5 STEM micrograph of DP393 (x50k)



----- 0.5 microns

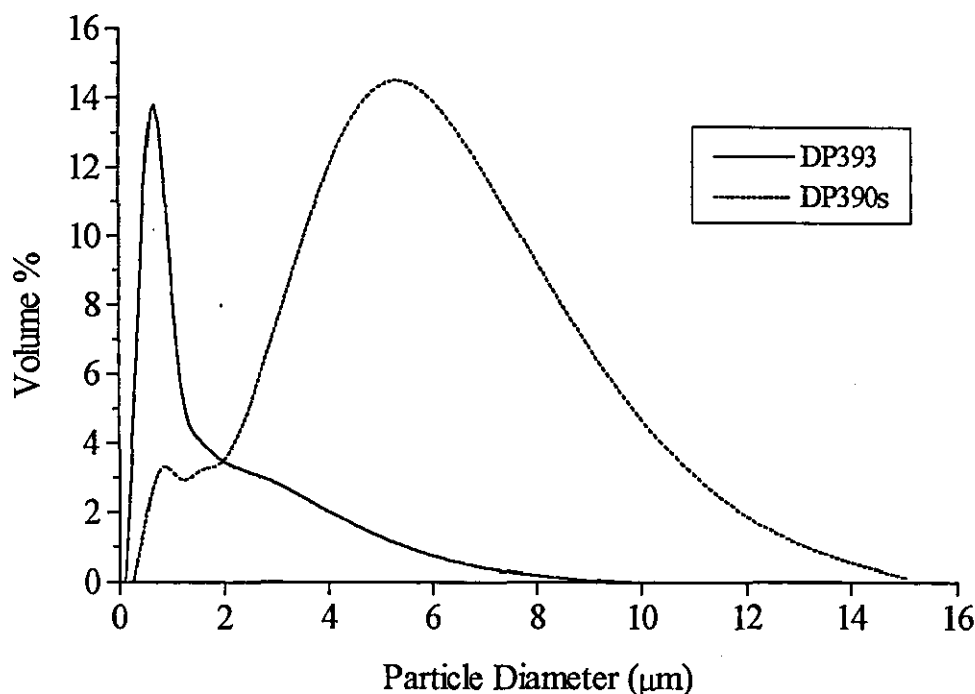
Fig. 4.6 STEM micrograph of DP390s (x50k)



----- 0.5 microns

The primary structure of uncoated fillers DP393 and DP390s can be seen in Figs. 4.5 and 4.6 respectively. From STEM analysis, DP393 is seen to be comprised of regular hexagonal plates of size 0.25 to 0.5 microns in diameter. Their aspect ratio is approximately 1. DP390s is seen to be comprised of stacks of hexagonal plates varying in length from 0.1 to 0.4 microns. Their aspect ratio is approximately 5.

Fig.4.7 PSD of DP393 and DP390s fillers



The particle size distribution of both filler types can be seen in Fig. 4.7. DP393 is monodispersive whereas the distribution of DP390s is bi-modal. From Fig. 4.8 the particle size distributions for both high density (HD-DP393) and standard density (DP393) have been shown to be essentially identical. However, from Fig. 4.9 it could be seen that HD-DP393 is an array of highly agglomerated DP393 primary particles with diameters up to one hundred microns. From Fig. 4.10 it has been seen that the particle size distribution of DP393 fillers varies between different batches.

Fig.4.8 PSD for standard and high density DP393

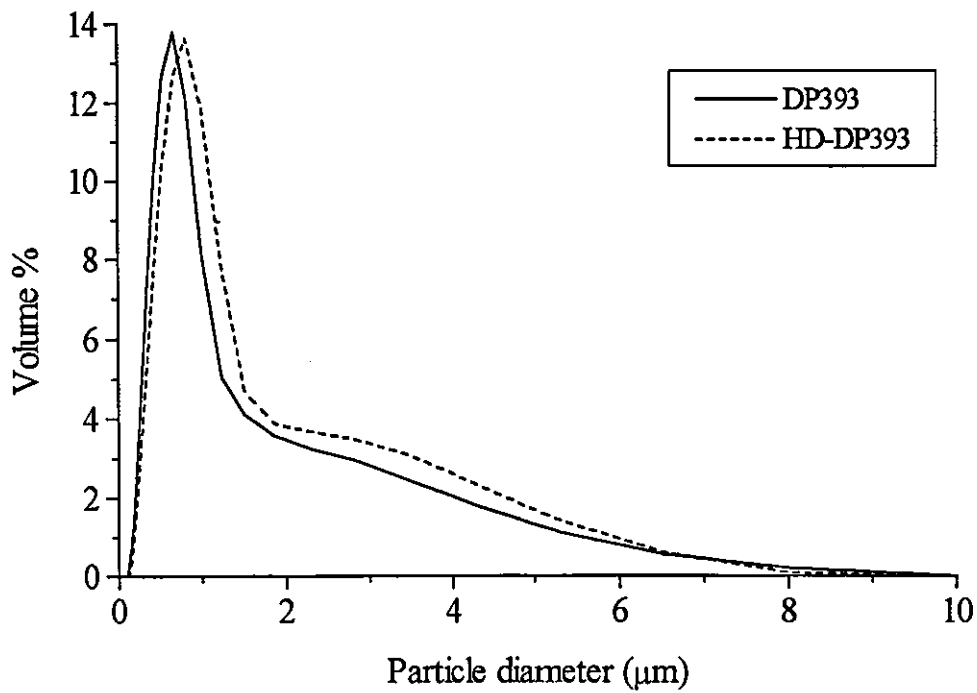


Fig. 5.5 SEM micrograph of HD-DP393 (x220)

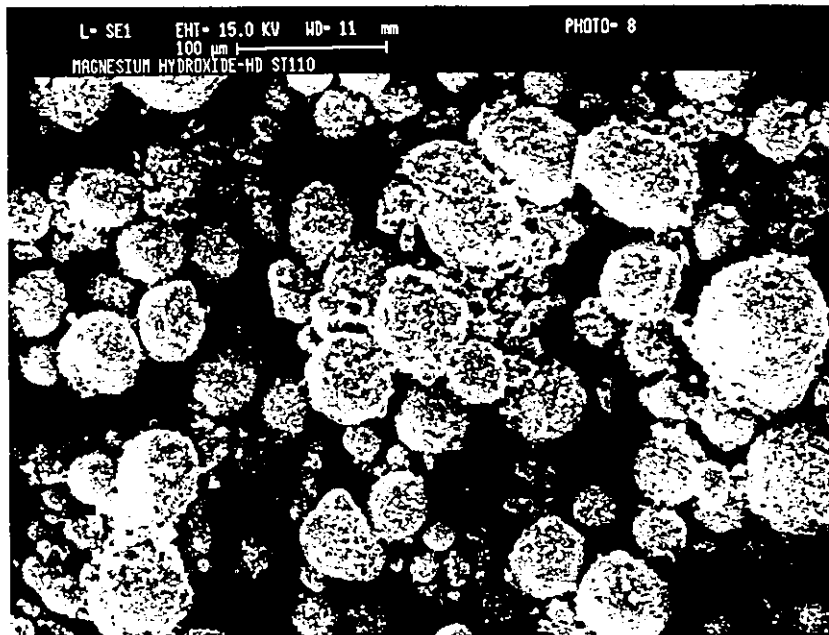


Fig. 4.10 PSD for different LOTS of DP393 fillers

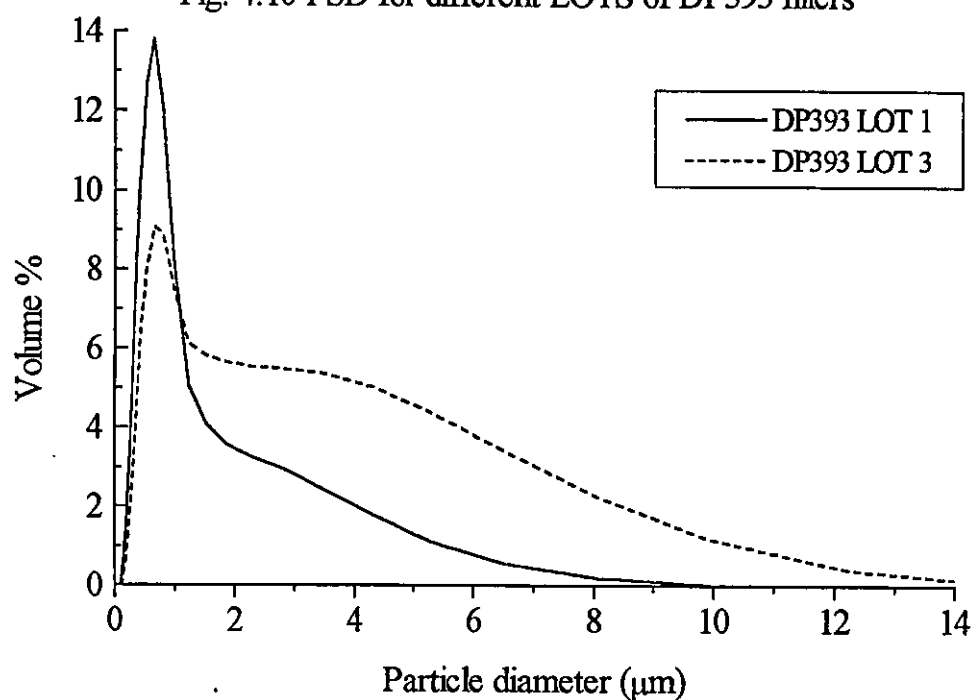
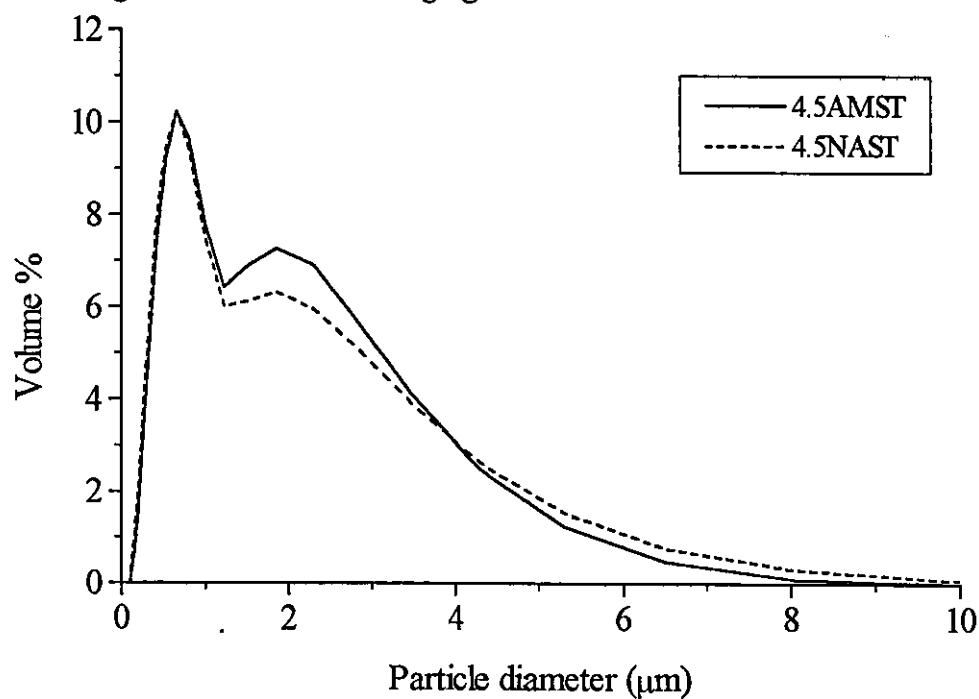


Fig. 4.11 Effect of coating agent on PSD of DP393 LOT 1 fillers



From Figs. 4.11, 4.12 and 4.13, it can be seen that coating agent has a negligible effect on the PSD of DP393 or DP390s fillers.

Fig 4.12 Effect of coating agent on PSD of DP393 LOT 2 fillers

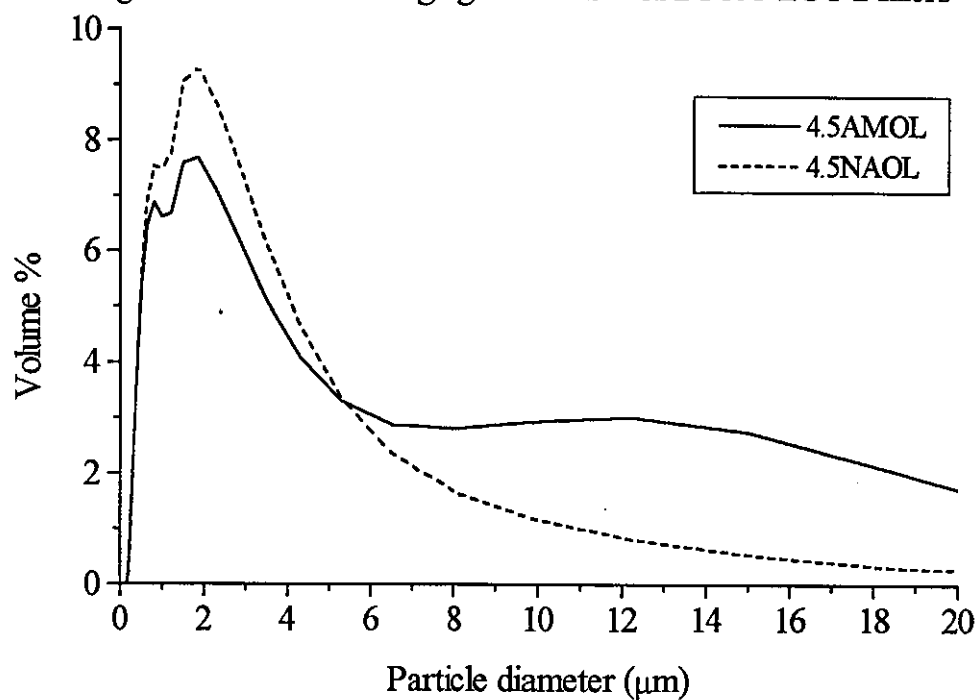


Fig. 4.13 Effect of coating agent on PSD of DP390s LOT 2 fillers

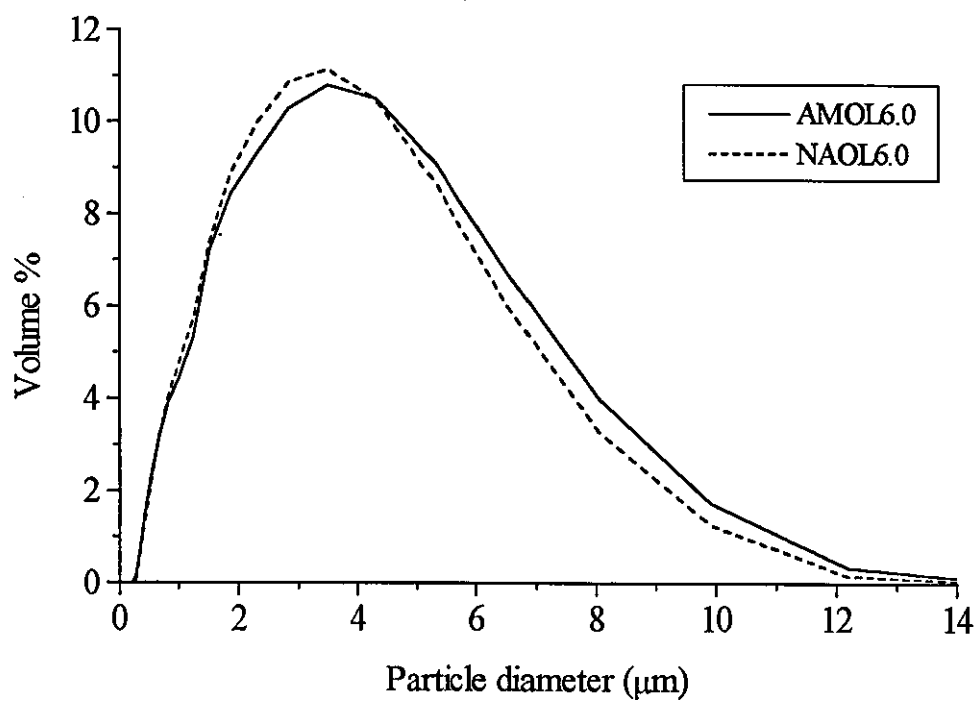


Fig. 4.14 PSD of stearate, oleate and rosin coated DP393

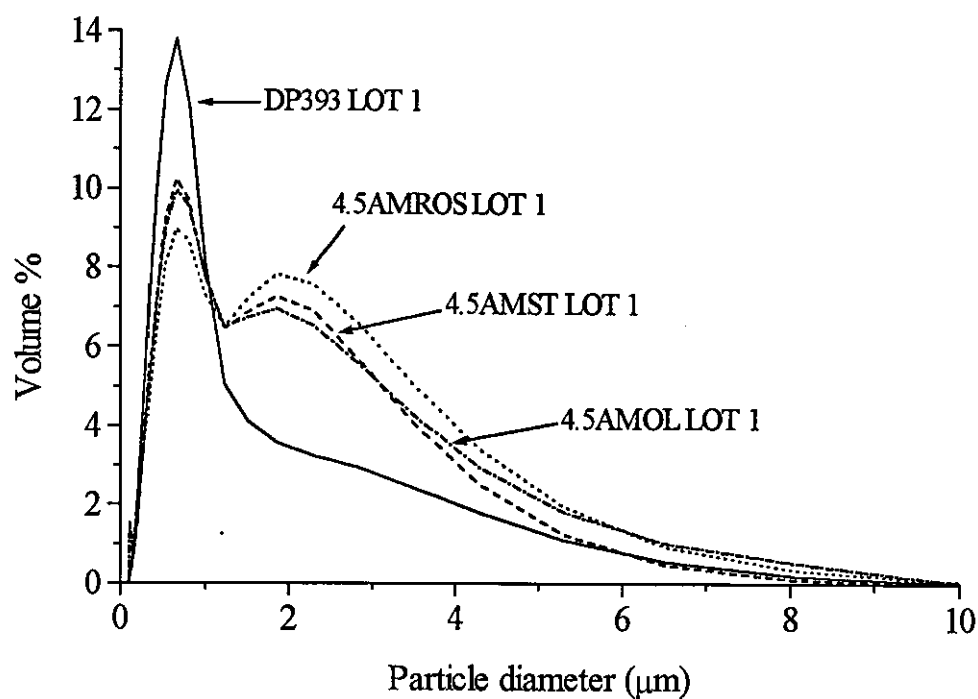
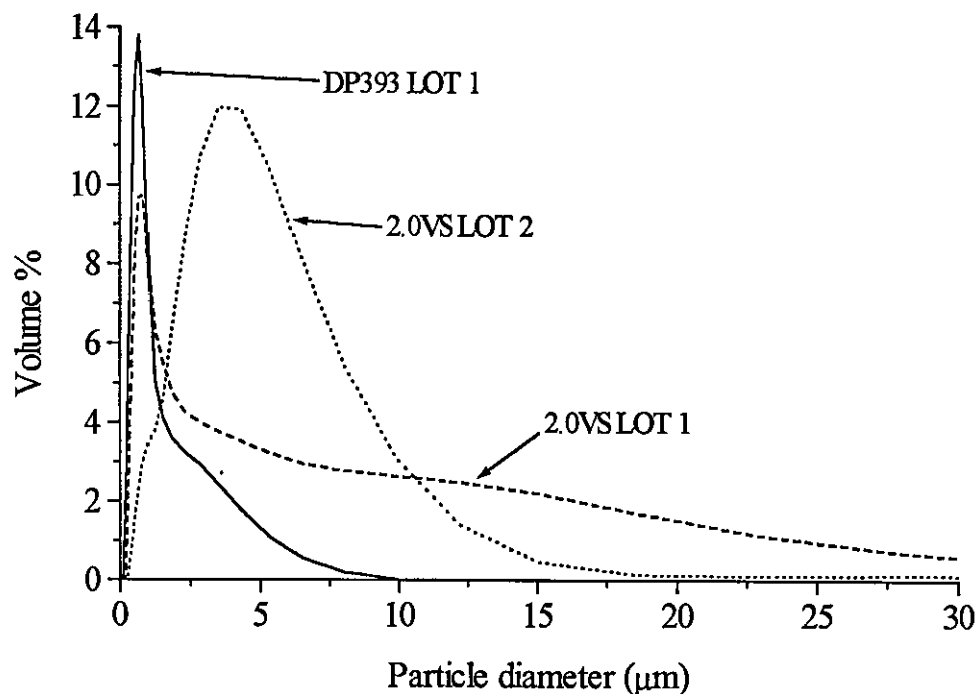


Fig. 4.15 PSD of vinyl silane coated DP393



It can be seen from Fig. 4.14 that the application of a fatty acid coating to DP393 causes agglomeration (indicated by a side mode around 2 μm). The different fatty acids do not affect PSD. From Fig. 4.15, it can be seen that coating method of vinyl silane

influences PSD. Fatty acid coating reduces the mean particle size of DP390s, as depicted in Fig. 4.16.

Fig. 4.16 PSD of stearate and oleate coated DP390s

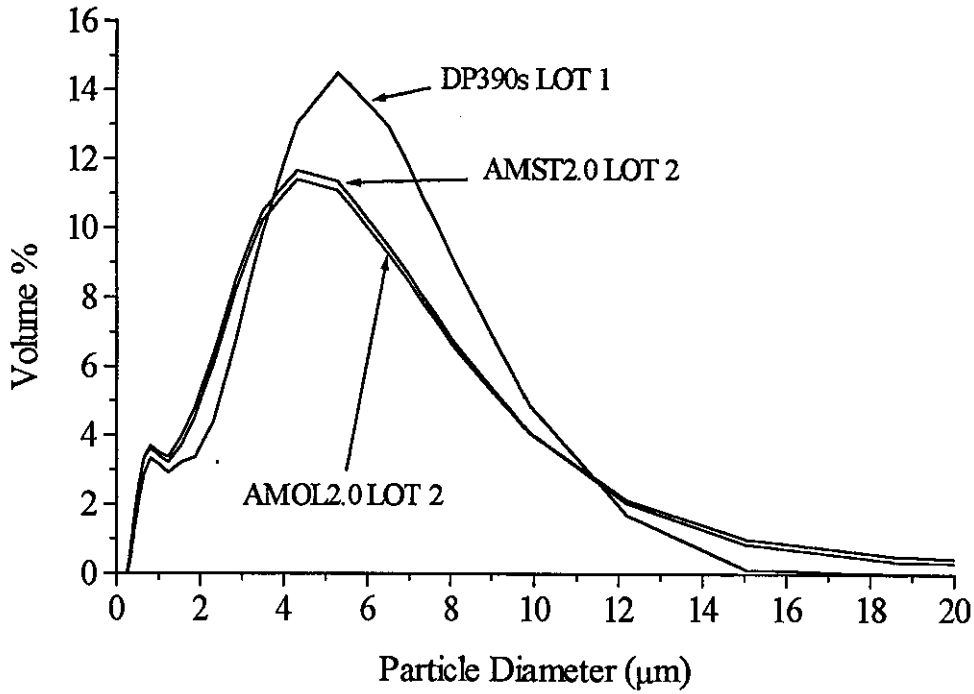


Fig. 4.17 PSD for stearate and oleate coated DP393
LOT 1 fillers at high and low levels

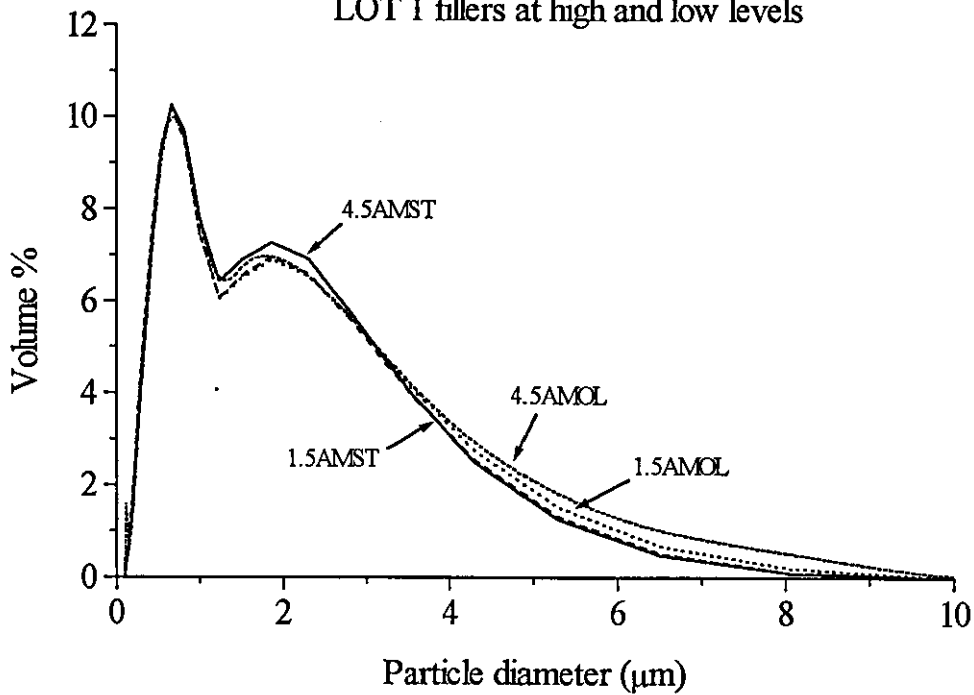
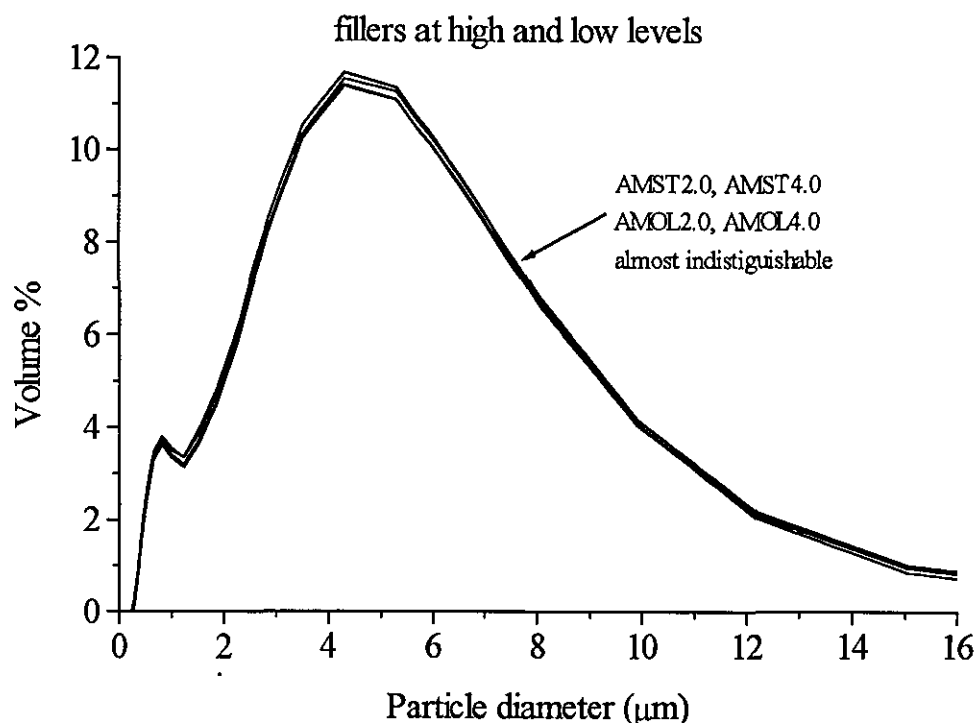


Fig. 4.18 PSD for stearate and oleate coated DP390s LOT 1

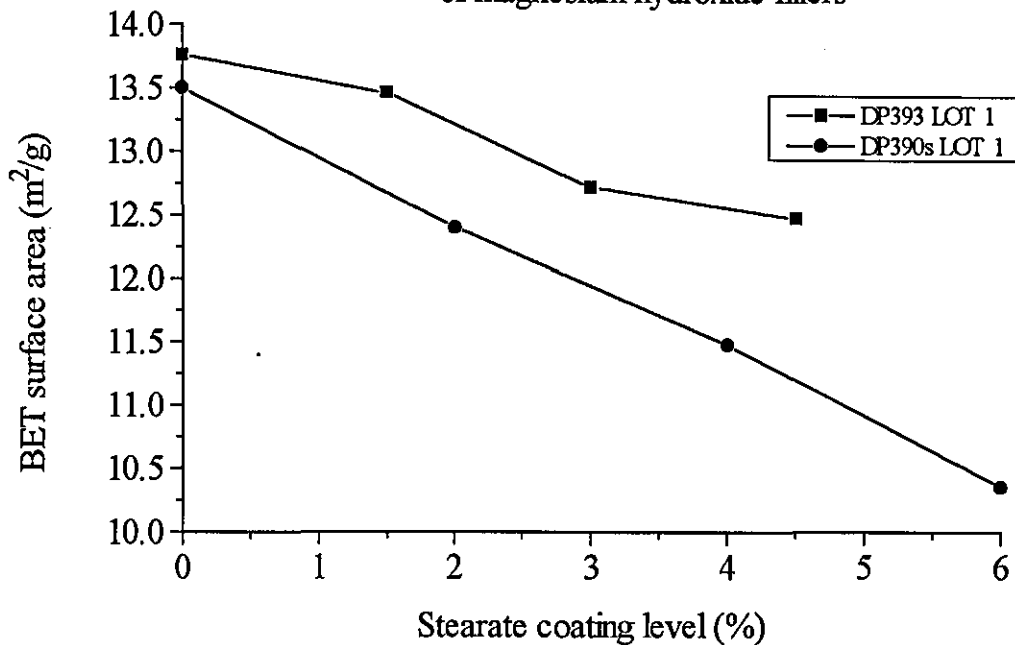


Addition of both low and high fatty acid coating levels has no effect on the particle size distribution of DP393 or DP390s fillers (Figs. 4.17 and 4.18 respectively).

4.1.3 Surface area

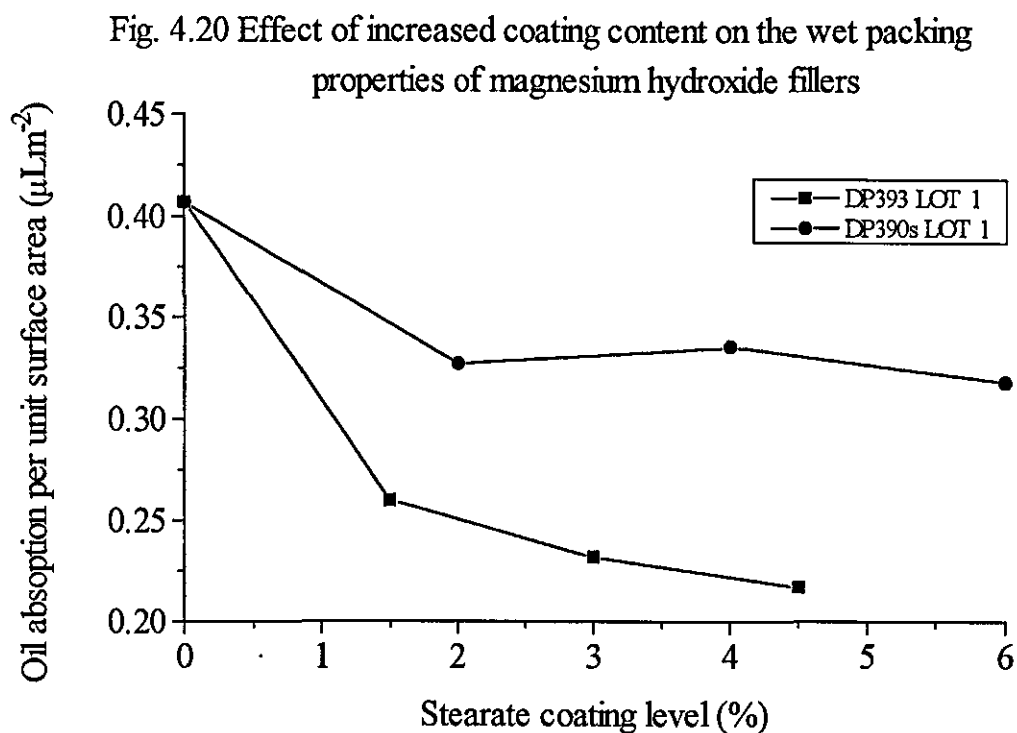
Comprehensive results of BET surface area for all DP393 and DP390s filler types can be found in Appendix C. Both uncoated fillers have almost identical surface areas (approximately $13.5\text{m}^2/\text{g}$) given their different mean secondary particle sizes. This was attributed to the irregular stacks of DP390s primary particles producing a porous structure, whereas DP393 was more regular. Filler coating has the effect of reducing surface area. The filler coatings covered the surface porosity, reducing the amount of micropores onto which the nitrogen gas could be adsorbed. This can be depicted for stearate coated magnesium hydroxide fillers in Fig. 4.19.

Fig. 4.19 Effect of stearate coating level on surface area of magnesium hydroxide fillers



4.1.4 Packing properties

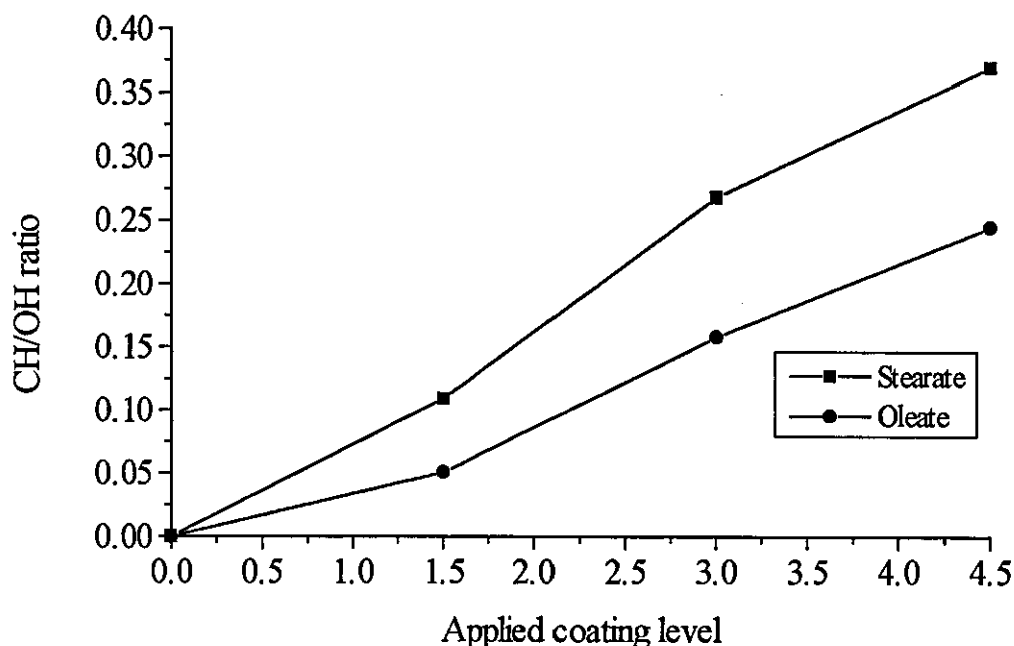
Bulk density defines the dry packing properties of the fillers whereas the oil absorption defines the wet packing properties of the fillers. An average of 3 bulk density determinations were made for each filler, the standard deviation of 3 runs was less than 0.01. The oil absorption values for the uncoated and coated fillers of different morphology were calculated using paraffin oil as the reagent. A mean of three determinations was taken, the standard deviation in all cases was less than 0.1. Results for the DP390s and DP393 fillers can be seen in Appendix D. The bulk densities of DP393 fillers are smaller than DP390s fillers mainly due to the differences in particle size distribution between the different morphologies. Filler coating improves dry packing by increasing inter-particle lubrication. Wet packing properties decrease for both filler types surface area, this being governed by filler coating content. The reduction in wet packing properties of both fillers can be depicted in Fig. 4.20.



4.1.5 FTIR DRIFT analysis

FTIR DRIFT analysis was mainly relevant for quantifying the amount of fatty acid coating agent present on the surface of both morphological types of magnesium hydroxide fillers. The ratioed CH (coating) to OH (substrate) levels for the DP393 and DP390s fillers can be seen in tables 4.8 and 4.9 respectively. A typical trace and the relevant peaks can be found in Appendix E. Due to the surface coating being present as the salt form, it could not be determined whether the fatty acid had fully reacted with the filler surface. However, from Fig. 4.21 it can be seen that an increase in applied coating level produces a larger CH/OH ratio (whether bound or unbound).

Fig. 4.21 Effect of increase in applied fatty acid coating level on CH/OH ratio of DP393 LOT 1 fillers



4.2 Compounding Characteristics

During continuous mixing on both the APV MP2015 and MP30TC intermeshing co-rotating mixing extruders, it was possible to measure the percentage of the maximum compounding torque (and pressures on the MP30TC). However, as machines differed, torques should not be directly compared. The melt state of the extrudates were also assessed visually. Unfilled polypropylene produced a torque of 50-60% and a pressure of 1.31-1.38MPa.

Compounding characteristics of all DP393 and DP390s filled composites can be seen in Figs. 4.1 to 4.4 and 4.5 to 4.6 respectively. In general, uncoated fillers were the most difficult to process (this not being possible for HD-DP393). DP393 filled compounds did compound slightly better than DP390s equivalent DP390s filled compounds. Increased filler levels increases the measured torque and pressure at the die head. Filler coatings improve processing characteristics, particularly for stearate and oleate. This was most pronounced at the highest coating levels. A greater explanation can be found within the rheology sections of chapter 5.

Table 4.1 DP393 LOT 1 uncoated and fatty acid formulations (MP2015)

<i>CODE</i>	<i>LOT</i>	<i>TORQUE</i> (%)	<i>PRESSURE</i>	<i>COMMENT</i>
DP393	1	25-30	Not available	Strand broke
HD-DP393	1	Exceeded	Not available	Would not extrude
1.5AMST	1	9-11	Not available	Continuous strand
3.0AMST	1	7-8	Not available	Continuous strand
4.5AMST	1	6-7	Not available	Continuous strand
1.5AMOL	1	9-10	Not available	Continuous strand
3.0AMOL	1	8-9	Not available	Continuous strand
4.5AMOL	1	7-8	Not available	Continuous strand
4.5NAST	1	7-8	Not available	Continuous strand
4.5NAOL	1	6-7	Not available	Continuous strand
4.5AMROS	1	9-10	Not available	Strand broke

Table 4.2 DP393 LOT 2 fatty acid formulations (MP30TC)

<i>CODE</i>	<i>LOT</i>	<i>TORQUE</i> (%)	<i>PRESSURE</i> (MPa)	<i>COMMENT</i>
1.5NAOL	2	60-70	2.62-2.78	Blockage
3.0NAOL	2	50-70	1.65-1.79	Continuous strand
4.5NAOL	2	40-60	1.38-1.52	Continuous strand
4.5AMOL	2	40-60	1.31-1.45	Continuous strand

Table 4.3 DP393 LOT 3 uncoated and fatty acid formulations (MP30TC)

<i>CODE</i>	<i>LOT</i>	<i>TORQUE</i> (%)	<i>PRESSURE</i> (MPa)	<i>COMMENT</i>
DP393	3	50-60	2.21-2.34	Strand broke
4.5AMOL	3	40-50	1.24-1.31	Continuous strand
4.5AMST	3	35-50	1.10-1.24	Continuous strand
4.5NAOL	3	40-50	1.24-1.31	Continuous strand

Table 4.4 DP393 LOTS 1 & 2 vinyl silane formulations (1A: MP2015, 1B: MP30TC)

<i>CODE</i>	<i>LOT</i>	<i>TORQUE</i> (%)	<i>PRESSURE</i> (MPa)	<i>COMMENT</i>
2.0VS50A	1	7-8	Not available	Continuous strand
2.0VS55A	1	9-10	Not available	Continuous strand
2.0VS60A	1	11-12	Not available	Continuous strand
2.0VS65A	1	15-18	Not available	Continuous strand
2.0VS70A	1	19-20	Not available	Strand broke
2.0VS20B	1	50-60	1.52-1.59	Continuous strand
2.0VS30B	1	50-60	1.52-1.59	Continuous strand
2.0VS40B	1	50-60	1.59-1.65	Continuous strand
2.0VS50B	1	55-65	1.79-1.86	Continuous strand
2.0VS60B	1	45-65	2.00-2.07	Continuous strand
2.0VS70B*	1	25-40	2.41-2.48	Blockage

* 400rpm

Table 4.5 DP390s LOT 1 formulations (MP30TC)

<i>CODE</i>	<i>LOT</i>	<i>TORQUE</i> (%)	<i>PRESSURE</i> (MPa)	<i>COMMENTS</i>
DP390s*	1	35-50	1.86-2.34	Strand broke
AMST2.0	1	60-85	1.38-1.52	Strand broke
AMST4.0	1	60-80	1.38-1.45	Continuous strand
AMST6.0	1	60-80	1.24-1.38	Strand broke
AMOL2.0	1	60-80	1.38-1.52	Continuous strand
AMOL4.0	1	60-80	1.31-1.45	Strand broke

* 400rpm

Table 4.6 DP390s LOT 2 formulations (MP30TC)

<i>CODE</i>	<i>LOT</i>	<i>TORQUE</i> (%)	<i>PRESSURE</i> (MPa)	<i>COMMENT</i>
NAOL1.5	2	70-85	2.14-2.34	Strand broke
NAOL3.0	2	35-55	1.38-1.65	Continuous strand
NAOL4.5	2	40-55	1.17-1.38	Continuous strand
NAOL6.0	2	30-40	0.83-1.24	Continuous strand
AMOL4.0	2	55-65	1.31-1.45	Continuous strand
AMOL6.0	2	30-50	1.31-1.45	Continuous strand

4.3 Characterisation of Pelletised Compounds

The pelletised extrudates were dried and subsequently characterised. Filled compounds had their final filler content and filler volume fraction calculated. Filled and unfilled polypropylene compounds were assessed in terms of their rheological characteristics.

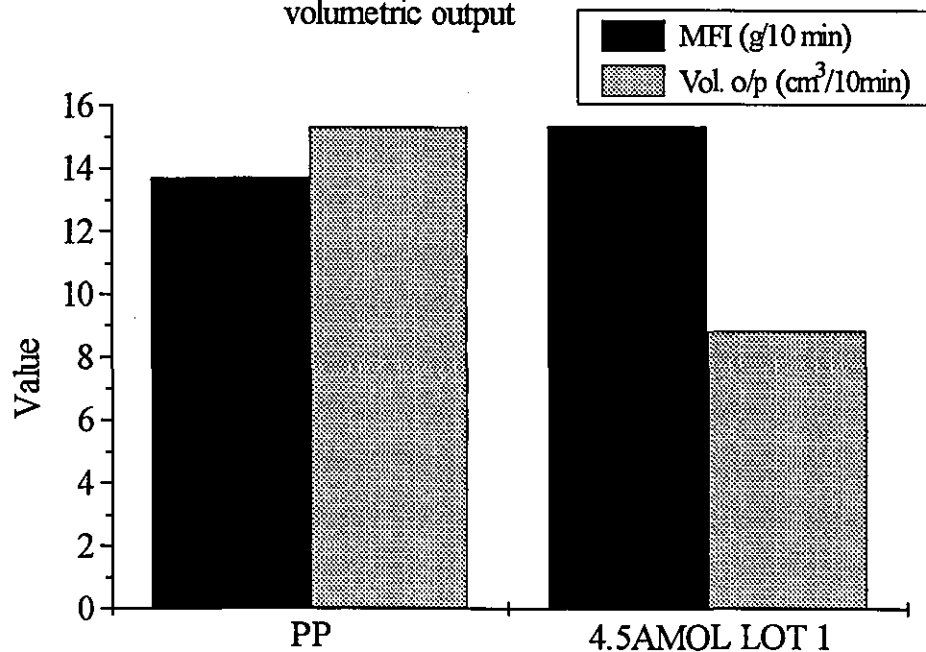
4.3.1 Final filler content

Final filler content and filler volume fraction for all DP393 and DP390s filled composites can be found in Appendix F. In general, DP393 composites were much easier to maintain at the 60% (by weight) loading level. DP390s fillers were more difficult to compound into polypropylene and the desired 60% by weight loading level, this level in actual fact never being attained. The reason for the reduced level of DP390s fillers was caused by the fillers general inferior packing properties to those of DP393. The higher bulk densities promoted bridging in the hopper and in general poor, flow properties into the extruder. The lower wet packing properties restricted wet out with the polypropylene melt.

4.3.2 Melt flow index

Melt flow index was calculated using the standard method [109]. Results of three determinations (per run) can be seen in Appendix G. Values in brackets are the standard deviations. Volumetric output is also provided in Appendix G. When filler loadings are high, the densities of the composites are higher than that of the unfilled polypropylene. The melt flow rates can be higher than that of the virgin polymer, indicating that the viscosity is lower. This can be depicted below in Fig. 4.22. Volumetric output provided a more real measure of polymer flow. However, this will still be influenced by the presence of the dense filler and by any lubricants (coatings). The MFI for uncoated filled compounds (DP393 LOTS 1& 2 and DP390s) was zero. This value was recorded because the flow rate per unit time was too low to measure using the standard equipment (even using a heavier 10kg charge weight). Increasing the preheat time to permit flow would cause ambiguities since the polymer would degrade within the heating chamber of the MFI unit.

Fig. 4.22 Bar chart showing discrepancies between MFI and volumetric output



4.3.3 Capillary rheometry

Measured values of shear stresses (τ_w) for a broad range of apparent shear rates ($\dot{\gamma}_A$), between 24 and 1200 s^{-1} , were used to construct shear flow curves and can be found in Appendix H.

Fig. 4.23 Shear flow curves for DP393 and DP390s filled PP

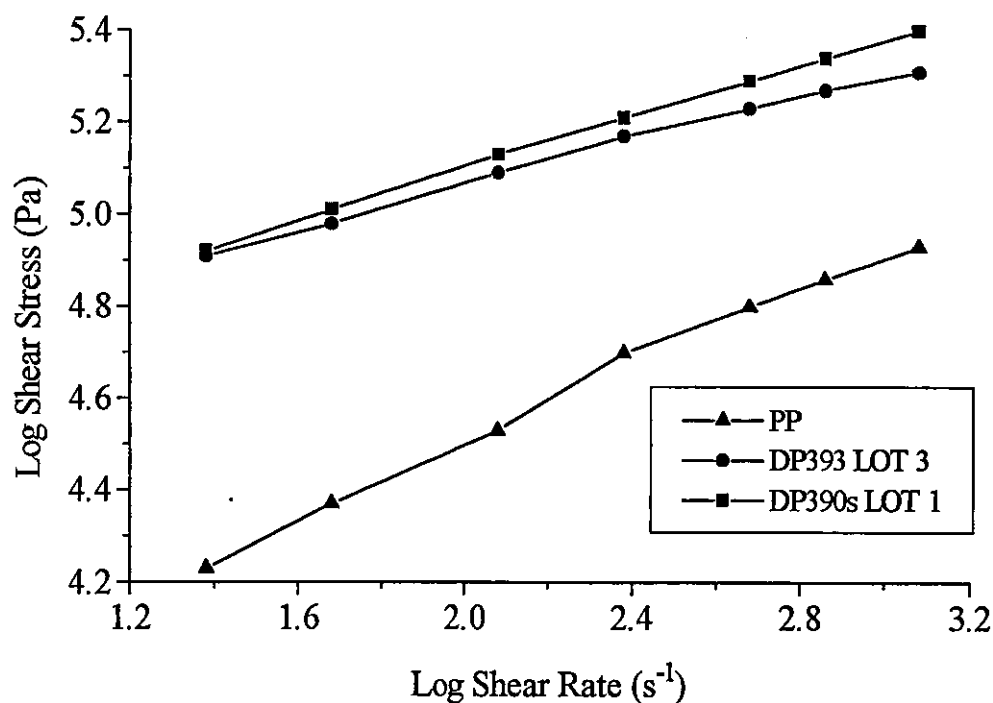
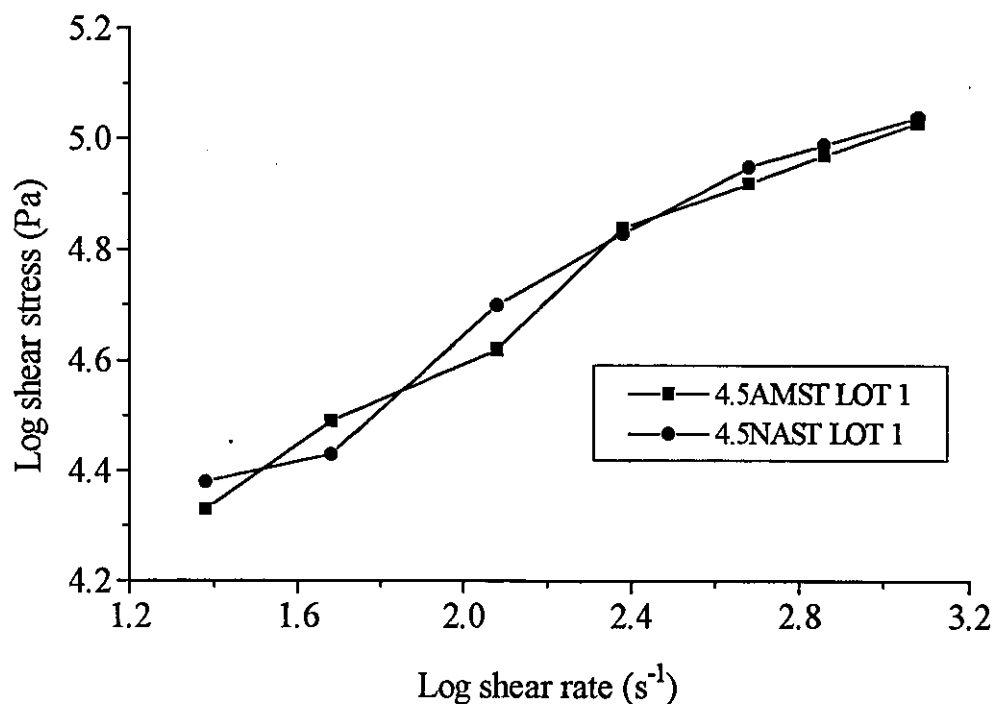


Fig. 4.24 Shear flow curves for DP393 with stearate coating agents



Addition of 60% $\text{Mg}(\text{OH})_2$ significantly increases the melt viscosity of PP, DP390s slightly more so than DP393 at higher shear rates (Fig. 4.23). However, altering the coating agent causes no change on the rheological properties of PP for either DP393 or DP390s (Figs. 4.24, 4.25 and 4.26 respectively) for stearate or oleate coating types.

Fig. 4.25 Shear flow curves for DP393 with oleate coating agents

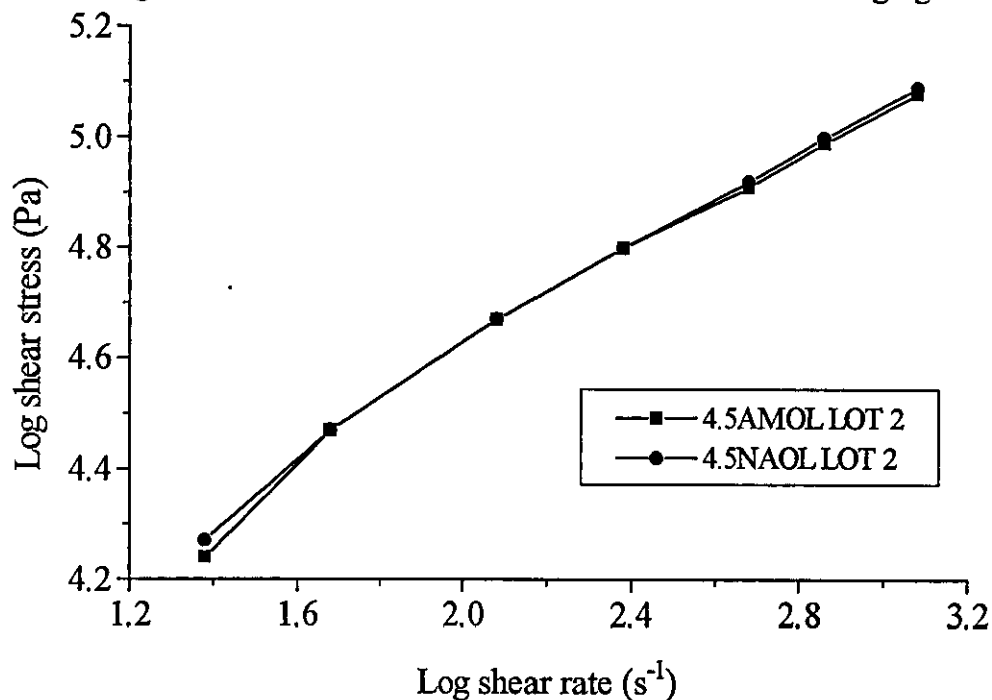


Fig. 4.26 Shear flow curve for DP390s with oleate coating agents

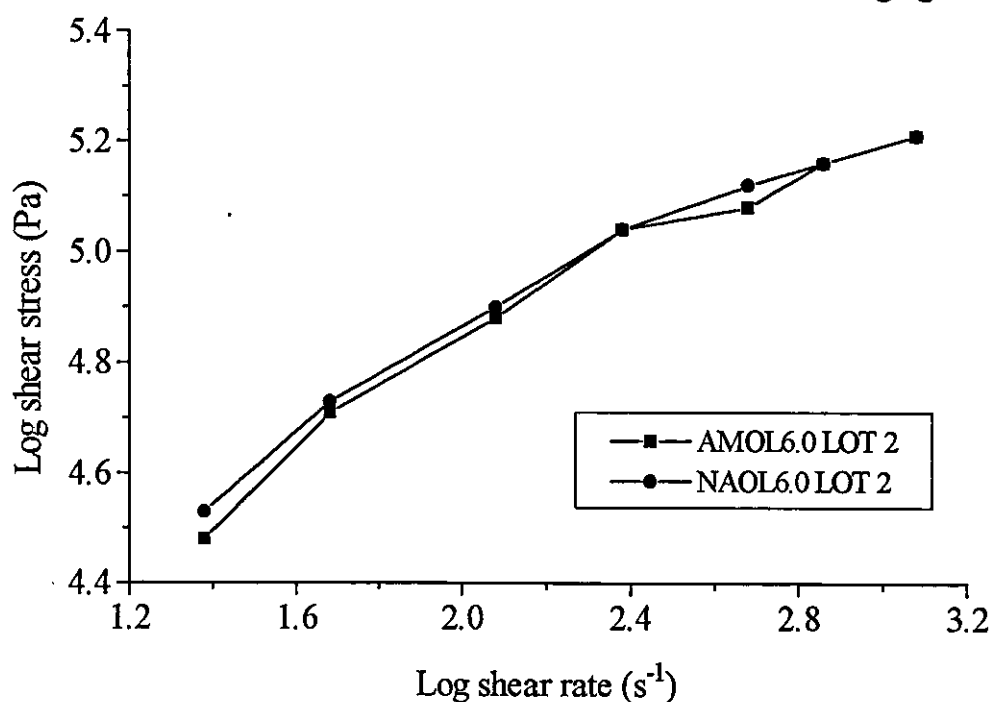
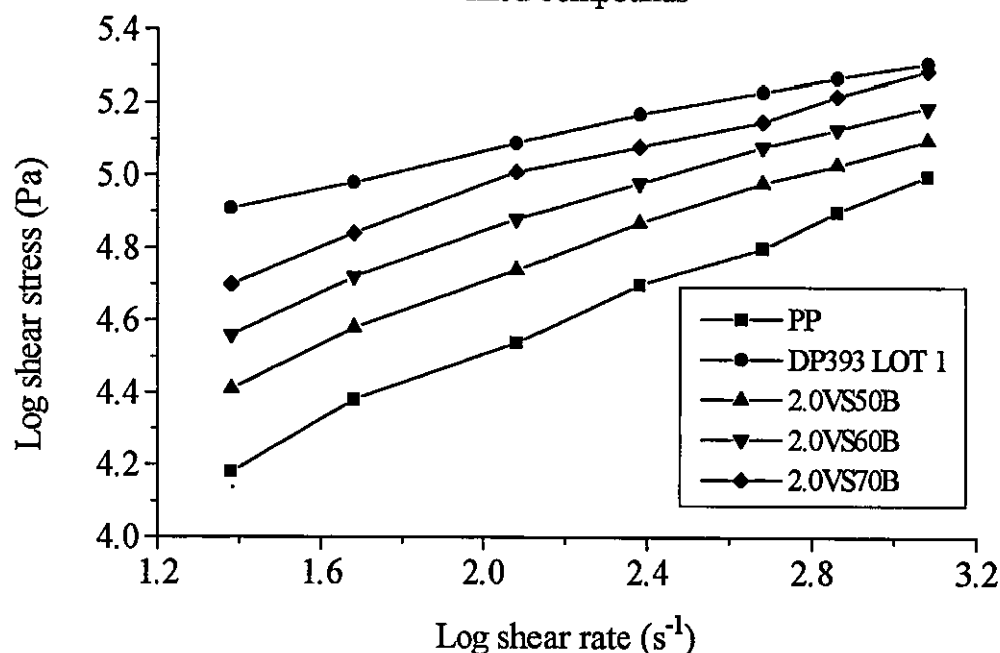


Fig. 4.27 Shear flow curves for vinyl silane coated DP393 filled compounds



Addition of high levels (>50%) of $Mg(OH)_2$ increases the melt viscosity of PP (Fig. 4.27). Coating agents reduce this below that of the uncoated fillers. Rosin gum has least effect, silane is intermediate. Stearate and oleate coatings have similar effects and reduce the melt viscosity towards that of unfilled PP (Figs. 4.28, 4.29 and 4.30).

Fig. 4.28 Shear flow curves of stearate, oleate, rosin and silane coated DP393 filled compounds

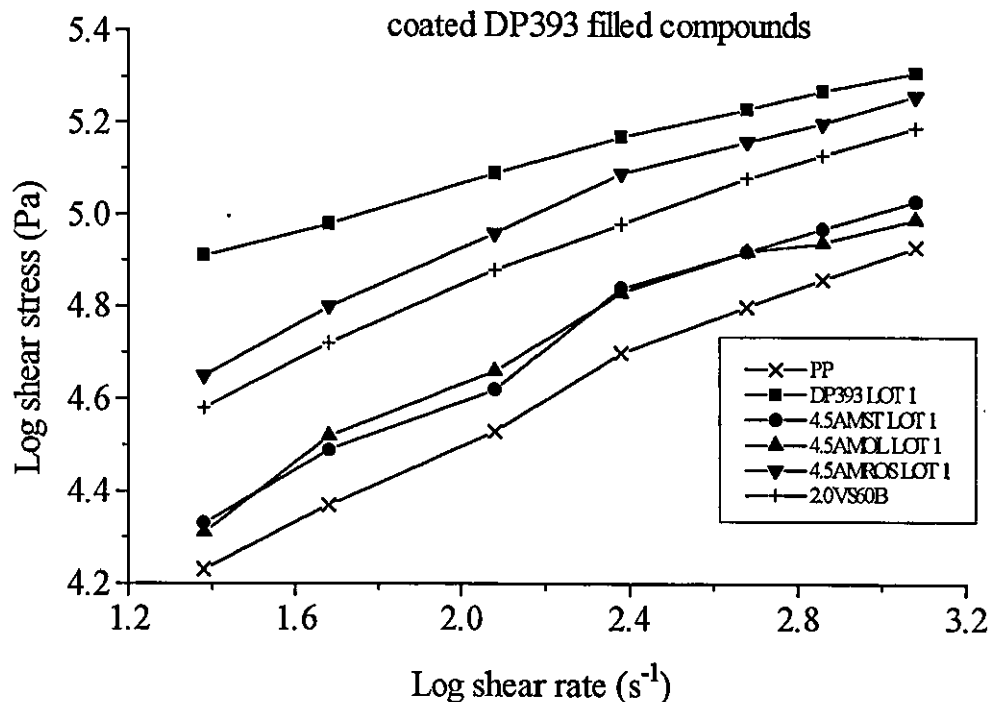


Fig. 4.29 Shear flow curves for stearate and oleate coated DP390s compounds

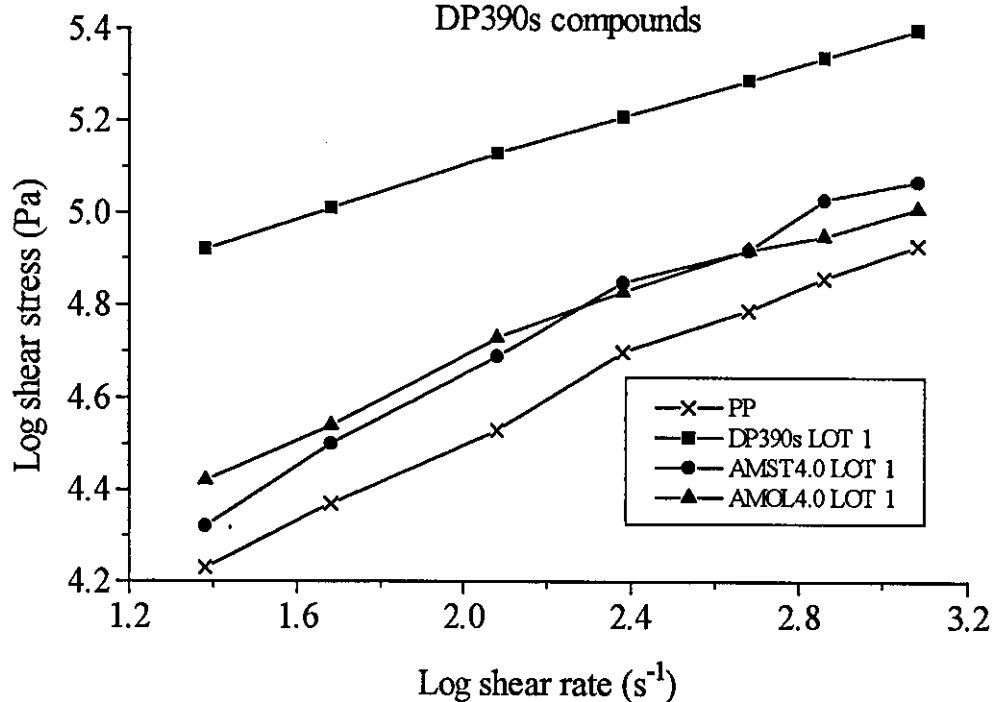


Fig. 4.30 Effect of increased oleate coating level on the rheological properties of DP393 filled PP

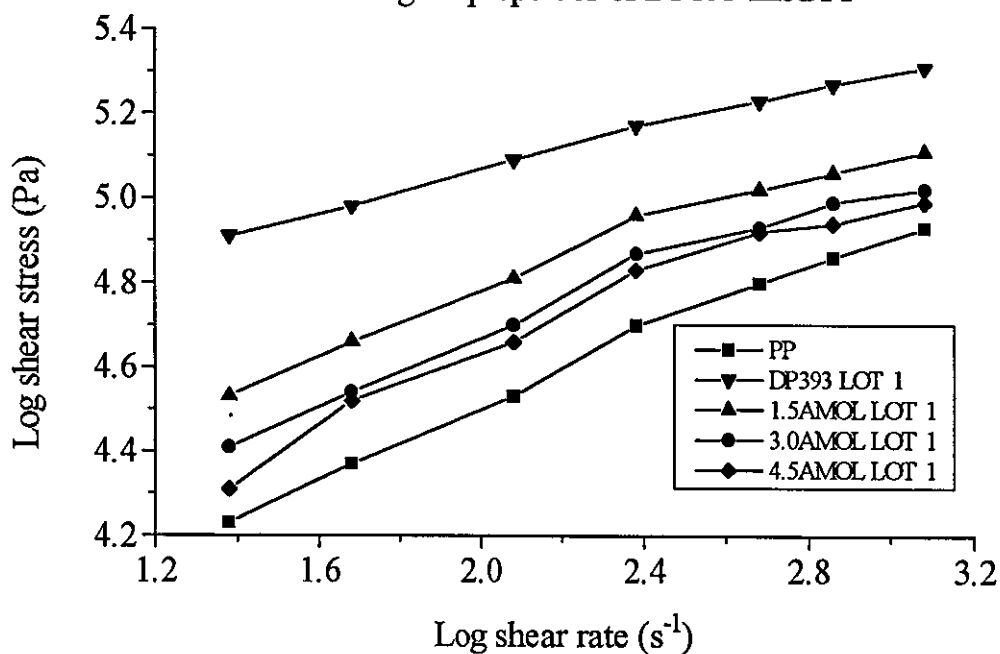
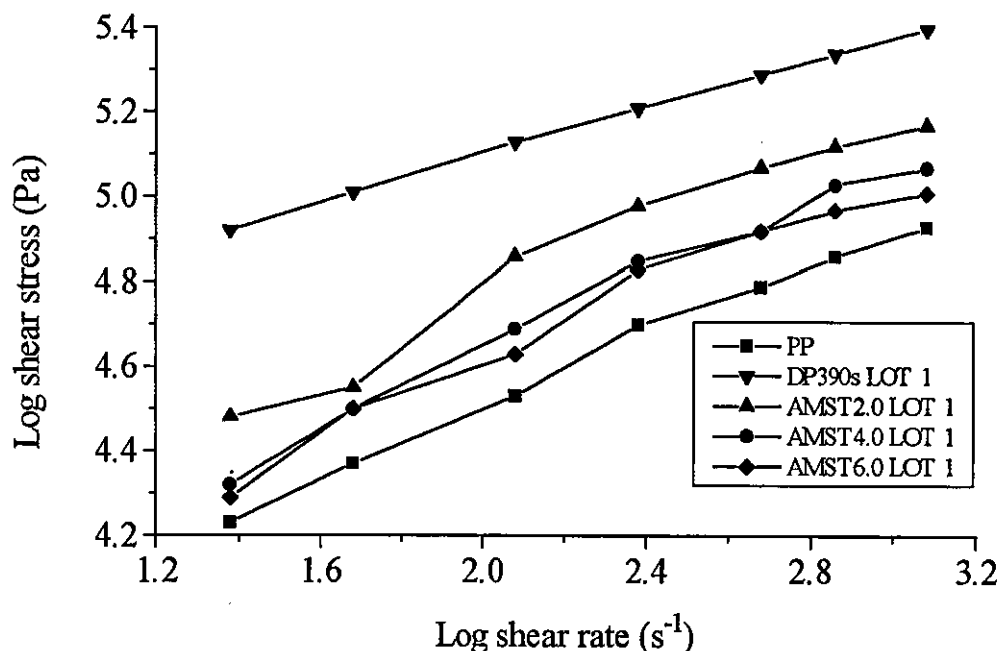


Fig. 4.31 Effect of increased stearate coating level on the rheological properties of DP390s filled PP



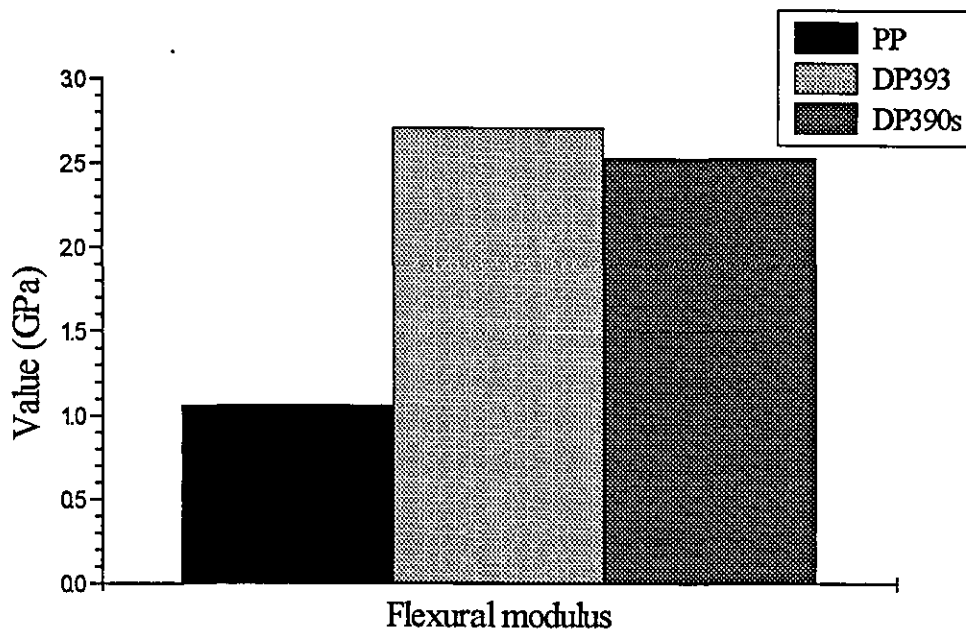
Addition of higher levels of oleate and stearate coating significantly reduced the melt viscosity of DP393 and DP390s filled compounds towards that of unfilled PP (Figs. 4.30 and 4.31).

4.4 Mechanical Properties

The mechanical properties of the unfilled, uncoated filled and coated filled composites were assessed in terms of their flexural and impact properties. These can be seen in sections 4.4.1 and 4.4.2 respectively.

4.4.1 Flexural properties

The flexural properties were analysed in terms of flexural modulus, flexural strength and extension to break, described in section 3.5.1. The results for all of the composites can be found in Appendix I, along with the method of calculating flexural parameters.

Fig. 4.32 Change in PP modulus with 55% addition of $Mg(OH)_2$ 

From Fig. 4.32, it can be seen that the addition of hard, rigid magnesium hydroxide fillers increases the flexural modulus of PP by over a factor of 2.5. This is more significant for the platey DP393 filler type.

Table 4.7 Effect of stearate coating agent on flexural properties of DP393 composites.

CODE	Flexural Modulus (GPa)	Flexural Strength (MPa)	Extension @ break (mm)
4.5AMST LOT 1	2.37 (0.10)	26.2 (0.8)	3.25 (0.47)
4.5NAST LOT 1	2.61 (0.04)	2.79 (0.7)	2.77 (0.30)

In Table 4.7, both composites contain similar filler loading levels. The differences in flexural properties have been attributed to residual (insoluble) sodium salts present within the matrix.

Table 4.8 Comparison of DP393 LOT 1 uncoated and coated fillers.

<i>CODE</i>	<i>Flexural Modulus (GPa)</i>	<i>Flexural Strength (MPa)</i>	<i>Extension @ break (mm)</i>
DP393	3.27 (0.06)	29.0 (1.2)	2.15 (0.15)
4.5AMST	2.37 (0.01)	26.2 (0.8)	3.25 (0.47)
4.5AMOL	1.92 (0.06)	25.5 (0.1)	2.62 (0.15)
4.5AMROS	4.14 (0.12)	31.3 (1.0)	1.44 (0.13)
2.0VS60B*	3.19 (0.11)	31.9 (0.7)	2.67 (0.26)

* 157 days post moulding

Table 4.9 Comparison of DP390s LOT 1 uncoated and coated fillers.

<i>CODE</i>	<i>Flexural Modulus (GPa)</i>	<i>Flexural Strength (MPa)</i>	<i>Extension @ break (mm)</i>
DP390s	2.53 (0.08)	31.4 (0.5)	3.70 (0.31)
AMST2.0	3.12 (0.05)	26.5 (0.5)	24.5 (0.05)
AMOL2.0	3.17 (0.04)	26.2 (0.2)	2.20 (0.04)

From Tables 4.8 and 4.9 it can be seen that fatty acid coatings decrease interfacial adhesion at the PP/Mg(OH)₂ interface when compared to the uncoated filler. The rosin gum and vinyl silane increase interfacial adhesion but reduced extension to failure with the rosin coating was caused by filler agglomeration.

Table 4.10 Comparison of fatty acid coating level for DP393 LOT 1 fillers.

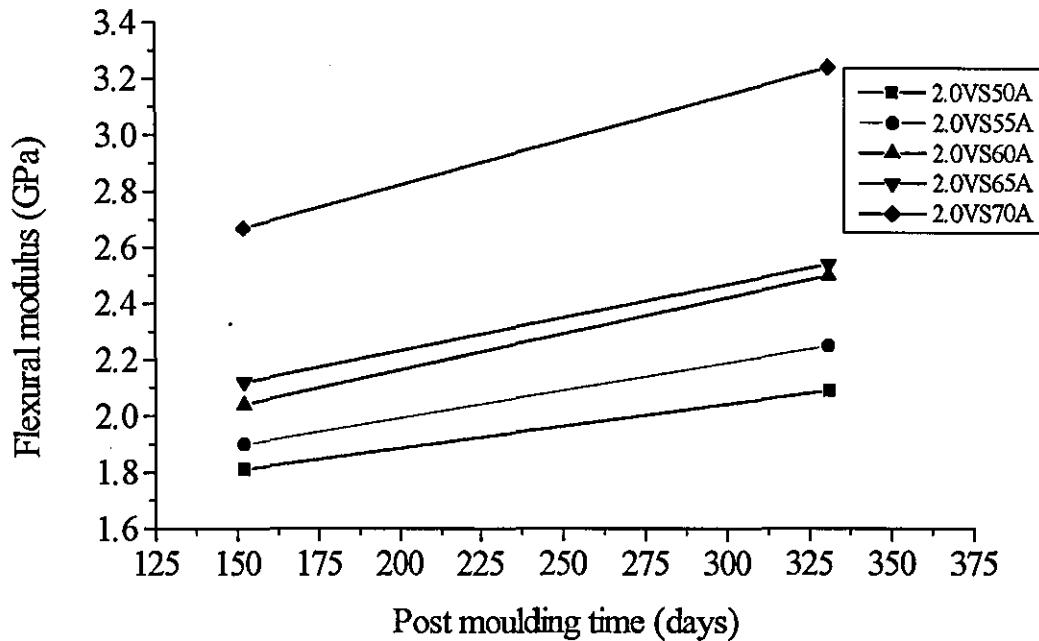
<i>CODE</i>	<i>Flexural Modulus (GPa)</i>	<i>Flexural Strength (MPa)</i>	<i>Extension @ break (mm)</i>
1.5AMST	2.70 (0.08)	28.2 (1.00)	2.13 (0.09)
3.0AMST	2.49 (0.09)	27.3 (0.8)	2.97 (0.26)
4.5AMST	2.37 (0.01)	26.2 (0.8)	3.25 (0.47)
1.5AMOL	2.63 (0.01)	29.4 (0.6)	2.44 (0.09)
3.0AMOL	2.07 (0.03)	26.3 (1.0)	2.33 (0.06)
4.5AMOL	1.92 (0.06)	25.5 (0.1)	2.62 (0.15)

Table 4.11 Comparison of fatty acid coating level for DP390s fillers

CODE	Flexural Modulus (GPa)	Flexural Strength (MPa)	Extension @ break (mm)
AMST2.0 LOT 1	3.12 (0.05)	26.5 (0.5)	2.45 (0.04)
AMST4.0 LOT 1	2.53 (0.03)	26.6 (0.3)	5.99 (0.10)
AMST6.0 LOT 1	1.89 (0.03)	26.3 (0.6)	9.10 (0.15)
NAOL1.5 LOT 2	3.44 (0.10)	33.0 (0.7)	2.73 (0.28)
NAOL3.0 LOT 2	2.66 (0.12)	30.1 (0.6)	4.14 (0.72)
NAOL4.5 LOT 2	2.45 (0.14)	29.6 (0.6)	5.04 (0.34)
NAOL6.0 LOT 2	2.31 (0.09)	30.1 (0.7)	7.42 (0.64)

From Tables 4.10 and 4.11 it can be seen that an increase in fatty acid coating levels decreases mechanical properties, suggesting a decrease in interfacial adhesion of the composites.

Fig. 4.33 Change in flexural modulus with time for vinyl silane coated DP393 composites



Flexural modulus can be seen to increase as a function of post moulding time for vinyl silane coated DP393 filled composites comprised of different filler levels (Fig. 4.33).

4.4.2 Impact testing.

The impact properties were analysed in terms of peak impact force, peak impact energy and peak deflection, described in section 3.5.1.2. Total impact energies are not included due to the inconclusive end point for the vast array of formulations. The propagation phase of the impact trace was wavy in many cases, and determining the true end point of the test was difficult. The results for all of the composites are given in Appendix J along with test conditions. Standard deviations are given in brackets. Total impact properties were omitted from the results section.

Table 4.12 Effect of 55% magnesium hydroxide addition on impact properties of PP

<i>Code</i>	<i>Peak impact force (N)</i>	<i>Peak impact energy (mJ)</i>	<i>Peak deflection (mm)</i>
PP	507 (64)	312 (77)	1.48 (0.15)
DP393	239 (58)	80 (15)	0.82 (0.82)
DP390s	207 (31)	75 (15)	0.74 (0.07)

Addition of 55% magnesium hydroxide significantly reduces the toughness of polypropylene Table 4.12). Both fillers act as stress concentrators but there is less difference between the different morphologies than expected.

Table 4.13 Effect of coating agent on impact properties of DP393 fillers

<i>Code</i>	<i>Peak impact force (N)</i>	<i>Peak impact energy (mJ)</i>	<i>Peak deflection (mm)</i>
4.5AMST LOT 1	162 (10)	59 (2)	0.80 (0.01)
4.5NAST LOT 1	147 (5)	51 (2)	0.80 (0.02)
4.5AMOL LOT 2	98 (14)	31 (5)	0.66 (0.05)
4.5NAOL LOT 2	106 (9)	33 (2)	0.66 (0.05)

From Table 4.13, it can be seen that when loading levels are similar, altering the fatty acid coating agent has a negligible effect on the toughness of magnesium hydroxide filled PP composites.

Table 4.14 Comparison of DP393 LOT 1 uncoated and coated fillers

<i>Code</i>	<i>Peak impact force (N)</i>	<i>Peak impact energy (mJ)</i>	<i>Peak deflection (mm)</i>
DP393	249 (26)	85 (16)	0.74 (0.08)
4.5AMST	162 (10)	59 (2)	0.80 (0.01)
4.5AMOL	159 (7)	54 (6)	0.80 (0.04)
4.5AMROS	92 (3)	29 (2)	0.60 (0.03)
2.0VS60B*	143 (0.11)	40 (5)	0.63 (0.26)

* 173 days

Table 4.14 shows the impact properties of polypropylene composites loaded with 60% DP393 fillers. Uncoated fillers produce superior properties, filler coating causes a decline. Fatty acids (stearate and oleate) give similar effects and due to their lubrication effects were the best coatings. Vinyl silane was intermediate whereas the rosin gives an inferior performance.

Table 4.15 Comparison of DP390s LOT 1 uncoated and coated fillers

<i>Code</i>	<i>Peak impact force (N)</i>	<i>Peak impact energy (mJ)</i>	<i>Peak deflection (mm)</i>
DP390s	207 (31)	70 (15)	0.74 (0.07)
AMST2.0	105 (5)	30 (2)	0.57 (0.05)
AMOL2.0	115 (9)	33 (4)	0.61 (0.03)

Fatty acid coating of DP390s reduces the toughness, but both have similar properties (Table 4.15).

Table 4.16 Effect of coating level on stearate coated DP393 LOT 1 fillers

<i>Code</i>	<i>Peak impact force (N)</i>	<i>Peak impact energy (mJ)</i>	<i>Peak deflection (mm)</i>
DP393	249 (26)	85 (15)	0.74 (0.08)
1.5AMST	117 (3)	33 (2)	0.62 (0.01)
3.0AMST	146 (10)	49 (2)	0.75 (0.01)
4.5AMST	162 (10)	59 (2)	0.80 (0.01)

Table 4.17 Effect of coating level on oleate coated DP390s LOT 1 fillers

<i>Code</i>	<i>Peak impact force (N)</i>	<i>Peak impact energy (mJ)</i>	<i>Peak deflection (mm)</i>
DP390s	207 (31)	70 (15)	0.74 (0.07)
AMOL2.0	105 (5)	30 (2)	0.57 (0.05)
AMOL4.0	142 (7)	41 (4)	0.61 (0.03)
AMOL6.0	157 (10)	48 (5)	0.66 (0.01)

From Tables 4.16 and 4.17, it can be seen that progressive fatty acid coating of magnesium hydroxide improves the toughness the composites towards that of the uncoated. DP393 fillers are slightly better than DP390s fillers.

4.5 Thermal Analysis

Selected composites have been thermally characterised utilising three thermal analysis techniques. These are differential scanning calorimetry (DSC), dynamic mechanical thermal analysis (DMTA) and Vicat softening point. These results can be seen below in sections 4.5.1, 4.5.2 and 4.5.3 respectively. A typical DSC and DMTA trace can be seen in Appendix K and L respectively.

4.5.1 Differential Scanning Calorimetry (DSC)

Composites were analysed by DSC at least 7 days after moulding. A mean of three determinations is given. Selected composites were further quantified using parameters determined by Maiti et al [103] (see Appendix K).

Table 4.18 Thermal properties of polypropylene

<i>CODE</i>	<i>T_m (°C)</i>	<i>%XL</i>	<i>T_c (°C)</i>	<i>%RC</i>
PP	170	36.8	119	37.9

Table 4.19 Thermal properties of DP393 LOT 1 fatty acid composites

<i>CODE</i>	<i>T_m</i> (°C)	<i>%XL</i>	<i>T_c</i> (°C)	<i>%RC</i>
DP393	167	40.2	133	43.6
1.5AMST	167	39.5	125	42.6
3.0AMST	167	41.4	124	43.9
4.5AMST	168	44.0	124	43.3
1.5AMOL	167	38.7	125	40.9
3.0AMOL	167	39.1	124	42.6
4.5AMOL	167	39.5	123	43.1
4.5NAST	168	42.6	125	43.2
4.5NAOL	168	39.4	126	41.9
4.5AMROS	166	40.3	120	40.3

Table 4.20 Thermal properties of DP393 LOT 2 fatty acid composites

<i>CODE</i>	<i>T_m</i> (°C)	<i>%XL</i>	<i>T_c</i> (°C)	<i>%RC</i>
1.5NAOL	168	35.2	128	35.2
3.0NAOL	168	33.4	127	38.3
4.5NAOL	169	32.1	127	36.2
4.5AMOL	168	32.3	126	33.7

Table 4.21 Thermal properties of DP393 LOT 3 fatty acid composites

<i>CODE</i>	<i>T_m</i> (°C)	<i>%XL</i>	<i>T_c</i> (°C)	<i>%RC</i>
DP393	166	35.7	131	40.3
4.5AMOL	167	33.4	121	33.4
4.5NAOL	168	33.7	123	35.2
4.5AMST	168	29.2	122	32.7

Table 4.22 Thermal properties of DP390s LOT 1 fatty acid composites

<i>CODE</i>	<i>T_m</i> (°C)	<i>%XL</i>	<i>T_c</i> (°C)	<i>%RC</i>
DP390s	166	35.8	132	35.4
AMST 2.0	167	39.1	123	39.2
AMST 4.0	167	37.4	123	40.0
AMST 6.0	168	37.0	120	36.8
AMOL2.0	167	38.2	124	39.7
AMOL4.0	168	37.2	121	39.0

Table 4.23 Thermal properties of DP390s LOT 2 fatty acid composites

<i>CODE</i>	<i>T_m</i> (°C)	<i>%XL</i>	<i>T_c</i> (°C)	<i>%RC</i>
NAOL1.5	167	34.7	127	38.0
NAOL3.0	167	34.8	125	38.5
NAOL4.5	167	31.9	126	35.8
NAOL6.0	168	31.8	122	35.5
AMOL4.0	168	31.8	120	35.5
AMOL6.0	167	32.2	124	35.0

From Tables 4.18, 4.19 and 4.22, the crystallisation onset temperature, T_c , is increased by the addition of magnesium hydroxide filler. This is reduced with an increase in filler coating level. DP393 fillers produce slightly higher crystallinity contents than DP390s fillers. From Tables 4.24, 4.25 and 4.26, it can be seen that unfilled polypropylene has the slowest crystallisation rates and has the widest crystallite size distribution. Uncoated fillers produce the fastest crystallisation rates and narrowest crystallite distributions. These tend back towards that of the unfilled polypropylene with an increase in filler coating level.

Table 4.24 Maiti [103] parameters for some DP393 LOT 1 composites

CODE	(T _c -T _p)	S _i	ΔW
DP393	4.7	10.4	26.0
1.5AMST	2.3	57.3	12.5
3.0AMST	3.3	57.3	13.5
4.5AMST	3.7	42.8	14.5
4.5NAST	4.0	19.1	16.5
1.5AMOL	3.1	86.0	13.0
3.0AMOL	3.7	21.2	16.5
4.5AMOL	3.9	32.0	16.0
4.5NAOL	3.3	66.8	15.5
4.5AMROS	3.9	21.4	17.0

Table 4.25 Maiti [103] parameters for some DP390s LOT 1 composites

CODE	(T _c -T _p)	S _i	ΔW
DP390s	6.1	9.5	25.5
AMST2.0	2.4	144.6	13.0
AMST4.0	2.1	42.8	12.0
AMST6.0	4.3	19.1	16.5
AMOL2.0	1.9	163.2	11.0
AMOL4.0	3.1	81.8	12.5

Table 4.26 Maiti [103] parameters for polypropylene

CODE	(T _c -T _p)	S _i	ΔW
PP	7.2	8.8	25.0

For the case of the vinyl silane coated DP393 fillers, much thermal analysis work was performed to investigate whether crystallisation effects were causing the change in mechanical properties with time. This was done long-term for LOT 1A and 1B filled composites and short-term for the LOT 2 batch mixed compounds. Maiti analysis [103] was also performed on some of these compounds.

Table 4.27 Onset temperature (°C) of vinyl silane coated DP393 LOT 1A composites

CODE	29 days	56 days	71 days	305 days
2.0VS50A	126	125	126	125
2.0VS55A	126	125	126	126
2.0VS60A	126	127	126	127
2.0VS65A	128	129	128	128
2.0VS70A	128	126	127	129

Table 4.28 % Crystallinity, XL (on heating) of vinyl silane coated DP393 LOT 1A composites

CODE	29 days	56 days	71 days	305 days
2.0VS50A	30.7	38.8	39.3	37.1
2.0VS55A	34.1	37.0	38.2	38.9
2.0VS60A	32.9	37.8	37.8	38.3
2.0VS65A	39.6	40.5	43.7	42.9
2.0VS70A	38.2	36.3	42.8	42.5

Table 4.29 % Crystallinity, RC (on cooling) of vinyl silane coated DP393 LOT 1A composites

CODE	29 days	56 days	71 days	305 days
2.0VS50A	34.6	40.3	43.7	39.7
2.0VS55A	26.8	39.1	40.9	42.5
2.0VS60A	32.3	41.6	38.2	40.6
2.0VS65A	43.4	46.0	46.1	46.1
2.0VS70A	40.4	41.8	42.6	41.7

From Table 4.27, it can be seen that onset temperature is influenced by magnesium hydroxide loading level. From Table 4.28 it can be seen that crystallinity of the mouldings increases with time.

Table 4.30 Onset temperature (°C) of vinyl silane coated DP393 LOT 1B composites

CODE	6/7 days	34/35 days	69/70 days	157/158 days
PP	120	120	120	120
2.0VS20B	126	125	125	125
2.0VS30B	126	126	125	126
2.0VS40B	126	127	128	127
2.0VS50B	130	129	129	130
2.0VS60B	130	131	130	130
2.0VS70B	131	129	130	129

Table 4.31 % Crystallinity, XL (on heating) of vinyl silane coated DP393 LOT 1B composites

CODE	6/7 days	34/35 days	69/70 days	157/158 days
PP	36.4	32.5	33.3	34.6
2.0VS20B	34.4	32.2	33.6	33.3
2.0VS30B	34.4	32.6	31.3	35.6
2.0VS40B	35.3	32.1	31.8	34.7
2.0VS50B	36.6	32.7	34.7	37.1
2.0VS60B	34.1	34.3	35.0	37.3
2.0VS70B	37.3	34.8	35.2	38.3

Table 4.32 % Crystallinity, RC (on cooling) of vinyl silane coated DP393 LOT 1B composites

CODE	6/7 days	34/35 days	69/70 days	157/158 days
PP	40.7	35.8	37.4	38.0
2.0VS20B	38.8	36.4	39.2	36.6
2.0VS30B	38.9	37.1	36.0	40.8
2.0VS40B	39.2	35.9	34.2	38.5
2.0VS50B	41.1	37.1	38.3	40.1
2.0VS60B	37.8	27.3	38.2	39.7
2.0VS70B	39.4	35.8	37.2	39.9

From Table 4.30, onset temperature increases with filler addition, over a wide range of filler levels. Anomalies in crystallinity (Table 4.31) can be seen after 6/7 days post moulding.

Table 4.33 Thermal analysis of batch mixed polypropylene and uncoated DP393 compounds.

TIME (hours)	PP				DP393			
	T _m (°C)	T _c (°C)	%XL	%RC	T _m (°C)	T _c (°C)	%XL	%RC
1	169	119	33.2	22.9	167	126	38.2	39.8
2	172	119	32.8	37.3	167	127	37.9	37.8
25	171	119	34.4	22.1	168	126	39.2	39.6
26	171	119	33.3	35.6	168	127	39.5	39.2
39	169	119	36.1	36.6	170	125	40.3	40.1
40	170	119	33.8	36.8	169	126	58.6	59.9
52	171	119	34.6	38.0	167	126	38.6	41.3
53	174	119	26.9	34.2	169	127	40.1	41.3
68	168	119	35.5	40.5	168	127	42.1	42.6
69	169	120	32.6	35.6	169	127	43.2	43.2

Table 4.34 Thermal analysis of batch mixed vinyl silane coated DP393 LOT 2 compounds.

TIME (hours)	20VS				60VS			
	T _m (°C)	T _c (°C)	%XL	%RC	T _m (°C)	T _c (°C)	%XL	%RC
1	169	124	36.1	41.7	167	124	36.2	38.5
2	168	125	37.9	40.6	168	124	26.5	26.6
25	168	123	37.1	33.8	168	----	38.5	----
26	169	124	33.7	36.9	170	123	35.0	35.3
39	170	122	37.4	40.1	166	124	36.5	36.4
40	171	123	35.5	34.1	166	124	37.4	35.3
52	167	124	40.3	30.5	167	124	35.1	26.6
53	168	124	33.8	29.6	168	124	40.4	31.2
68	167	124	36.6	41.3	167	125	43.9	42.2
69	167	124	42.6	44.9	165	126	43.5	45.1

From Tables 4.33 and 4.44, the crystallinity of magnesium hydroxide filled compounds does not increase with time, up to a period of 69 hours.

Table 4.35 Overall crystallisation rate (T_c-T_p) of vinyl silane coated DP393 LOT 1B composites

CODE	6/7 days	34/35 days	69/70 days	157/158 days
PP	6.4	5.8	5.8	6.2
2.0VS20B	2.3	2.1	2.1	2.3
2.0VS30B	2.4	2.3	2.3	2.2
2.0VS40B	2.8	2.8	2.8	2.9
2.0VS50B	5.0	4.7	4.7	4.0
2.0VS60B	4.6	5.2	5.2	4.8
2.0VS70B	5.0	7.2	7.2	4.9

Table 4.36 Nucleation rate (S_i) of vinyl silane coated DP393 LOT 1B composites

CODE	6/7 days	34/35 days	69/70 days	157/158 days
PP	9.8	45.4	9.6	9.1
2.0VS20B	95.5	74.0	61.1	107.4
2.0VS30B	95.5	76.0	54.6	60.3
2.0VS40B	40.1	41.9	66.9	33.4
2.0VS50B	39.3	24.6	54.6	37.1
2.0VS60B	47.8	27.3	21.1	32.7
2.0VS70B	76.4	20.3	24.0	30.1

Table 4.37 Crystallite size distribution (ΔW) of vinyl silane coated DP393 LOT 1B composites

CODE	6/7 days	34/35 days	69/70 days	157/158 days
PP	22.8	22.5	23.5	22.5
2.0VS20B	15.8	14.8	14.8	13.3
2.0VS30B	14.9	15.3	15.5	13.3
2.0VS40B	15.5	15.5	16.0	14.5
2.0VS50B	22.6	22.5	20.8	20.0
2.0VS60B	21.8	24.3	21.3	20.8
2.0VS70B	24.0	24.4	20.3	21.5

Table 4.38 Maiti analysis of polypropylene and uncoated DP393 batch mixed compounds

TIME (hours)	PP			DP393		
	T_c-T_p	S_i	ΔW	T_c-T_p	S_i	ΔW
1	12.2	12.7	24.0	7.1	42.8	14.5
2	11.3	22.9	25.0	6.6	143.2	13.0
25	15.1	15.1	24.0	7.2	286.5	16.0
26	15.3	6.6	26.0	6.9	573.0	15.0
39	13.3	5.7	25.0	8.1	573.0	13.5
40	12.5	6.3	21.0	7.7	42.8	18.0
52	13.3	7.6	26.5	7.1	38.2	16.5
53	13.9	7.1	30.0	6.9	57.3	16.0
68	13.4	6.8	23.0	6.9	47.7	15.0
69	13.1	9.5	22.0	7.3	34.3	16.0

Table 4.39 Maiti analysis of vinyl silane coated DP393 batch mixed compounds

TIME (hours)	2.0VS20B			2.0VS60B		
	T_c-T_p	S_i	ΔW	T_c-T_p	S_i	ΔW
1	9.9	14.3	20.5	8.2	17.9	16.0
2	9.5	11.7	19.5	8.9	33.7	16.0
25	11.5	14.3	20.0	----	----	----
26	10.7	7.4	21.0	8.6	15.9	16.5
39	11.5	17.9	18.5	8.7	19.1	15.0
40	9.3	15.1	21.5	8.8	14.7	15.0
52	10.0	20.8	20.5	7.9	19.7	15.0
53	9.5	14.3	19.0	9.0	20.4	15.0
68	8.6	15.1	18.0	7.9	28.6	15.0
69	9.8	24.9	16.0	8.2	19.7	14.0

From Tables 4.35 to 4.37, increased filler loading level decreases the crystallisation rate of polypropylene but increases the crystallite size distribution. The thermal analysis parameters of these LOT 1B fillers do not alter as a function of time. From Tables 4.38 and 4.39, thermal analysis parameters of vinyl silane coated DP393 filled compounds do not change with time up to a period of 69 hours.

4.5.2 Differential mechanical thermal analysis (DMTA)

LOT 1A DP393 vinyl silane coated composites were analysed using DMTA to investigate the effect of high filler loading levels on the glass transition temperature of polypropylene. The traces were noisy and required smoothing. The $\tan \delta$ curve was particularly noisy and made the T_g determination difficult. This was measured from the loss modulus curve (E''). However, the results appeared unrealistic and have not been used within the discussion. These values can be found, with the theory of DMTA and a typical trace, in Appendix L.

4.5.3 Vicat softening point

The investigation of filler loading on the Vicat softening point of polypropylene was determined using LOT 1 DP393 vinyl silane coated compounds and can be seen in Table 4.40.

Table 4.40 Vicat softening point for polypropylene and some vinyl silane coated DP393 composites

<i>CODE</i>	<i>VICAT SOFTENING POINT (°C)</i>
PP	150.0 (---)
2.0VS20B	150.0 (---)
2.0VS30B	150.0 (---)
2.0VS40B	150.8 (0.4)
2.0VS50B	152.0 (---)
2.0VS60B	154.0 (---)
2.0VS70B	157.8 (0.4)

It can be seen from Table 4.40, that the Vicat softening point of PP is only affected at filler loading levels of nominally 40% and above. This is thought to be due to a critical volume fraction that also influences mechanical properties and flame retardancy.

4.6 Flame Retardancy

The flame retardance of selected composites was assessed using UL94 vertical burning assessment, limiting oxygen index (LOI) and cone calorimetry. The results for UL94 and LOI can be found in section 4.6.1 whereas cone calorimetry data can be found in section 4.6.2.

4.6.1 UL94 Vertical burning test and limiting oxygen index.

The results for the UL94 vertical burning assessment and limiting oxygen index (LOI) can be seen below. Tables 4.41 to 4.44 are for DP393 fillers whereas Tables 4.45 to 4.46 are for DP390s fillers.

Table 4.41 DP393 LOT 1 fatty acid composites UL94 and LOI results

<i>CODE</i>	<i>% FILLER</i>	<i>UL94 RATING</i>	<i>LOI (%)</i>
DP393	59.3	V0	27.8
1.5AMST	60.3	V0	27.9
3.0AMST	60.0	V0	27.0
4.5AMST	58.7	V0	26.5
1.5AMOL	57.3	V1	27.0
3.0AMOL	62.7	V0	28.5
4.5AMOL	61.7	V0	28.0
4.5NAST	58.1	V0	26.8
4.5NAOL	54.7	V1	26.6
4.5AMROS	60.8	V1	27.5

Table 4.42 DP393 LOT 2 fatty acid composites UL94 and LOI results

<i>CODE</i>	<i>% FILLER</i>	<i>UL94 RATING</i>	<i>LOI (%)</i>
1.5NAOL	61.1	V0	27.4
3.0NAOL	60.5	V0	28.0
4.5NAOL	58.6	V0	27.0
4.5AMOL	59.0	V0	27.3

Table 4.43 DP393 LOT 3 fatty acid composites UL94 and LOI results

<i>CODE</i>	<i>% FILLER</i>	<i>UL94 RATING</i>	<i>LOI (%)</i>
DP393	54.5	Unclassified	25.1
4.5AMOL	60.7	V0	28.1
4.5AMST	56.0	Unclassified	25.9
4.5NAOL	58.6	V0	27.9

Table 4.44 DP393 LOT 1 vinyl silane composites UL94 and LOI results

<i>CODE</i>	<i>% FILLER</i>	<i>UL94 RATING</i>	<i>LOI</i>
2.0VS50A	46.2	Unclassified	23.3
2.0VS55A	50.1	Unclassified	24.1
2.0VS60A	53.7	Unclassified	25.5
2.0VS65A	57.0	V1	27.1
2.0VS70A	63.3	V0	29.6

Table 4.45 DP390s LOT 1 fatty acid composites UL94 and LOI results

<i>CODE</i>	<i>% FILLER</i>	<i>UL94 RATING</i>	<i>LOI</i>
DP390s	55.5	Unclassified	25.0
AMST2.0	58.8	V1	26.4
AMST4.0	58.2	V1	25.8
AMST6.0	53.9	Unclassified	25.7
AMOL2.0	57.0	V1	26.3
AMOL4.0	56.0	Unclassified	25.9

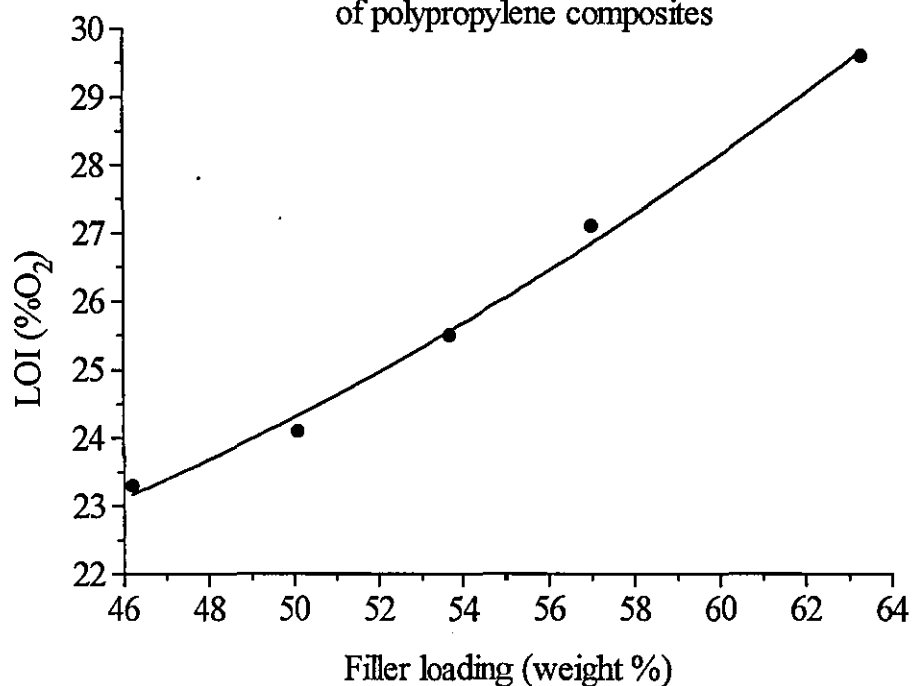
Table 4.46 DP390s LOT 2 fatty acid composites UL94 and LOI results

<i>CODE</i>	<i>% FILLER</i>	<i>UL94 RATING</i>	<i>LOI</i>
NAOL1.5	56.8	V1	26.7
NAOL3.0	56.7	V1	26.1
NAOL4.5	55.0	Unclassified	25.9
NAOL6.0	54.5	Unclassified	25.7
AMOL4.0	55.2	Unclassified	25.8
AMOL6.0	56.1	V1	27.0

Table 4.47 Polypropylene (unfilled) UL94 and LOI results

<i>CODE</i>	<i>% FILLER</i>	<i>UL94 RATING</i>	<i>LOI</i>
PP	0.00	Unclassified	16.6

Fig. 4.34 Effect of DP393 filler loading on LOI of polypropylene composites

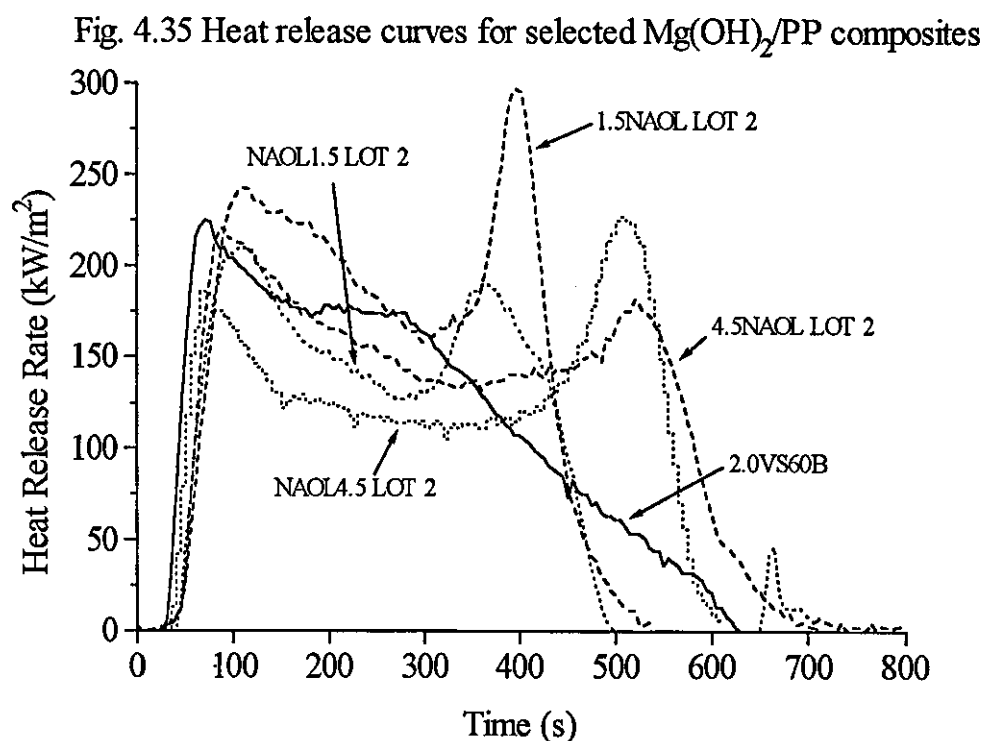


The limiting oxygen index of vinyl silane coated DP393 filled PP appears to increase exponentially as a function of filler content (Fig. 4.34). This indicates that the filler was not just acting as a diluent. UL94 properties are dramatically affected by filler loading. A minimum loading level of 58.1% is required to attain a V0 rating for DP393 fillers.

However, a V0 rating was never reached for DP390s fillers, due to the problems associated with filler incorporation.

4.6.2 Cone calorimetry

Cone calorimetry was performed on similar DP393 and DP390s LOT 2 oleic acid coated composites. A DP393 vinyl silane coated composite was also studied. The results can be seen below.



From Fig. 4.35, it can be seen that magnesium has a two-phase burn when incorporated into PP. The maximum heat release rate measured was approximately 300kW/m^2 . Variations in filler loading level will also be a major factor influencing the cone calorimetry results. Composite 1.5NAOL LOT 2 had the largest secondary heat release peak, but had a larger particle size than the silane coated DP393 filler. Higher coating levels appear to delay the onset of the secondary peak.

Table 4.48 Cone calorimetry data for some magnesium hydroxide filled polypropylene composites

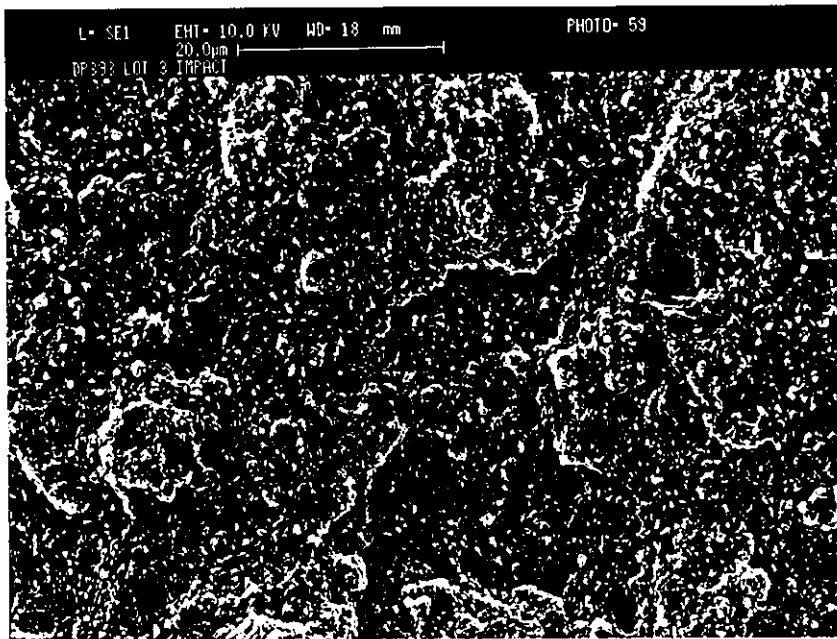
<i>CODE</i>	<i>FILLER</i>	<i>IGNITION TIME, T_i (s)</i>	<i>FLAMEOUT (s)</i>	<i>TOTAL HEAT EVOLVED (MJ/m²)</i>	<i>% MASS LOSS</i>
2.0VS60B	DP393 LOT 1	39	631	73.8	59.4
1.5NAOL	DP393 LOT 2	55	509	80.8	57.3
4.5NAOL	DP393 LOT 2	55	667	88.0	57.5
NAOL1.5	DP390s LOT 2	48	561	65.9	57.7
NAOL4.5	DP390s LOT 2	41	588	73.9	60.8

From Table 4.48, it can be seen that vinyl silane coating magnesium hydroxide increases the ignition time of PP. DP393 filled composites have a shorter ignition time than equivalent DP390s filled composites. The heat evolved is highest for fatty acid filled composites.

4.7 Fracture surface analysis

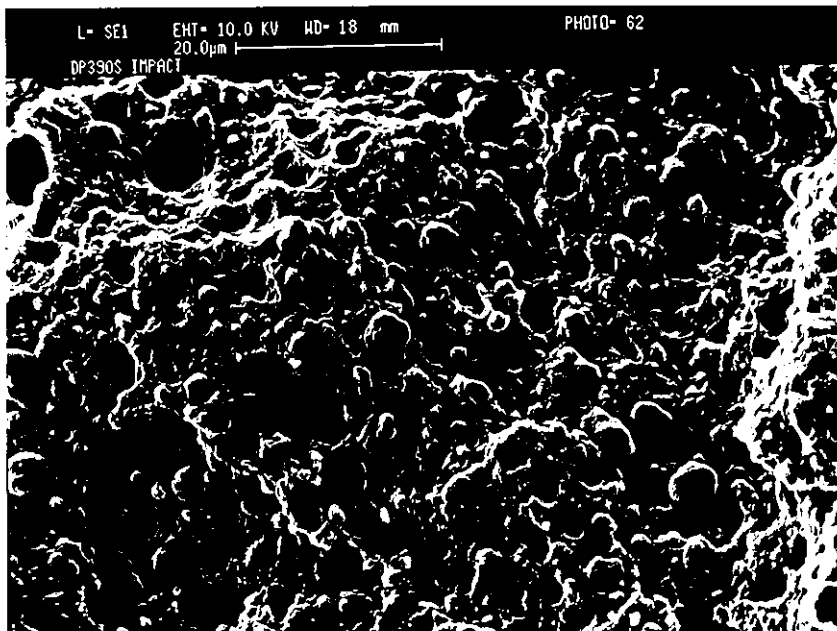
Both flexural and impact fracture surfaces were observed to compare the effect of filler morphology on the failure mechanisms of filled polypropylene. Flexural failure is induced at low strain rates whereas impact failure is induced at high strain rates. Fractures surfaces of a selected range of composites can be seen in Figs. 4.36 to 4.42.

Fig. 4.36 Impact fracture surface of composite DP393 LOT 3 (x5k)



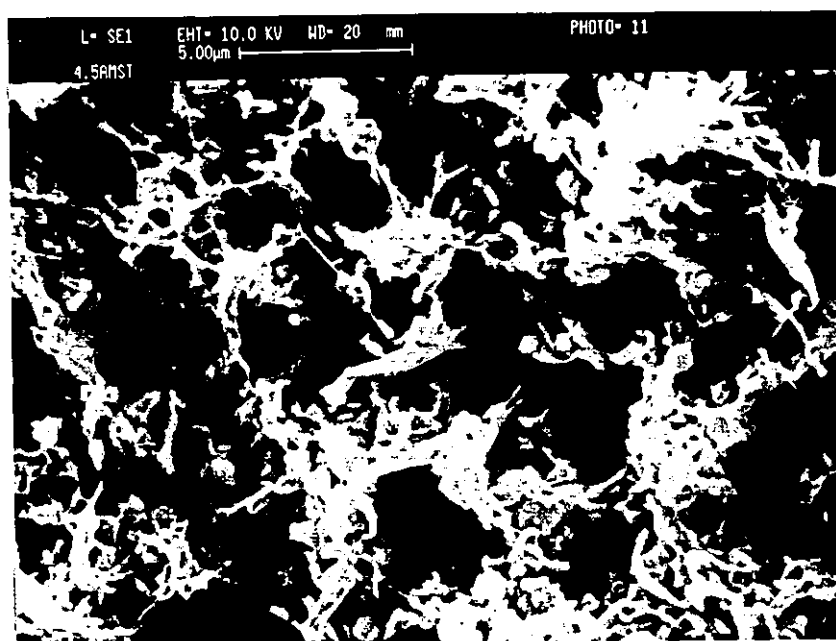
Brittle failure revealing delamination across anisotropic filler planes.

Fig. 4.37 Impact fracture surface of composite DP390s LOT 1



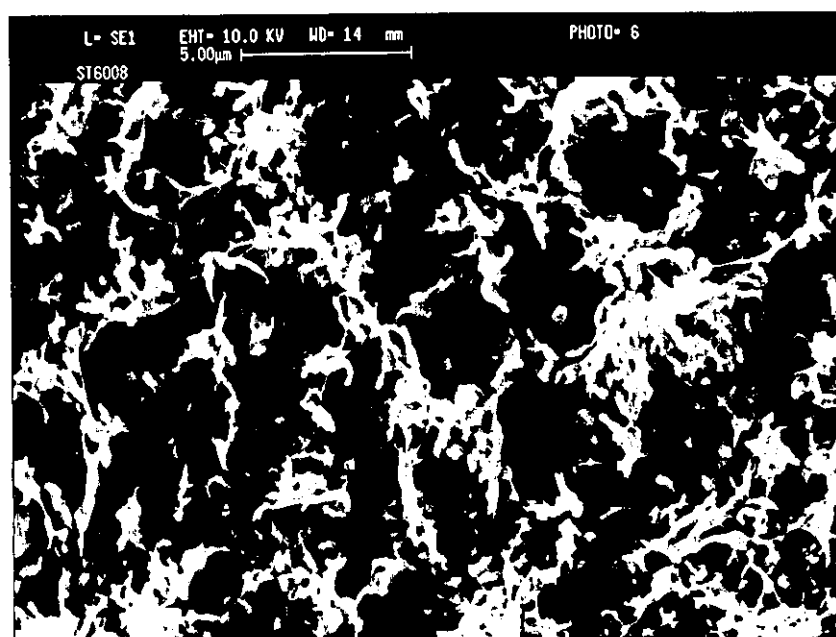
Brittle failure revealing debonding of isotropic filler particles.

Fig. 4.38 Flexural fracture surface of composite 4.5AMST LOT 1 (x5k)



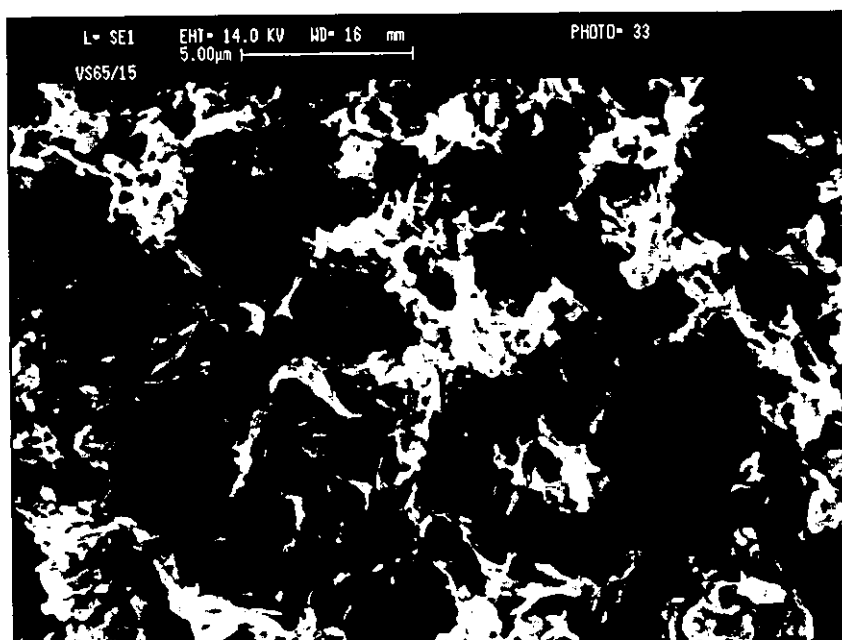
Brittle failure due to poor filler/matrix adhesion. Some microfibrils are observed.

Fig. 4.39 Flexural fracture surface of composite DP393 LOT 1 (x5k)



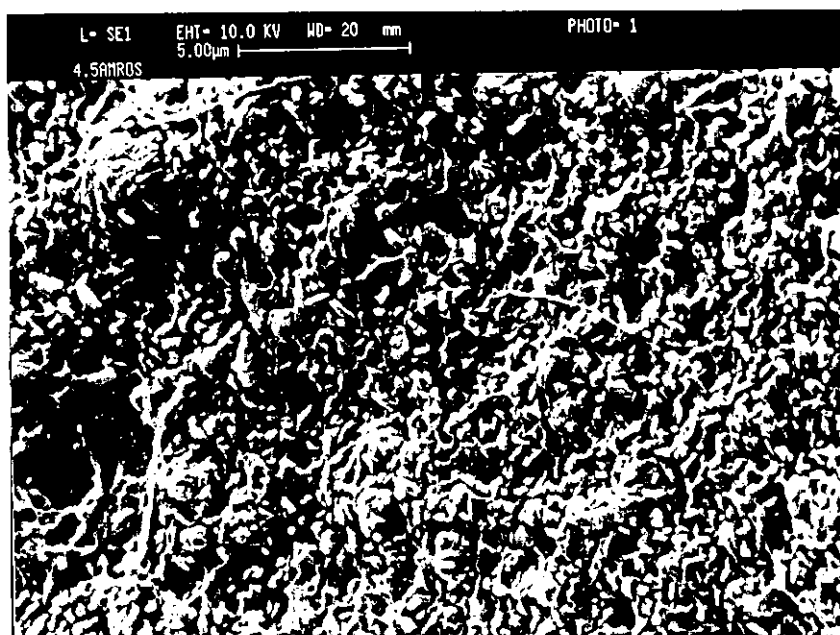
Brittle failure due to poor filler/matrix adhesion. Some microfibrillation observed.

Fig. 4.40 Flexural fracture surface of composite 2.0VS65A (x5k)



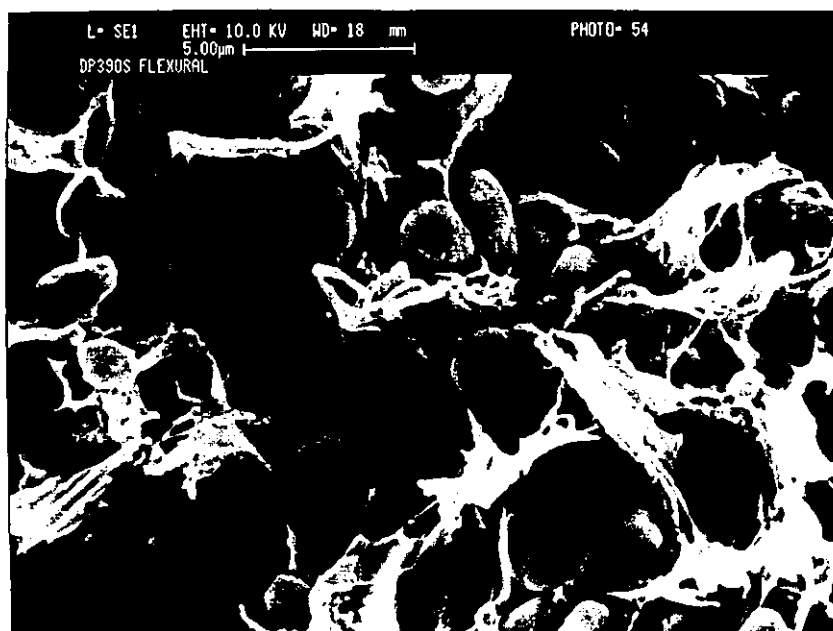
Brittle failure, with less microfibrillation than fatty acid coatings.

Fig. 4.41 Flexural fracture surface of composite 4.5AMROS LOT 1 (x5k)



Brittle failure unique to this filler type. No microfibrillation produced.

Fig. 4.42 Flexural fracture surface of composite DP390s (x5k)

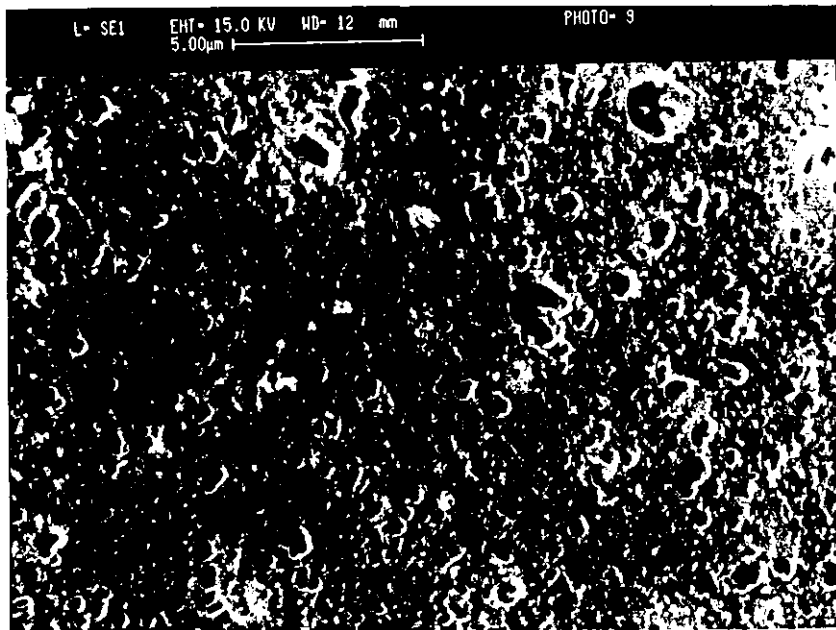


Brittle failure induced by poor filler/matrix adhesion.

4.8 Filler dispersion analysis

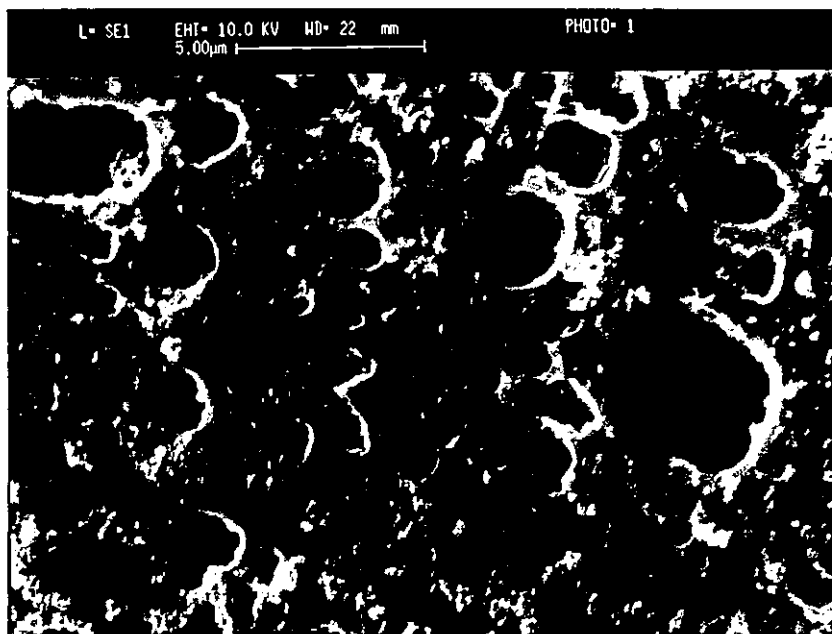
Filler dispersion analysis was performed on all magnesium hydroxide filled composites. The cryogenic polishing and acid etching technique is an excellent method for qualitatively assessing the filler dispersion and distribution within the polypropylene matrix. Black holes within the matrix are regions where the filler particles reside. Figs. 4.43 to 4.49 are micrographs for a selected range of DP393 and DP390s filled composites, used for indicating filler dispersion.

Fig. 4.43 Etched surface of composite DP393 LOT 1 showing filler dispersion (x5.5k)



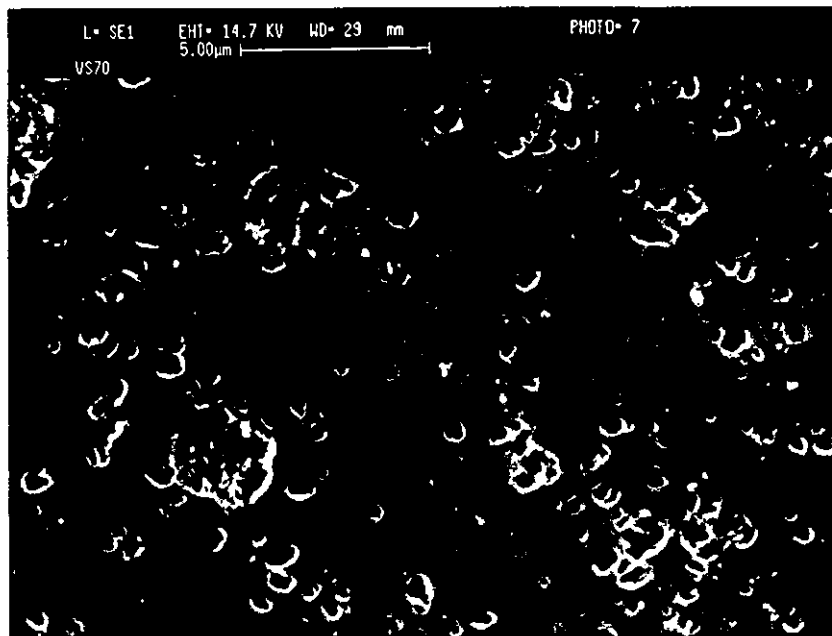
Good filler dispersion and distribution produced by compounding.

Fig. 4.44 Etched surface of composite DP390s LOT 1 showing filler dispersion (x5.5k)



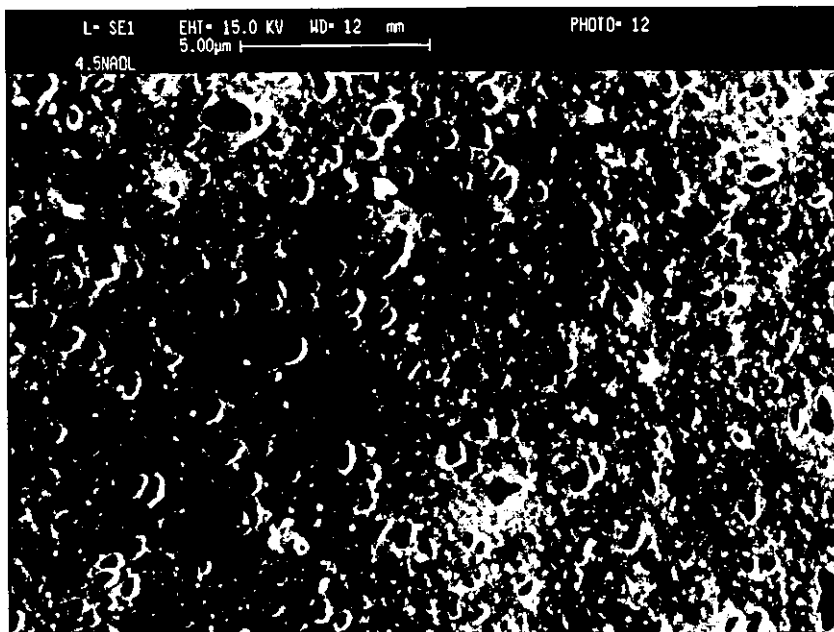
Good dispersion and distribution produced by compounding.

Fig. 4.45 Etched surface of composite 2.0VS70A showing filler dispersion (x5.5k)



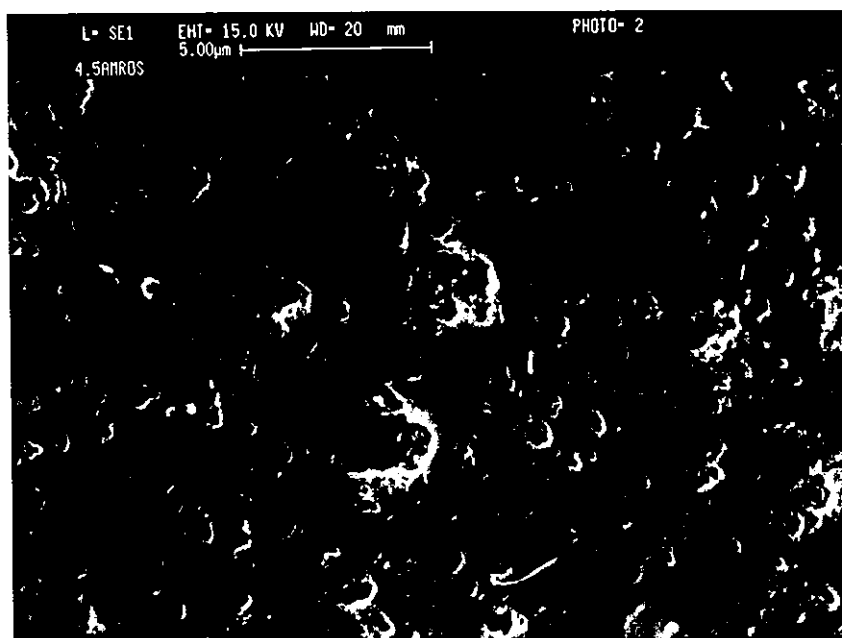
Improved dispersion and good distribution produced by compounding.

Fig. 4.46 Etched surface of composite 4.5NAOL LOT 1 showing filler dispersion (x5.5k)



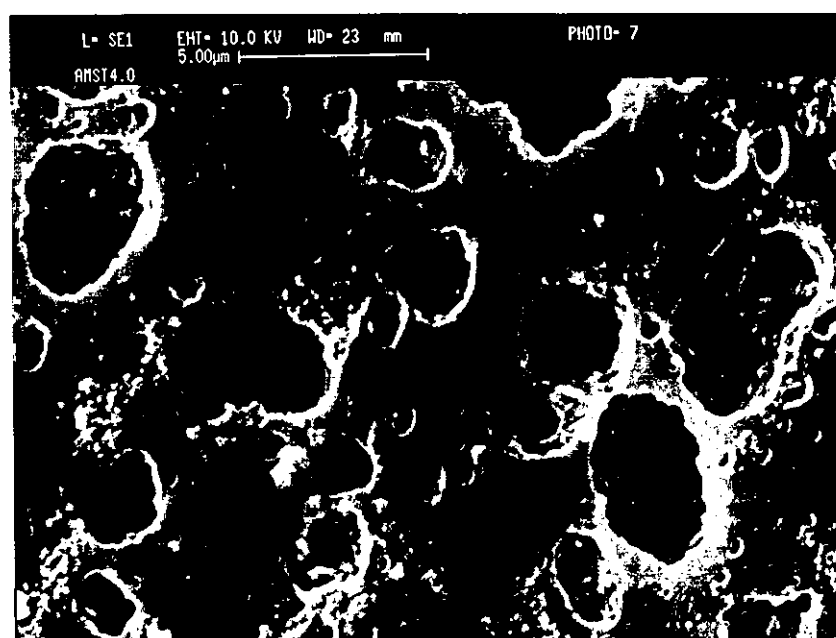
Good dispersion and distribution produced by compounding.

Fig. 4.47 Etched surface of composite 4.5AMROS LOT 1 showing filler dispersion (x5.5k)



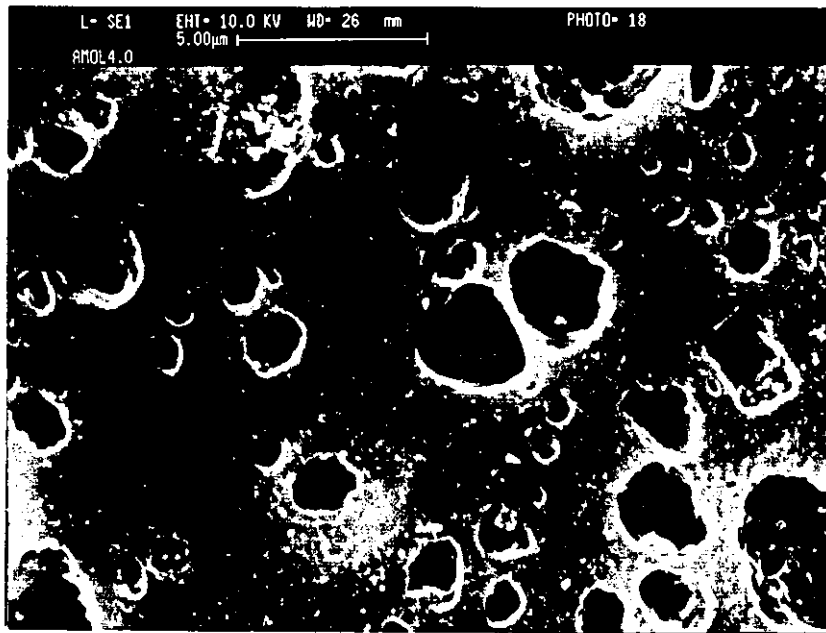
Poor dispersion but good distribution produced by compounding.

Fig. 4.48 Etched surface of composite AMST4.0 LOT 1 showing filler dispersion (x5.5k)



Good dispersion and distribution produced by compounding.

Fig. 4.49 Etched surface of composite AMOL4.0 LOT 1 showing filler dispersion (x5.5k)



Good dispersion and distribution produced by compounding.

CHAPTER 5

DISCUSSION

The major aim of the project was to surface modify a commercially available filler, with an optimised coating, to obtain good all round properties including effective flame retardancy when compounded, at high filler levels into polypropylene.

In broad terms this involved determining the effect of filler morphology, coating agent, coating type and coating level on the physical, rheological and mechanical properties of polypropylene.

5.1 Filler Morphology

The effect of filler morphology was studied using two different grades of synthetic magnesium hydroxide, one of which required significantly less preparation. The preparation route of both fillers can be found in Fig. 3.1. Both fillers had the same origin but filler DP393 underwent more precipitation stages than DP390s.

5.1.1 Filler structure

Magnesium hydroxide, like all minerals contains various levels of structure, from the basic crystal structure up to the final filler particle size. The basic crystal structure was studied using X-ray diffraction (XRD). Fig. 4.1 and data in Appendix A shows the position of the XRD peaks for both uncoated DP393 and DP390s fillers. For the resolution of the scanning speed used, it can be seen that the positions and relative intensities of the diffracted peaks of both fillers overlap. This proves that the basic crystal structure of magnesium hydroxides DP393 and DP390s are identical. When the d (interplanar) spacing was compared to the standard XRD file for magnesium hydroxide [115], it was confirmed that the crystal structure of the fillers were hexagonal (trigonal) with lattice parameters $a = 0.3174\text{nm}$ and $c = 0.4769\text{nm}$.

The primary particle size and secondary particle size (filler particle) can be observed using scanning transmission electron microscopy (STEM). A magnification of 50k revealed the primary particle size of both fillers to be distinctly different. Micrographs of the DP393 and DP390s fillers can be seen in Figs. 4.5 and 4.6. DP393 consisted of regular hexagonal plates of size 0.25 to 0.5 microns in diameter with small groups of plates (primary particles) agglomerating into secondary particles. These agglomerates had a mean particle size (d50) of 0.75 microns. DP390s appeared to be comprised of stacks of many hexagonal plates (primary particles). The plates varied in length from 0.1 to 0.4 microns. These agglomerated plates formed pseudo spherical secondary particles, much bigger than for filler DP393, producing a snowball type morphology. The morphology of DP390s was therefore designated as porous when compared to that of DP393. Particle sizing data (Appendix B) showed the mean secondary particle size (d50) of DP390s to be 4.78 microns. The size distribution of both fillers, seen in Fig. 4.7 were in general found to be monodispersive although DP390s contained a small side mode at approximately 1 micron.

Filler DP393 also existed in a high density form, HD-DP393. This high density material is the aggregated form of DP393 produced when the material has been washed and dried. This aggregated form is pin milled to produce the free flowing powder, DP393. The particle size distribution for both these fillers can be seen in Fig. 4.8. Both of these fillers have almost identical characteristics. This must be due to sample preparation. As aggregated lumps of HD-DP393 could not be truly particle sized, gentle reduction to a powder by pestle and mortar was necessary, essentially producing DP393. Their primary particle size will obviously be identical, but as received their secondary particle size was very different. A poor dispersion of fine material existed with many rounded agglomerates up to a particle diameter of 100 microns. This can be seen in Fig 4.9. The surface areas of the two fillers were almost identical (Appendix C), because of their identical primary morphology, it was just that HD-DP393 was weakly aggregated into lumps.

Fillers DP393 and DP390s have similar surface areas (Appendix C), this being due to the porous nature of DP390s creating extra surface area into which nitrogen molecules can be absorbed.

Finally, elemental analysis by energy dispersive X-ray analysis was performed on both uncoated DP393 and DP390s. Although not quantitative, DP393 was found to contain a trace of calcium, probably calcium oxide. DP390s also contained this level of calcium with additional smaller traces of chlorine and sulphur. These may be present as magnesium chloride and sulphate respectively. Differences in the purity may affect the regularity of the crystal structure, surface energy and nucleation properties.

5.1.2 Replication of morphology

The reproducibility of both filler types, either uncoated or coated, using exactly the same production method, proved difficult. This is apparent from the three LOTS of DP393 fillers and two LOTS of DP390s fillers prepared.

During the precipitation of magnesium hydroxide, settling and filtration characteristics of the precipitate are poor, but are considerably increased by recirculation of the product as seed. The precipitation and seeding processes are produced in large settling tanks which are constantly exposed to atmospheric conditions. This means that the temperature, hence the kinetics of the precipitation procedure, may not be constant. It has been shown [117] that a change in the precipitation temperature and/or a slight adjustment in pH can alter the crystallite size in the 110 and 001 directions.

From Fig. 4.10 (and data in Appendix B) it can be seen that the particle size distribution of two different LOTS of uncoated DP393 have varied. Although both distributions are monodispersive, the LOT 1 filler has a narrower distribution with a lower volume of particles with larger particle diameters. Exposure to extensive ultrasound (d50, 15 minutes) reduces the mean particle size of the DP393 LOT 3 uncoated filler, whereas the LOT 1 filler remains the same. These weakly bound agglomerates are broken down by prolonged exposure to ultrasound indicating that

secondary particle size distribution is also dependent on physical breaking of aggregates, such as in the pin milling stage of production. The differences observed in secondary particle size distribution were therefore believed to be due to agglomeration rather than growth in crystallite size.

With the application of a filler coating, the secondary particle size of DP393 fillers increased. This indicates that filler primary particles have more of a tendency to agglomerate than disperse. However, the application of a filler coating to DP390s had the opposite effect, the secondary particle size is reduced. This will change the filler morphology and packing properties. These points will be covered in more detail later.

5.1.3 Dry packing properties

The dry packing properties (bulk density) are influenced by particle size distribution and morphology of the filler particles (Appendix D). DP390s has a bulk density nearly twice as high as that for DP393 (Tables 4.6 & 4.7). On production, DP390s is a slightly denser material than DP393, but this does not account for the large difference. A more likely explanation is that due to the wide particle size distribution of DP390s, the side mode of particles about 1 micron in diameter compliments packing.

DP393 and HD-DP393 have been shown to have different secondary particle sizes (Fig. 4.8). The particle diameters for HD-DP393 ranges from sub-micron up to approximately 100 microns. The bulk density of this filler is not surprisingly higher than for the pin milled DP393. The presence of aggregated particles creates free volume between adjoining particles into which the smaller particles can fill and hence improve the dry packing properties.

5.1.4 Wet packing properties

The uncoated DP393 (LOT 1 and 3) and HD-DP393 fillers have the highest oil absorption values of all fillers (Appendix D). Uncoated fillers have the highest polarity, due to the presence of metal ions on the substrate surface. This high polarity makes it

more difficult for the fillers to be wet out. As the oil absorption method involves mechanically working the oil into the filler, the aggregates in the high density filler will be broken down, to produce effectively DP393. Both fillers now have the same particle size distribution and their oil absorption values are the same.

Considering the large difference in the secondary particle size of fillers DP393 and DP390s, it is interesting that they have almost identical surface areas (Appendix C). The secondary particle structure of DP393 is created from a few, well aggregated primary particles. However, the secondary particle structure of DP390s is created from a multitude of primary particles, creating a porous structure. It is this porous structure that increases the surface area of this filler type. Oil absorption involves the physical wetting of the filler structure by a wetting oil. Although the filler morphologies are entirely different, their oil absorption values are almost the same. This is due to the fact that both fillers have similar surface areas onto which the oil can be absorbed.

5.1.5 Compounding

Compounding of LOT 1 DP393 and HD-DP393 was performed on a MP2015 APV twin screw extruder (L:D = 15:1), whereas LOT 1 DP390s and LOT 3 DP393 were produced on a MP30TC APV twin screw extruder (L:D = 30:1). Pressure measurements were unavailable on the MP2015 and due to the different nature of the machines and compounds produced direct comparisons cannot be made. Screw profiles and barrel temperatures for both extruders can be seen in Tables 3.9 and 3.10 respectively.

However, DP393 LOT 3 and DP390s LOT 1 were both produced on the MP30TC and contain a similar filler content of approximately 55%. Compounding characteristics of these two filler types can be seen in Tables 4.3 and 4.5 respectively. In both cases, a continuous strand could not be produced; the broken strands were cooled in the water bath and fed through the granulator by hand. The DP393 filled compound could be produced at the standard screw speed of 250rpm, whereas this speed had to be increased to 400rpm for DP390s to prevent the extruder becoming blocked. This

increased screw speed resulted in a lower torque and pressure than for DP393, obviously making processing easier. Uncoated DP390s was therefore more difficult to produce than uncoated DP393, due to the larger secondary particle size. A fuller rheological explanation can be found in section 5.1.6. However, in both cases, when the extruder had been run for approximately 30 to 60 minutes, the clutch disengaged, making further compounding impossible. This is attributed to large amounts of dry, unlubricated filler being retained within the feed end of the screw, eventually causing blockage.

Attempts were made to compound the unmilled HD-DP393 on the MP2015. However, this proved unsuccessful as the extrudate sputtered periodically from the die, making the formation of a strand impossible. Due to the fact that the milled filler was not processable, it can be assumed that at least some of the large agglomerated secondary particles were retained within the melt, causing the difficulties. As none of the HD-DP393 filled compound could be produced, no further results could be obtained.

5.1.6 Rheology

The main purpose of filler incorporation is to create composites with a prescribed set of mechanical properties, which are dependent on filler content, shape and distribution within the matrix. However, a major concern is that such addition may increase the viscosity of the melt. Neilson [118] modified an equation relating the melt viscosity of a particulate filled composite to the elastic modulus. It was deduced that the addition of filler to a base polymer would cause an increase in the strength characteristics of the composite, this being due to the ability of filler to form its own structural network within the matrix. Also, the agglomeration of filler particles were shown to cause an increase in the viscosity and modulus of the solid composite [119].

The flow properties of polymer melts can be measured using capillary rheometers. These are characterised by high shear rates, but are insensitive to material structure as the structure is substantially destroyed in the melt state [44]. Fig 4.23 compares the shear flow properties of uncoated DP393 and DP390s loaded at 55% in polypropylene

to the virgin polymer itself. It can be clearly seen that the incorporation of 55% by weight of magnesium hydroxide to polypropylene, greatly increases the viscosity, hence the shear stress. This difference in viscosity is greater at higher shear rates with a larger particle size filler (as confirmed by Hornsby [84]). At low shear rates (24s^{-1}), the shear stress of both DP393 and DP390s filled compounds are almost identical. This is reinforced by melt flow index values. Melt flow index occurs at a very low shear rate and both uncoated filled compounds have the same MFI (Appendix G). At higher shear rates, the shear flow curves for the filled compounds diverged, the DP390s filled compound experiencing the higher shear rates. As the surface area of both fillers is essentially the same (Appendix C), the larger particle size of the DP390s filler must account for the increase in viscosity. DP393 is formed from regular hexagonal crystals, aggregating in small numbers to form an approximately platey secondary particles (Fig 4.5). DP390s is formed from very large groups of irregular plates forming an approximately spherical secondary particle (Fig. 4.6). Platey fillers, such as in the case of DP393 are known to align in the direction of flow in the melt state [54, 55]. At the higher shear rates, the induced anisotropy may be increased, promoting better flow fields, hence reducing the effective viscosity. If the particle size is increased, the flow fields will become disturbed, and turbulent at higher shear rates, restricting flow. This anisotropy was confirmed by Fig. 4.3. Also, microporous particles, such as DP390s are known to promote an immobilised layer of polypropylene on their surface [56]. This decrease in polypropylene mobility, and the possibility that the immobile PP may act as a bonding agent between adjoining filler particles will also account for an increase in viscosity for DP390s filled composites.

5.1.7 Crystallinity

The crystallisation of polypropylene, although a homogeneous process, is complex. The final crystallinity content can be altered by the incorporation of heterogeneous nuclei (nucleants).

From the results in Tables 4.18, 4.19 and 4.22, it can be seen that the incorporation of uncoated magnesium hydroxide increases the onset temperature of polypropylene quite

significantly. However, the change in morphology from DP393 to DP390s appears to be a contributing factor and does affect the crystallinity content (%XL). DP393 increases the crystallinity above the unfilled (Tables 4.19 and 4.18 respectively). The incorporation of DP390s does not cause a change in the measured crystallinity value above the unfilled polypropylene (Tables 4.22 and 4.18 respectively). The injection moulded morphology thermal history of the unfilled and filled composites was destroyed by heating above 220°C. On cooling (isothermal), the crystallinity (%RC) of the recrystallised unfilled and filled composites was measured (Tables 4.18, 4.19 and 4.22). The percentage crystallinity of the unfilled and DP390s filled composites remained at levels similar to those produced on moulding (%XL). However, that of the DP393 filled was significantly increased by over 3%. Although the filled composites have a high viscosity (Fig 4.23), it may be possible that after melting, the smaller platey DP393 particles may be able to reorientate themselves permitting greater crystallinity whereas the larger DP390s particles are not affected. Also, the DP390s particles are essentially round and have the same orientation at any position within the polypropylene matrix. This reorientation, and isothermal crystallisation process may allow DP393 filled composites to reach a higher crystallinity.

The overall crystallisation rate ($T_c - T_p$) of the DP393 and DP390s filled composites is significantly faster than for unfilled polypropylene (Tables 4.24, 4.25 and 4.26 respectively). Therefore, the incorporation of magnesium hydroxide increases the crystallisation rate, the fillers acting as heterogeneous nuclei. DP393 nucleates at a faster rate filler than that of DP390s. As the surface areas are similar, this must be due to primary particle structure and morphology. The primary particles of DP393 are very regular hexagonal plates which stack neatly into secondary particles (Fig. 4.5). The well defined geometry, and sharp edges of these particles may favour the faster formation of the polypropylene structure. Alternatively, the poorly defined primary particles associated with DP390s and porosity (Fig. 4.6) may cause the slower crystallisation rate, and lower crystallinity content, due to less surface being exposed to the polymer. The values for crystallite size distribution (ΔW) between the unfilled and both filled composites (Tables 4.24, 4.25 and 4.26) are approximately the same. This does not mean that the crystallites are the same size though. The slow homogeneous

crystallisation rate of polypropylene promotes the formation of few, large crystallites. The nucleated filled polypropylenes favour the formation of many small crystallites.

X-ray diffraction was also used to assess the crystallinity and morphology of both the unfilled and 55% magnesium hydroxide loaded polypropylene. It has been shown that talc (platey) particles align parallel to the flow direction, and crystallisation progresses with the 040 planes of polypropylene stacking on the plate planes of filler particles [55]. Magnesium hydroxides used in this study were platey in their primary structure, therefore samples were analysed in their through (normal) direction, i.e. perpendicular to the flow direction. Polypropylene normally exists in its most stable α form and diffracts strongly in both the 110 and 040 directions. Ratioing the intensity of the α -PP 110 peak to the α -PP 040 peak (I_{110}/I_{040}) relates the crystal a and b axis orientations. If the ratio is less than 1.3, then the b axis is orientated parallel to the surface under examination. If the ratio is greater than 1.5, the a axis is orientated parallel to the surface under examination. The sample is isotropic (randomly orientated) if the ratio of the intensities is in the range 1.3 to 1.5 [54].

For the case of unfilled polypropylene the ratio of intensities was 1.14 (Fig. 4.2). This indicates that there is some degree of anisotropy, with polypropylenes b axis (040) being orientated parallel to the samples surface. This slight orientation may have been caused by the shear flow action induced when processed in the melt state. However, with the incorporation of DP393 filler, this value decreases to 0.41, indicating that these filler particles are aiding orientation (Fig. 4.3). That is, the polypropylenes b axis is orientated parallel to the fillers surface. The DP393 filled composite had a very strong intensity caused by the 001 axis of the magnesium hydroxide, with a very weak intensity in the 101 direction. The crystal structure of the platey DP393 magnesium hydroxide is highly orientated in its 001 axis. It would appear that crystals in the 001 planes are being orientated parallel to the composites surface. This 001 plane corresponds to the basal plane of magnesium hydroxide, the hexagonal top face of the crystal structure. For DP390s (Fig. 4.4), there was a strong intensity also in the 001 axis but this is almost equalled by an intensity in the 101 direction. This means that neither plane is specifically oriented, therefore the roughly spherical DP390s filler

particles are lying unoriented within the matrix. The ratio I_{110}/I_{040} for the matrix though is 0.67, the polypropylene *b* axis being specifically orientated parallel to the moulded surface. The incorporation of the DP390s filler therefore increases this orientation above the unfilled, but not so greatly as for DP393. The 001 (basal) plane is therefore responsible for nucleation.

The β phase of polypropylene is detected by a shoulder on the 040 peak on the α trace at 16.7° . The traces of unfilled polypropylene and polypropylene filled at 60% with DP393 and DP390s can be seen in Figs. 4.2, 4.3 and 4.4. No shoulder corresponding to the presence of the β phase was detected in either the unfilled or filled samples. The magnesium hydroxide fillers, were therefore not changing the morphology from the stable α form, but were altering the orientation of the polypropylene morphology.

5.1.8 Flexural properties

Flexural modulus is a bulk property and is dependent on filler geometry, modulus, particle size distribution and concentration within the matrix. Flexural strength is more complex, and is dependent also on spatial distribution and interface thickness. Incorporation of nominally 36% by volume magnesium hydroxide filler has substantially altered the flexural properties of polypropylene. Flexural data can be found in Appendix I.

The flexural modulus of composites filled with both uncoated DP393 and uncoated DP390s are over twice that of polypropylene alone (Fig. 4.32). This is due to the fact that the fillers have higher elastic moduli (approximately 64GPa) than that of the matrix. The movement of the matrix is constrained by the hard, immobile filler particles. The flexural modulus of DP393 filled composites (both LOT 1 and 3) are higher than for DP390s. As the modulus, surface area, oil absorption values and filler concentrations of these different grades of magnesium hydroxide are similar, the changes must be due to filler geometry and particle size distribution. From X-ray diffraction, DP393 filler particles are thought to lie predominantly parallel to the

injection direction (Fig. 4.3), whereas the more symmetrical DP390s fillers are less orientated (Fig. 4.4).

It has been shown that the shape and orientation of magnesium hydroxide filler particles are influential on composite modulus [58]. Fibrous particles were shown to be highly orientated and reinforcing. Platey fillers were orientated to a lesser degree but still reinforcing. Spherical particles were isotropic with the least reinforcing effect. DP393 fillers are small (1 micron) in diameter with a regular hexagonal plate structure, whereas DP390s fillers are larger (over 4 microns) pseudo-spherical. The flexural modulus of composites filled with uncoated DP393 are higher than that of DP390s. The platey structure of DP393 particles, with particles lying perpendicular to the applied load will enhance reinforcement when compared to the porous spherical shape of DP390s. The increase in crystallinity of the DP393 filled composites will also contribute to increased stiffness.

Addition of magnesium hydroxide to the matrix reduces the effective area of PP for load bearing, however the flexural strength is either retained or increased (Tables 4.8 and 4.9). As the amount of ductile matrix has been reduced, the load must be carried by the filler particles too, indicating that there is some degree of adhesion between the filler particles and the matrix. This adhesion cannot be chemical due to the filler and matrix having different polarities. It may be that the high flexural strength may have been caused by physical adhesion between the polypropylene and the rough (porous) filler surface, which has been reported to reinforce PP/wollastonite composites [120].

Extension to failure of polypropylene has been greatly reduced by the incorporation of uncoated magnesium hydroxide particles (Tables 4.8 and 4.9). At high filler levels, with no interfacial adhesion, failure will occur due to microplastic deformation around particles. The reduction in extension to failure is largest for composites comprised of sharp, platey particles, as in the case of DP393. Although lying perpendicular to the load direction and providing reinforcement, the sharp edges will contribute as areas of stress concentration, reducing the energy required for crack propagation. There is a slight difference in values for LOT 1 and 3 composites which is due to the loading level of LOT 3 being slightly lower than desired. The DP390s particles are more

geometrically well defined, and provide less sharp edges to promote internal stresses, therefore composites containing these fillers can undergo larger deformations.

5.1.9 Impact properties

It is well documented [65,69,70,71] that filler morphology (filler shape and particle size distribution), loading and dispersion are the main factors influencing the falling weight impact strength of polypropylene. Good filler dispersion is of overriding importance when discussing the effect of mineral fillers on impact strength. Impact data can be found in Appendix J.

From Table 4.12, one can see that the incorporation of approximately 36% by volume of magnesium hydroxide to polypropylene causes a significant reduction in the impact properties of polypropylene compared to that of the unfilled material.

From thermal analysis in section 5.1.6, it has been found that both uncoated DP393 and DP390s act as nucleants to polypropylene (Tables 4.19 and 4.20), and increase the overall crystallisation rate (Tables 4.24 and 4.25). The morphology of the filled polypropylene will significantly differ to the unfilled polymer. It has been found [71] that an increase in crystallisation rate produces a reduction in falling weight impact strength of polypropylene. As the crystallisation rate is faster, the formation of smaller crystallites will be favoured. It may be that this change in morphology has contributed to the reduction in matrix toughness.

From Table 4.12, the peak energies of the DP393 filled composites (80mJ) are markedly higher than for the DP390s filled composites (70mJ), both filled at 55% by weight. This is due to the particle size difference of the fillers. The DP393 fillers have a mean particle size (d_{50}) of 1 micron, being of platey in shape, whereas the DP390s fillers have a mean particle size of approximately 5 microns, essentially spherical in shape. Larger filler particles act as flaws from which cracks can propagate. With a reduction in the number of flaw sites, the impact energy can be dissipated throughout the matrix more efficiently. Also, in section 5.1.7, DP393 fillers have been shown to

orientate parallel to the moulded surface (perpendicular to the applied load). The matrix having a higher crystallinity content and matrix orientation may contribute to the increased toughness of the composite.

Considering the difference in size of the fillers, the peak force to restrict crack propagation is only slightly better for DP393 filled composites than DP390s filled composites (Table 4.12). DP390s filler particles are essentially round with a low aspect ratio. This type of particle are known to act as crack blockers to hinder the motion of the crack tip [69]. However as the orientation of the matrix for the DP390s composites is less than for DP393. Once the crack blocking mechanism has occurred, continuation throughout the matrix will occur. The less tough matrix will allow the crack to propagate quicker than in the matrix of DP393 filled composites. DP393 filler particles, although much smaller, have a larger aspect. Large stress concentrations will occur in the region of these sharp edges. However, filler particles are thought to lie parallel to the composites surface, so less of the sharp edges will be orientated in the direction of crack propagation.

5.1.10 Flame retardancy

According to literature [22,29], magnesium hydroxide requires to be loaded into polypropylene at 60% by weight or greater in order to produce a significant flame retardant effect. For uncoated fillers, flame retardancy was studied using a vertical burn method (UL94) and limiting oxygen index (LOI) test procedure. For both tests, the samples were mounted vertically. With LOI tests, samples are ignited at the top but with UL94, samples are ignited at the bottom.

From the results in section 4.6.1, it can be seen that the burning characteristics of polypropylene can be significantly altered by addition of high levels of uncoated magnesium hydroxide. Polypropylene alone burns rapidly with a dripping flame. For the UL94 test, polypropylene is rated unclassified (Table 4.47) because its combined burning time exceeds the time specified for the lowest rating (V2). Also, the dripping flame ignites cotton wool situated below the flaming sample, spreading flames in a real

fire situation. For the LOI test, polypropylene achieved a rating of 16.6 (Table 4.47), again dripping.

Incorporation of uncoated DP393 was achieved at two levels, 59.3% and 54.5%, although the desired level was 60%. For the LOI test, addition of a higher level of DP393 increased the LOI rating (Tables 4.41 and 4.43 respectively). This is due to the dilution of the flammable matrix with the hydrated filler. Gal [121] deduced that the heat of combustion of a hydrated mineral filled matrix will decrease linearly with filler content. As LOI increases linearly with the decrease in heat of combustion, LOI should increase linearly with filler content. However, LOI is sensitive to the amount of heat transmitted back from the flame to unburned sample. Ash formation can reduce this feedback, and therefore increased LOI (Fig 4.34). For the case of DP393, the ash mounted in a stable manner on top of the unburned sample, without spalling. Therefore, flame retardance was influenced in the solid phase by preventing oxygen from supplying the flame. With UL94 tests, loading levels of uncoated DP393 were more significant with respect to the composite achieving V0 rating (Tables 4.41 and 4.43), as heat was redirected back into the sample on burning. Again, the layer of ash acted as a screen to the oxygen supply. For both tests, the high level of filler restricted the polymer from dripping, therefore spreading fire. This was to be expected due to the poor melt flow properties. The composites also burned much more slowly than for unfilled polypropylene. However, the increase in filler content from 54.5 to 59.3% altered the UL94 rating from unclassified to V0. It can be deduced that at least 59.3% of uncoated DP393 will produce a flame retardant formulation.

Addition of uncoated DP390s at 55.5% loading level also reduced the rate of burning of polypropylene and prevented dripping. However, for the UL94 test, a rating of unclassified was obtained (Table 4.45). Therefore a higher loading level of uncoated DP390s would be required to achieve effective flame retardance. Again, ash formation was stable and spalling was not observed. The LOI value of 25.0 is comparable to that of the DP393 composite with 54.5% filler (Table 4.43). The DP390s filled composite had 1% greater filler content than the DP393 LOT 3 composite, yet had the same LOI rating. From this it can be assumed that uncoated DP393 is a slightly better flame

retardant filler than uncoated DP390s. The filler chemistry of the two filler types differ, with DP393 being purer than DP390s. Hornsby [22] showed that in a PP homopolymer at 60% weight loading, there was a variation in LOI from 25.4 up to 28.6. Differences in crystal size and purity levels were thought to be a contributory factor, but also good dispersion was considered.

Both filler types have been shown to be well dispersed in the matrix (section 5.1.12). Flame retardancy will be optimised with good filler dispersion, which in turn will limit void creation. This is due to the better balance of heat generation in the matrix being absorbed by the hydrated filler particles. More of the matrix will be in contact with the filler. This ensures that the heat of combustion of the matrix is transferred rapidly to the hydrated filler particles (low thermal conductivity), allowing them to decompose endothermically. However, it appears that for uncoated magnesium hydroxide fillers, there is a transition period between 55 and 60% filler loading, after which composites can restrict the burning properties of polypropylene to make them very flame retardant.

5.1.11 Fracture surface analysis

To fully understand the effect that magnesium hydroxide morphology has on the mechanical properties of polypropylene, the fracture surfaces of both impact and flexural samples were viewed using scanning electron microscopy. Fracture surface analysis should compliment the mechanical properties assessment in sections 5.1.8 and 5.1.9.

To standardise the effect of filler loading, LOT 3 DP393 is compared to DP390s filled polypropylene (54.5 and 55.5% filler loadings respectively). DP393 and DP390s filled polypropylene impact fracture surfaces can be seen in Figs. 4.36 and 4.37 respectively. From observation of these impact fracture surfaces, it is obvious that both composites have failed in a brittle manner. Failure has occurred at the polymer/filler interface, indicating poor interfacial adhesion. The DP393 filled composite has a slight resemblance to a laminated system. Fracture may have occurred this way due to the layers of orientated filler platelets, in which the crack propagates along a plane of these

anisotropic filler particles. With the DP390s filled composite, the fracture surface is more uneven. However, the pseudo-spherical filler particle debonding can be clearly depicted, crack propagation will have occurred along the line of weakest interfacial adhesion.

The flexural fracture surfaces of DP393 and DP390s filled composites were also compared (Fig. 4.39 and 4.42), although less information was obtained. Again, interfacial adhesion was poor as filler particles debonded from the polymer matrix. However, there was some ductile failure, because microfibrils could be observed from both morphologies. This fibrillation tended to obscure the smaller DP393 filler particles and made conclusions more difficult. It is interesting that these two composites, comprised of different filler morphologies have almost identical flexural properties. However, poor filler/matrix adhesion was depicted, particularly for DP390s.

5.1.12 Filler dispersion

The dispersion of both filler morphologies was observed using the cryogenic etching technique. The dispersion cannot be quantified, but very good observational analysis is possible.

The composites observed were the same as for the fracture surface analysis, both with similar filler contents. Etched filler particles exist as black holes within the grey matrix background. Both filler types were well distributed within the polymer matrix. DP393 filler particles in general were well dispersed within the filler matrix, residing at their mean secondary particle size of approximately 1 micron (Fig. 4.43). Some slight agglomeration was observed, but this was not serious as agglomerates were no larger than about 3 microns. This is not surprising, since small platey fillers have a tendency to agglomerate. However, twin screw extrusion proved sufficient to keep the agglomeration to a minimum. DP390s filler particles were also very well dispersed within the matrix (Fig. 4.44). Although some particles resided at their mean secondary particle of approximately 5 microns, particles smaller than a micron were visible. It is

obvious that the abrasion caused by twin screw extrusion has caused some of the many primary particles to become detached from the secondary particles.

5.2 Coating Agent

The effect of coating agent was studied using two different types of fatty acid salts on the two morphologically different magnesium hydroxide fillers. The fatty acid salts used were either in ammonium or sodium form, the fatty acids used were stearic and oleic acid. The effect of coating type and level on the physical, mechanical and rheological properties of polypropylene, will be covered more concisely in sections 5.3 and 5.4 respectively.

5.2.1 Filler structure

The filler structure for both uncoated DP393 and DP390s has been clearly defined in section 5.1.1 in terms of crystal, primary and secondary structure.

Addition of a fatty acid coating agent to DP393 fillers has the effect of increasing the mean particle size of the filler. This has been attributed to the agglomeration of primary particles. However, altering the coating agent from sodium to ammonium has had little effect on the morphology of similarly coated fillers. The primary crystal structure was defined at the precipitation stage, so altering the coating agent will not affect this part of the filler structure. The primary particles remain as essentially regular hexagonal platelets, as seen in Fig 4.5. The agglomeration of these primary particles into secondary particles can be observed using scanning transmission electron microscopy (STEM). However, no noticeable difference in the secondary particle size is observed using this technique. This is best illustrated by particle size analysis.

Addition of a fatty acid coating agent to DP390s had the effect of decreasing the secondary mean particle size of the filler. This has been attributed to the coating agent being able deagglomerate some of the irregular primary particles. Altering the cation from sodium to ammonium produced no change in the primary structure, this being

determined, again at the precipitation stage. As STEM showed little difference in secondary particle structure, from that of the uncoated filler (Fig. 4.6), therefore particle size analysis was utilised.

5.2.2 Particle size distribution

Particle size analysis was performed on corresponding DP393 fillers with different coating agents. The particle size distribution for DP393 fillers coated with stearic and oleic acids using different coating agents is best exemplified in Figs. 4.11 and 4.12 respectively. From PSD analysis, it was found that altering the cation of the stearate coating agent caused no change in the mean particle size or distribution of DP393 filler particles. With oleate coatings, the mean particle size and distribution appears to be slightly more sensitive to altering the cation of the coating agent, especially at larger particle diameters. This effect though is not considered a significant finding. Differences in size analysis will be dependent on coating efficiency and dispersion within the Malvern particle sizer.

The effect of coating DP390s fillers has the tendency of deagglomerating primary particles to produce a smaller secondary particle size. Although no corresponding stearate coated DP390s fillers have been produced, the particle size distribution for oleate coated fillers can be seen in Fig. 4.13. Altering the cation from sodium to ammonium produces no significant change in the mean particle size or distribution.

5.2.3 Surface area

Once reacted onto the filler surface, coating agents should liberate bound magnesium stearate/oleate. The ammonium/sodium salts produced from this reaction should be removed by washing. The efficiency of the reaction will depend upon coating conditions, substrate purity and coating agent reactivity (section 2.3.2). Surface area determinations can be found in Appendix C.

For DP393 coated with stearate coating agents (LOT 1), surface areas of corresponding fillers are the same. As coating conditions and substrate purity should be identical, it can be assumed that to produce identical surface coverage, the reactivity of sodium and ammonium stearate are comparable. From FTIR DRIFT analysis, these two fillers also have similar CH/OH ratios (Appendix E), indicating that the amount of stearate in the composites (whether bound or unbound) is similar. With oleate coating agents, there are slight fluctuations of surface area for corresponding fillers. These fluctuations were also detected with FTIR DRIFT analysis. As the reactivity of stearate coating agents is the same, it is assumed the same is true for oleate. However, other workers [29], believe that oleic acid can also bond chemically through the double bond, located at the mid point of its aliphatic chain, which would therefore increase their overall reactivity. It is considered that coating conditions govern this reaction and not the change in coating agent.

5.2.4 Packing properties

For uncoated fillers, dry packing properties are mainly governed by particle size distribution. When coatings are applied, interparticle lubrication may also influence dry packing properties. Wet packing properties will be mainly governed by surface coverage and compatibility with the wetting oil. Packing data is found in Appendix D.

With corresponding DP393 fillers of the same LOT, bulk densities are similar (Appendix D). As the change in coating agent causes no significant change in particle size distribution, any change in bulk density must be due to coating effects. When measuring the bulk density of coated fillers, the coatings had a tendency to stick some of the platey filler particles to the side of the measuring cylinder used in obtaining bulk density values. This attraction may have prevented the movement of some particles by the tapping movement, which in itself was sufficient to cause the discrepancies.

Oil absorption measurements should be governed by the coating content upon the fillers surface which it has been shown is not governed by the cation. Therefore a change in coating agent will not affect the oil absorption measurements.

Bulk density and oil absorption measurements for corresponding oleate coated DP390s fillers are almost identical (Appendix D). The larger, round particles had less tendency to adhere to the measuring cylinder. Surface areas of the fillers were almost equal therefore similar amounts of oil were required to wet out the fillers.

Altering the coating agent on magnesium hydroxide fillers has caused no change in the packing properties, these are influenced by other factors.

5.2.5 Compounding

From the results in Tables 4.1 to 4.3 and Tables 4.5 to 4.6, it can be seen that a change in coating agent caused no change in the respective processing characteristics of fatty acid coated DP393 or DP390s fillers. Any slight discrepancies were due to fluctuations in filler loadings between the corresponding compounds.

5.2.6 Rheology

The application of a fatty acid coating using different coating agents did not significantly affect the primary particle size or size distribution (Figs. 4.11 to 4.13). Therefore any changes in the rheological properties of the compounds will be governed by the surface coatings of the fillers. The coatings affect filler morphology but it has not been possible to quantify whether the coating agents have fully reacted with the filler surfaces to become bound as magnesium stearate.

The rheological properties of DP393 filled compounds coated with stearate and oleate coating agents can be seen in Figs. 4.25 and 4.25 respectively. In both cases, the shear flow curves can almost be transposed onto each other. This would indicate that there is no difference in using ammonium over sodium as the carrier cation. If the coating agents have fully reacted with the filler surface, then the same amount of magnesium stearate/oleate will be produced. If only partial reaction has taken place, the presence of the coating agent upon the fillers surface will act as a lubricant too.

Although only one example of oleate coating agents can be given for DP390s (Fig. 4.26), again the shear flow curves almost overlap. Again this would suggest that the salt of the coating agent does not influence rheological properties, especially if it has fully reacted with the substrate surface.

5.2.7 Crystallinity

As crystallisation of polypropylene can be triggered by heterogeneous nuclei, the influence of coating agents could be expected to be most influential. Changing the cation from ammonium to sodium alters very few of the fillers physical characteristics, but ammonium salts are readily removed whereas sodium salts are not. The presence of impurities, even catalyst residues [102] can affect the crystallisation process.

From XRD and DSC analysis, differences in morphology of uncoated magnesium hydroxide have been shown to affect the crystallinity and orientation of the polypropylene matrix. Coating using a fatty acid coating agent was assessed using thermal analysis and Maiti's parameters [103].

For DP393 filled composites, corresponding fillers coated with different coating agents were shown to have similar onset temperatures and crystallinity contents (Table 4.19). Oleate coatings produced composites with the closest values. Crystallisation parameters of fatty acid coated DP393 LOT 1 filled compounds were also analysed (Table 4.24). Overall nucleation (S_i) and crystallisation rate ($T_c - T_p$) were the same for both the sodium and ammonium oleate coated filler. Crystallite size distribution did show a slight fluctuation for stearate coatings. As PSD (Fig. 4.12), surface area (Appendix C) and filler content (Appendix F) of these composites was so similar, it may be that residual insoluble sodium salts were responsible for these fluctuations.

Corresponding DP390s fillers coated with oleate coating agents also had similar onset temperatures and crystallinity contents (Table 4.22). Overall crystallisation rates were also similar (Table 4.25), but these uncoated pseudo-spherical particles were shown to have less of an effect than DP393 fillers.

As only certain crystal faces of filler particles are thought to act as nucleation centres [46], the fact that the both filler morphologies have strong XRD intensities in the 001 plane (Figs. 4.3 and 4.4) causing orientation effects in the matrix, it is assumed that this plane is the nucleation centre for magnesium hydroxide.

5.2.8 Flexural properties

The effect of filler coatings on the flexural properties of magnesium hydroxide/polypropylene composites will be covered more comprehensively in section 5.3 and 5.4. However, the effect of applying the coating using different agents will be dealt with here. Flexural data can be found in Appendix I.

Flexural properties of DP393 fillers coated with different fatty acid coating agents appear to vary. Difficulty in obtaining the desired 60% filler loading levels for corresponding LOTS of DP393 coated fillers was experienced. Polymers when loaded with filler produce composites with a higher modulus, but lower flexural strength and extension to break. Fillers compounded with stearate coating agents (LOT 1), contain the same filler level, so flexural properties can be directly compared (Table 4.7). The sodium stearate coated fillers have produced a composite with a slightly higher modulus, flexural strength and lower extension to break. As the surface area and wettability of the stearate coated fillers are the same, it may be the residual sodium salts that are causing fluctuations. LOT 2 oleate coated fillers are compounded at almost the same filler levels, and the flexural properties using different coating agents are the same. However, with LOT 3 oleate coated fillers, extension to break varies dramatically with only a small variation in filler content. This must be due to the difference in particle size distribution of the fillers, since the bulk density of the sodium oleate coated filler is much higher than for the ammonium oleate (0.72 compared with 0.54 respectively). Better packing properties will lead to a better dispersion of filler, limiting premature failure.

DP390s fillers coated with different oleate coating agents show a difference in flexural properties (Appendix I). This however, is attributed to the differences in filler content and not coating agents.

From the above results, it is deduced that fluctuations in filler level and particle size distribution are significantly more influential than coating agent when considering flexural properties.

5.2.9 Impact properties

Polypropylene is a highly ductile material at low strain rates yet can exhibit brittle characteristics at high strain rates. Falling weight impact testing induces deformations at high rates. Therefore, flaws within the matrix structure will be influential upon the failure mechanism. Impact data can be found in Appendix J.

The variation in impact properties for corresponding LOTS of DP393 treated with different fatty acid coating agents is more dramatic with a slight variation in filler content (Appendix I). Composites comprising of LOT 1 stearate coated and LOT 2 oleate coated fillers are loaded at similar levels. The corresponding impact properties are the same, accounting for standard deviations (Table 4.13). However, with a large difference (7%) in filler loading, such as for the oleate treated LOT 1 fillers, the impact properties decline with filler content. Volume fraction is therefore the most influential factor affecting impact properties and not coating agent. It would appear that there is a large change in impact properties between filler loading levels of 55 and 60%, a transitional zone. This is unfortunate because the upper limit is required for effective flame retardancy.

Differences in the impact properties DP390s coated with oleate coating agents can only be accounted for by differences in filler content, as only one pair of corresponding composites were studied.

5.2.10 Flame retardancy

Limiting oxygen index (LOI) is governed primarily by filler content whereas UL94 tests are also influenced by matrix rheology, since samples are lit at the bottom. Also, assuming that coatings are fully reacted at 4.5% level and fillers are loaded at 60%, each composite contains approximately 2.7% by weight bound fatty acid. LOI and UL94 results can be found in section 4.6.1.

When filler loading levels are similar, for corresponding LOTS of DP393 fillers treated with different coating agents, LOI values are also similar (Tables 4.41, 4.42 and 4.43). Also, if filler contents are 58.6% or over, their UL94 ratings are identical too. Therefore a very small difference in coating content (Appendix E) or crystallinity (Table 4.19) caused by the change in cation on coating agents causes no change in the flame retardant properties of the polypropylene composites. If filler contents do differ greatly, such as in the case of the LOT 1 oleate coated fillers, the change in LOI and especially UL94 ratings can change. This again is not attributed to the difference in coating agents.

DP390s fillers also show the same trend of improved flame retardance with filler content (Tables 4.45 and 4.46). The changes caused by the difference in coating agents are too small to affect the flame retardant properties.

5.2.11 Fracture surface analysis

To truly assess the affect of coating agent on the fracture behaviour of polypropylene, corresponding composites with similar filler content must be assessed. However, no visible differences in the fracture pattern were detected in either flexure or under impact.

5.2.12 Filler dispersion

Filler dispersion analysis by the polishing and etching technique provides an excellent way of observing filler dispersion in polypropylene. However, as the method was not quantitative, dispersion could only be categorised qualitatively.

Filler dispersion analysis revealed that fatty acid coating agents provided good filler dispersion for magnesium hydroxide fillers. However, no differences could be observed when using different coating agents.

5.3 Coating Type

The effect of using different cations as carriers for corresponding fatty acid coatings on DP393 and DP390s fillers have been discussed in section 5.2. However, DP393 fillers were also coated with a rosin gum and a vinyl silane coating, as well as the fatty acid coatings. Rosin coated DP393 was incorporated at 60% weight level, whereas silane coated DP393 was incorporated over a range from 20 to 70% weight level.

5.3.1 Filler structure

Observation of coated DP393 and DP390s fillers using scanning electron microscopy (STEM) revealed their primary and secondary structure (Figs. 4.5 and 4.6). The effect of applying any of the filler coatings to either filler type did not influence the shape or size of the primary particles. Therefore, the basic crystal and primary structure of the magnesium hydroxide fillers can be said to have been governed by the precipitation stages involved in production.

Although the basic shape of DP393 and DP390s secondary particles were retained after the application of coatings, it is difficult to determine small changes that may have arisen in secondary particle size. These will be revealed by particle size analysis.

5.3.2 Particle size distribution

The application of coatings (independent of level or type) to DP393 fillers had the effect of increasing the mean particle size of the fillers. Therefore, primary particles had a tendency to agglomerate with the application of a coating. However, the application of coatings (independent of level or type) to DP390s fillers had the effect of decreasing the mean particle size of the fillers. Agglomerates of primary particles had the tendency to deagglomerate with the application of a coating. Particle sizing data can be found in Appendix B.

Observation of DP393 coated fillers indicates that coating method can influence the final secondary particle size of the fillers. Slurry coating (stearate, oleate, rosin), produced a secondary particle size of approximately 1 micron in diameter. DP393 fillers in slurry form are coated prior to wet milling. In the slurry the primary particles are in a loosely bound network. Wet milling breaks up this network and exposes surfaces of uncoated filler. Primary particles have a tendency to group together in aggregates which lower their surface energy, which may involve adhering together by attraction or entanglement of the coatings. Stearate and oleate coatings can be expected to behave in the same way since they have similar characteristics. Rosin, however is a cyclic molecule, comprised mainly of abietic acid, but has the same secondary particle size as fatty acid coated DP393. The agglomeration of the primary particles of all three of these coating types has the effect of producing a secondary peak approximately 2 microns in diameter. Particle size distributions for DP393 fillers coated with stearate, oleate and rosin can be seen in Fig. 4.14.

Vinyl silane coatings were applied to DP393 by both spray and dry methods, after the fillers had been dried and milled. Filler treatment with vinyl silane coatings greatly increased the mean particle size of magnesium hydroxide when compared to the uncoated filler, especially when dry coating (LOT 2). The particle size distribution of these fillers can be seen in Fig 4.15. Spray coating consisted of applying the silane as a spray to a uniformly spread layer of filler. This method should apply the coating more uniformly on DP393. The PSD for this filler is similar to that of uncoated DP393

except for the presence of a small number of agglomerates up to 35 microns in diameter. These agglomerates were not detected using STEM, thus it can be concluded that they were only loosely held together. As the sprayed silane dried, it may have caused adjoining particles to adhere into clumps which further pin milling would have reduced. Dry coating in the laboratory (LOT 2) produced a totally different particle size distribution to other DP393 LOT 1 fillers, with a mean secondary particle size of approximately 3 microns. This crude mixing technique would not be uniform, with some regions of filler receiving little or no coating, with others receiving excess. This may have caused aggregation of primary filler particles into larger than normal secondary particles. The lack of large agglomerates experienced with LOT 1, may have been avoided due to the mechanical working of the silane into the filler, thus breaking down weak aggregates.

Fatty acid coatings were also applied to DP390s fillers in slurry form. Here, the mean particle size was reduced from approximately 5 to 4 microns in diameter. This can be seen in Fig 4.16. DP390s particles are pseudo-spherical particles comprised of many irregular hexagonal primary particles. When in slurry form, a combination of the addition of coatings along with the stirring motion, may cause weakly bound aggregates to disperse. This has caused the small shift in size of the major peak from 5 to 4 microns, the shape of the PSD itself remaining the same.

These changes detected in the mean secondary particle size of DP393 fillers when coatings are applied will influence the behaviour once incorporated into the polypropylene matrix. However, the compounding method itself will also affect the extremes to which the particles are dispersed.

5.3.3 Surface Area

The addition of filler coatings to magnesium hydroxide fillers causes a reduction in the surface area. This is due to the surface coatings smoothing out the micropores upon the substrate surface, allowing less nitrogen to be absorbed during their BET measurement. Surface area determinations can be found in Appendix C.

The amount to which the surface area will be reduced is governed by the quantity of coating applied, the size of the coating molecule, how the molecule is positioned upon the surface when it has reacted and the size of the micropores on the surface. For DP393 and DP390s fillers, total surface coverage with fatty acids and rosin are calculated to be at their upper coating content weight levels respectively. On DP393, vinyl silane is calculated to totally cover the surface at 2% weight level. Fatty acids cause a greater reduction in surface area at the same coverage than vinyl silane. This is probably due to the fatty acid chains being longer, covering up more of the fillers surface.

The increase in surface area with the DP393 LOT 2 fillers cannot be accounted for. However, their primary structure was the same as for LOT 1. The surface area measurements were also double checked. The increase in mean particle size would be expected to produce a smaller surface area. It may be that for these fillers in which there was a difficulty in repeating the exact filler morphology, a slightly more porous structure was present.

5.3.4 Packing properties

Packing properties of the magnesium hydroxide fillers studied were defined in terms of dry packing (bulk density) and wet packing properties (oil absorption). Bulk density will be influenced by particle size distribution and coating, whereas oil absorption will be mainly influenced by surface area and surface treatment. Packing properties can be found in Appendix D.

Figs. 4.14 and 4.15 show the effects of fatty acid, rosin and silane surface coatings on the particle size distribution of DP393 fillers which differ from uncoated DP393. From Appendix D, one can see that the application of a surface coating to DP393 increases the bulk density.

Application of stearate, oleate and rosin coatings to DP393 (Fig. 4.14) alters the particle size distribution. Although this difference in PSD compared with the uncoated

filler could be improving the dry packing properties, it must be the surface coatings that are most influential. Comparison, of either wet or dry packing, between stearate and oleate coated DP393 fillers (at the same coating level) show little difference. As the fatty acids have similar physical (solubility) characteristics, this was to be expected. Fatty acid coated fillers have optimum packing properties. This is due to their good interparticle lubrication promoting good dry packing. This lubrication can allow normally static particles to slide over each other to attain a higher order of packing. Also good compatibility with the wetting oil promotes good wet packing properties. The rosin coated DP393 has a high bulk density, indicating improved dry packing and interparticle lubrication. However, the higher oil absorption value may have arisen, because the compatibility of the rosin was lower than that of a fatty acid.

The two different LOTS of silane coated DP393 have significantly different particle size distributions (Fig 4.15), yet their bulk densities are similar, and only slightly larger than the uncoated filler. Although the PSD difference from the uncoated filler may be having some influence, the silane coating may be having a slight lubrication effect. The slight decrease in oil absorption compared to the uncoated filler indicates that the silane coated DP393 takes less oil to wet out. This will be due to the reduction in surface area caused by the coating, but also some compatibility with the wetting oil.

Packing properties of DP390s fillers are also improved by fatty acid coating, and were higher than for DP393 fillers. This was due to the fillers being more dense, but the particle size distribution of the pseudo-spherical particles being superior. From Appendix D, it could be suggested that high oleate coating levels produced the highest bulk densities. Oil absorption was improved with fatty acid treatment, but no obvious advantage of oleate over stearate was observed, again due to the fatty acids having similar physical and chemical characteristics.

5.3.5 Coating consistency

The amount of stearic acid coating present on magnesium hydroxide can be quantified by using FTIR DRIFT analysis [88]. The area of the CH peak caused by the coatings

alkyl chain substrate is ratioed to the area of the hydroxyl peak from the substrate. If the stearic acid had reacted onto the filler's surface, it would form magnesium stearate. Any unreacted stearic acid could be detected because it produces an IR peak at a different position to the reacted stearate. However, with this project, the coating agent was in salt form, so it was not possible to detect whether the coating agent had reacted onto the magnesium substrate or remained in its ammonium/sodium form (all of which have the same IR peak). Therefore the CH/OH ratio reveals the total amount of magnesium stearate and coating salt in the compound. Exactly the same situation exists for the oleate coating. Stearic acid possesses 16 alkyl CH₂'s whereas oleic acid possesses only 14, so the CH/OH ratio for stearate should be slightly stronger.

The CH/OH ratios for DP393 fillers can be seen in Appendix D. The highest ratio observed for stearate coatings is 0.396, whereas with oleates it is 0.318. In all cases for corresponding LOTS of fillers at the same coating contents, the CH/OH ratio is higher for stearate coated fillers. This simply shows that for DP393 fillers, the 16 stearate CH₂'s are producing a stronger signal than the 14 oleate CH₂'s. However, sometimes the difference in CH/OH ratios is greater than a 16/14 ratio. This may be due to the fact that any unbound fatty acid salt may have been removed from the filler surface by washing following milling, thus lowering the signal.

The CH/OH ratios for DP390s fillers can be seen in Appendix D. The highest ratio for stearate is 0.665 and for oleate is only 0.328, these being on the same LOT of fillers. It may be possible that with these larger, porous fillers, the oleate is reacting with its acid group and at the double bond. If this is the case, then only 7 CH₂'s are exposed from the fillers surface, capable of producing a signal of only half the strength. Washing will also remove some of the unreacted coating agent.

5.3.6 Compounding

To compare the compounding characteristics of DP393 fillers LOT 1 were used for the fatty acids and the rosin (Table 4.1), and LOT 1A was used for the silane (Table 4.4), since all of these compounds have a similar PSD and were all produced on the same

extruder. It can be seen from Tables 4.1 and 4.4, that the addition of a filler coating has significantly reduced the processing torque. The lowest torque was experienced with the fatty acids, stearate being slightly superior to oleate. This was to be expected since fatty acids are used for lubrication purposes in other polymer formulations. The processing torque of the rosin filled compound was only marginally higher, indicating its role as a processing aid. The vinyl silane coated filler produced the largest torque. It may be initially assumed that its lubrication properties were inferior to the other 3 coatings. However, the additional torque may have resulted from the break up of the large agglomerates detected by electron microscopy. With stearate, oleate and rosin, none of these large agglomerates (up to 35 microns) were detected. Capillary rheometry in section 5.3.7 was used to assess the melt flow properties of these compounds.

The processing characteristics of DP390s fillers can be assessed in terms of torque and extrusion pressure (Tables 4.5 and 4.6). Although the uncoated filler was produced at a higher screw speed, it can be seen from these tables that addition of a fatty acid coating still reduced the pressure at the die. There was no difference between stearate or oleate coated fillers, both having the same processing characteristics.

5.3.7 Rheology

From section 5.1.5, the morphology of magnesium hydroxide fillers has been shown to influence the rheological behaviour of polypropylene. Smaller, platey filler particles which can align in the flow direction, cause less laminar shear flow. Microporous fillers can produce an immobilised layer of polymer at their surface, increasing the viscosity. However, the difference in viscosity between DP393 and DP390s filled compounds, particularly at low shear rates, was not great (Fig. 4.23).

The effect of incorporating different levels of filler into polypropylene can distinctly alter its viscosity. This is illustrated in Fig. 4.27 using vinyl silane coated DP393 at nominal filler levels of 50, 60 and 70% (0.29 to 0.42 volume fractions) and 60% filled with uncoated DP393 as a reference point. Filler levels from 20 to 40% of vinyl silane

coated DP393 (0.1 to 0.19 volume fractions) were also incorporated into the matrix but surprisingly did not influence the viscosity of the matrix above that of the unfilled polymer. However, it is known [44] that high molecular weight polymers suffer less variation in relative viscosity with increased filler content than do polymers of low molecular weight. Small particle size fillers can form a strong structural network in a polymer melt. At volume fractions below 0.29, the affinity for neighbouring filler particles may be low, so a network is not formed because the interparticle spacing is too large. These platey fillers, orientate in the flow direction, and do not restrict the flow motion of the melt. At volume fractions over 0.29, the distance between neighbouring filler particles is reduced, and the tendency to form a network will be increased. With a network, the filler becomes less of a discontinuous phase, fluid mechanics of the polymer melt will be altered, and as a result the viscosity increases.

The effect on rheology of vinyl silane as a coating for DP393 can be compared against stearate, oleate and rosin in Fig. 4.28. All compounds are loaded at 60% weight level. Uncoated DP393 and unfilled polypropylene are included as boundary limits. As filler structures, mean particle sizes (and loading levels to a certain degree) are essentially the same for all compounds, any differences in rheological properties must be due solely to coatings. The rosin coating has the highest viscosity of all the coated fillers. At higher shear rates, the shear flow curve tends towards that of the uncoated filled system. The rosin coating is comprised mainly of abietic acid. This is a bulky, cyclic organic acid. If abietic acid had fully reacted with the substrate, the bulky molecule would be exposed from the fillers surface. Obviously some lubrication had been produced, since the viscosity is less than for uncoated DP393, but the bulky nature of the molecule restricted good lubrication. The vinyl silane coated filler has produced a shear flow curve intermediate between the uncoated filled system and polypropylene alone. The silane molecule is the shortest of the coatings used, therefore the coating molecules on the fillers surface should be less restricted to reorientate when under external shearing motion. This would explain the superior rheological properties over the rosin. Fatty acid coated DP393 produced rheological properties which are close to that of the unfilled polypropylene. There is a slight indication that oleate may be better than stearate, although this effect is not a significant one, as both chain lengths are

identical. Fatty acid molecules, at high coating levels, are thought to orientate themselves outwards from the fillers surface. The longer chain length permits a more effective lubrication than for the shorter silane molecules. Also, fatty acids are known to be good lubricants anyway, and are used for this purpose in many polymeric formulations.

The effect of fatty acid coatings on DP390s filled compounds can be seen in Fig. 4.29. Due to compounding difficulties, uncoated DP390s is present at 55.5% whereas stearate and oleate coated DP390s are present at 58.2 and 56.0% loading levels respectively. The viscosity of both the stearate and oleate coated fillers are comparable, the stearate being slightly lower at lower shear rates. This cannot be accounted for by the slight discrepancies in loading level since the loading level of oleate coated DP390s is higher, therefore favouring increased melt viscosity. However, the oleate coating may also react through its double bond, thus restricting the effective chain length, hence lubrication.

Oil absorption values give an indication of the wettability of fillers when incorporated into PP. It has been seen (Appendix D) that lower oil absorption values for both stearate and oleate coatings on both filler types have yielded the lowest rheological characteristics. This trend was not followed with silane and rosin. The rosin may be more compatible with the wetting oil, yet its bulky structure has restricted its ability to lubricate.

Finally, filler coating appears to be more influential than filler morphology in governing the rheological properties of magnesium hydroxide filled polypropylene compounds than the morphology of filler particles. Both DP393 and DP390s fillers coated with fatty acids produce PP compounds with similar viscosities. However, when uncoated, the platey structure of DP393 had superior flow properties compared to the pseudo-spherical structure of DP390s.

5.3.8 Crystallinity

DSC analysis was mainly used to assess the crystallinity of composites filled with magnesium hydroxide with various coatings. Crystallisation parameters were also investigated using Maiti [103] analysis. To give a direct comparison of coating types, coating levels corresponding to total surface coverage will be used (assuming complete reaction with the substrate), this being in all cases, the highest coating level produced.

X-ray diffraction analysis has shown that DP393 composites are anisotropic with the filler particles lying parallel to the moulded surface. DP390s fillers are shown to be isotropic within the matrix, therefore must retain their spherical shape during compounding. The effect of filler orientation produced a higher crystallinity content and orientation within the polypropylene matrix than the isotropic filler particles. The effect of filler coating will reduce the surface area and may reduce the number of 001 planes required for nucleation.

LOT 1 coated DP393 fillers were used to compare the effect of filler coating on crystallinity (Table 4.19), since the PSD and loading levels were very similar. Coating DP393 with vinyl silane and loading at various levels in polypropylene produced interesting effects on crystallinity as a function of time, and will be covered in detail in section 5.3.9. Addition of a fatty acid coating to DP393 reduced its onset temperature by about 8°C (Table 4.19), preventing the formation of the higher melting crystallites. Coating with the rosin however caused little change in onset temperature from the unfilled polypropylene, indicating little nucleation. Crystallinity contents for oleate and rosin coated DP393 were the same as for the uncoated filler, yet stearate coated DP393 produced a slightly higher content (which occurred with both coating agents). The overall crystallisation rate ($T_c - T_p$), of the stearate, oleate and rosin coated fillers (Table 4.24) were significantly increased above the unfilled PP (Table 4.26), and slightly increased above PP containing the uncoated filler (Table 4.24). Galeski [46] found that stronger adhesion between the matrix and fillers surface lowers chain mobility, which slows down the overall crystallisation rate. Surface modifiers restored this rate. The crystallisation rates and crystallite size distributions of the stearate, oleate

and rosin coatings were indistinguishable however. As the surface area and wettability of the fatty acid and rosin coatings differed so much, these factors have had little effect. As the surfaces of these fillers were totally covered, but possessed similar amounts of orientated 001 crystal planes within the polymer matrix, it must be this latter factor that is equalising their nucleation properties.

The nucleation properties of coated DP390s fillers were assessed using LOT 1 materials, but only stearate and oleate coatings were applied. Application of a fatty acid coating reduced the onset temperature of DP390s by approximately 8°C (Table 4.22). The surface tension of magnesium hydroxide fillers must also play a role in the formation of polypropylene crystallites, since higher melting crystallites were formed with uncoated DP390s. The crystallinity levels of the fatty acid coated fillers were similar, but slightly higher than the uncoated filler. The overall crystallisation rate of stearate coated DP390s was slightly lower than for oleate, but both yielded similar crystallite size distributions (Table 4.25).

Uncoated DP390s is more impure than DP393, this may have been one factor contributing to the reduction in the crystallisation properties of this filler. Once coated, the surface chemistry of the fillers will be similar, therefore having crystallisation rates that are alike. At total surface coverage, there appears to be little difference between stearate, oleate or rosin coatings in the crystallisation and nucleation properties of each filler morphology (Table 4.24). Rosin however does not increase the onset temperature above the unfilled, restricting the formation of higher melting point crystallites. Surface coated DP393 fillers do produce marginally higher crystallinity contents (Table 4.19) than corresponding DP390s fillers (Table 4.22), due to the orientation of the 001 planes within the matrix. Maiti [103] also found that polypropylene crystallisation rates increased with filler surface coating, but only one coating level was studied.

5.3.9 Ageing of vinyl silane composites

Investigation of the influence of LOT 1A silane coated DP393 on the crystallinity and mechanical properties of polypropylene gave an indication that these properties were

influenced by post moulding time. As only a small range of loading levels were studied (46.2 to 63.3% weight fraction) a second LOT of this filler was compounded at a wider range of filler loadings (22.5 to 65.9%), and coded LOT 1B, to investigate these changes further.

The initial investigation performed on LOT 1A, consisted of measuring the crystallinity soon after moulding and up to 305 days post moulding. It can be seen (Table 4.28) that for all of the highly filled composites, there is a distinct change in crystallinity up to 56 days. This would be expected to influence mechanical properties, which were measured quite a time after moulding. However, flexural (Fig. 4.33) properties were seen to change between 152 and 351 days after moulding, a period when the crystallinity was expected to have stabilised.

In order to understand these effects in more detail, a new programme was set up, in which vinyl silane coated DP393 composites were loaded at levels from 20 to 70% by weight, and compared to the unfilled polypropylene. Crystallinity levels and mechanical properties were measured from one week up to 158 days post moulding. From the results in Table 4.30, it can be seen that there is an increase in onset temperature from unfilled PP up to that containing a filler level of 65.9%. The highest filled composite has the same value as for 59.3% uncoated DP393. The increase in onset temperature appears to happen in two stages. Stage one from unfilled to 38.5%, stage two above this level to the highest filler content. The presence of more nucleation centres may permit the high temperature crystallites to be formed, thus causing the rise in onset temperature. There is however no change in onset temperature with time. Although a standard deviation is not given, the scatter in crystallinity measurements was significantly larger for readings taken 6/7 days post moulding (Table 4.31). This can be expected as the polymer matrix is reaching a uniform state. However, the mean values were still high. Beyond this time, the crystallinity of the mouldings appeared to increase as a function of time (Table 4.31), hence so did flexural modulus and strength (Appendix I). The extremely low flexural properties measured 6/7 days post moulding cannot be explained in terms of crystallinity effects.

Thermal analysis data was examined in more detail using crystallisation parameters. It can be seen that unfilled polypropylene has the lowest crystallisation rate (Table 4.35). Incorporation of vinyl silane coated DP393 has the effect of increasing the crystallisation rate (Table 4.35) and narrowing the crystallite size distribution (Table 4.37). Nucleation properties also appear to occur in two stages (Table 4.36). From 22.5 to 38.5% filler, the crystallisation rates are fast causing a narrow crystallite size distribution. Above this level, crystallisation rates are reduced, producing a larger crystallite size distribution. There is an indication that the highly loaded composites are slightly more crystalline (Table 4.31), probably due to the presence of the higher melting point crystallites, producing a larger spread in crystallite sizes. This coexistence of large and small crystallites may account for the decrease in flexural strength of the highest filled composites, also observed by Maiti [103], due to the less well defined morphology. There is however no indication that these crystallisation parameters are influenced by post moulding time (Tables 4.35 to 4.37). Changes in flexural properties must be due to filler/matrix interfacial effects. The exact factor governing the change in flexural properties could not be determined, but migration of the silane from the filler surface may have contributed, causing an increase in interfacial adhesion between the filler and matrix, therefore increasing low strain rate properties. The impact properties of the composites however were not altered by time (Appendix J), therefore no change occurred at high strain rates. Therefore, impact results for vinyl silane coated DP393 filled polypropylene can be directly compared to the other coatings in section 5.3.11.

The strange crystallinity values obtained after 6/7 days (Table 4.31) were further investigated by incorporation of a fresh vinyl silane coated DP393 filler at nominally 20 and 60% coating levels. These compounds were compared to both unfilled and 60% uncoated DP393 filled polypropylene. Although these compounds were batch mixed, they have some relevance to the above composites. Their crystallinity content and rates were measured immediately after preparation and up to a period of 69 hours, although only one point data could be used. The unfilled polypropylene had the lowest onset temperature (Table 4.33). Vinyl silane coated DP393 produced compounds with the same onset temperature (Table 4.34), whereas the uncoated filler was marginally

higher (Table 4.33). Results indicated that there was no change in crystallinity content with time. Polypropylene had the lowest crystallinity level, whereas the filled compounds had about the same level (Tables 4.33 and 4.34). Measurement of crystallisation parameters revealed that uncoated DP393 produced the fastest crystallisation rate (Table 4.38). Highly filled silane coated DP393 produced a rate just higher than that at the lower level. This was not observed when continuous mixing was used. The crystallite size distribution for this low filler content was also wider than the highly filled compounds. It must be noted that the particle size distribution of this LOT 2 vinyl silane coated filler was significantly different to that in LOT 1.

From the various vinyl silane programmes, it has been deduced that the crystallinity of vinyl silane coated DP393 composites, in general do not alter as a function of time. Slow strain rate mechanical tests, such as flexural testing, do show an increase in bulk properties, whereas fast strain rate impact properties are unaffected. Varying the filler content does influence the crystallisation rate which defines the range of crystallites formed. These rates are dependent on the filler particle size and shear stress exerted upon the melt during preparation, which influences the extent of filler dispersion.

5.3.10 Flexural properties

The flexural properties of vinyl silane coated DP393 filled polypropylene have been shown in section 5.3.9 to increase as a function of time. Therefore, these composites cannot be directly compared to other composites containing magnesium hydroxide with the other coatings. Flexural data can be found in Appendix I.

Again, LOT 1 DP393 filled composites have been chosen to show the effect of filler coating on the flexural properties of their composites, since filler particle size distributions and loadings are similar (Appendix B and F). Incorporation of fatty acid coated fillers causes a reduction in the flexural properties of uncoated DP393 filled polypropylene composites (Table 4.8). Fatty acid treatment has been shown to reduce the oil absorption, therefore should enhance compatibility with the matrix. Jancar [61] stated that fatty acid surface treatment reduced the amount of immobilised

polypropylene on the fillers surface by lowering the thermodynamic work of adhesion. Fatty acids therefore reduce the interfacial adhesion at the polymer/filler interface, causing lubrication. Comparison of stearate and oleate coatings at total surface coverage reveal that the flexural modulus and strength of the oleate coated filler is lower than that of the stearate (Table 4.8). Jancar also proposed that the reaction of stearic acid deactivates the reactive centres on the magnesium hydroxide surface, causing a reduction in the interfacial work of adhesion. If oleic acid can also react through its double bond, then more reactive sites on the fillers surface can be deactivated. This would further reduce the interfacial work of adhesion and account for the decrease in flexural properties of the oleate coated DP393 when compared to the stearate. The higher flexural modulus and strength of the uncoated filled composites must be due to higher interfacial adhesion caused by the formation of immobilised polypropylene around the fillers surface. This so-called transcrystalline region [46] must allow loads to be transferred onto the filler, which is more difficult with the lubrication effect experienced with fatty acids.

The rosin coated filler produced the highest flexural properties of all DP393 filled composites even though the wettability of this filler is higher than for fatty acids (Table 4.8). This would indicate that there is increased interfacial adhesion between the filler and coating. As there are no more groups except the acid group expected to react, it could be deduced that the coating is altering the morphology of the polypropylene around the filler particles. Although the onset temperature is different, the crystallinity and crystallisation parameters do not significantly differ from the fatty acid coated filled composites. The rosin coating however is mainly comprised of abietic acid, but does contain organic impurities. The blocky structure of the abietic acid molecule with its propyl chain at the opposite end to the substrate may be enough to cause physical entanglement with the matrix, improving the interfacial adhesion. However, from dispersion analysis, rosin causes filler particles to agglomerate. These weakly bound agglomerates will increase the flexural modulus due to the improved load transfer onto the larger particles, but their poor cohesion will cause premature failure through them.

Although flexural properties of vinyl silane coated DP393 filled PP are time dependent, the flexural modulus of 60% filled composites are higher than for fatty acids (Table 4.8). The high oil absorption value and short chain length of the silane may permit the matrix to interact with active sites on the filler surface to promote load bearing transcrystalline regions, like that those on the uncoated DP393.

DP390s fillers were only treated with fatty acid coatings. Accounting for the slight difference in filler loading, stearate and oleate coated filled composites have similar flexural properties to each other (Table 4.9). The uncoated filled composite has a flexural modulus almost identical to the composites containing fatty acid coated magnesium hydroxide. This can be accounted for by two factors. Firstly, the loading level is the lowest of all these composites (Appendix F). Secondly, the mean secondary particle size is approximately 5 microns, whereas the coated fillers are only 4 microns. Flexural strengths of the fatty acid coated fillers are lower than the uncoated material, and can be accounted for by the decrease in interfacial adhesion caused by the decrease in wettability.

5.3.11 Impact properties

The impact properties of vinyl silane coated DP393 filled composites have been shown not to be time dependent, therefore they can be compared directly to other coatings (Appendix J). Again, to maximise the number of coatings compared and restrict the number of variables affecting material properties, composites comprised of LOT 1 fillers for both DP393 and DP390s were studied.

Incorporation of DP393 filler particles reduced the peak impact energy to at least one quarter of that for unfilled polypropylene (Table 4.12). This is because the platey fillers act as stress concentrators from which cracks can propagate. Uncoated DP393 produced higher impact properties than all of the filled systems except for those coated with vinyl silane (Appendix J). As peak impact force is analogous to flexural strength, this would reinforce the theory that interfacial adhesion for the uncoated filler is higher than for fatty acid and rosin coated fillers. This would ensure that more impact load is

transferred onto the filler particle. This load bearing would occur through the transcrystalline region at the polymer/filler interface caused by immobilisation of polypropylene by reactive sites upon the substrate. Filler coating with a fatty acid has shown little difference in impact properties between stearate and oleate, when both filler loadings are similar. Fatty acid treatment will reduce the interfacial adhesion, but at high strain rates was not as significant as with flexural testing. Rosin coated DP393, although having a high flexural modulus and strength (Table 4.8), had poor impact properties (Table 4.14). The peak impact energy was almost half of that for fatty acids. The bulkiness of the cyclic structure may have been ineffective at load bearing/lubrication at high strain rates. Finally, the silane had impact properties midway between that of a fatty acid and rosin (Table 4.14). The wettability of the filler was high, indicating poor interfacial lubrication. The shortness of the silane chain may have been ineffective in transferring load from the matrix onto the filler.

Coating of DP390s fillers followed the same trends as for DP393 fillers (Table 4.15). Fatty acid surface treatment lowered the toughness of the composite, but both stearate and oleate coatings produced similar values.

In instrumented falling weight impact tests, Hornsby [67] found that fatty acid coatings applied in salt form at high coating levels to magnesium hydroxide at high filler levels resulted in a substantial increase in the impact strength. Fatty acid salts gave better results than fatty acids, however unreacted magnesium stearate gradually migrated to the mouldings surface causing a reduction in mechanical properties. This may indicate that the filler coating conditions on both DP393 and DP390s fillers were not ideal, and unreacted coating agent may have resided upon the fillers surface, with a potential to bloom out and cause detrimental effects on mechanical properties.

5.3.12 Flame retardancy

The flame retardant effects of the coated filled composites were assessed using limiting oxygen index (LOI) and UL94 tests. These results can be found in section 4.6.1.

The effect of vinyl silane coated DP393 as flame retardant filler for polypropylene was studied using filler loading levels from 46.2 to 63.3% (0.25 to 0.40 volume fraction). From Fig 4.34, it can be seen that over this range the limiting oxygen index increased exponentially as a function of loading level. Although the range of loading levels is quite small, the filler is not simply acting as a diluent, also observed by Hornsby [15]. At these high filler loadings, the burning characteristics and accumulation of residual ash was similar, with no spalling of ash from the burning composite being observed. With UL94 tests however, the trend was not so simple (Table 4.44). With filler levels of 53.7% and under, the composites were rated unclassified, and although the burning rate was suppressed, the composites did not extinguish. When the filler loading level was increased to 57%, a rating of V1 was reached. Although the filler was releasing water vapour through endothermic decomposition (as with the two lower loading levels), the dilution of the matrix was sufficiently high to achieve some flame retardancy. Eventually, at 63.3% loading, vinyl silane coated DP393 achieved the necessary V0 rating, acting not only as a diluent but the oxide being present in adequate quantity to act as a screen to the heat source. The UL94 test varies compared to the LOI test since more heat is redirected into the bottom lit samples.

The influence of filler coatings on the flame retardant properties of DP393 filled composites was investigated using silane, stearate, oleate and rosin coatings. To give comparable results (Tables 4.41 and 4.44), LOT 1 fillers at maximum coating levels were used (since the rosin and silane only exist in this extreme). The primary structure and particle size distribution of these fillers is also very similar, although filler loading levels do vary slightly. The uncoated filler was compounded at 59.3% and was rated at 27.8% for LOI and V0 for UL94. Incorporation of a fatty acid treated filler, at a very similar level also produced a UL94 rating of V0. The rosin coated filler was loaded at a slightly higher level, and produced a UL94 rating of V1 and an LOI of 27.5. It may be that the presence of the rosin gum coating, although only present in a small quantity, increases the flammability and reduces the LOI compared to the uncoated filler. The LOI of the stearate coated DP393 filled composites were slightly lower than those of the oleate, yet this is because these composites had the lower filler contents. At least 63.3% vinyl silane coated filler was required to attain a V0 rating, however this

composite had the highest filler content of the group and produced the highest LOI. It is difficult to rank the DP393 filler coatings in their contribution to flame retardance. None of the filler coatings (even the fatty acids), even at these high coating levels significantly altered the rheological properties of the composites when burning, to promote dripping. No spalling of the ash was experienced for any of the composites, therefore from these simple tests, it can be assumed that their burning mechanisms are very similar.

DP390s fillers were more difficult to compound at 60% level and the scatter in loading levels was greater. Uncoated DP390s and oleate coated at 4% were in the matrix at similar levels. Both produced the same UL94 ratings and similar LOI values (Table 4.45). The corresponding stearate coated filler, contained over 2% more filler had a higher UL94 rating. However, the LOI was no better than that of the oleate at a lower level. Therefore, if the filler coating is influencing the flammability, then it is the free fatty acid which is causing the change rather than the bound. At the highest fatty acid coating levels, with low filler loadings (AMST6.0, LOT 1 and NAOL6.0, LOT 2), the effects of this additional lubrication was to enhance dripping of the composites, igniting cotton wool situated below the samples.

For highly filled magnesium hydroxide composites, the filler loading level is the main factor governing the flame retardant effects and not the filler coating. Differences in coatings did not appear to produce differences in the burning characteristics but direct comparisons could not be drawn due to the difficulty in producing samples loaded at exactly 60%.

5.3.13 Fracture surface analysis

Fracture surface analysis of uncoated DP393 and DP390s filled polypropylene, particularly impact specimens, revealed slight differences in their fracture mechanism. The effect of filler coating on fracture analysis is given below.

LOT 1 DP393 filled composites were again used to compare the effect of coating type on fracture behaviour, since they have similar particle size distributions and filler loadings. Fatty acid coated fillers had similar flexural fracture surfaces, a typical flexural surface for a stearate coated filler can be seen in Fig. 4.38. Ductility within the matrix is revealed by the formation of a degree of fibrillation. Filler particles can be seen dispersed within the matrix. However, holes within the matrix where the filler particles have pulled out indicate poor adhesion with the matrix. The fracture surface is not dissimilar to that of uncoated DP393 loaded at 60% (Fig. 4.39). The vinyl silane flexural surface, loaded at a similar level (Fig. 4.40), indicates that the incorporation of this filler reduces the ductility of the system. There is some indication of drawing of the matrix, but fibrils are shorter than for fatty acid coated fillers. Filler debonding can be depicted and holes where agglomerates have pulled out the matrix are also visible. These agglomerates are no larger than 5 microns. The flexural fracture surface of the rosin is totally different from the other coated fillers (Fig. 4.41). There is no sign of matrix ductility, indicated by fibrillation, which therefore accounts for the small elongation at break. Some filler agglomerates, no larger than 5 microns can be seen. Fracture has again occurred by the filler debonding from the matrix. Fatty acid coated DP390s filled polypropylene flexural surfaces are almost identical and resemble that of the uncoated material (Fig. 4.42). Filler particles are well distributed throughout the matrix. The composites have failed in the matrix, as the formation of fibrils around the filler particles. There is no indication of any cohesion with the matrix.

Impact fracture surfaces are less revealing than flexural, since the strain rate is much faster and all samples fail in a brittle manner. The fracture behaviour for DP393 and DP390s is comparable to that of the uncoated filled matrix (Figs. 4.36 and 4.37). DP393 fails along the matrix, indicating a degree of lamination, probably caused by the anisotropic filler particles. Fatty acid filler particles look well dispersed within the matrix. The lower fracture toughness of the silane and rosin coated fillers is accounted for by the presence of agglomerates, up to 5 microns in diameter. Filler agglomeration increases the effective particle size of the filler particle, and if weakly bound, will provide an easier route for crack propagation. Fatty acid coated DP390s are well dispersed within the matrix and fail by debonding of the filler particles.

5.3.14 Filler dispersion

Filler dispersion analysis of magnesium hydroxide filled composites was achieved using the polished etching technique. Although the method was not quantitative, an excellent visual representation was possible.

DP393 fillers were coated in fatty acid, silane and rosin coatings. The filler distribution for both uncoated and coated fillers was shown to be good. Filler particles that have been removed from the matrix are represented by black holes. Particle size analysis of the vinyl silane coated filler revealed that particles up to a diameter of approximately 35 microns were present in the uncompounded filler (Fig. 4.15). However, one can see from a representative sample shown in Fig 4.45, that filler dispersion is good. Most filler particles exist at their mean particle size of about 1 micron. Very few agglomerates were detected, and where present these were no larger than 5 microns. Stearate and oleate coatings created no difference in the dispersion of the DP393 fillers. The particles again existed at their mean particle size of 1 micron. No cases of agglomeration were detected on the samples prepared. The similarity in wettability and surface properties of the fatty acids was the reason for their similarity in dispersion. The dispersion of an oleate coated filled composite can be seen in Fig. 4.46 The rosin coating was the only coating that caused significant agglomeration, as detected by holes greater than 3 microns in diameter, seen in Fig. 4.47.

DP390s fillers were only coated with fatty acids. The dispersion of both stearate and oleate coated fillers was very good, with no indication of agglomeration. This can be seen in Figs. 4.48 and 4.49 respectively. The mean particle size obtained by particle sizing was retained in the matrix.

It can be deduced that magnesium hydroxide coating with fatty acids promotes good filler dispersion in polypropylene. With vinyl silane some agglomeration does occur but is reduced by compounding. Rosin coating has the tendency to cause filler agglomeration, which occurred during compounding.

5.4 Coating Level

The effects of coating level was studied using two different types of fatty acids on the two morphologically different magnesium hydroxide fillers. The fatty acids used were stearic and oleic acid. The effect of coating agent and type on the physical, mechanical and rheological properties of polypropylene, were covered more extensively in sections 5.2 and 5.3 respectively.

5.4.1 Filler structure

The filler structure for both uncoated DP393 and DP390s has been clearly defined in section 5.1.1 in terms of crystal, primary and secondary structure.

Addition of a fatty acid coating agent to DP393 fillers has the effect of increasing the mean particle size of the filler. This has been attributed to the agglomeration of primary particles. However, increasing the coating level of either fatty acid had no significant effect on the morphology of DP393 fillers. The primary crystal structure was defined at the precipitation stage, so altering the coating level will not affect this part of the filler structure. The primary particles remain as essentially regular hexagonal platelets, as seen in Fig 4.5 It should be possible to observe the agglomeration of these primary particles into secondary particles using scanning transmission electron microscopy (STEM). However, no noticeable difference in the secondary particle size was observed using this technique. Particle size analysis was used to investigate the effect of coating level on the particle size distribution of DP393 fillers.

DP390s secondary particles deagglomerated slightly with the addition of a fatty acid coating. As the primary particle structure was defined at the precipitation stage (Fig. 4.6), STEM was used to observe the differences in secondary particle size of the fillers. No noticeable difference was seen between different coating levels, so particle size analysis was again used.

5.4.2 Particle size distribution

To ensure that the effect of increasing both fatty acid coating levels on both magnesium hydroxide types, LOT 1 fillers were used for comparison in all cases. Particle sizing data can be found in Appendix B.

The particle size distribution for DP393 filler coated with stearic and oleic acid at high and low levels can be seen in Fig. 4.17. It is known that changing the coating agent and coating type, has no effect on the particle size distribution. It can be seen from Fig. 4.17 that an increase in coating levels also causes no change in the PSD for DP393 fillers. Once DP393 is coated with fatty acid at a low level, the high surface polarity is reduced. This permits particles to agglomerate into a structure with a lower surface energy. Progressive coating will only reduce the surface energy slightly, when compared to the uncoated, so no advantage is gained by reordering into another structure. As both stearic and oleic acid have similar physical properties, their polar and dispersion components should be identical at equivalent coating levels. It has been shown [47] that the largest incremental change in these parameters occur when a small level of fatty acid coating is applied to an uncoated filler.

Particle size distributions for fatty acid coated DP390s at different coating levels can be seen in Fig. 4.18. Like DP393 fatty acid coated fillers, altering the coating agent and coating type has no significant effect on the fillers particle size distribution. Increasing the fatty acid coating level also causes no change in the particle size distribution of the fillers, this again been attributed to the small changes in surface tension between coated fillers.

5.4.3 Surface area

The application of stearic and oleic acid coatings to magnesium hydroxide fillers is thought to reduce the surface area by the same amount, since both molecules have the same chain length and similar physical properties. However, if the oleate can react through its double bond as well as its acid group under certain conditions, this may

cause discrepancies between the two fatty acids. Surface area determinations can be found in Appendix C.

The effect of surface area on the progressive coating of magnesium hydroxides with different morphology can be seen in Fig. 4.19. The surface area of both filler types, initially very similar, progressively decreases with an increase in filler coating level. Due to the large surface area of the pseudo-spherical DP390s filler, it has been deduced that this filler morphology is 'porous', created by many 'micropores' between the irregular primary platelets. The reduction in surface area with coating content is most significant for this filler morphology. It may be that fatty acid molecules, when bound to the substrate, prevent nitrogen molecules being absorbed into the tiny micropores. This would retain extensive undetectable internal porosity after coating, as confirmed by Hornsby [67]. The effect of increasing the coating level has the effect of macroscopically smoothing out any discontinuities on both filler surfaces. This has the effect of lowering the effective surface area.

5.4.4 Packing Properties

It has been seen, that the addition of a filler coating can significantly increase the dry and wet packing properties of magnesium hydroxide fillers. The effect of increasing fatty acid coating content on these properties can be seen below. It appears that packing properties are mainly governed by particle size distribution and coating type.

The dry packing properties of DP393 fillers can be seen in Appendix D. It can be seen that an increase in coating level, for LOT 1 or 2 fillers, caused no increase in the bulk density of these fillers. The fatty acid coating causes an interparticle lubrication effect and permits filler particles to pack to a higher order than when uncoated. However, the particle size distribution will limit the extent to which the packing can occur. Therefore, although further additions of a fatty acid coating, provide further lubrication, the upper limit of packing is restricted by the PSD. The bulk densities of DP390s fillers also increase with fatty acid content for LOT 1 and 2 fillers. This again being due to the increase in interparticle lubrication, allowing primary particles to slide

past each other to attain a higher order of packing. The increase over the uncoated material is larger with DP393 fillers due to the smaller platey filler particles being able to fill interstices created by adjoining filler particles. This is more difficult for the significantly larger pseudo-spherical DP390s fillers.

The wet packing properties of DP393 fillers can be found in Appendix D. It can be seen that oil absorption decreases with an increase in fatty acid coating content. This is due to the fact that as more coating is applied, the surface energy and solubility parameters of the filler are altered and the filler becomes more compatible with the wetting oil. As the particle size distribution is not affected by changes in coating content, the effect is solely due to coating content. The same effect is true for DP390s fillers, except an increase in coating level causes less of a reduction in oil absorption. Both fillers have essentially the same surface area when uncoated. However, DP390s being porous can retain oil within these pores thus increasing the wet packing properties. This trend can be depicted in Fig. 4.20., a plot of oil absorption per unit surface area versus stearate coating content. Both uncoated magnesium hydroxide fillers originate from the same upper point on the graph. As a stearate coating is applied, the oil absorption per unit surface area decreases, as some of the surface coverage is reduced. However, as progressive coating occurs, the oil absorption per unit surface area decreases less, and tends to level out.

5.4.5 Coating consistency

Although FTIR drift analysis cannot quantify whether the fatty acid chain is bound to the fillers surface, it can detect the amount of fatty acid salt present in the compound. This could be in the form of bound or unbound magnesium stearate or as the unreacted coating agent. Knowledge of the amount of fatty acid salt upon the fillers surface assists in an understanding of the fillers rheological and crystallisation properties.

From Appendix E, the CH/OH ratios for fatty acid coated DP393 and DP390s fillers can be seen. It is clear that an increase in fatty acid coating level produces an increase in the CH/OH level for both filler types. That is there is more fatty acid, in whatever

form, present in the compound as more coating agent is applied. The CH/OH ratios appear to increase linearly as a function of applied coating level. Therefore, highly coated filler would be expected to have superior lubrication properties. Gilbert [88] found that non porous magnesium hydroxide reached a saturation coating level at 3% (comparable to DP393) and a porous grade at 7-8% weight coating (comparable to DP390s). This is why DP390s filler has a higher applied coating level to achieve saturation (6.0%) when compared to DP393 (4.5%), even though their surface areas are so similar. The slight difference in signal strength for oleate compared to stearate arises from the fact that the double bond on the oleate chain reduces the CH₂ signal.

5.4.6 Compounding

From Tables 4.1 to 4.6 it can be seen that an increase in the fatty acid coating level causes a decrease in the processing torque and pressure of both morphologies of magnesium hydroxide. This again was attributed to the fatty acid coating (magnesium stearate/oleate) acting as a lubricant. The coatings should act as both internal and external lubricants. Internal lubrication would reduce inter-particle friction whereas external lubrication would reduce friction between the polymer and the barrel/screw arrangement. Increasing the coating level will simply increase the amount of lubricant present, therefore easing processability.

5.4.7 Rheology

It has been seen that the platey DP393 fillers produce a lower melt viscosity when incorporated into polypropylene than the pseudo-spherical DP390s fillers. Fatty acid coatings reduce the shear viscosity on both filler types by similar amounts.

The change in melt viscosity of polypropylene with increased oleate coating level on DP393 fillers can be seen in Fig. 4.30. Uncoated DP393 and unfilled PP are included as the upper and lower limits of viscosity. It can be seen that an increase in oleate coating level reduces the melt viscosity of DP393/PP compounds. Even the addition of the lowest level of coating (1.5%) has a pronounced effect. When the coating reached

the intermediate level, the reduction in melt viscosity compared with that at total coverage, was not so great. It may be that at the lowest coating level, some of the filler surface is left exposed, causing high frictional forces producing higher shear stresses. Above this level, most of the fatty acid chains are packed tightly enough together to prevent the filler surface making contact with any external media. Identical trends were found as with compounding characteristics, the fatty acid coating possessing lubrication properties.

Fig 4.31 shows the effect of increased stearate coating level on the rheological properties of the porous DP390s filled PP. Identical trends to those observed for the DP393 coated fillers are seen. Addition of a filler coating appears to influence the rheological characteristics of magnesium hydroxide filled polypropylene more than the morphology. Hornsby [84] found that when a porous grade of magnesium hydroxide was treated with an excess of stearate coating agent (magnesium stearate), the melt viscosity of the compound was reduced below that of the unmodified polypropylene. Apart from the excess magnesium stearate acting as a dispersion aid, it was deduced that it was also acting as a plasticizer or external lubricant for polypropylene. This was not observed with DP393 or DP390s, indicating that an excess of coating level was not applied to these filler morphologies, and that magnesium stearate (bound or unreacted) does have lubrication properties.

5.4.8 Crystallinity

The morphology of the two magnesium hydroxide types has been shown to affect the crystallinity of the polypropylene composites. The effect of increased fatty acid coating content on crystallinity can be seen below.

As the coating level of fatty acid coated DP393 fillers increases, it can be assumed that the crystallinity remains approximately constant (Table 4.19). Stearate coatings appear to increase slightly in crystallinity, but this may be accounted for by statistical variation. The onset temperature can be seen to decrease marginally with increased coating level. The change is only great between uncoated and coated filler. Once a

filler coating has been applied, the decrease in surface tension of the filler is only small, therefore little change in the nucleating properties would be expected. Observation of the crystallisation parameters (Table 4.24) reveals that the crystallisation rate decreases as the coating level increases. The effect is most noticeable for the lowest coating content, which produces the fastest crystallisation rate and smallest crystallite size distribution. This will favour the formation of many small crystallites, producing a fine structure. At higher coating levels, the crystallisation is slower, favouring the formation of larger crystallites, of a wider crystallite size distribution. This slower growth of crystallites may lead to more well defined boundaries, producing optimum mechanical properties. Similar effects were seen with DP390s, except that crystallinity contents were slightly lower (Table 4.27). However, nucleation properties were similar (Table 4.25).

It has been seen that filler morphology affects the nucleation properties of magnesium hydroxide fillers (section 5.1.7). However, surface treatment also affects nucleation properties. Firstly the surface tension of the filler is reduced with fatty acid coating, but secondly the surface area is also reduced, altering the morphology. Only certain crystal faces of filler particles are thought to have the ability to nucleate polypropylene. When uncoated, these faces will be exposed, but their poor wettability, due to the high surface energy, may limit their nucleating properties. At low coating levels, the surface energy is reduced, improving nucleation. At high coating levels, the surface area has been reduced by the smoothing of discontinuities on the fillers surface. This may have obstructed some of the crystal faces necessary for nucleation, therefore reducing the crystallisation rate.

5.4.9 Flexural properties

It has been found that the filler morphology of magnesium hydroxide fillers affects the flexural properties of polypropylene. DP393 fillers are platey, align in the flow direction of the melt, and cause superior flexural properties to the unorientated pseudo-spherical DP390s fillers. At total surface coverage, oleate coatings cause

slightly more of an interfacial lubrication effect than stearates. The effect of coating the fillers at levels ranging from uncoated to total surface coverage can be seen below.

It can be seen from Table 4.10, that as the fatty acid coating level increases, the flexural properties of DP393 LOT 1 filled polypropylene composites are modified. An increase in coating level causes a reduction in the flexural modulus and flexural strength, whereas the extension to break increased. This was true for LOT 2 fillers, with mean secondary particle sizes of 2 microns compared with 1 micron for LOT 1. As the filler coating level was increased, the surface area and oil absorption of the fillers were reduced. This will have improved the wettability with the polypropylene matrix. Increased wettability has been shown [47] to decrease interfacial tension and work of adhesion of fatty acid treated calcium carbonate. The reduction in the interfacial work of adhesion with the polymer matrix, will have the effect of producing less immobilised polypropylene on the fillers surface, which is responsible for load bearing. This is reflected by the reduction in flexural strength with coating content, for both stearate and oleate coatings. The fatty acid coatings were proposed to be acting as internal lubricants at the polymer filler interface at these slow strain rates, the polymer chains themselves being long enough to interact with the matrix [67], but not long enough to form physical entanglements [62].

The same trends are seen with both LOT 1 (Table 4.11) and LOT 2 of DP390s oleate coated fillers of mean secondary particles sizes 4 and 3 microns respectively. The change in flexural properties with coating level is predominantly due to the interfacial lubrication effects. However, the change in flexural modulus with coating level is more pronounced for these porous fillers. The increased surface coating causes reduction in surface area which will be caused by the smoothing of the rough surface of the filler. As coarse morphology is thought [120] to be responsible for increased physical adhesion with the matrix, filler coating of DP390s has more of an effect in reducing this adhesion, which is less prominent with platey (DP393) fillers.

5.4.10 Impact properties

It has been seen in section 5.1.9 that the incorporation of DP393 and DP390s types of magnesium hydroxide at a high loading level has detrimental effects on the impact properties of polypropylene. However, the toughness of such composites increased as the level of fatty acid coating increased; the toughness never reaching that of the polypropylene containing uncoated filler. This is shown in Table 4.16 for stearate coated DP393 LOT 1 fillers and in Table 4.17 for oleate coated DP390s fillers.

According to Riley [69], impact properties of polypropylene are governed by particle size, aspect ratio, dispersion and nucleation properties. As the first two factors are the same for corresponding magnesium hydroxide types and filler dispersion has been shown to be good in all fatty acid compositions, then nucleation properties of the fillers must be of great importance to the micromorphology of the polypropylene matrix. However, interfacial effects must also be taken into consideration.

The decrease in crystallisation rate with coating level for magnesium hydroxide fillers (Tables 4.24 and 4.25) will yield larger, more well defined crystallites. These crystallites may be tougher than smaller less well defined ones, therefore accounting for the improvement in impact properties with coating level. However, the increase in coating level may also toughen polypropylene during the failure mechanism. As the surface tension is reduced, there is less interaction with the matrix, which therefore permits higher chain mobility. This increased chain mobility will permit the matrix and filler to slide over each other under deformation, reducing localised stresses and heat build up. A combination of the differences in matrix morphology and interface crystallinity will produce the overall changes in impact properties with coating level.

DP390s filler particles follow identical trends as for DP393 coated fillers, except that the toughness of these composites is lower. It may be that DP393 may be that the anisotropic DP393 particles may be able to reorientate in the impact direction, reducing stress zones, caused by the increased interfacial lubrication.

5.4.11 Flame retardancy

Flame retardancy so far reported has been characterised by two simple procedures, UL94 and LOI. It has been seen that filler loading is the main factor governing flame retardance. However, the effect of coating level has also been studied using cone calorimetry. The flame retardant effect of $\text{Mg}(\text{OH})_2$ fillers can be seen in section 4.6.

It can be seen from Appendix F, that stearate coated LOT 1 and oleate coated LOT 2 fillers are all loaded at similarly suitable levels to achieve V0 ratings. The increase in coating level has no noticeable effect on the UL94 ratings (Tables 4.41 and 4.42). The LOI values for stearate coated fillers do decrease with coating level, but this is attributed to the fact that filler loading levels decreased with coating level. Similar trends were followed with increased oleate coating levels, indicating that when present, magnesium stearate/oleate is not such a fire hazard as depicted by its chemistry, even at higher levels.

Due to the difficulty experienced in compounding DP390s fillers, a high enough filler content, to achieve V0 rating was not obtained (Appendix F). Stearate coated DP390s at 2 and 4% coating levels were incorporated at similar loading levels, and both attain similar UL94 and LOI (Table 4.45). LOT 2 oleate coated fillers exhibited a decrease with coating content. Below 56.1%, the composites were rated unclassified, LOI values decrease as a function of filler loading.

Cone calorimetry provided more data on the burning characteristics of DP393 and DP390s filled composites (Table 4.48). LOT 2 fillers were used, having a mean secondary particle size of 2 and 3 microns respectively. The heat release plots for fatty acid treated DP393 and DP390s can be seen in Fig. 4.35. Silane coated DP393 was also included. The ignition time of the vinyl silane coated DP393 filler was the shortest. Composites comprised of oleic acid coated DP393 fillers were more difficult to ignite than corresponding DP390s fillers. Polypropylene is known to have a one phase burning mechanism with a peak heat release value of approximately 1000kW/m^2 [122]. Additions of 60% magnesium hydroxide can be seen to reduce this heat release

rate to as low as 225kW/m^2 , where the burning mechanism is altered to a two phase burn. This is more apparent for oleic acid treated fillers. The hydrated filler decomposes endothermically and will release water above 350°C . This increased thermal stability of the composite and the dilution of hot gases in the vapour phase will result in a significant decrease in the measured heat release. Once the majority of the water of hydration has been released, the flame retardant properties will be reduced. Magnesium oxide is produced in the form of a grey char. Although an after glow is produced, this will not be significantly hot enough to account for the second phase of the burn. It may be that the filler contents are not high enough to promote enough magnesium oxide formation, capable of reducing all of the thermal feedback to the polymer, therefore causing ignition of unburned material. This may stop when a critical thickness of magnesium oxide has been formed. From cone calorimetry, it can be seen that an increase in oleate coating level caused an increase in the total heat evolved and the time to flameout. Therefore, at higher heat fluxes, magnesium oleate will contribute as a fuel. The total heat evolved is less for DP390s fillers. Although these composites ignite faster than those containing DP393, it may be that the damping down of the matrix is more effective. Finally, the potential toxicity of flame retardant formulations can be deduced by measuring the ratio of CO_2 to CO throughout the burn. With the oleic acid coatings, most of the toxic carbon monoxide was released at the end of the burning process. For the vinyl silane coated filler, most of the carbon monoxide was released over the first 400s of burning, therefore making it the most toxic formulation tested.

5.4.12 Fracture surface analysis

To truly assess the effect of fatty acid coating level on the fracture behaviour of polypropylene, corresponding composites with similar filler content must be assessed. Although different coating levels did produce differences in the mechanical test results, no distinct differences in the fracture pattern were detected in either flexure or under impact.

5.4.13 Filler dispersion

Filler dispersion analysis by the polishing and etching technique provides an excellent way of observing filler dispersion in polypropylene. Filler particles could be detected as holes within the polypropylene matrix.

It has been seen that changing the coating agent or fatty acid type causes no distinct change in the dispersion of magnesium hydroxide fillers. Filler contents did vary slightly between composites loaded with fatty acid coated fillers at different coating levels. Filler dispersion analysis revealed that an increase in fatty acid coating level caused no noticeable difference in filler dispersion, which was good in all cases. This being attributed to the wettability of the coated fillers being similar.

CHAPTER 6

CONCLUSIONS

The major aim of this project was to optimise a filler which would be commercially available with a coating, to obtain good all round properties when compounded into polypropylene at a filler level high enough to attain a UL94-V0 flame retardant rating. These major aims were subdivided into four discrete areas; filler morphology, coating agent, coating type and coating level. This involved determining the effect of these variables on the physical, rheological and mechanical properties of polypropylene. The conclusions drawn from each area are concisely given below.

6.1 Filler Morphology

- DP393 and DP390s both have identical crystallographic structure, but different primary and secondary structures. DP393 is a non porous platey filler of high purity, whereas DP390s is a porous pseudo-spherical filler with a higher impurity content.
- Structural replication of both filler types by current production methods is unsatisfactory.
- HD- DP393 requires pin milling to reduce the large aggregates to make twin screw extrusion possible.
- Incorporation of DP393 at the desired high filler loadings proved easier than with DP390s fillers due to the platey particles orientating in the flow direction.
- Flame retardant formulations greatly increased the melt viscosity of polypropylene, at high shear rates.
- Larger filler particle size produces higher melt viscosities for PP compounds.
- Incorporation of uncoated magnesium hydroxide increases the overall crystallisation rate of polypropylene, causing orientation of the polymers b axis parallel to the samples surface. The magnesium hydroxides 001 plane is responsible for nucleation of the matrix.
- Platey DP393 filler particles orientate during the melt flow process and PP crystallises parallel to the moulded surfaces. Spherical DP390s filler particles reside isotropically within the matrix.

- Smaller, platey particles produce superior bulk mechanical properties than larger spherical particles. This is attributed to the flow induced platey particles producing reinforcement and an increase in content of the crystalline phase.
- LOI measurements were proportional to magnesium hydroxide content. However, with UL94 measurements, a transitional region occurred between 55 and 60% loading level where ratings increased dramatically from unclassified up to V0.

6.2 Coating Agent

- Altering the coating agent caused no significant change in the physical properties of magnesium hydroxide fillers of the same type.
- Altering the coating agent caused no significant change in the rheological, mechanical or crystallisation characteristics of subsequent magnesium hydroxide filled polypropylene composites.
- Although quantifying whether fatty acid coatings were fully bound was difficult, it was deduced that ammonium and sodium salts have similar reactivities.

6.3 Coating Type

- Coating of DP393 fillers had a tendency to cause agglomeration of primary particles into larger secondary particles, whereas the opposite was true for DP390s fillers.
- Spray coating of DP393 with vinyl silane caused agglomeration which was dispersed using twin screw extrusion.
- Filler coating is more important than morphology in governing the rheological properties of magnesium hydroxide filled PP compounds. Filler coating decreases the melt viscosity towards that of the unfilled matrix, fatty acids being superior due to their lubrication properties.
- Crystallisation rates of polypropylene are decreased with magnesium hydroxide coating. At equivalent coating levels, fatty acids and rosin produce similar PP crystallisation rates, which is attributed to 001 planes of filler particles, responsible for nucleation, being orientated by the shear flow motion during compounding.

- The crystallinity of vinyl silane coated DP393 composites does not increase as a function of time. However, an increase in flexural modulus is attributed to the migration of silane from the filler surface, reducing interfacial lubrication effects.
- Incorporation of coated fillers into the matrix reduces the bulk properties of composites compared to the incorporation of uncoated material. The increased wettability of fillers, particularly fatty acid coated, reduces the interfacial work of adhesion, increasing chain mobility.
- Cone calorimetry revealed vinyl silane coated fillers to be the most toxic formulation, releasing carbon monoxide throughout the burning mechanism.
- Fatty acid coated fillers facilitate good dispersion whereas rosin produced some agglomeration. Twin screw extrusion significantly reduced agglomeration of spray coated vinyl silane coated fillers.

6.4 Coating Level

- An increase in fatty acid coating level causes a reduction in surface area by smoothing out discontinuities on the fillers surface.
- Wettability increased linearly with increased fatty acid treatment. The linear increase is dependent on filler morphology, porous morphologies being more difficult to wet out.
- Increasing the fatty acid coating level improves the processability of magnesium hydroxide filled polypropylene compounds. This is attributed to stearate/oleate salts acting as lubricants.
- Flexural modulus and strength decrease with increased coating level. This is due to a decrease in interfacial adhesion reducing the amount of immobilised polypropylene.
- Increasing the fatty acid coating level improves material toughness towards that of the compound containing uncoated filler.
- Increasing the oleate coating level causes an increase in the heat evolved and time to flameout during the burning process.

REFERENCES

1. ICI Petrochemicals and Plastics, 'Properties of Propathene', ICI technical centre, Wilton, Middlesborough, Reference P1/1/05/91.
2. Mark, H. F., Bikales, N. M., Overberger, C. G., Menges, G. M., *Encyclopaedia of Polymer Science and Engineering*, 13, Wiley Interscience, 2nd Ed., New York.
3. Himont U.K., 'An Introduction to Polypropylene - A one day training seminar', Montell Polyolefins, Milton Keynes Ltd.
4. Billmeyer, F. W., *Textbook of Polymer Science*, John Wiley and Sons Inc., 3rd Ed., 1984, New York.
5. Kakugo, M., Sadatsoshi, H., Yokoyama, M., Kojima, K., *Macromol.* 22, 1989, p547.
6. Putanov, P., Kis, E., *Tetrahedron* 8 (13/14), 1989, p1867.
7. Kakugo, M., Sadatoshi, H., Sakai, J., Yokoyama, M., *Macromol.* 22, 1989, p3172.
8. Brydson, J., *Plastics Materials*, 3rd Ed., Butterworths, 1984, New York.
9. Mark, H. F., Bikales, N. M., Overberger, C. G., Menges, G. M., *Encyclopaedia of Polymer Science and Engineering*, 7, Wiley Interscience, 2nd Ed., New York.
10. Grassie, N., *Polymer Degradation and Stability*, 30, 1990, p3.
11. Holloway, L. R., *Rubb. Chem. Tech.*, 61 (2), 1988, p186.
12. Kirschbaum, G., *Flame Retardants Conference Proceedings*, Jan 19/20, London 1990, p143.
13. Wypych, G. W., *Fillers*, Chem Tech Publishing, 1993, Ontario, Canada.
14. Hornsby, P. R., Wang, J., Cosstick, K., Rothon, R., Jackson, G., Wilkinson, G., *Progress in Rubber and Plastics Technology*, 10 (3), 1994, p204.
15. Hornsby, P. R., *Plas. Rubb. Proc. Appl.*, 11 (1), 1989, p45.
16. Rothon, R.N., *Flame Retardants Conference Proceedings*, Jan 17/18, London 1990, p156.
17. Rothon, R. N. (Ed.), *Particulate Filled Polymer Composites*, Longmans, 1995.
18. Hornsby, P.R., *Eurofillers Conference Proceedings*, Sep. 11/14, Mulhouse, France, 1995, p419.

19. Toure, B., Lopez Cuesta, J. M., Gaudon, P., Benhassaine, A., Crepsy, A., Eurofillers Conference Proceedings, Sep. 11/14, Mulhouse, France, 1995, p423.
20. Premier Periclase Limited, 'Leading the world in the production of highest quality sintermagnesia'.
21. Premier Periclase Limited, 'Premier DP393, An ultrafine magnesium hydroxide fire retardant filler from Premier Periclase Limited for polymeric applications'.
22. Hornsby, P. R., *Fire and Materials*, **18**, 1994, p269.
23. Premier Periclase 'Premier DP393 Chemical Safety Sheet' February 1992, Premier Periclase Limited, Drogheda, Ireland.
24. Steetley Magnesia Products Limited 'Information Brochure', Hartlepool Works.
25. Sherman, L. M; *Plast. Tech.*, July, 1992, p56.
26. Hatke Van Ven, S., Dallavia, A; *Society of Plastic Engineer, Antec*, 1988, p1415.
27. Hornsby, P. R., Watson, C. L., *Polym. Deg. Stab.*, **30**, 1990, p73.
28. Hornsby, P.R., Watson, C. L., *Plast. Rubb. Proc. Appl.*, **6** (2), p169.
29. Miyata, S., Imahashi, T., Anabuki, H., *J. Appl. Polym. Sci.*, **25**, 1980, p415.
30. Rychley, J., Vesely, K., Gal, E., Kummer, M., Jancar, J., Rychla, I., *Polym. Deg. Stab.*, **30**, 1990, p 57.
31. Jancar, J., *J. Mat. Sci. Let.*, **26**, 1991, p4123.
32. *Plast. Rubb. Weekly*, No 1438, June 6, p10.
33. Baird, T., Braterman, P., Cochrane, H., Spoors, G., *J. Cryst. Growth*, **91**, 1988, p610.
34. Rothon, R.N., *Conference Proceedings, Eurofillers, Mulhouse, France, Sep 11/14, 1995*, p72.
35. Fernandez-Lozano, J., *Fifth International Symposium on Salt, Northern Ohio Geological Society*, p269.
36. *Plastics Additives and Modifiers Handbook* (Ed. Edembaum, J), Chapter 81, 4th Ed., Van Nostrand Reinhold, New York, 1993.
37. Martinswerk, 'Magnifin Halogen Free Flame Retardancy', Croxton and Garry, Dorking, Surrey, Reference number Magnifin E/92/1000/A.
38. Martinswerk, 'Magnifin Halogen Free Polypropylene Flameproofing', Croxton and Garry, Dorking, Surrey, Reference number Polypropylene E/92/1000/A.

39. United States Patent, 4145404, March 20, 1979.
40. Jilken, L., Malhammer, G., Seldon, R., *Polym. Test.*, 10, 1991, p329.
41. Jancar, J., Kucera, J., Vesely, P., *J. Mat. Sci. Let.*, 7, 1988, p1377.
42. Turcsanyi, B., Pukansky, B., Tudos, F., *J. Mat. Sci. Let.*, 7, 1988, p160.
43. Kornetka, Z. W., *Int. Polym. Sci. Tech.*, 15, 1985, p76.
44. Enikolopyan, N. S. (Ed.), *Advances in Polymer Science*, 96, Filled Polymers 1, Springer Verlag, 1990, New York.
45. Katz, H., Milewski, J., *Handbook of Fillers for Plastics*, Van Nostrand Reinhold Company, 1987, New York.
46. Galeski, A., *Controlled Interphases in Composite Materials* (Ed. Ishida, H.), *Proceedings of the Third International Conference on Composite Interfaces (ICCI-III)*, p623, Elsevier Science Publishing Company, 1990, New York.
47. Pukansky, B., Fekete, E., Tudos, F., *Makromol. Chem. Macromol. Symp.*, 28, 1989, p165.
48. Berlin, A. A., Volfson, S. A., Enikolopyan, N. S., Negmatov, S. S., *Principles of Polymer Composites*, Springer Verlag, 1986, New York.
49. Barth, H. G., *Modern Methods of Particle Size Analysis*, John Wiley and Sons, 1984, New York.
50. Hoy, K. L., *Org. Cot. Sci. Technol.*, 5, 1983, p123.
51. Bigg, D. M., *Polymer Composites*, 8 (2), 1987, p115.
52. Wickson, E. J. (Ed.), *Handbook of PVC Formulating*, Chapter 13, John Wiley and Sons, 1993, New York.
53. Neilson, L. E., *J. Polym. Sci. Polym. Phys.*, 17, 1979, p1897.
54. Rybnicar, F., *J. Appl. Polym. Sci.*, 38, 1989, p1479.
55. Fujiyama, M., Wakino, T., *J. Appl. Polym. Sci.*, 42, 1991, p9.
56. Jancar, J., *J. Mat. Sci.*, 24, 1989, p4268.
57. Jancar, J., *J. Mat. Sci.*, 26, 1991, p4878.
58. Jancar, J., *J. Mat. Sci.*, 24, 1989, p3947.
59. Turcsanyi, B., Pukansky, B., Tudos, F., *J. Mat. Sci. Let.*, 7, 1988, p160.
60. Turcsanyi, B., Tudos, F., Jancar, J., Kolarik, J., *J. Mat. Sci. Let.*, 8, 1989, p1040.
61. Jancar, J., Kucera, J., *Polym. Eng. Sci.*, 30 (12), 1990, p707.
62. Jancar, J., Kucera, J., *Polym. Eng. Sci.*, 30 (12), 1990, p714.

63. Jancar, J., Dianselmo, A., Dibenedetto, A. T., *Polym. Eng. Sci.*, 32 (18), 1992, p1394.
64. Calvert, D. J., Haworth, B., Stephenson, R. C., *Plast. Rubb. Proc. Appl.*, 15, 1991, p229.
65. Jilken, L., Malhammer, G., Seldon, R., *Polymer Testing*, 10, 1991, p329.
66. Fu, Q., Wang, G., *Polym. Eng. Sci.*, 32 (2), 1992, p94.
67. Hornsby, P. R., Watson, C. L., *J. Mat. Sci.*, 30, 1995, p5347.
68. Suetsuga, Y., *Intern. Polym. Proc.*, V (3), 1990, p84.
69. Riley, A. M., Paynter, C. D., McGenity, P. M., Adams, J. M., *Plast. Rubb. Proc. Appl.*, 14, 1990, p85.
70. Hutley, T. J., Darlington, M. W., *Polym. Comm.*, 25, 1984, p226.
71. Hutley, T. J., Darlington, M. W., *Polym. Comm.*, 26, 1985, p264.
72. Miyata, S., Imahashi, T., Anabuki, H., *J. Appl. Polym. Sci.*, 25, 1990, p415.
73. Griffiths, J. B., *Plast. Rubb. Proc. Appl.*, 13, 1990, p3.
74. Morrell, S. H., *Plast. Rubb. Proc. Appl.*, 1, 1981, p179.
75. Suetsuga, Y., White, J. L., Kym, T., *Adv. Polym. Tech.*, 7 (4), 1987, p427.
76. BS2782: Part 1: Method 1106A: 1983: Assessment of pigment dispersion in polyolefin pipe and fittings: Microtome method.
77. BS2782: Part 8: Method 823A & 823B: 1978: Methods for the assessment of carbon black dispersion in polyolefins using a microscope.
78. Burke, M., Young, R. J., Stanford, J. L., *Plast. Rubb. Proc. Appl.*, 20 (3), 1981, p121.
79. Liauw, C. M., Ph.D Thesis, Manchester Metropolitan University, April, 1994, Influence of surface modification of aluminium hydroxide on the processing and mechanical properties of aluminium hydroxide/polypropylene composites.
80. Colbert, J., Society of Plastic Engineer, Antec, 1988, p76.
81. Lea, J. D., 'Developments in twin screw extrusion', APV Baker Limited, Ref. 12/26, p1.
82. Dillon, M., 'Extruders for masterbatch applications', APV Baker Limited, Newcastle under Lyme.
83. Hornsby, P. R., *Plast. Rubb. Proc. Appl.*, 7, 1987, p237.
84. Hornsby, P. R., *J. Mat., Sci. Let.*, 29, 1994, p5293.

85. Ishida, H., *Polym. Comp.*, **15** (2), 1984, p101.
86. OSi Specialities (UK) Limited, Filler Treatment Brochure, Harefield, Middlesex.
87. Haworth, B., Birchenough, C., Conference Proceedings, Eurofillers, Mulhouse, France, Sep 11/14, 1995, p365.
88. Gilbert, M., Sutherland, I., Guest, I., BPF, Filplas Conference Proceedings, Manchester, May, 1992.
89. Fekete, E., Pukanszky, B., Toth, A., Bertoti, I., *J. Colloid Interface Sci.*, **1**, 1990, p200.
90. Gospel, E., A Study of the Effects of Coating on Magnesium Hydroxide Surfaces, Dept. Chemistry, Loughborough University, June 1995.
91. Venables, R., PhD Thesis, Loughborough University, 1995, Structure and properties of alkyl-trimethyl-oxysilane modified talc/polypropylene composites.
92. Porro, T. J., Pattacini, S. C., *Appl. Spect.*, **44** (7), 1990, p1170.
93. Porro, T. J., Pattacini, S. C., *J. Adhesion. Sci. Technol.*, **6** (1), 1992, p73.
94. Jancar, J., Kucera, J., Vesely, P., *J. Mat. Sci. Let.*, **26**, 1991, p4883.
95. Jancar, J., *J. Mat. Sci.*, **26**, 1991, p4123.
96. Beck, H. N., Ledbetter, H. D., *J. Appl. Polym. Sci.*, **9**, 1965, p2131.
97. Belina, K., Vorster, O., *Plastics South Africa*, November, 1991, p25.
98. Turner Jones, A, Aizlewood, J. M., Beckett, D. R., *Makromol. Chem.*, **75**, 1964, p134.
99. Shi, G., Chu, F., Gui-en, L., Han, Z., *Makromol. Chem.*, **190**, 1989, p907.
100. Rybnikar, F., *Polymer*, **10**, 1969, p747.
101. Binsbergen, F. N., *J. Appl. Polym. Sci. Polym. Phy. Ed.*, **11**, 1973, p117.
102. Rybnikar, F., *J. Appl. Polym. Sci.*, **27**, 1982, p1479.
103. Maiti, S. N., Mahapatro, P. K., *Intern. J. Polym. Mat.*, **14**, 1990, p205.
104. Taylor, D., Paynter, C .D., Conference Proceedings, Eurofillers, Mulhouse, France, Sep 11/14, 1995, p361.
105. BS2782: Part 6: Method 621D: Determination of compacted apparent bulk density of PVC resins.
106. BS3483: Part B7: 1982: Determination of oil absorption value.
107. BS2782: Part 3: Method 320B: 1976: Tensile strength, elongation and elastic modulus.

108. BS2782: Part 4: Method 470A: 1991: Determination of ash (general methods).
109. BS2782: Part 7: Method 720A: 1979: Determination of melt flow rate of thermoplastics.
110. ASTM D790-86: Standard test method methods for flexural properties of unreinforced and reinforced plastic and electrical insulating materials (metric).
111. Mark, H. F., Bikales, N. M., Overberger, C. G., Menges, G. M., *Encyclopaedia of Polymer Science and Engineering*, Wiley Interscience, 13, 2nd Ed, 1988, New York, p481.
112. BS2782: Part 1: Method 120A: 1990: Determination of Vicat softening temperature of thermoplastics.
113. UL94: Underwriters laboratory: 1980: Tests for flammability of plastic materials for parts in devices and applications.
114. BS476: Part 15: 1993: Method for measuring the rate of heat release of products.
115. X-ray diffraction file 7-239: Magnesium Hydroxide.
116. Hancock, M. J., *Polym. Sci, Polym. Sci. Ed.*, 18, 1980, p3211.
117. Copperthwaite, M., Brett, N. H., *Sci. Ceram.*, 8, 1976, p85.
118. Neilson, L.E., *J. Mat. Sci.*, 2, 1968, p120.
119. Lewis, T. B., Neilson, L. E., *Trans. Soc. Rheol.*, 12, 1968, p21.
120. Ramsteiner, F., Theyston, R., *Composites*, 15, 1984, p121.
121. Gal, E., Pal, A., Rychly, J., Tarapcikova, K., *Flame Retardants Conference Proceedings*, Jan 17/18, London, 1990, p134.
122. Paul, K. J., *Fire Safety Journal*, 22, 1994, p62.

APPENDIX A

X-ray diffraction peaks for Mg(OH)₂ fillers

X-ray diffraction data for DP393 and DP390s uncoated fillers

<i>2θ</i> <i>DP393</i>	<i>2θ</i> <i>DP390s</i>	<i>d</i> <i>spacing/nm</i> <i>DP393</i>	<i>d</i> <i>spacing/nm</i> <i>DP390s</i>	<i>hkl plane</i>	<i>RELATIVE</i> <i>INTENSITY</i>
18.45	18.45	0.4805	0.4805	001	2
32.85	32.70	0.2724	0.2736	100	9
37.80	37.80	0.2378	0.2378	101	1
50.70	50.55	0.1799	0.1799	102	3
58.50	58.35	0.1576	0.1576	110	4
61.95	61.80	0.1497	0.1497	111	5
68.10	67.95	0.1376	0.1376	103	6
71.85	71.85	0.1313	0.1313	201	7
81.00	81.00	0.1186	0.1186	202	8

X-ray diffraction patterns for both these filler types can be seen in section 4.1.1.

Bragg's equation used for determining the interplanar spacing (*d*) is given:

$$2d\sin\theta = n\lambda$$

where,

θ is the incident X-ray angle causing constructive interference,

n is an integer (1, 2, 3....),

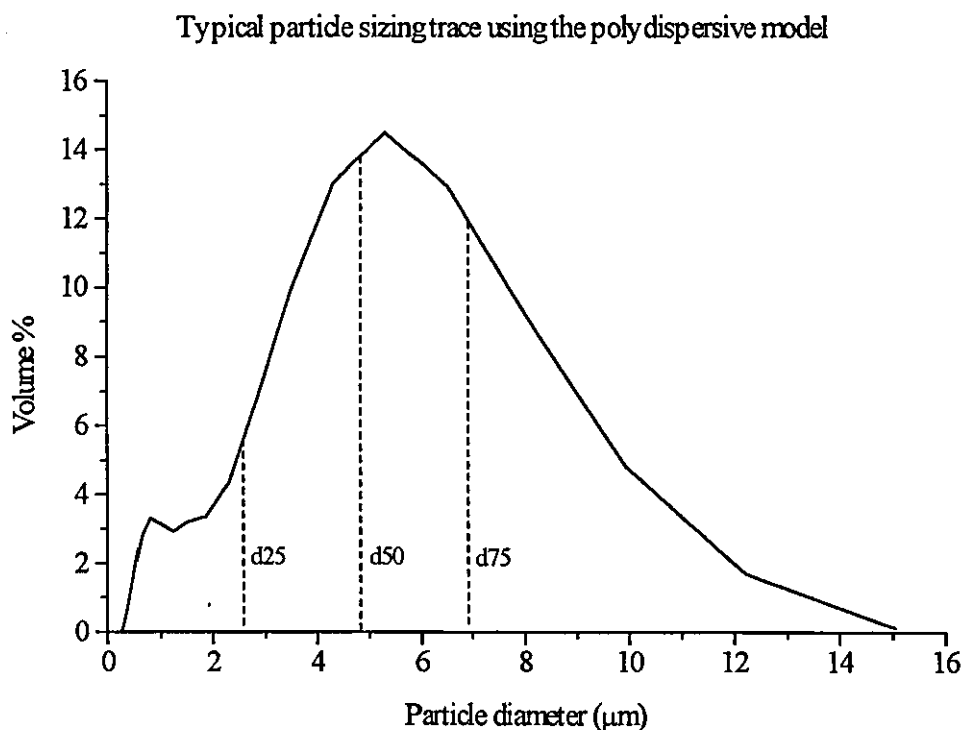
λ is the wavelength of the monochromatic X-ray source.

The intensities of the peaks are normalised with the most intense peak to produce a relative intensity value.

APPENDIX B

Particle sizing parameters and data

The d50 value was used to define the mean secondary particle size of the filler. The d25 and d75 values were used to indicate the type of size distribution. The values d50, d25 and d75 refer to the particle diameters of the filler that resides at 50%, 25% and 75% of the total volume of filler particles present. All of these values were taken after 5 minutes of ultrasound. Also, the d50 value for 15 minutes exposure to ultrasound was given to examine the cohesive strength of the filler particles. A typical PSD for a polydispersive filler can be seen below indicating the above parameters.



Particle sizing data for all DP393 and DP390s fillers, indicating their d50, d25 and d75 values, can be seen below. The abbreviation u/s refers to ultrasound. The most relevant plots can be seen in section 4.1.2 and are explained in section 5.

Particle sizing data for DP393 fillers

<i>CODE</i>	<i>LOT</i>	<i>d50 (μm), 5 min u/s</i>	<i>d25 (μm), 5 min u/s</i>	<i>d75 (μm), 5 min u/s</i>	<i>d50 (μm), 15 min u/s</i>
DP393	1	0.73	0.50	1.23	0.73
HD-DP393	1	0.73	0.47	1.16	0.69
2.0VS	1	1.32	0.73	4.00	1.13
1.5AMST	1	0.95	0.55	2.02	0.95
3.0AMST	1	0.95	0.56	2.01	0.94
4.5AMST	1	0.98	0.58	2.04	0.97
1.5AMOL	1	0.96	0.56	2.07	0.95
3.0AMOL	1	0.88	0.53	1.79	0.88
4.5AMOL	1	1.02	0.59	2.16	0.99
4.5NAST	1	0.92	0.54	1.97	0.89
4.5NAOL	1	0.83	0.50	1.89	0.70
4.5AMROS	1	1.14	0.62	2.36	1.17
2.0VS	2	3.03	1.76	4.71	3.02
1.5NAOL	2	2.10	1.07	3.95	1.86
3.0NAOL	2	1.83	0.96	3.34	1.45
4.5NAOL	2	1.74	0.90	3.16	1.50
4.5AMOL	2	1.94	0.92	4.37	1.48
DP393	3	1.26	0.68	3.12	1.09
4.5AMST	3	0.74	0.47	1.23	0.69
4.5AMOL	3	1.06	0.62	2.69	0.88
4.5NAOL	3	1.40	0.75	3.24	1.27

Particle sizing data for DP390s fillers

<i>CODE</i>	<i>LOT</i>	<i>d50 (μm), 5min u/s</i>	<i>d25 (μm), 5 min u/s</i>	<i>d75 (μm), 5 min u/s</i>	<i>d50 (μm), 15 min u/s</i>
DP390s	1	4.78	2.59	6.90	4.71
AMST2.0	1	4.07	2.06	6.40	4.06
AMST4.0	1	4.06	1.99	6.45	4.08
AMST6.0	1	4.17	2.07	6.65	4.16
AMOL2.0	1	4.17	2.10	6.64	4.12
AMOL4.0	1	4.17	2.10	6.59	4.13
NAOL1.5	2	3.07	1.72	4.97	3.07
NAOL3.0	2	3.11	1.71	5.05	3.12
NAOL4.5	2	3.06	1.69	5.03	3.01
NAOL6.0	2	2.94	1.66	4.72	2.94
AMOL4.0	2	3.02	1.69	4.87	3.02
AMOL6.0	2	3.09	1.70	5.08	3.03

APPENDIX C

BET surface area calculations and data

Calculation of BET surface area

The specific surface area per unit mass, S_m of the filler was calculated from n_m^s , the uptake of gas corresponding to monomolecular coverage of the solid surface, by assessing a value a_m for the average area occupied by each molecule. The following equation relates these quantities:

$$S_m = \frac{n_m^s a_m N_A}{m}$$

where N_A is Avagadro's number, m is the sample mass and a_m is 0.162nm^2 for nitrogen. The equation then becomes:

$$S_m = \frac{n_m^s}{m} 9.76 \times 10^4$$

The monolayer amount, n_m^s is obtained by determining the adsorbed amount, n^s , at a series of relative pressures, x . The data are interpreted by means of the BET equation of the form:

$$\frac{x}{(1-x)n^s} = \frac{1}{n_m^s C} + \frac{(C-1)x}{n_m^s C}$$

where C is a constant.

The plot of $x / \{n^s (1-x)\}$ against x should be a straight line of slope $(C-1) / (n_m^s C)$ and intercept $1 / (n_m^s C)$ from which:

$$n_m^s = 1 / (\text{slope} + \text{intercept}) \text{ and } C = 1 + (\text{slope} / \text{intercept}).$$

BET surface area of DP393 fillers

<i>CODE</i>	<i>LOT</i>	<i>BET SURFACE AREA (m²/g)</i>
DP393	1	13.76
HD-DP393	1	14.43
2.0VS	1	13.13
1.5AMST	1	13.46
3.0AMST	1	12.72
4.5AMST	1	12.47
1.5AMOL	1	13.68
3.0AMOL	1	12.18
4.5AMOL	1	9.29
4.5NAST	1	12.36
4.5NAOL	1	11.15
4.5AMROS	1	13.90
2.0VS	2	7.89
1.5NAOL	2	21.46
3.0NAOL	2	22.49
4.5NAOL	2	18.68
4.5AMOL	2	20.85
DP393	3	11.47
4.5AMST	3	14.58
4.5AMOL	3	9.03
4.5NAOL	3	7.76

BET surface area of DP390s fillers

<i>CODE</i>	<i>LOT</i>	<i>BET SURFACE AREA (m²/g)</i>
DP390s	1	13.50
AMST2.0	1	12.40
AMST4.0	1	11.48
AMST6.0	1	10.36
AMOL2.0	1	11.37
AMOL4.0	1	6.89
NAOL1.5	2	12.43
NAOL3.0	2	9.97
NAOL4.5	2	7.01
NAOL6.0	2	7.64
AMOL4.0	2	7.41
AMOL6.0	2	8.17

APPENDIX D
Filler packing data

Packing properties for DP393 fillers

<i>CODE</i>	<i>LOT</i>	<i>BULK DENSITY</i> (kg/m ³)	<i>OIL ABSORPTION</i> (ml/100g)
DP393	1	430	56.0
HD-DP393	1	670	56.0
2.0VS	1	470	54.0
1.5AMST	1	560	35.0
3.0AMST	1	600	29.5
4.5AMST	1	590	27.0
1.5AMOL	1	570	37.5
3.0AMOL	1	620	29.0
4.5AMOL	1	570	27.0
4.5NAST	1	640	29.0
4.5NAOL	1	670	25.0
4.5AMROS	1	580	38.5
2.0VS	2	470	50.0
1.5NAOL	2	680	45.0
3.0NAOL	2	680	35.0
4.5NAOL	2	700	27.5
4.5AMOL	2	700	25.0
DP393	3	540	56.0
4.5AMST	3	500	29.5
4.5AMOL	3	540	23.5
4.5NAOL	3	720	24.5

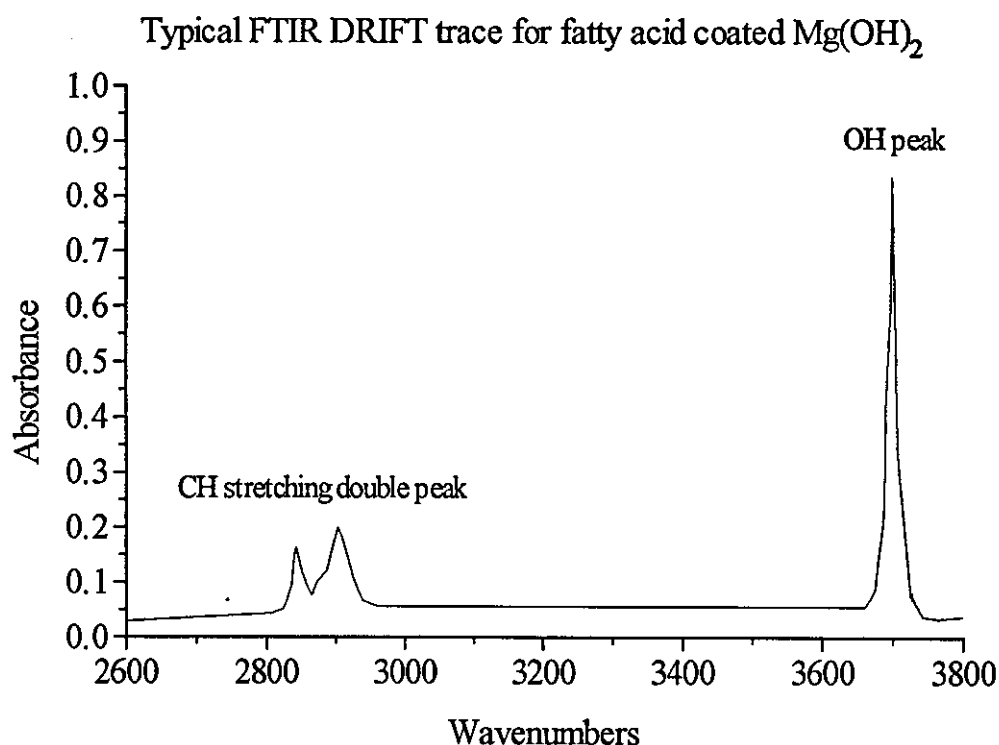
Packing properties for DP390s fillers

<i>CODE</i>	<i>LOT</i>	<i>BULK DENSITY</i> <i>(kg/m³)</i>	<i>OIL ABSORPTION</i> <i>(ml/100g)</i>
DP390s	1	820	55.0
AMST2.0	1	880	40.5
AMST4.0	1	890	38.5
AMST6.0	1	850	33.0
AMOL2.0	1	940	42.0
AMOL4.0	1	970	39.0
NAOL1.5	2	940	44.0
NAOL3.0	2	1070	33.0
NAOL4.5	2	1060	30.0
NAOL6.0	2	1060	29.5
AMOL4.0	2	1070	32.5
AMOL6.0	2	1090	30.0

APPENDIX E

FTIR analysis and data

FTIR DRIFT analysis was used to characterise the coating content upon the magnesium hydroxide filler surface. The absorption species of interest were the single OH magnesium hydroxide (filler substrate) peak and the double CH alkyl (coating) peaks. The OH peak was present for all filler types and was a constant used for ratioing purposes. The CH peak area was dependent upon the amount of coating present. The OH peak area was integrated between $2970\text{--}2800\text{cm}^{-1}$ and the CH peak area was integrated between $3735\text{--}3625\text{cm}^{-1}$. A typical trace can be seen below.



CH/OH peak area ratios for all DP393 and DP390s fatty acid (stearate and oleate) coated fillers at all coating levels can be seen below. CH/OH ratios for fatty acid coated DP393 and DP390s fillers can be seen over leaf.

CH/OH ratios for fatty acid coated DP393 fillers

<i>CODE</i>	<i>LOT</i>	<i>CH/OH RATIO</i>
1.5AMST	1	0.109
3.0AMST	1	0.268
4.5AMST	1	0.370
1.5AMOL	1	0.051
3.0AMOL	1	0.158
4.5AMOL	1	0.245
4.5NAST	1	0.396
4.5NAOL	1	0.318
1.5NAOL	2	0.056
3.0NAOL	2	0.185
4.5NAOL	2	0.246
4.5AMOL	2	0.222
4.5AMST	3	0.262
4.5AMOL	3	0.183
4.5NAOL	3	0.135

CH/OH ratios for fatty acid coated DP390s fillers

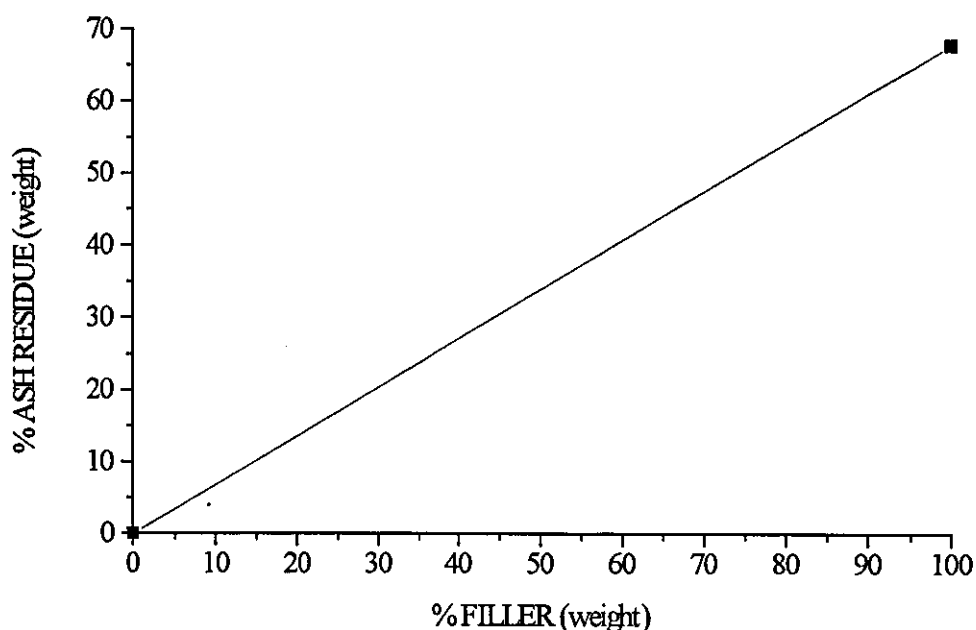
<i>CODE</i>	<i>LOT</i>	<i>CH/OH RATIO</i>
AMST2.0	1	0.262
AMST4.0	1	0.446
AMST6.0	1	0.665
AMOL2.0	1	0.176
AMOL4.0	1	0.328
NAOL1.5	2	0.006
NAOL3.0	2	0.105
NAOL4.5	2	0.203
NAOL6.0	2	0.242
AMOL4.0	2	0.180
AMOL6.0	2	0.186

APPENDIX F

Filler content data

Ash analysis was performed in accordance with the BS2782: Part 4: Method 470A: 1991 [108]. In order to calculate the final filler content of a composite, an ashing calibration plot was prepared for each filler. This was done using two points. The first point (0% filler) was obtained by ashing the unfilled polypropylene and measuring the percentage residual weight of the ash (0.00%). The second point (100% filler) was obtained by ashing solely the filler and measuring the weight of the ash residue, MgO (67.62%). An assumption was made that the percentage ash residue from any pyrolysed PP/Mg(OH)₂ composite comprised of these two components will lie between the upper and lower limits (and that the relationship is linear). The ashing calibration plot for DP393 LOT 1 can be seen below.

Ashing calibration plot for filler DP393 LOT 1



When observing the filler dispersion within the polypropylene matrix, the weight percentage loading is often misleading (as the density of the magnesium hydroxide filler is approximately 2.5 that of the base polymer). It is also necessary to express the filler content as a volume fraction. The polymer composite is comprised of 2 phases these being the polymer and the filler. If the filler is coated, a third phase must be taken into account. When the filler weight percent has been established, the volume fraction of the composite (V_{fc}) can be calculated from its constituents, using the following equation:

$$V_{fc} = \left(\frac{M}{\rho} \right)_{PP} + \left(\frac{M}{\rho} \right)_{FILLER} + \left(\frac{M}{\rho} \right)_{COATING}$$

where, M is mass and ρ is density.

The density of the materials used are given below.

Material	Density (kg/m ³)
Polypropylene	900
Magnesium hydroxide	2360
Stearic acid	840
Oleic acid	900
Rosin gum	1070
Vinyl silane	1040

The final filler content and filler volume fractions for all of the filled polypropylene formulations can be seen below. The standard deviations of three determinations are shown in brackets.

DP393 LOT 1 uncoated and fatty acid formulations

<i>CODE</i>	<i>COATING</i>	<i>LOT</i>	<i>FILLER LEVEL</i> (wt%)	<i>FILLER VOLUME</i> <i>FRACTION</i>
DP393	Uncoated	1	59.3 (0.1)	0.36
DP393*	Uncoated	1	58.9 (0.8)	0.35
1.5AMST	Stearate	1	60.3 (0.1)	0.37
3.0AMST	Stearate	1	60.0 (0.1)	0.36
4.5AMST	Stearate	1	58.7 (0.1)	0.35
1.5AMOL	Oleate	1	57.3 (0.1)	0.34
3.0AMOL	Oleate	1	62.7 (0.1)	0.39
4.5AMOL	Oleate	1	61.7 (0.8)	0.38
4.5NAST	Stearate	1	58.1 (0.1)	0.35
4.5NAOL	Oleate	1	54.7 (0.2)	0.32
4.5AMROS	Rosin	1	60.8 (0.1)	0.37

* Batch mixed

DP393 LOT 2 fatty acid formulations

<i>CODE</i>	<i>COATING</i>	<i>LOT</i>	<i>FILLER LEVEL</i> (wt%)	<i>FILLER VOLUME</i> <i>FRACTION</i>
1.5NAOL	Oleate	2	61.1 (0.1)	0.38
3.0NAOL	Oleate	2	60.5 (0.1)	0.37
4.5NAOL	Oleate	2	58.6 (0.2)	0.35
4.5AMOL	Oleate	2	59.0 (0.1)	0.36

DP393 LOT 3 uncoated and fatty acid formulations

<i>CODE</i>	<i>COATING</i>	<i>LOT</i>	<i>FILLER LEVEL</i> (wt%)	<i>FILLER VOLUME</i> <i>FRACTION</i>
DP393	Uncoated	3	54.50 (0.09)	0.31
4.5AMOL	Oleate	3	60.70 (0.11)	0.37
4.5AMST	Stearate	3	56.00 (0.07)	0.33
4.5NAOL	Oleate	3	58.62 (0.52)	0.35

DP393 LOTS 1 and 2 vinyl silane formulations

<i>CODE</i>	<i>COATING</i>	<i>LOT</i>	<i>FILLER LEVEL</i> (wt%)	<i>FILLER VOLUME</i> <i>FRACTION</i>
2.0VS50A	Vinyl silane	1	46.2 (0.3)	0.25
2.0VS55A	Vinyl silane	1	50.1 (0.5)	0.28
2.0VS60A	Vinyl silane	1	53.7 (0.3)	0.31
2.0VS65A	Vinyl silane	1	57.0 (0.5)	0.34
2.0VS70A	Vinyl silane	1	63.3 (0.4)	0.40
2.0VS20B	Vinyl silane	1	22.5 (0.1)	0.10
2.0VS30B	Vinyl silane	1	30.1 (0.1)	0.14
2.0VS40B	Vinyl silane	1	38.4 (0.1)	0.19
2.0VS50B	Vinyl silane	1	51.4 (0.1)	0.29
2.0VS60B	Vinyl silane	1	58.5 (0.1)	0.35
2.0VS70B	Vinyl silane	1	65.9 (0.4)	0.42
2.0VS20*	Vinyl silane	2	19.5 (0.1)	0.09
2.0VS60*	Vinyl silane	2	60.8 (0.1)	0.37

* Batch mixed

DP390s LOT 1 formulations

<i>CODE</i>	<i>COATING</i>	<i>LOT</i>	<i>FILLER LEVEL</i> (wt/wt%)	<i>FILLER VOLUME</i> <i>FRACTION</i>
DP390s	Uncoated	1	55.5 (0.4)	0.32
AMST2.0	Stearate	1	58.8 (1.1)	0.35
AMST4.0	Stearate	1	58.2 (0.1)	0.35
AMST6.0	Stearate	1	53.9 (0.1)	0.32
AMOL2.0	Oleate	1	57.0 (0.6)	0.34
AMOL4.0	Oleate	1	56.0 (0.1)	0.33

DP390s LOT 2 formulations

<i>CODE</i>	<i>COATING</i>	<i>LOT</i>	<i>FILLER LEVEL</i> (wt/wt%)	<i>FILLER VOLUME</i> <i>FRACTION</i>
NAOL1.5	Oleate	2	56.8 (0.4)	0.33
NAOL3.0	Oleate	2	56.7 (0.1)	0.33
NAOL4.5	Oleate	2	55.0 (0.5)	0.32
NAOL6.0	Oleate	2	54.5 (1.3)	0.31
AMOL4.0	Oleate	2	55.2 (0.5)	0.32
AMOL6.0	Oleate	2	56.1 (0.7)	0.33

APPENDIX G

Melt flow calculations and data

Calculation of MFI and volumetric output

The melt flow index (MFI) can be calculated in grams per reference time, by the formula:

$$\text{MFI (T, F)} = (S \times m) / t$$

where,

T is the test temperature,

F is the force,

S is the reference time (s)

m is the average mass (g) of the cut-offs

t is the cut-off interval (s)

Final units are expressed in g/10min or dg/min..

The volumetric output can be calculated in volume per reference time. Firstly, the total density of the filled composite must be established using the following equation:

$$\rho_c = \rho_p \times M_p + \rho_f \times M_f \text{ (g/cm}^3\text{)}$$

where,

ρ_c is the total composite density,

ρ_p is the density of the polymer (0.9g/cm³),

ρ_f is the density of the filler (2.36g/cm³),

M_p is the weight fraction of polymer in the formulation,

M_f is the weight fraction of filler in the formulation.

To obtain the volumetric output of the composite, the following equation is used:

$$\text{Volumetric output} = \text{MFI} / \rho_c$$

Final units are expressed in cm³/10min.

DP393 LOT 1 uncoated and fatty acid formulations

<i>CODE</i>	<i>COATING</i>	<i>LOT</i>	<i>MFI</i> (g/10min)	<i>VOLUMETRIC O/P</i> (cm ³ /10min)
DP393	Uncoated	1	0.00 (-----)	0.00
DP393*	Uncoated	1	0.00 (-----)	0.00
1.5AMST	Stearate	1	7.30 (0.43)	4.37
3.0AMST	Stearate	1	11.35 (0.66)	6.39
4.5AMST	Stearate	1	12.00 (0.41)	6.83
1.5AMOL	Oleate	1	4.72 (0.58)	2.72
3.0AMOL	Oleate	1	10.20 (0.33)	5.62
4.5AMOL	Oleate	1	13.12 (0.12)	7.31
4.5NAST	Stearate	1	12.26 (0.47)	7.02
4.5NAOL	Oleate	1	15.01 (0.52)	8.83
4.5AMROS	Rosin	1	1.77 (0.21)	0.98

* Batch mixed

DP393 LOT 2 fatty acid formulations

<i>CODE</i>	<i>COATING</i>	<i>LOT</i>	<i>MFI</i> (g/10min)	<i>VOLUMETRIC O/P</i> (cm ³ /10min)
1.5NAOL	Oleate	2	0.00 (-----)	0.00
3.0NAOL	Oleate	2	1.33 (0.14)	0.76
4.5NAOL	Oleate	2	7.65 (0.05)	4.36
4.5AMOL	Oleate	2	7.25 (0.08)	4.11

DP393 LOT 3 uncoated and fatty acid formulations

<i>CODE</i>	<i>COATING</i>	<i>LOT</i>	<i>MFI</i> (g/10min)	<i>VOLUMETRIC O/P</i> (cm ³ /10min)
DP393	Uncoated	3	0.00 (-----)	0.00
4.5AMOL	Oleate	3	9.52 (0.36)	5.33
4.5AMST	Stearate	3	11.18 (0.55)	6.59
4.5NAOL	Oleate	3	9.50 (0.14)	5.41

DP393 LOTS 1 and 2 vinyl silane formulations

<i>CODE</i>	<i>COATING</i>	<i>LOT</i>	<i>MFI</i> (g/10min)	<i>VOLUMETRIC O/P</i> (cm ³ /10min)
2.0VS50A	Vinyl silane	1	5.07 (0.16)	3.22
2.0VS55A	Vinyl silane	1	4.54 (0.16)	2.78
2.0VS60A	Vinyl silane	1	2.85 (0.10)	1.69
2.0VS65A	Vinyl silane	1	2.55 (0.16)	1.47
2.0VS70A	Vinyl silane	1	0.41 (0.07)	0.22
2.0VS20B	Vinyl silane	1	11.20 (0.20)	9.12
2.0VS30B	Vinyl silane	1	9.00 (0.30)	6.72
2.0VS40B	Vinyl silane	1	4.30 (0.10)	2.53
2.0VS50B	Vinyl silane	1	3.70 (0.20)	2.24
2.0VS60B	Vinyl silane	1	3.30 (0.10)	1.89
2.0VS70B	Vinyl silane	1	0.31 (0.02)	0.17
2.0VS20*	Vinyl silane	2	10.80 (0.05)	9.11
2.0VS60*	Vinyl silane	2	3.00 (0.10)	1.68

* Batch mixed

DP390s LOT 1 formulations

<i>CODE</i>	<i>COATING</i>	<i>LOT</i>	<i>MFI</i> (g/10min)	<i>VOLUMETRIC</i> <i>O/P</i> (cm ³ /10min)
DP390s	Uncoated	1	0.00 (-----)	0.00
AMST2.0	Stearate	1	2.03 (0.18)	1.15
AMST4.0	Stearate	1	7.30 (0.43)	4.32
AMST6.0	Stearate	1	7.71 (0.29)	4.56
AMOL2.0	Oleate	1	2.41 (0.33)	1.40
AMOL4.0	Oleate	1	6.51 (0.27)	3.78

DP390s LOT 2 formulations

<i>CODE</i>	<i>COATING</i>	<i>LOT</i>	<i>MFI</i> (g/10min)	<i>VOLUMETRIC O/P</i> (cm ³ /10min)
NAOL1.5	Oleate	2	0.33 (0.06)	0.19
NAOL3.0	Oleate	2	7.80 (0.12)	4.51
NAOL4.5	Oleate	2	8.36 (0.21)	4.91
NAOL6.0	Oleate	2	9.13 (0.22)	5.39
AMOL4.0	Oleate	2	8.49 (0.24)	4.98
AMOL6.0	Oleate	2	9.20 (0.26)	5.35

Appendix H

Capillary rheometry calculations and data

From the piston speed it is possible to calculate the volumetric output (Q) and the apparent shear rate (γ_{WA}). From the true pressure (ΔP) it is possible to calculate the shear stress (τ_w) of the melt. Equations governing these parameters can be seen below.

$$\tau_w = \frac{R\Delta P}{2L}$$

$$\gamma_{WA} = \frac{4Q}{\pi R^3} \quad (Q = \text{melt velocity} \times \text{area of extrusion})$$

where,

R is the radius of the die (1mm),

ΔP is the true pressure,

L is the corrected length of the die ($L_{20/2} - L_{0/2}$),

Q is the volumetric output of material through the die per unit time .

A plot of apparent shear stress versus shear rate is termed a shear flow curve, from which the rheological behaviour of any melt can be characterised.

Piston speed settings and apparent shear rates

Setting	1	2	3	4	5	6	7
Q (m ³ s ⁻¹) x 10 ⁻⁶	3.93	7.85	19.6	39.3	78.5	117.8	196.0
Piston speed (mm/min)	5	10	25	50	100	150	250
Apparent shear rate, γ_A (s ⁻¹)	24.0	48.0	120.0	240.0	480.0	720.0	1200.0

Measured pressure drop (ΔP) and calculated wall shear stresses (τ_w)

DP393 LOT 1 uncoated and fatty acid coated compounds

DP393

Setting	1	2	3	4	5	6	7
ΔP (Pa) $\times 10^6$	1.63	1.90	2.47	2.97	3.39	3.70	4.07
τ_w (Pa) $\times 10^4$	8.17	9.52	12.34	14.83	16.96	18.48	20.34

1.5AMST

Setting	1	2	3	4	5	6	7
ΔP (Pa) $\times 10^6$	0.61	0.77	1.17	1.63	2.14	2.26	2.76
τ_w (Pa) $\times 10^4$	3.03	3.86	5.86	8.14	10.69	11.31	13.79

3.0AMST

Setting	1	2	3	4	5	6	7
ΔP (Pa) $\times 10^6$	0.48	0.70	1.09	1.48	1.86	2.10	2.37
τ_w (Pa) $\times 10^4$	2.39	3.52	5.45	7.38	9.31	10.48	11.86

4.5AMST

Setting	1	2	3	4	5	6	7
ΔP (Pa) $\times 10^6$	0.43	0.62	0.83	1.39	1.68	1.86	2.17
τ_w (Pa) $\times 10^4$	2.13	3.10	4.17	6.96	8.41	9.31	10.83

1.5AMOL

Setting	1	2	3	4	5	6	7
ΔP (Pa) $\times 10^6$	0.68	0.91	1.31	1.81	2.11	2.32	2.59
τ_w (Pa) $\times 10^4$	3.41	4.59	6.53	9.03	10.55	11.58	12.96

3.0AMOL

Setting	1	2	3	4	5	6	7
$\Delta P \text{ (Pa)} \times 10^6$	0.51	0.69	0.99	1.48	1.69	1.94	2.12
$\tau_w \text{ (Pa)} \times 10^4$	2.55	3.45	4.97	7.38	8.45	9.72	10.58

4.5AMOL

Setting	1	2	3	4	5	6	7
$\Delta P \text{ (Pa)} \times 10^6$	0.41	0.66	0.91	1.34	1.65	1.72	1.97
$\tau_w \text{ (Pa)} \times 10^4$	2.07	3.31	4.55	6.69	8.27	8.62	9.86

4.5NAST

Setting	1	2	3	4	5	6	7
$\Delta P \text{ (Pa)} \times 10^6$	0.48	0.54	0.99	1.35	1.77	1.97	2.18
$\tau_w \text{ (Pa)} \times 10^4$	2.41	2.69	4.97	6.76	8.83	9.86	10.90

4.5NAOL

Setting	1	2	3	4	5	6	7
$\Delta P \text{ (Pa)} \times 10^6$	0.46	0.61	0.84	1.23	1.49	1.59	1.79
$\tau_w \text{ (Pa)} \times 10^4$	2.28	3.03	4.22	6.14	7.45	7.93	8.96

4.5AMROS

Setting	1	2	3	4	5	6	7
$\Delta P \text{ (Pa)} \times 10^6$	0.90	1.27	1.82	2.47	2.87	3.16	3.64
$\tau_w \text{ (Pa)} \times 10^4$	4.48	6.34	9.10	12.34	14.34	15.79	18.20

DP393 LOT 2 fatty acid compounds

1.5NAOL

Setting	1	2	3	4	5	6	7
$\Delta P \text{ (Pa)} \times 10^6$	1.16	1.30	1.72	2.20	2.85	3.25	3.72
$\tau_w \text{ (Pa)} \times 10^4$	5.79	6.52	8.60	11.03	14.24	16.27	18.62

3.0NAOL

Setting	1	2	3	4	5	6	7
$\Delta P \text{ (Pa)} \times 10^6$	0.58	0.83	1.21	1.65	2.17	2.56	3.10
$\tau_w \text{ (Pa)} \times 10^4$	2.90	4.14	6.07	8.27	10.86	12.82	15.51

4.5NAOL

Setting	1	2	3	4	5	6	7
$\Delta P \text{ (Pa)} \times 10^6$	0.37	0.60	0.94	1.26	1.68	1.99	2.48
$\tau_w \text{ (Pa)} \times 10^4$	1.86	3.00	4.69	6.31	8.41	9.93	12.41

4.5AMOL

Setting	1	2	3	4	5	6	7
$\Delta P \text{ (Pa)} \times 10^6$	0.34	0.59	0.91	1.26	1.63	1.94	2.40
$\tau_w \text{ (Pa)} \times 10^4$	1.72	2.93	4.55	6.31	8.14	9.69	12.00

DP393 LOT 1 Vinyl Silane Compounds

2.0VS50A

Setting	1	2	3	4	5	6	7
$\Delta P \text{ (Pa)} \times 10^6$	0.62	0.85	1.16	1.63	1.97	2.18	2.54
$\tau_w \text{ (Pa)} \times 10^4$	3.10	4.24	5.79	8.14	9.83	10.89	12.69

2.0VS55A

Setting	1	2	3	4	5	6	7
$\Delta P \text{ (Pa)} \times 10^6$	0.61	0.83	1.31	1.85	1.93	2.17	2.55
$\tau_w \text{ (Pa)} \times 10^4$	3.03	4.14	6.55	9.24	9.65	10.83	12.76

2.0VS60A

Setting	1	2	3	4	5	6	7
$\Delta P \text{ (Pa)} \times 10^6$	0.80	1.06	1.42	2.17	2.35	2.63	3.06
$\tau_w \text{ (Pa)} \times 10^4$	4.00	5.31	7.10	10.83	11.74	13.17	15.31

2.0VS65A

Setting	1	2	3	4	5	6	7
$\Delta P \text{ (Pa)} \times 10^6$	0.77	0.94	1.50	1.85	2.25	2.47	2.85
$\tau_w \text{ (Pa)} \times 10^4$	3.86	4.68	7.48	9.24	11.24	12.34	14.27

2.0VS70A

Setting	1	2	3	4	5	6	7
$\Delta P \text{ (Pa)} \times 10^6$	1.14	1.48	1.97	2.90	3.12	3.36	3.97
$\tau_w \text{ (Pa)} \times 10^4$	5.72	7.38	9.86	14.49	15.58	16.82	19.93

2.0VS20B

Setting	1	2	3	4	5	6	7
$\Delta P \text{ (Pa)} \times 10^6$	0.32	0.50	0.76	0.11	1.35	1.71	2.13
$\tau_w \text{ (Pa)} \times 10^4$	1.58	2.48	3.78	5.23	6.73	8.53	10.63

2.0VS30B

Setting	1	2	3	4	5	6	7
$\Delta P \text{ (Pa)} \times 10^6$	0.39	0.59	0.82	1.12	1.39	1.76	2.15
$\tau_w \text{ (Pa)} \times 10^4$	1.95	2.95	4.10	5.63	6.95	8.75	10.75

2.0VS40B

Setting	1	2	3	4	5	6	7
$\Delta P \text{ (Pa)} \times 10^6$	0.44	0.63	0.94	1.26	1.57	1.86	2.20
$\tau_w \text{ (Pa)} \times 10^4$	2.20	3.15	4.70	6.30	7.83	9.28	11.00

2.0VS50B

Setting	1	2	3	4	5	6	7
$\Delta P \text{ (Pa)} \times 10^6$	0.52	0.76	1.11	1.49	1.90	2.16	2.54
$\tau_w \text{ (Pa)} \times 10^4$	2.60	3.78	5.55	7.43	9.48	10.78	12.68

2.0VS60B

Setting	1	2	3	4	5	6	7
$\Delta P \text{ (Pa)} \times 10^6$	0.76	1.05	1.53	1.93	2.42	2.71	3.08
$\tau_w \text{ (Pa)} \times 10^4$	3.78	5.23	7.63	9.63	12.10	13.53	15.38

2.0VS70B

Setting	1	2	3	4	5	6	7
$\Delta P \text{ (Pa)} \times 10^6$	1.00	1.39	2.06	2.43	2.83	3.38	3.90
$\tau_w \text{ (Pa)} \times 10^4$	5.00	6.95	10.30	12.15	14.13	16.90	19.50

DP393 LOT 3 uncoated and fatty acid compounds

DP393

Setting	1	2	3	4	5	6	7
$\Delta P \text{ (Pa)} \times 10^6$	1.54	1.88	2.43	2.90	3.37	3.65	3.96
$\tau_w \text{ (Pa)} \times 10^4$	7.72	9.38	12.13	14.48	16.86	18.24	19.78

4.5AMST

Setting	1	2	3	4	5	6	7
$\Delta P \text{ (Pa)} \times 10^6$	0.36	0.58	0.82	1.20	1.48	1.57	1.78
$\tau_w \text{ (Pa)} \times 10^4$	1.78	2.88	4.10	6.00	7.40	7.84	8.90

4.5AMOL

Setting	1	2	3	4	5	6	7
$\Delta P \text{ (Pa)} \times 10^6$	0.39	0.63	0.90	1.30	1.63	1.72	1.96
$\tau_w \text{ (Pa)} \times 10^4$	1.96	3.17	4.51	6.48	8.14	8.62	9.79

4.5NAOL

Setting	1	2	3	4	5	6	7
$\Delta P \text{ (Pa)} \times 10^6$	0.37	0.62	0.92	1.32	1.65	1.76	1.99
$\tau_w \text{ (Pa)} \times 10^4$	1.84	3.09	4.60	6.59	8.27	8.79	9.95

DP390s LOT 1 uncoated and fatty acid coated compounds

DP390s

Setting	1	2	3	4	5	6	7
$\Delta P \text{ (Pa)} \times 10^6$	1.66	2.03	2.68	3.21	3.92	4.42	5.04
$\tau_w \text{ (Pa)} \times 10^4$	8.28	10.13	13.40	16.05	19.58	22.08	25.22

AMST2.0

Setting	1	2	3	4	5	6	7
$\Delta P \text{ (Pa)} \times 10^6$	0.61	0.72	1.44	1.91	2.35	2.62	2.93
$\tau_w \text{ (Pa)} \times 10^4$	3.03	3.58	7.18	9.53	11.73	13.10	14.63

AMST4.0

Setting	1	2	3	4	5	6	7
$\Delta P \text{ (Pa)} \times 10^6$	0.42	0.64	0.98	1.41	1.66	2.13	2.36
$\tau_w \text{ (Pa)} \times 10^4$	2.08	3.18	4.90	7.03	8.28	10.63	11.80

AMST6.0

Setting	1	2	3	4	5	6	7
$\Delta P \text{ (Pa)} \times 10^6$	0.39	0.63	0.85	1.35	1.66	1.88	2.07
$\tau_w \text{ (Pa)} \times 10^4$	1.93	3.13	4.25	6.75	8.28	9.38	10.35

AMOL2.0

Setting	1	2	3	4	5	6	7
$\Delta P \text{ (Pa)} \times 10^6$	0.77	1.07	1.56	1.93	2.33	2.54	3.15
$\tau_w \text{ (Pa)} \times 10^4$	3.85	5.35	7.80	9.65	11.65	12.68	15.73

AMOL4.0

Setting	1	2	3	4	5	6	7
$\Delta P \text{ (Pa)} \times 10^6$	0.53	0.70	1.08	1.35	1.65	1.77	2.04
$\tau_w \text{ (Pa)} \times 10^4$	2.63	3.48	5.38	6.75	8.25	8.83	10.20

DP390s LOT 2 fatty acid coated compounds

NAOL1.5

Setting	1	2	3	4	5	6	7
$\Delta P \text{ (Pa)} \times 10^6$	1.03	1.77	1.99	2.83	3.53	4.00	4.64
$\tau_w \text{ (Pa)} \times 10^4$	5.14	8.83	9.94	14.13	17.66	20.00	23.18

NAOL3.0

Setting	1	2	3	4	5	6	7
$\Delta P \text{ (Pa)} \times 10^6$	0.77	1.08	1.68	2.29	2.70	3.05	3.39
$\tau_w \text{ (Pa)} \times 10^4$	3.84	5.42	8.38	11.45	13.52	15.25	16.97

NAOL4.5

Setting	1	2	3	4	5	6	7
$\Delta P \text{ (Pa)} \times 10^6$	0.69	1.08	1.66	2.29	2.70	2.95	3.31
$\tau_w \text{ (Pa)} \times 10^4$	3.45	5.40	8.28	11.45	13.52	14.77	16.56

NAOL6.0

Setting	1	2	3	4	5	6	7
$\Delta P \text{ (Pa)} \times 10^6$	0.68	1.08	1.60	2.20	2.65	2.90	3.23
$\tau_w \text{ (Pa)} \times 10^4$	3.38	5.38	8.00	11.00	13.25	14.49	16.15

AMOL4.0

Setting	1	2	3	4	5	6	7
$\Delta P \text{ (Pa)} \times 10^6$	0.61	1.08	1.60	2.18	2.75	3.19	3.48
$\tau_w \text{ (Pa)} \times 10^4$	3.04	5.38	8.00	10.90	13.74	15.94	17.39

AMOL6.0

Setting	1	2	3	4	5	6	7
$\Delta P \text{ (Pa)} \times 10^6$	0.61	1.02	1.52	2.21	2.41	2.90	3.26
$\tau_w \text{ (Pa)} \times 10^4$	3.04	5.11	7.59	11.07	12.08	14.49	16.28

Unfilled Polypropylene

PP

Setting	1	2	3	4	5	6	7
$\Delta P \text{ (Pa)} \times 10^6$	0.34	0.47	0.68	1.01	1.25	1.45	1.71
$\tau_w \text{ (Pa)} \times 10^4$	1.72	2.35	3.41	5.03	6.24	7.24	8.55

APPENDIX I

Flexural calculations and data

The flexural modulus (E) and the flexural strength (σ) of the filled composites were calculated according to the following equations:

$$E = \frac{l^3 m}{4bd^3}$$

$$\sigma = \frac{3nl}{2b^2 d}$$

where,

l is the span (60 mm),

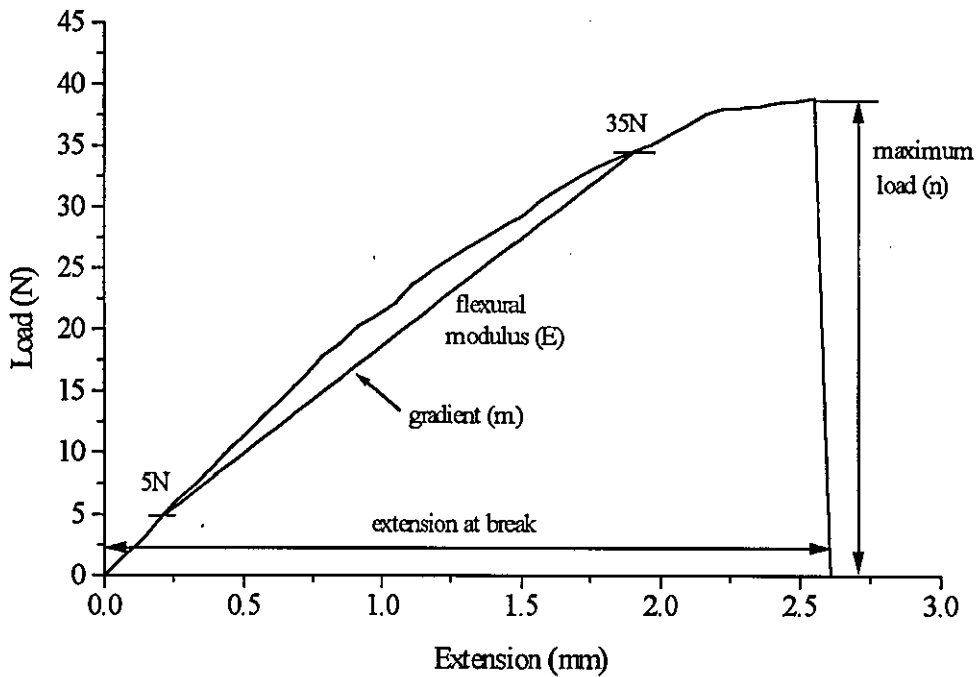
b is the sample thickness (3.2 mm),

d is the sample width (12.6 mm),

n is the maximum load (N),

m is the slope of the curve between 5 and 35N (N/mm).

Typical trace for PP filled with 60% $\text{Mg}(\text{OH})_2$



PP, DP393 and DP390s uncoated filled composites

<i>CODE</i>	<i>FLEXURAL MODULUS (GPa)</i>	<i>FLEXURAL STRENGTH (MPa)</i>	<i>EXTENSION @ BREAK (mm)</i>
PP ductile	1.03	28.3	>15.0
	1.09	28.9	>15.0
	1.00	29.6	>15.0
	1.03	28.5	>15.0
	1.09	29.2	>15.0
	1.10	29.3	>15.0
	1.06	29.0	>15.0
	1.06	29.1	>15.0
	1.06 (0.03)	29.0 (0.8)	>15.0 (—)
DP393 (LOT 1) brittle	2.71	27.9	1.95
	3.30	29.2	2.04
	3.12	27.2	2.07
	3.19	28.5	2.15
	3.25	29.1	2.29
	3.25	31.5	2.73
	3.28	28.1	2.11
	2.79	28.8	2.42
	3.43	30.4	2.18
	3.24 (0.03)	29.0 (1.2)	2.15 (0.15)
DP393 (LOT 3) brittle	2.62	33.5	3.45
	2.51	32.8	3.47
	2.69	33.7	3.95
	2.74	33.5	3.11
	2.75	34.3	3.33
	2.76	33.6	3.25
	2.89	34.3	3.53
	2.68	33.7	3.33
	2.71 (0.04)	33.7 (0.6)	3.44 (0.09)
DP390s (LOT 1) brittle	2.72	31.6	3.47
	2.43	31.1	4.00
	2.50	31.4	3.55
	2.76	32.0	3.80
	2.65	32.0	4.30
	2.57	31.0	3.56
	2.61	31.1	3.37
	2.60	30.8	3.56
	2.61 (0.08)	31.4 (0.5)	3.70 (0.31)

Averages are given in bold (standard deviations in brackets).

Values denoted by >15.0mm did not break within the limits of the test.

DP393 LOT 1 fatty acid coated filled composites

CODE	FLEXURAL MODULUS (GPa)	FLEXURAL STRENGTH (MPa)	EXTENSION @ BREAK (mm)
1.5AMST brittle	2.61	28.6	2.27
	2.62	27.8	2.14
	2.77	29.2	2.20
	2.77	27.8	2.02
	2.59	26.9	2.13
	2.69	26.7	2.03
	2.81	29.8	2.18
	2.74	28.2	2.09
	2.70 (0.08)	28.2 (1.0)	2.13 (0.09)
3.0AMST brittle	2.53	27.3	2.70
	2.51	27.4	2.87
	2.47	26.4	3.17
	2.54	27.6	2.59
	2.56	28.5	2.90
	2.54	27.8	3.47
	2.35	26.3	2.82
	2.42	26.6	2.96
	2.49 (0.09)	27.3 (0.8)	2.97 (0.26)
4.5AMST brittle	2.41	26.2	2.71
	2.41	26.5	3.25
	2.23	26.5	3.76
	2.38	26.4	3.74
	2.32	25.5	3.06
	2.38	25.2	3.25
	2.52	27.2	2.77
	2.31	26.1	3.46
	2.37 (0.09)	26.2 (0.8)	3.25 (0.47)
1.5AMOL brittle	2.57	29.1	2.55
	2.62	28.7	2.38
	2.62	29.5	2.45
	2.68	28.8	2.36
	2.70	30.3	2.47
	2.63	28.9	2.33
	2.62	30.2	2.57
	2.63	29.7	2.43
	2.63 (0.01)	29.4 (0.6)	2.44 (0.09)
3.0AMOL brittle	2.07	25.6	2.33
	2.08	27.1	2.34
	2.12	27.2	2.39
	2.03	26.5	2.41
	2.04	25.7	2.33
	2.01	27.7	2.36
	2.09	25.2	2.23
	2.11	25.2	2.22
	2.07 (0.03)	26.3 (1.0)	2.33 (0.06)
4.5AMOL brittle	1.82	24.0	2.40
	1.89	26.1	2.65
	1.95	25.3	2.59
	1.97	25.6	2.89
	1.93	25.7	2.56
	1.91	25.4	2.60
	1.95	26.0	2.74
	1.95	26.0	2.53
	1.92 (0.07)	25.5 (1.1)	2.62 (0.15)
4.5NAST brittle	2.62	26.4	2.44
	2.59	28.1	3.25
	2.63	27.9	2.55
	2.57	28.6	2.45
	2.71	27.8	2.91
	2.54	28.2	2.97
	2.57	28.2	2.99
	2.54	28.0	2.61
	2.61 (0.04)	27.9 (0.7)	2.76 (0.30)
4.5NAOL quasi-ductile	1.61	29.4	4.94
	1.61	28.1	4.78
	1.49	27.6	4.76
	1.59	28.6	4.78
	1.55	28.2	4.75
	1.59	28.6	4.79
	1.68	27.9	4.78
	1.54	28.6	4.69
	1.58 (0.08)	28.4 (0.5)	4.78 (0.18)
4.5AMROS brittle	4.03	31.1	1.46
	4.39	31.5	1.35
	4.16	30.3	1.39
	4.16	31.4	1.46
	4.08	30.7	1.49
	4.25	33.5	1.46
	4.03	31.4	1.48
	4.04	31.0	1.49
	4.13 (0.12)	31.3 (1.0)	1.44 (0.13)

DP393 LOT 2 fatty acid coated filled composites

CODE	FLEXURAL MODULUS (GPa)	FLEXURAL STRENGTH (MPa)	EXTENSION @ BREAK (mm)
1.5NAOL brittle	3.49	29.6	2.22
	3.58	29.5	2.18
	3.37	28.3	1.90
	3.49	28.3	1.69
	3.43	28.6	1.86
	3.32	28.7	1.94
	3.50	28.0	1.67
	3.38	28.0	2.04
	3.44 (0.09)	28.6 (0.6)	1.94 (0.20)
3.0NAOL brittle	2.55	27.7	2.62
	2.80	28.8	2.62
	2.87	29.3	2.65
	2.58	27.2	2.18
	2.63	28.1	2.73
	2.62	27.5	2.54
	2.70	28.4	2.65
	2.70	27.5	2.13
	2.68 (0.11)	28.0 (0.8)	2.52 (0.22)
4.5NAOL brittle	1.99	27.2	2.74
	2.11	27.1	3.08
	2.02	26.4	2.83
	1.96	26.7	3.26
	2.08	26.0	3.27
	2.03	26.0	3.09
	2.06	26.0	3.12
	1.93	26.3	3.67
	2.02 (0.06)	26.5 (0.5)	3.01 (0.23)
4.5AMOL brittle	2.03	27.2	3.26
	2.06	27.1	2.77
	1.86	26.4	3.41
	1.94	26.3	2.85
	1.95	26.7	3.21
	1.91	26.0	2.91
	1.85	26.0	2.86
	1.85	26.0	2.87
	1.93 (0.08)	26.5 (0.5)	3.02 (0.24)

DP393 LOT 3 fatty acid coated filled composites

CODE	FLEXURAL MODULUS (GPa)	FLEXURAL STRENGTH (MPa)	EXTENSION @ BREAK (mm)
4.5AMST quasi-ductile	1.89	28.8	10.78
	1.77	28.9	10.64
	1.96	29.6	13.40
	1.91	29.4	11.22
	2.00	29.6	13.41
	1.88	29.3	11.23
	1.91	28.9	10.77
	1.93	29.1	10.65
	1.91 (0.02)	29.2 (1.0)	11.5 (0.78)
4.5AMOL brittle	1.99	27.7	3.51
	1.95	26.3	3.27
	2.01	26.7	3.04
	2.00	26.9	3.22
	2.06	26.9	2.92
	2.17	28.0	3.71
	2.08	27.3	3.41
	2.04	26.7	3.02
	2.03 (0.02)	28.0 (0.8)	3.26 (0.10)
4.5NAOL brittle	2.14	28.0	6.15
	2.15	27.7	6.40
	2.24	28.4	7.61
	2.24	28.7	8.10
	2.16	27.8	6.06
	2.23	28.1	5.99
	2.12	28.0	6.58
	2.23	28.1	6.78
	2.19 (0.02)	28.1 (0.1)	6.71 (0.29)

DP390s LOT 1 fatty acid coated filled composites

<i>CODE</i>	<i>FLEXURAL MODULUS (GPa)</i>	<i>FLEXURAL STRENGTH (MPa)</i>	<i>EXTENSION @ BREAK (mm)</i>
AMST2.0 brittle	3.10	25.7	2.45
	3.29	26.9	2.41
	3.10	25.6	2.49
	3.24	27.9	2.56
	3.32	27.2	2.39
	2.89	25.4	2.36
	3.16	26.7	2.47
	3.12	26.3	2.43
	3.14 (0.17)	26.5 (0.5)	2.45 (0.04)
AMST4.0 quasi-ductile	2.43	27.1	5.84
	2.45	26.6	5.99
	2.56	27.4	6.37
	2.43	26.1	6.10
	2.38	26.2	5.75
	2.39	26.1	5.89
	1.94	26.8	6.00
	2.44	26.4	5.98
	2.44 (0.03)	26.6 (0.3)	5.99 (0.10)
AMST6.0 quasi-ductile	2.49	25.9	8.86
	2.02	25.9	9.68
	1.94	24.9	8.98
	2.00	26.1	8.83
	2.20	27.7	9.27
	1.85	27.8	8.98
	2.10	26.5	9.30
	2.06	26.1	8.90
	2.08 (0.10)	26.3 (0.6)	9.10 (0.15)
AMOL2.0 brittle	3.27	27.0	2.18
	3.27	26.3	2.16
	3.14	26.4	2.26
	3.14	27.3	2.28
	3.05	26.1	2.28
	3.24	26.3	2.11
	3.08	26.9	2.16
	3.15	26.6	2.20
	3.17 (0.04)	26.6 (0.2)	2.20 (0.04)
AMOL4.0 brittle	2.22	24.6	3.03
	2.41	24.4	2.94
	2.44	25.4	2.66
	2.41	24.0	2.96
	2.36	24.5	3.04
	2.31	25.5	2.97
	2.38	24.9	2.95
	2.34	24.5	2.91
	2.36 (0.04)	24.7 (0.3)	2.93 (0.06)

DP390s LOT 2 fatty acid coated filled composites

<i>CODE</i>	<i>FLEXURAL MODULUS (GPa)</i>	<i>FLEXURAL STRENGTH (MPa)</i>	<i>EXTENSION @ BREAK (mm)</i>
NAOL1.5 brittle	3.45	32.9	2.40
	3.63	33.9	2.82
	3.36	32.4	2.96
	3.35	32.1	2.44
	3.42	32.6	2.36
	3.70	33.8	2.97
	3.52	33.3	2.83
	3.39	33.3	3.06
	3.44 (0.13)	33.0 (0.7)	2.73 (0.3)
NAOL3.0 brittle	2.79	30.4	4.02
	2.80	30.7	3.76
	2.50	29.5	3.50
	2.78	30.7	4.60
	2.62	29.9	3.60
	2.67	30.0	4.35
	2.62	30.5	5.44
	2.50	29.3	3.33
	2.66 (0.12)	30.1 (0.6)	4.14 (0.72)
NAOL4.5 brittle	2.53	29.7	5.39
	2.40	29.5	4.58
	2.32	29.1	4.93
	2.40	29.3	4.99
	2.48	30.9	5.03
	2.29	29.3	5.15
	2.41	29.6	4.65
	2.74	29.2	5.56
	2.45 (0.14)	29.6 (0.6)	5.04 (0.34)
NAOL6.0 quasi-ductile	2.35	30.9	9.89
	2.47	30.9	9.89
	2.41	30.5	6.38
	2.31	30.5	7.18
	2.28	29.8	5.91
	2.19	29.6	7.51
	2.22	29.1	5.62
	2.27	29.8	6.69
	2.31 (0.09)	30.1 (0.7)	7.45 (1.69)
AMOL4.0 quasi-ductile	2.07	29.9	5.47
	2.30	30.6	4.59
	2.13	29.5	5.29
	2.19	30.0	5.69
	2.20	30.1	4.54
	2.23	29.9	5.18
	1.98	31.1	6.67
	2.10	29.1	4.90
	2.14 (0.10)	30.0 (0.6)	5.29 (0.70)
AMOL6.0 quasi-ductile	2.42	30.1	6.91
	2.19	28.3	5.97
	2.77	28.5	5.49
	2.25	29.4	6.61
	2.16	28.0	5.71
	2.16	28.6	6.66
	2.22	28.4	6.14
	2.31	28.8	5.02
	2.25 (0.09)	28.8 (0.7)	5.97 (0.61)

Flexural properties of vinyl silane coated LOT 1A composites 152 days post moulding

<i>CODE</i>	<i>FLEXURAL MODULUS (GPa)</i>	<i>FLEXURAL STRENGTH (MPa)</i>	<i>EXTENSION @ BREAK (mm)</i>
2.0VS50A brittle	1.70	33.7	1.08
	1.88	36.9	1.01
	1.83	36.2	1.15
	1.86	36.7	1.12
	1.83	35.1	1.12
	1.78	45.8	1.01
	1.78	34.1	1.01
	1.80	34.4	1.08
	1.81 (0.06)	36.6 (3.9)	1.08 (0.06)
2.0VS55A brittle	1.93	36.8	1.06
	1.89	36.9	1.72
	1.91	36.8	1.06
	1.92	36.2	1.01
	1.89	35.2	0.96
	1.94	37.1	1.06
	1.94	36.1	1.03
	1.81	35.9	1.07
	1.90 (0.04)	36.4 (0.4)	1.07 (0.10)
2.0VS60A brittle	2.03	35.9	1.07
	2.11	34.0	0.87
	2.01	34.5	0.84
	2.09	34.2	0.87
	2.04	35.1	0.86
	2.05	35.0	0.91
	1.99	33.3	0.85
	2.02	32.8	1.09
	2.04 (0.04)	34.4 (1.0)	0.92 (0.10)
2.0VS65A brittle	2.11	34.0	0.83
	2.18	32.7	0.84
	2.13	33.3	0.80
	2.03	32.4	0.77
	2.13	33.5	0.82
	2.08	33.2	0.82
	2.12	34.5	0.83
	2.15	34.6	0.84
	2.12 (0.05)	33.9 (3.0)	0.82 (0.10)
2.0VS70A brittle	2.68	32.5	0.63
	2.65	32.5	0.64
	2.58	32.0	0.61
	2.77	32.6	0.61
	2.75	31.9	0.61
	2.69	32.3	0.63
	2.53	31.6	0.64
	2.72	32.8	0.63
	2.67 (0.08)	32.2 (1.0)	0.63 (0.01)

Flexural properties of vinyl silane coated LOT 1A composites 351 days post moulding

<i>CODE</i>	<i>FLEXURAL MODULUS (GPa)</i>	<i>FLEXURAL STRENGTH (MPa)</i>	<i>EXTENSION @ BREAK (mm)</i>
2.0VS50A brittle	2.13	38.1	0.96
	2.11	37.2	0.96
	2.08	39.1	0.96
	2.09	37.8	0.96
	1.99	38.4	0.96
	2.15	38.2	0.99
	2.13	37.4	0.91
	2.03	36.4	0.90
	2.09 (0.05)	37.8 (0.8)	0.95 (0.03)
2.0VS55A brittle	2.26	38.0	0.85
	2.15	36.1	0.87
	2.31	37.4	0.84
	2.28	37.8	0.85
	2.28	37.6	0.86
	2.26	37.7	0.84
	2.27	37.4	0.84
	2.21	37.5	0.82
	2.25 (0.05)	37.5 (0.6)	0.85 (0.01)
2.0VS60A brittle	2.48	35.0	0.65
	2.44	35.5	0.71
	2.43	34.6	0.64
	2.52	35.7	0.67
	2.60	36.3	0.66
	2.55	36.3	0.71
	2.53	36.9	0.73
	2.46	34.9	0.70
	2.50 (0.08)	35.6 (0.8)	0.68 (0.03)
2.0VS65A brittle	2.46	33.9	0.63
	2.62	35.8	0.63
	2.67	35.7	0.62
	2.53	34.1	0.61
	2.52	34.4	0.63
	2.52	33.9	0.61
	2.50	34.8	0.66
	2.48	34.3	0.64
	2.54 (0.08)	34.6 (1.8)	0.63 (0.02)
2.0VS70A brittle	3.30	34.3	0.49
	3.20	33.3	0.49
	3.21	33.8	0.51
	3.30	32.1	0.49
	3.32	35.1	0.47
	3.11	34.1	0.50
	3.19	33.5	0.46
	3.26	32.9	0.49
	3.24 (0.07)	33.7 (0.9)	0.48 (0.02)

Flexural properties of vinyl silane coated DP393 LOT 1B composites 6 days post moulding

CODE	FLEXURAL MODULUS (GPa)	FLEXURAL STRENGTH (MPa)	EXTENSION @ BREAK (mm)
2.0VS20B ductile	0.39	20.9	>15.0
	0.39	20.8	>15.0
	0.39	20.7	>15.0
	0.40	20.9	>15.0
	0.39	20.7	>15.0
	0.39	20.7	>15.0
	0.40	21.0	>15.0
	0.38	19.4	>15.0
	0.39 (0.07)	20.6 (0.5)	>15.0 (—)
2.0VS30B ductile	0.52	23.1	>15.0
	0.52	22.8	>15.0
	0.51	22.8	>15.0
	0.52	23.0	>15.0
	0.49	23.3	>15.0
	0.47	22.1	>15.0
	0.49	22.4	>15.0
	0.48	22.2	>15.0
	0.50 (0.02)	22.7 (0.4)	>15.0 (—)
2.0VS40B ductile	0.68	24.9	>15.0
	0.63	23.7	>15.0
	0.64	24.1	>15.0
	0.65	24.4	>15.0
	0.63	24.3	>15.0
	0.62	23.8	>15.0
	0.64	23.1	>15.0
	0.62	24.0	>15.0
	0.64 (0.02)	24.0 (0.6)	>15.0 (—)
2.0VS50B quasi-ductile	0.94	24.7	8.18
	0.91	24.3	7.94
	0.95	25.1	7.87
	0.93	24.6	7.87
	0.89	24.4	7.46
	0.89	24.2	8.51
	0.87	24.3	7.70
	0.91	24.8	7.52
	0.91 (0.03)	24.6 (0.3)	7.88 (0.35)
2.0VS60B brittle	1.18	24.6	5.04
	1.16	24.3	4.94
	1.14	24.1	5.00
	1.14	23.9	4.97
	1.11	23.5	4.84
	1.14	24.3	5.12
	1.16	23.9	5.04
	1.12	24.1	5.12
	1.14 (0.02)	24.1 (0.3)	5.01 (0.09)
2.0VS70B brittle	1.45	23.4	3.46
	1.50	23.0	3.18
	1.46	22.3	3.36
	1.44	22.2	3.29
	1.39	22.1	3.18
	1.47	23.8	3.45
	1.48	22.4	3.46
	1.49	23.2	3.29
	1.46 (0.04)	22.8 (0.6)	3.35 (0.14)
PP ductile	0.31	15.3	>15.0
	0.29	15.3	>15.0
	0.29	16.6	>15.0
	0.31	15.3	>15.0
	0.31	15.2	>15.0
	0.29	14.9	>15.0
	0.32	15.5	>15.0
	0.28	14.6	>15.0
	0.30 (0.01)	15.3 (0.6)	>15.0 (—)

Flexural properties of vinyl silane coated DP393 LOT 1B composites 34 days post moulding

CODE	FLEXURAL MODULUS (GPa)	FLEXURAL STRENGTH (MPa)	EXTENSION @ BREAK (mm)
2.0VS20B ductile	1.02	34.1	>15.0
	1.08	34.9	>15.0
	1.01	34.1	>15.0
	1.08	34.3	>15.0
	1.08	34.9	>15.0
	1.10	35.1	>15.0
	1.04	34.5	>15.0
	1.03	35.5	>15.0
	1.05 (0.03)	34.5 (0.5)	>15.0 (—)
2.0VS30B ductile	1.34	35.8	>15.0
	1.42	36.3	>15.0
	1.31	35.2	>15.0
	1.36	36.0	>15.0
	1.39	36.2	>15.0
	1.33	35.6	>15.0
	1.42	36.8	>15.0
	1.39	36.1	>15.0
	1.37 (0.04)	36.0 (0.5)	>15.0 (—)
2.0VS40B ductile	1.70	35.5	>15.0
	1.61	34.7	>15.0
	1.59	34.4	>15.0
	1.62	34.7	>15.0
	1.57	34.1	>15.0
	1.68	35.1	>15.0
	1.64	35.0	>15.0
	1.61	34.6	>15.0
	1.63 (0.04)	34.8 (0.4)	>15.0 (—)
2.0VS50B brittle	2.23	33.3	4.70
	2.47	35.7	5.35
	2.41	34.9	4.99
	2.34	33.7	4.25
	2.33	34.5	5.06
	2.13	32.9	4.32
	2.27	33.8	4.40
	2.23	33.8	5.15
	2.31 (0.10)	34.1 (0.9)	4.77 (0.42)
2.0VS60B brittle	2.58	31.5	2.80
	2.57	31.9	2.63
	2.76	33.1	3.69
	2.65	33.3	3.39
	2.70	32.5	2.64
	2.74	33.7	3.35
	2.69	32.1	2.55
	2.71	32.7	2.70
	2.67 (0.07)	32.6 (0.7)	2.97 (0.44)
2.0VS70B brittle	3.39	30.9	2.32
	3.52	29.5	1.56
	3.56	29.3	1.80
	3.60	32.1	2.07
	3.52	30.8	2.51
	3.33	30.3	1.90
	3.26	31.3	2.05
	3.56	30.3	2.01
	3.47 (0.11)	30.5 (0.9)	2.03 (0.35)
PP ductile	1.04	28.0	>15.0
	1.07	28.6	>15.0
	1.01	28.4	>15.0
	0.99	28.6	>15.0
	1.09	29.3	>15.0
	1.01	29.0	>15.0
	1.01	28.7	>15.0
	1.07	27.5	>15.0
	1.04 (0.04)	28.4 (0.6)	>15.0 (—)

Flexural properties of vinyl silane coated DP393 LOT 1B composites 69 days post moulding

CODE	FLEXURAL MODULUS (GPa)	FLEXURAL STRENGTH (MPa)	EXTENSION @ BREAK (mm)
2.0VS20B ductile	1.37	35.4	>15.0
	1.38	35.7	>15.0
	1.39	36.1	>15.0
	1.35	35.5	>15.0
	1.34	36.1	>15.0
	1.39	34.7	>15.0
	1.30	36.1	>15.0
	1.38	35.3	>15.0
	1.36 (0.03)	35.5 (0.5)	>15.0 (—)
2.0VS30B ductile	1.55	34.1	>15.0
	1.58	36.7	>15.0
	1.54	36.8	>15.0
	1.46	35.7	>15.0
	1.55	36.8	>15.0
	1.47	36.2	>15.0
	1.45	36.1	>15.0
	1.40	35.5	>15.0
	1.50 (0.07)	36.0 (0.9)	>15.0 (—)
2.0VS40B ductile	1.67	34.4	>15.0
	1.74	35.1	>15.0
	1.61	33.8	>15.0
	1.68	34.7	>15.0
	1.67	34.5	>15.0
	1.60	33.7	>15.0
	1.65	36.6	>15.0
	1.60	33.9	>15.0
	1.65 (0.05)	34.5 (1.0)	>15.0 (—)
2.0VS50B brittle	2.51	35.1	4.51
	2.34	33.6	5.08
	2.26	32.9	4.50
	2.24	33.2	4.64
	2.27	32.7	3.83
	2.44	35.2	4.76
	2.31	32.9	3.99
	2.29	33.7	5.05
	2.33 (0.09)	33.7 (1.5)	4.54 (0.45)
2.0VS60B brittle	2.68	31.7	2.59
	2.65	31.6	2.61
	2.73	31.8	2.55
	2.94	33.5	3.21
	2.94	33.3	3.27
	2.85	33.2	3.29
	2.84	32.8	2.65
	2.64	31.2	2.55
	2.78 (0.12)	32.4 (0.9)	2.84 (0.34)
2.0VS70B brittle	3.96	31.6	2.11
	3.84	32.0	2.28
	3.77	31.7	2.31
	3.77	32.2	2.40
	3.67	30.4	2.27
	3.64	29.9	1.86
	3.70	29.9	1.90
	3.71	30.6	1.76
	3.78 (0.11)	31.0 (0.9)	2.11 (0.26)
PP ductile	1.08	30.9	>15.0
	1.08	30.6	>15.0
	1.04	29.7	>15.0
	1.01	29.3	>15.0
	1.04	29.5	>15.0
	1.01	30.3	>15.0
	1.08	29.9	>15.0
	1.06	29.6	>15.0
	1.05 (0.03)	30.0 (0.6)	>15.0 (—)

Flexural properties of vinyl silane coated DP393 LOT 1B composites 157 days post moulding

CODE	FLEXURAL MODULUS (GPa)	FLEXURAL STRENGTH (MPa)	EXTENSION @ BREAK (mm)
2.0VS20B ductile	1.35	34.7	>15.0
	1.30	33.9	>15.0
	1.25	33.3	>15.0
	1.33	34.5	>15.0
	1.29	33.7	>15.0
	1.25	33.2	>15.0
	1.29	33.6	>15.0
	1.31	32.4	>15.0
	1.30 (0.04)	33.7 (0.7)	>15.0 (—)
2.0VS30B ductile	1.58	34.7	>15.0
	1.54	33.9	>15.0
	1.57	35.0	>15.0
	1.61	34.5	>15.0
	1.57	34.9	>15.0
	1.57	34.7	>15.0
	1.51	34.0	>15.0
	1.58	34.9	>15.0
	1.57 (0.03)	34.6 (0.4)	>15.0 (—)
2.0VS40B ductile	2.08	35.7	>15.0
	2.05	35.3	>15.0
	2.05	35.4	>15.0
	2.01	34.8	>15.0
	1.99	34.6	>15.0
	2.16	35.9	>15.0
	2.00	34.1	>15.0
	2.09	34.4	>15.0
	2.05 (0.06)	34.9 (0.6)	>15.0 (—)
2.0VS50B brittle	2.78	34.1	4.85
	2.81	33.5	4.52
	2.63	33.3	4.79
	2.44	32.1	4.55
	2.51	32.5	4.20
	2.67	33.1	4.24
	2.64	32.6	4.32
	2.62	32.7	4.32
	2.64 (0.12)	33.0 (0.7)	4.45 (0.25)
2.0VS60B brittle	3.30	32.4	2.56
	3.26	32.7	3.07
	3.33	32.8	2.55
	3.20	31.7	2.52
	3.16	31.9	3.25
	3.15	31.5	3.27
	3.09	31.3	2.29
	3.03	31.0	3.25
	3.19 (0.11)	31.9 (0.7)	2.67 (0.26)
2.0VS70B brittle	3.94	30.9	2.05
	3.85	30.3	1.79
	3.84	30.0	1.76
	3.82	29.5	1.70
	3.76	29.5	1.73
	3.82	30.3	1.76
	3.83	31.5	1.80
	3.83	30.5	1.81
	3.83 (0.05)	30.3 (0.7)	1.80 (0.12)
PP ductile	1.07	30.3	>15.0
	1.04	29.3	>15.0
	1.02	28.1	>15.0
	1.03	28.0	>15.0
	1.07	29.2	>15.0
	1.08	30.3	>15.0
	1.11	29.6	>15.0
	1.04	29.0	>15.0
	1.06 (0.03)	29.0 (0.8)	>15.0 (—)

APPENDIX J

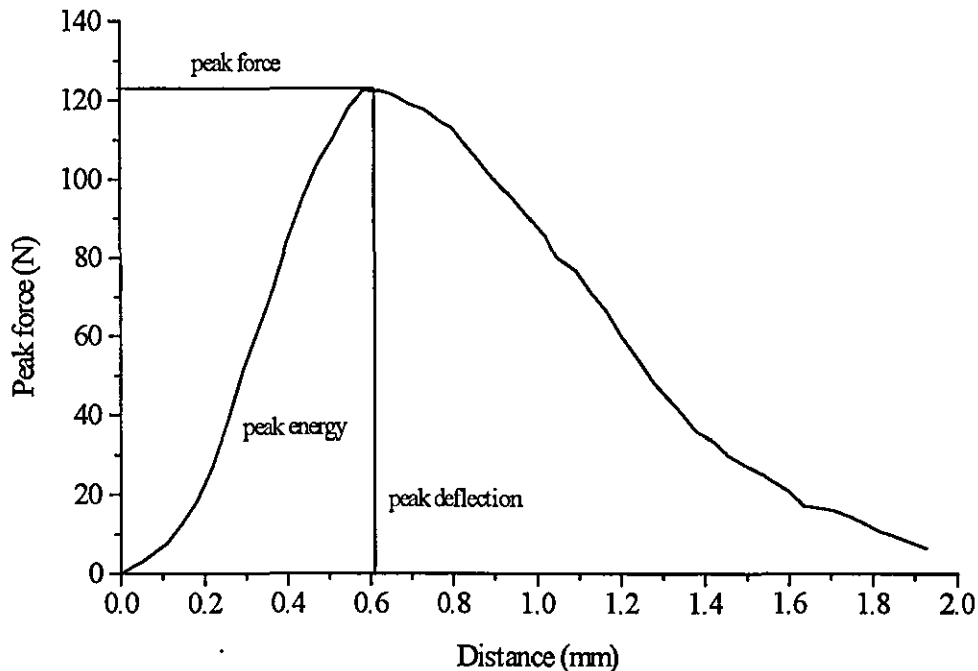
Impact parameters and data

The impact test conditions for the instrumented falling weight impact test can be seen below.

<i>PARAMETER</i>	<i>VALUE</i>
Mass	25kg
Dart	Charpy
Drop speed	3.0m/s
Drop height	464mm
Filter frequency	1.5KHz
Sweep time	10ms

The parameters used from an impact trace were peak force, peak energy and peak deflection. Failure information was not used, due to the difficulties in determining the end point of the impact event. In all cases, samples failed in a brittle mode. A typical impact trace for a 60% filled composite can be seen below.

Typical IFW impact trace for PP filled with 60%Mg(OH)₂



Peak impact data for all composites studied can be seen below. Averages are quoted in bold type and values in brackets are standard deviations of 8 samples.

PP, DP393 and DP390s uncoated filled composites

<i>CODE</i>	<i>PEAK IMPACT FORCE (N)</i>	<i>PEAK IMPACT ENERGY (mJ)</i>	<i>PEAK DEFLECTION (mm)</i>
PP	571	401	1.62
	428	226	1.33
	476	253	1.32
	569	388	1.63
	533	339	1.55
	441	246	1.37
	450	249	1.37
	581	398	1.66
	507 (64)	312 (77)	1.48 (0.15)
DP393 (LOT 1)	243	75	0.67
	227	69	0.66
	208	65	0.66
	253	90	0.76
	255	92	0.78
	279	103	0.83
	276	104	0.83
	242	89	0.71
	261	96	0.77
	249 (26)	85 (26)	0.74 (0.08)
DP393 (LOT 3)	191	53	0.71
	211	65	0.71
	211	89	0.97
	211	84	0.98
	208	72	0.89
	240	90	0.89
	348	99	0.71
	289	85	0.71
	239 (58)	80 (15)	0.82 (0.10)
DP390s (LOT 1)	218	72	0.78
	193	55	0.70
	197	68	0.79
	231	77	0.78
	208	59	0.70
	194	65	0.73
	221	72	0.76
	211	66	0.75
	210 (16)	66 (9)	0.75 (0.05)

DP393 LOT 1 fatty acid coated filled composites

CODE	PEAK IMPACT FORCE (N)	PEAK IMPACT ENERGY (mJ)	PEAK DEFLECTION (mm)
1.5AMST	116	30	0.62
	116	33	0.62
	122	36	0.62
	116	31	0.62
	114	33	0.62
	119	34	0.62
	115	31	0.62
	118	33	0.62
	117 (3)	32 (2)	0.62 (0.01)
3.0AMST	144	42	0.71
	156	57	0.82
	145	47	0.71
	131	47	0.71
	156	48	0.71
	154	57	0.80
	133	45	0.72
	148	52	0.80
	146 (19)	49 (2)	0.75 (0.01)
4.5AMST	154	58	0.80
	158	59	0.80
	172	59	0.80
	163	64	0.80
	168	56	0.81
	179	58	0.81
	157	61	0.80
	148	56	0.80
	162 (10)	59 (2)	0.80 (0.01)
1.5AMOL	122	34	0.62
	125	39	0.71
	132	37	0.62
	128	33	0.63
	119	35	0.62
	131	36	0.62
	124	35	0.63
	125	33	0.62
	126 (5)	35 (2)	0.64 (0.02)
3.0AMOL	135	45	0.72
	147	54	0.80
	148	55	0.81
	148	55	0.81
	135	41	0.71
	143	49	0.71
	143	54	0.80
	144	48	0.71
	143 (5)	50 (5)	0.76 (0.05)
4.5AMOL	160	51	0.80
	169	63	0.80
	157	51	0.80
	150	46	0.71
	153	61	0.80
	160	52	0.80
	167	56	0.80
	154	50	0.71
	159 (7)	54 (6)	0.80 (0.04)
4.5NAST	151	51	0.80
	152	55	0.80
	147	51	0.83
	150	52	0.76
	149	52	0.79
	138	47	0.79
	143	49	0.83
	146	50	0.79
	147 (5)	51 (2)	0.80 (0.02)
4.5NAOL	328	142	0.95
	329	147	1.09
	306	138	1.10
	309	129	1.10
	322	149	1.14
	312	134	1.09
	286	121	1.05
	335	151	1.13
	317 (4)	140 (9)	1.07 (0.08)
4.5AMROS	89	29	0.62
	101	33	0.61
	87	29	0.62
	93	29	0.62
	90	29	0.58
	94	27	0.58
	97	34	0.61
	95	30	0.57
	92 (3)	29 (2)	0.60 (0.03)

DP393 LOT 2 fatty acid coated filled composites

CODE	PEAK IMPACT FORCE (N)	PEAK IMPACT ENERGY (mJ)	PEAK DEFLECTION (mm)
1.5NAOL	92	26	0.63
	106	33	0.63
	89	30	0.63
	107	29	0.63
	99	32	0.63
	95	26	0.54
	95	26	0.54
	94	26	0.63
	97 (7)	29 (3)	0.61 (0.04)
3.0NAOL	102	30	0.63
	90	26	0.63
	100	26	0.63
	95	26	0.63
	98	28	0.62
	102	27	0.63
	97	26	0.63
	97	26	0.63
	98 (4)	27 (2)	2.52 (0.04)
4.5NAOL	101	33	0.63
	109	38	0.72
	92	32	0.63
	117	32	0.63
	117	32	0.63
	107	33	0.72
	99	33	0.63
	104	31	0.72
	105 (6)	33 (2)	0.66 (0.05)
4.5AMOL	86	27	0.63
	84	26	0.63
	90	30	0.63
	85	25	0.63
	118	38	0.71
	101	34	0.71
	117	36	0.71
	103	32	0.63
	98 (14)	31 (5)	0.66 (0.05)

DP393 LOT 3 fatty acid coated filled composites

CODE	PEAK IMPACT FORCE (N)	PEAK IMPACT ENERGY (mJ)	PEAK DEFLECTION (mm)
4.5AMST	232	94	0.88
	239	85	0.89
	225	86	0.89
	245	90	0.80
	235	80	0.80
	225	74	0.89
	260	103	0.97
	283	114	0.89
	243 (20)	91 (13)	0.87 (0.06)
4.5AMOL	154	49	0.70
	143	43	0.71
	155	47	0.70
	156	48	0.71
	151	50	0.71
	149	41	0.71
	159	48	0.71
	143	46	0.71
	151 (6)	47 (3)	0.71 (0.02)
4.5NAOL	161	65	0.98
	187	60	0.80
	166	61	0.80
	169	60	0.80
	168	58	0.80
	165	50	0.71
	185	56	0.70
	171	59	0.80
	171 (10)	59 (5)	0.80 (0.09)

DP390s LOT 1 fatty acid coated filled composites

<i>CODE</i>	<i>PEAK IMPACT FORCE (N)</i>	<i>PEAK IMPACT ENERGY (mJ)</i>	<i>PEAK DEFLECTION (mm)</i>
AMST2.0	111	29	0.53
	97	28	0.61
	108	27	0.52
	109	30	0.61
	106	31	0.52
	102	34	0.61
	105	30	0.58
	102	30	0.61
	105 (5)	30 (2)	0.58 (0.05)
AMST4.0	150	39	0.61
	130	39	0.60
	147	45	0.61
	145	46	0.61
	149	39	0.61
	135	34	0.61
	138	44	0.61
	146	44	0.61
	142 (7)	41 (4)	0.61 (0.02)
AMST6.0	162	47	0.70
	159	45	0.61
	160	53	0.69
	157	43	0.61
	163	58	0.71
	146	44	0.61
	143	48	0.70
	175	52	0.61
	157 (10)	48 (5)	0.66 (0.05)
AMOL2.0	107	31	0.61
	116	38	0.61
	125	36	0.61
	113	37	0.60
	121	34	0.61
	105	28	0.61
	101	30	0.61
	126	32	0.60
	115 (9)	26.6 (0.2)	0.61 (0.03)
AMOL4.0	121	38	0.61
	107	33	0.61
	118	35	0.61
	130	39	0.61
	124	37	0.61
	124	33	0.61
	126	38	0.61
	119	34	0.61
	121 (7)	36 (2)	0.61 (0.01)

DP390s LOT 2 fatty acid coated filled composites

<i>CODE</i>	<i>PEAK IMPACT FORCE (N)</i>	<i>PEAK IMPACT ENERGY (mJ)</i>	<i>PEAK DEFLECTION (mm)</i>
NAOL1.5	119	39	0.62
	113	39	0.70
	111	32	0.62
	121	31	0.62
	116	38	0.61
	122	37	0.71
	123	38	0.62
	120	32	0.62
	118 (4)	36 (3)	0.64 (0.04)
NAOL3.0	130	37	0.62
	133	42	0.71
	144	47	0.71
	133	47	0.79
	132	43	0.71
	126	36	0.62
	117	34	5.44
	134	39	0.70
	132 (8)	41 (5)	0.69 (0.06)
NAOL4.5	159	51	0.71
	144	53	0.79
	158	51	0.79
	147	49	0.71
	164	60	0.80
	161	52	0.79
	150	56	0.80
	179	71	0.89
	158 (11)	55 (7)	0.79 (0.06)
NAOL6.0	147	52	0.88
	151	57	0.97
	165	62	0.88
	176	69	0.97
	176	69	1.07
	195	82	0.89
	165	68	0.97
	189	73	0.97
	170 (17)	67 (9)	0.95 (0.06)
AMOL4.0	181	73	1.06
	176	73	1.06
	174	70	1.05
	179	63	0.98
	169	67	0.98
	165	65	1.06
	180	74	1.15
	173	62	0.98
	175 (5)	68 (5)	1.04 (0.06)
AMOL6.0	157	55	0.89
	127	47	0.88
	153	57	0.89
	155	56	0.97
	148	58	0.98
	144	58	0.89
	155	49	0.88
	152	49	0.88
	148 (9)	54 (4)	0.91 (0.04)

Impact properties of vinyl silane coated LOT 1A composites 20 days post moulding

<i>CODE</i>	<i>PEAK IMPACT FORCE (N)</i>	<i>PEAK IMPACT ENERGY (mJ)</i>	<i>PEAK DEFLECTION (mm)</i>
2.0VS50A	183	91	0.84
	207	98	0.84
	213	105	0.84
	222	108	0.83
	194	91	0.83
	209	106	0.83
	213	103	0.84
	217	101	0.79
	207 (13)	100 (7)	0.83 (0.02)
2.0VS55A	182	90	0.84
	197	97	0.83
	190	94	0.83
	180	97	0.83
	170	89	0.83
	180	94	0.84
	183	87	0.79
	184	87	0.83
	183 (8)	92 (4)	1.07 (0.10)
2.0VS60A	181	87	0.79
	167	86	0.84
	156	85	0.84
	179	87	0.84
	158	81	0.84
	161	89	0.83
	166	89	0.86
	187	90	0.89
	169 (12)	87 (3)	0.83 (0.02)
2.0VS65A	143	80	0.83
	154	85	0.88
	176	114	0.93
	189	91	0.79
	168	89	0.84
	168	91	0.88
	150	81	0.83
	180	91	0.83
	165 (15)	90 (11)	0.85 (0.04)
2.0VS70A	152	124	1.23
	148	121	1.23
	152	130	1.24
	154	126	1.19
	157	123	1.23
	151	124	1.19
	157	132	1.24
	147	128	1.24
	152 (3)	126 (4)	1.22 (0.02)

Impact properties of vinyl silane coated LOT 1A composites 274 days post moulding

<i>CODE</i>	<i>PEAK IMPACT FORCE (N)</i>	<i>PEAK IMPACT ENERGY (mJ)</i>	<i>PEAK DEFLECTION (mm)</i>
2.0VS50A	123	39	0.61
	123	36	0.61
	122	36	0.61
	117	34	0.61
	118	36	0.62
	127	36	0.61
	122	36	0.61
	122	39	0.61
	122 (3)	37 (2)	0.61 (0.04)
2.0VS55A	121	38	0.61
	123	36	0.62
	118	37	0.61
	120	39	0.62
	119	37	0.61
	120	34	0.57
	119	36	0.61
	114	32	0.61
	119 (3)	36 (2)	0.61 (0.02)
2.0VS60A	110	34	0.61
	105	29	0.57
	110	33	0.57
	116	36	0.62
	104	31	0.61
	111	32	0.57
	110	35	0.61
	114	35	0.61
	110 (2)	33 (2)	0.60 (0.03)
2.0VS65A	109	32	0.57
	114	35	0.61
	108	31	0.57
	114	35	0.61
	118	34	0.61
	110	31	0.61
	114	36	0.61
	109	34	0.61
	112 (3)	33 (2)	0.60 (0.02)
2.0VS70A	95	28	0.57
	94	26	0.53
	93	24	0.53
	95	25	0.53
	99	29	0.56
	89	26	0.53
	90	25	0.57
	90	26	0.56
	94 (3)	26 (2)	0.54 (0.02)

Impact properties of vinyl silane coated DP393 LOT 1B composites 7 days post moulding

<i>CODE</i>	<i>PEAK IMPACT FORCE (N)</i>	<i>PEAK IMPACT ENERGY (mJ)</i>	<i>PEAK DEFLECTION (mm)</i>
2.0VS20B	372	168	1.09
	292	124	1.01
	353	156	1.06
	301	127	1.01
	379	180	1.09
	348	147	1.06
	272	101	0.93
	304	122	0.97
	328 (40)	141 (27)	1.03 (0.06)
2.0VS30B	292	108	0.93
	273	100	0.93
	326	133	1.00
	270	100	0.92
	319	133	0.97
	297	111	0.93
	316	129	0.98
	280	106	0.93
	297 (22)	115 (14)	0.95 (0.03)
2.0VS40B	236	84	0.84
	219	89	0.79
	262	80	0.83
	219	77	0.78
	196	65	0.75
	196	64	0.84
	255	94	0.79
	248	85	0.79
	229 (26)	80 (11)	0.80 (0.03)
2.0VS50B	146	49	0.70
	178	61	0.71
	148	49	0.66
	163	50	0.66
	156	48	0.67
	141	44	0.66
	136	44	0.66
	144	44	0.62
	152 (15)	49 (6)	0.67 (0.03)
2.0VS60B	130	36	0.57
	122	37	0.62
	139	41	0.61
	132	41	0.62
	127	36	0.62
	136	39	0.62
	125	38	0.62
	125	39	0.62
	130 (6)	38 (2)	0.61 (0.02)
PP	571	401	1.62
	428	226	1.33
	476	253	1.32
	569	388	1.63
	533	339	1.55
	441	246	1.37
	450	249	1.37
	581	398	1.66
	507 (64)	312 (77)	1.48 (0.15)

Impact properties of vinyl silane coated DP393 LOT 1B composites 35 days post moulding

<i>CODE</i>	<i>PEAK IMPACT FORCE (N)</i>	<i>PEAK IMPACT ENERGY (mJ)</i>	<i>PEAK DEFLECTION (mm)</i>
2.0VS20B	279	123	1.08
	375	176	1.16
	362	163	1.16
	378	165	1.07
	272	122	1.07
	324	137	0.98
	344	147	1.15
	278	116	1.07
	329 (43)	145 (22)	1.10 (0.06)
2.0VS30B	288	104	0.99
	255	103	0.98
	310	119	0.99
	264	102	0.99
	310	136	1.07
	274	108	0.98
	241	94	0.98
	251	95	0.89
	274 (28)	108 (15)	0.98 (0.05)
2.0VS40B	206	66	0.80
	247	85	0.81
	240	80	0.80
	228	81	0.81
	231	77	0.81
	214	82	0.89
	217	72	0.80
	256	94	0.90
	230 (17)	80 (8)	0.83 (0.04)
2.0VS50B	141	48	0.72
	148	44	0.72
	141	47	0.72
	137	42	0.71
	152	52	0.71
	153	56	0.81
	128	43	0.72
	137	44	0.72
	142 (8)	47 (5)	0.73 (0.03)
2.0VS60B	119	42	0.72
	135	37	0.63
	117	38	0.63
	134	36	0.63
	132	35	0.63
	115	40	0.72
	122	42	0.72
	129	42	0.72
	2.67 (0.07)	39 (3)	0.67 (0.05)
PP	498	359	1.70
	378	207	1.43
	438	248	1.43
	555	385	1.70
	529	348	1.60
	401	203	1.52
	539	341	1.60
	546	370	1.60
	497 (67)	319 (71)	1.58 (0.10)

Impact properties of vinyl silane coated DP393 LOT 1B composites 70 days post moulding

<i>CODE</i>	<i>PEAK IMPACT FORCE (N)</i>	<i>PEAK IMPACT ENERGY (mJ)</i>	<i>PEAK DEFLECTION (mm)</i>
2.0VS20B	281	117	0.98
	296	124	1.06
	370	148	1.06
	295	117	0.98
	369	166	1.06
	350	156	1.07
	378	163	1.07
	297	121	0.99
	330 (41)	139 (21)	1.03 (0.04)
2.0VS30B	325	133	0.98
	334	133	0.98
	296	124	1.06
	314	144	1.08
	286	106	0.89
	275	101	0.89
	302	106	0.89
	301	111	0.97
	304 (20)	120 (16)	0.97 (0.08)
2.0VS40B	222	75	0.80
	233	78	0.80
	208	66	0.80
	230	76	0.80
	225	82	0.90
	205	70	0.80
	246	85	0.80
	229	77	0.79
	225 (13)	76 (6)	0.81 (0.03)
2.0VS50B	137	48	0.71
	151	49	0.72
	146	40	0.62
	148	44	0.71
	125	40	0.72
	146	50	0.72
	151	50	0.72
	146	50	0.71
	144 (9)	46 (4)	0.71 (0.03)
2.0VS60B	137	37	0.62
	133	35	0.62
	126	38	0.63
	123	38	0.63
	127	38	0.63
	130	36	0.63
	132	37	0.62
	116	34	0.62
	128 (6)	37 (2)	0.63 (0.03)
PP	466	287	1.43
	549	331	1.51
	481	267	1.43
	432	250	1.42
	447	233	1.34
	583	384	1.60
	489	273	1.43
	563	352	1.61
	502 (56)	297 (53)	1.47 (0.09)

Impact properties of vinyl silane coated DP393 LOT 1B composites 173 days post moulding

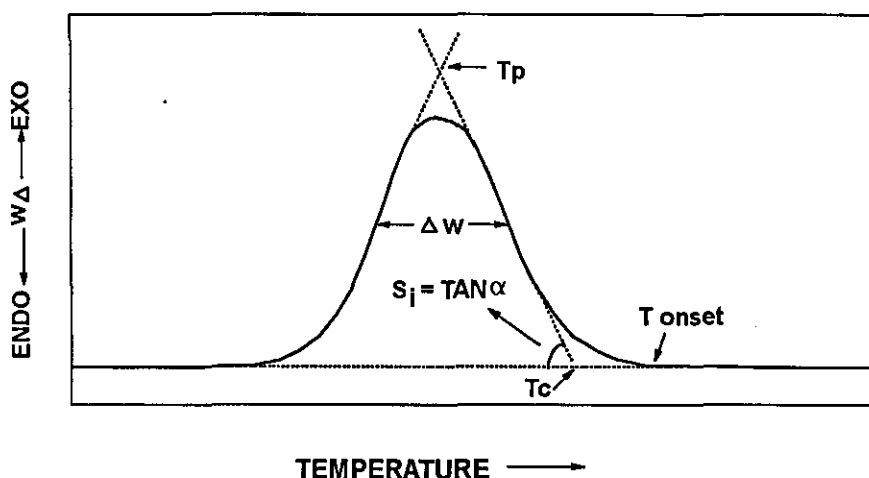
<i>CODE</i>	<i>PEAK IMPACT FORCE (N)</i>	<i>PEAK IMPACT ENERGY (mJ)</i>	<i>PEAK DEFLECTION (mm)</i>
2.0VS20B	290	124	0.98
	361	156	1.06
	390	158	1.06
	298	120	0.98
	294	98	0.80
	342	141	0.98
	280	107	0.98
	349	160	1.06
	326 (41)	133 (24)	0.99 (0.02)
2.0VS30B	250	90	0.88
	293	110	0.98
	280	110	0.97
	308	127	0.98
	309	113	0.88
	316	124	0.98
	315	118	0.89
	270	104	0.89
	293 (24)	112 (12)	0.93 (0.05)
2.0VS40B	201	65	0.80
	229	82	0.80
	209	73	0.80
	234	79	0.80
	209	64	0.71
	201	78	0.80
	228	75	0.80
	250	89	0.80
	220 (18)	76 (8)	0.79 (0.03)
2.0VS50B	150	53	0.71
	143	48	0.71
	146	51	0.71
	147	39	0.62
	147	43	0.62
	134	36	0.62
	134	40	0.71
	132	36	0.62
	142 (7)	43 (7)	0.66 (0.05)
2.0VS60B	141	47	0.71
	148	47	0.62
	151	48	0.71
	136	37	0.62
	141	40	0.62
	130	34	0.62
	143	41	0.62
	153	35	0.53
	143 (8)	40 (5)	0.63 (0.06)
PP	529	349	1.51
	509	327	1.51
	520	342	1.50
	510	277	1.41
	533	347	1.52
	537	276	1.06
	523	320	1.42
	522	320	1.42
	523 (11)	320 (31)	1.42 (0.16)

APPENDIX K

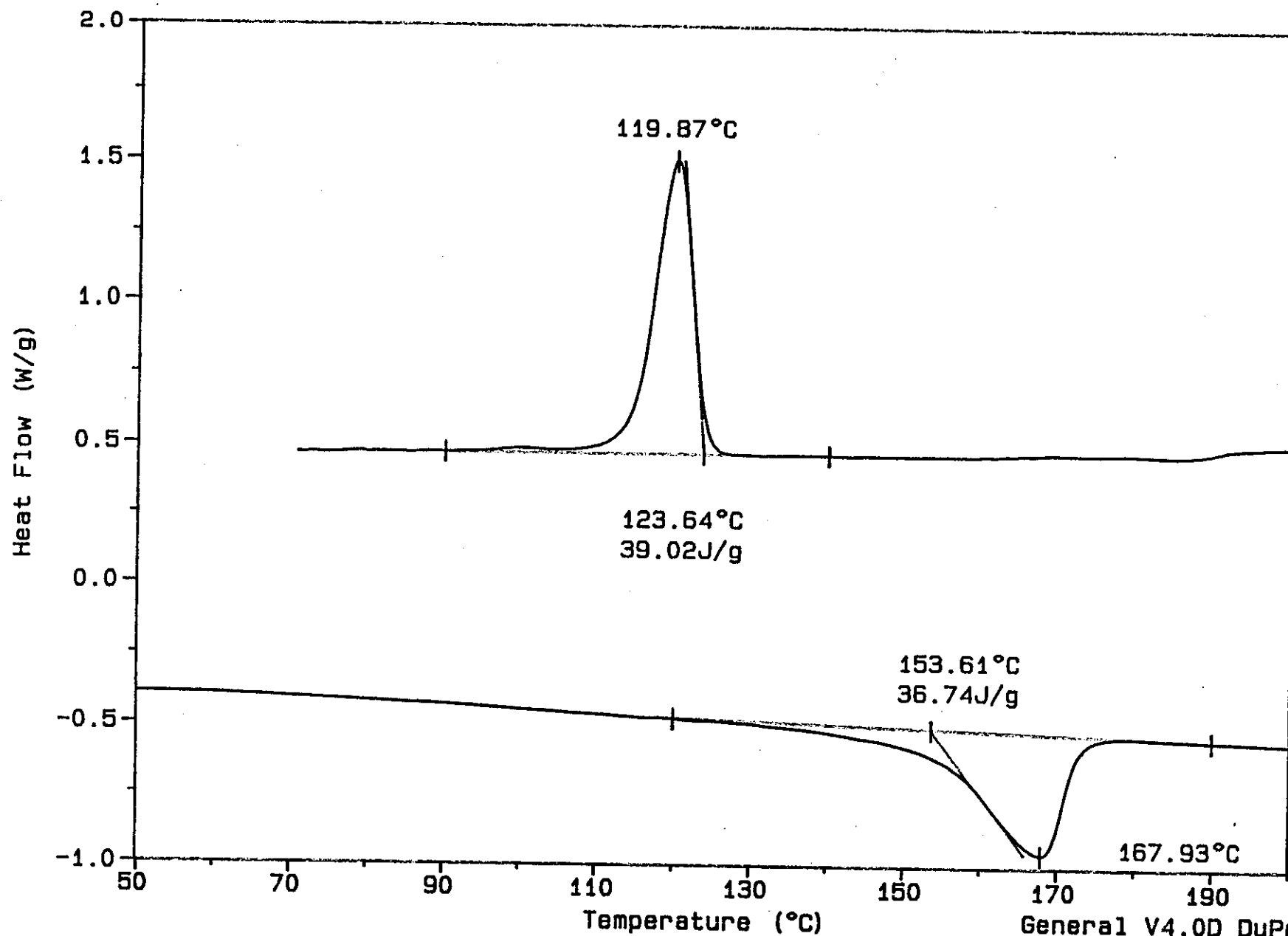
DSC analysis and parameters

Using the Maiti [103] method of analysing the cooling exotherm of a DSC trace, three useful parameters are yielded. These are $(T_c - T_p)$, S_i and ΔW (see schematic figure below). $(T_c - T_p)$ is a measure of overall crystallisation growth rate where T_p is the peak temperature of the crystallisation exotherm and T_c is the temperature at the intercept of the tangents at the base line on the high temperature side of the exotherm. Small values of $(T_c - T_p)$ indicate a high crystallisation growth rate. S_i is indicative of nucleation rate which is measured from the initial slope of the high temperature side of the exotherm. ΔW is a measure of crystallite size distribution and is obtained from measuring the width at half height of the exotherm peak. This is shown below. A typical DSC trace can be seen over leaf.

Method of determining Maiti parameters from DSC crystallization exotherm peak



Typical DSC trace for 60% magnesium hydroxide filled polypropylene composite



General V4.0D DuPont 2000

APPENDIX L

DMTA theory and data

Polymeric materials are viscoelastic, and in a dynamic stress state, the resulting strain is sinusoidally out of phase with the applied stress due to energy dissipation observed as heat or damping. This damping depends on the physical state of the samples. The Young's modulus is related to the square of the resonance frequency as the dynamic modulus of the samples is described as:

$$E^* = E' + E''$$

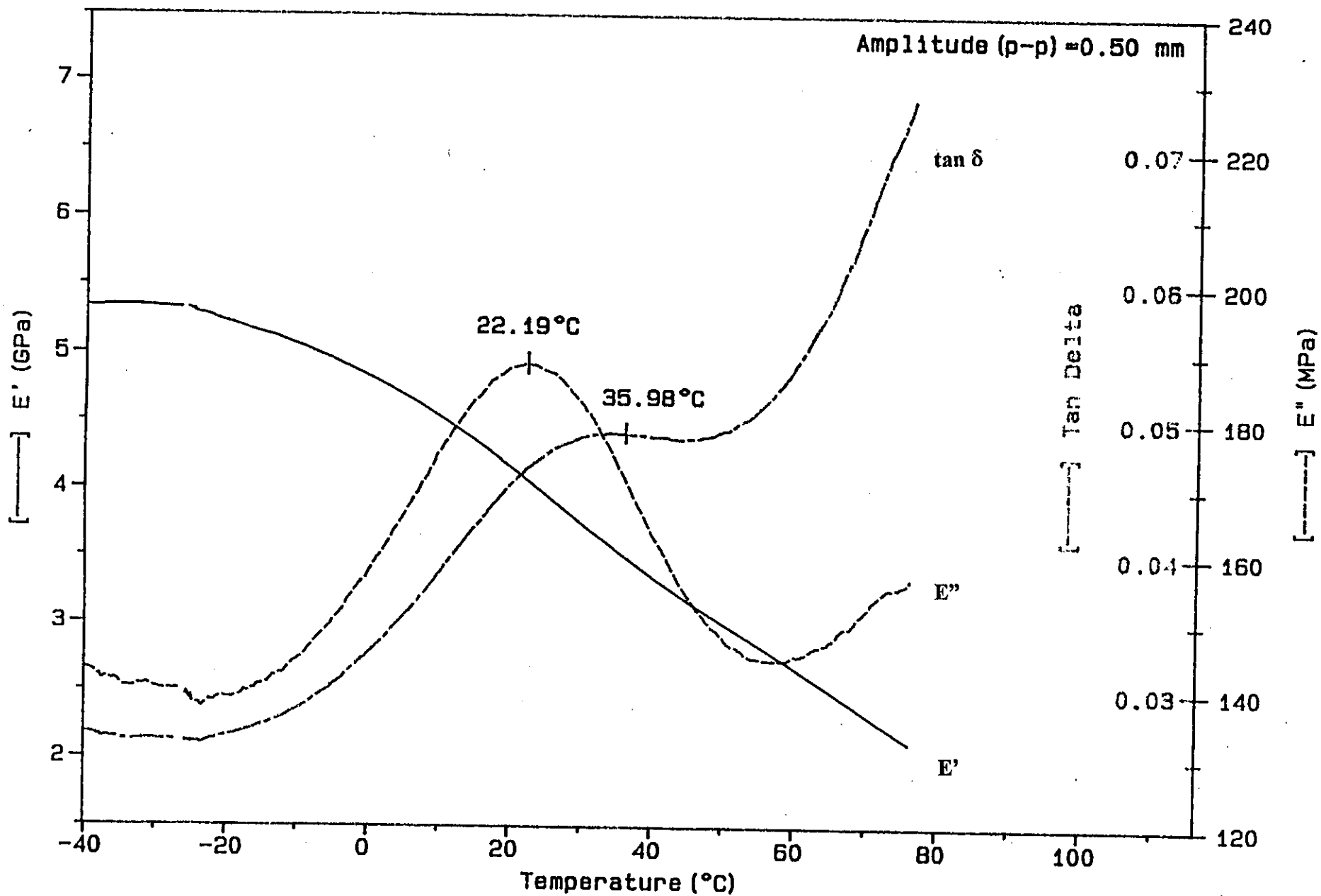
The storage modulus (E') is related to the elastic component of the materials and related to the recoverable strain. The loss modulus (E'') is related to the materials energy dissipation (viscous component). The ratio of these determines the phase angle, $\tan\delta$, where:

$$\tan\delta = E''/E'$$

These three terms are characteristics of the polymers along with their T_g . The results for vinyl silane LOT 1A composites are given below. T_g was determined from the loss modulus curve (E''), indicated by the DMTA trace included over leaf.

DMTA data for vinyl silane LOT 1A coated DP393 composites

<i>CODE</i>	<i>T_g (1)</i>	<i>T_g (2)</i>	<i>T_g (3)</i>	<i>T_g (mean)</i>
PP	17	24	23	21
2.0VS50A	24	25	22	24
2.0VS55A	22	25	22	23
2.0VS60A	22	25	21	23
2.0VS65A	22	25	21	23
2.0VS70A	26	28	24	26



Typical DMTA trace for $\text{Mg}(\text{OH})_2/\text{PP}$ composite

